

Dynamic wetting in pressure-infiltration of ceramic particle preforms by molten metal

Thèse N° 9673

Présentée le 27 septembre 2019

à la Faculté des sciences et techniques de l'ingénieur
Laboratoire de métallurgie mécanique
Programme doctoral en science et génie des matériaux

pour l'obtention du grade de Docteur ès Sciences

par

Gionata SCHNEIDER

Acceptée sur proposition du jury

Prof. A. Fontcuberta i Morral, présidente du jury
Prof. A. Mortensen, Dr L. Weber, directeurs de thèse
Prof. W. C. Carter, rapporteur
Prof. O. Dezellus, rapporteur
Prof. F. Stellacci, rapporteur

2019

Per me si va ne la città dolente
per me si va ne l'eterno dolore
per me si va tra la perduta gente
[...]

Lasciate ogni speranza, voi ch'entrate'
— Advice to each Ph.D. Student

Acknowledgements

The thesis is never a lone journey, but is a long path crossed by many people, which helped me in different ways to achieve the ultimate goal: having the red book (not Mao's but EPFL's)!// Firstly I would like to thank Andreas Mortensen and Ludger Weber, without whom this journey could not have ended positively, or even have started. They have helped me and supported me throughout the tortuous path; morally, when the light at the end of the tunnel was still hidden, and practically, giving precious and welcoming advices, through stimulating discussions and helping to correct the manuscript and the articles that have been (or will be) published as a consequence of my hard labour. During the five years spent under their supervision, even if the discussions were like a roller coaster, with many ups and downs, where you want to scream and/or you may sometime feel sick, at the end, once you are back on the ground, you are happy and you know that everything was worth it!

I would like to thank Prof. Francesco Stellacci, who had been following my project, starting from the egg, observing its transformation from an ugly and problematic caterpillar, and finally rising as a butterfly.

I am grateful to Prof. Craig Carter and Prof. Olivier Dezellus for their time and attending of my thesis defence as jury members, and for their useful comments and suggestions to my manuscript and for the highlighting discussions. I would like to thank Prof. Ana Fontcuberta i Morral for presiding the jury during my presentation.

All major explorations need sponsors; like America's exploration, which was founded by Spain or Australia's one, which was founded by Dutch. Dynamic infiltration exploration however, was kindly founded by Swiss National Science Foundation (SNSF, project 200021_149899) and Ecole Polytechnique Fédérale de Lausanne (EPFL), providing the resources, the manpower and the tools to pursue this long and incredible journey.

I would like to thank all the ATMX team, starting by the boss, Pierre-André who accepted all my last-minute requests after breaking a part of my machine or having a sudden inspiration on how to improve it and going there with a hand-drawn plan, and still accepting it! Thanks to Werner and Severino, to whom I could always go for a last minute touch, to have advices on how to improve the machine, or just to rectify a small mistake on the drawing. I am grateful to Jean-Pierre, Jean-Marc, Yves, Eric and Martial for their excellent work, without which I would still be holding a drill and a screwdriver to try to open my machine! And most important, I really enjoyed spending time with you all before Christmas for the annual "dîner de l'atelier"! I am thankful to all the CIME team, from Fabienne to Grégoire, Colette and Danièle for helping and training me to the electron microscopes and the samples preparation.

Acknowledgements

And now, the place where I spent almost more time than at home: LMM!

Firstly to Alain, who left me many interesting things to discover and explore in the pressure-infiltration domain! Thank you for initiating me to the machine, and to the wonderful world of metal matrix composites!

Thank you Fabienne for the discussions, the fun and withstanding my lame jokes for the last five years! Cyril... Without your help, I would not have been able to have a functional machine! Even if you did not spend so much time with us at the coffee since we live on the ground floor, I really appreciated spending time with you and having all the discussions we had.

Martin, Vaclav and Goran, thank you! For all the time spent during the coffee breaks, the interesting (and often silly) discussions, for the football matches and all the moments spent together! It was a pleasure having you as co-workers!

Gabi and Ana, we did not spend much time together, but it was a pleasure to meet you, talk to you and having many discussions around the coffee!

Marta, after 10 years spent in Vaud, I was finally able to speak Italian with someone! Thank you for everything! Both for helping me through the experiments with your expertise in ceramics, and for your kindness during the many discussions that we had!

Alejandra and Luciano, the newcomer in LMM. We did not spend so much time together, but it was a pleasure to share many moments both in the lab and outside!

Raph... We shared the office for five years, but the time that we actually spent together there is not more than a few working days! But apart from that, thanks for all the essential help though all my project and all the talks, jokes, anecdotes that you shared with me! It was an honour to meet you and to cross your path.

Lionel, I know that you know that "j'ai toujours raison"! Sometimes I was a bit annoying and my jokes were not always funny! Lionel and Mélina, knowing you, sharing all the moments together, especially those outside the lab: the hikes, the skiing, the dinners and all other activities that we did! A special thanks for coming to my wedding in Indonesia, it was a pleasure to share this moment with you and it will always stay in my memory! You are the proof that a Valaisan can be friend with a Ticinese, a Vaudoise and a Fribourgeoise, so there is still hope for the integration and acceptance of diversity in this world!

Léa, probably Andreas will delete this part, but it was a pleasure to spend 5min every hours with you! When I was infiltrating, if I did not come up every hour, you would come down to see if I was still alive! But apart from that, thank you for everything, for standing my lame jokes, for all the moments spent together: the hikes, the talks, the dinners, the bike ride (even if I think that it was more to be sure that I actually did it!) and to you too, to share the experience of my Chinese wedding in Indonesia! Thank you very much for everything!

Hamed... I really do not know where to start... maybe from the project that I did with you. There I started to know you better as a person. During the following years, I got to know you better and better, sharing many moments, which I am not able to list all here because it will be too long, but I will however thank you for two things: first, thank you for punching my eye, it was a once-in-a-lifetime experience! Second, thank you for the saffron rice and chicken! But seriously, thank you for being my best man and coming to the other side of the world to

attend our wedding, for all the small things that you did for the last 5 years and I am sure you will continue to do! As Americans would say, Thank you Bro!

Maïté.. It has been already 10 years that we know each other! From the shy girl in the first year, you became a very close friend, on which I could always count on, the wise voice of calm and tranquillity when everything seems out of control! Thanks mainly (and now let's include Alex) for all the things that we shared outside EPFL! And to you two too, thanks for sharing the unforgettable Indonesian wedding. It was a pleasure to share this moment with you!

Thanks to all my gym friends: George, Yvan, Jean-Claude and James, the few brave enough to train at 5:30! And Julien, who tortures me every morning, and with whom (and Sonia) I made the craziest hike ever. . . I am thanking you, but my legs for sure are not!

I am thankful to my parents, Paul and Cri, who, even without understanding a single word of what I was doing, were always asking me how I was doing and were concerned about my well-being, calling me after the meetings always with words of comfort and moral support! I am grateful to my sister Eia, for her smiles and kindness. Finally, to my brother Teseo and his family, who already ticked the Ph.D. box, giving me advices and support during the "downs" moments (and occasionally if I had problems with programming or math, he was always available for some tips!).

I would like to thank my family-in-law, Ago, Nurhajati, Ryco, Nyco and Viren, for even with all the communication problems that we have, they were always asking me how I was doing and giving precious encouragement! It was a pleasure to spend a few weeks in your warm island! Kamshia! Terima Kasih banyank! Saya tau kita tidak bisa bicara karena saya bicara sedikit Bahasa Indonesia, tetapi saya bahagia telah mempunyai anda seperti mertua!

Finally my (now) wife, who had to stand my mood swings, but who however always stayed on my side, giving me drinks when she saw that I was not in the best mood for various (work-related) reasons, supporting me and believing in my success even when my faith in science was flickering, and never losing hope and always being understandable! You were and still are my Rock even when I roll! Makasih Sayang manis! Saya cinta kamu, dan saya pasti tentang itu! Saya sangat bahagia karena kamu istriku!

Lausanne, le 15 août 2019

G. S.

Abstract

This thesis investigates the interaction between mechanically induced flow of a liquid metal into a porous solid, and kinetic effects at the triple line. The approach is experimental and focuses on metal-ceramic systems for which the literature gives values of wetting and local kinetic parameters (θ , σ_{LV} , and interfacial phenomena near the triple line) at high temperature, gleaned by means of the sessile drop experiment. We investigate the infiltration with Al of Al_2O_3 preforms at 1000°C , 1050°C and 1100°C , and the infiltration with Cu-x (x=Si, Ti or Cr) of porous C_{Gr} between 1050°C and 1200°C . Those three alloys are known to form carbides better wetted by the liquid than is graphite.

If measurements are taken at various values of applied metal overpressure, in the presence of thermally activated processes at the triple line, time intervenes in capillarity and the front does not stabilise. We observe that the metal continues to invade slowly the porous medium, gradually “creeping” into its pores under the action of local phenomena that take place at the triple line. We characterise such dynamic infiltration by measuring rates of steady isobaric infiltration, measuring also the variation of infiltration rates at P_{th} and $P_{th}+0.05\text{MPa}$. Saturation rates are then computed by means of a linear regression over 100s of the measured saturation for each pressure step. Data are interpreted using an analogy with high-temperature plasticity. This leads to assume that the applied pressure contributes a proportional reduction in the activation energy of the process that governs the rate of preform infiltration, the constant of proportionality defining an activation volume that characterises the thermally activated process.

Cu-46at.pct.Si infiltrating carbon is a mildly reactive system that forms SiC at the interface. Isobaric saturation rates of infiltration and their dependence on variations in the applied pressure were conducted between 1050°C and 1200°C . It is found that an activation volume on the order of $\approx 200\text{nm}^3$ makes the data compatible with the Arrhenius law, with an estimated activation energy value of $\approx 400 \frac{\text{kJ}}{\text{mol}}$, which is realistic for a process limited by the rate of SiC growth along the interface.

Aluminium infiltrating three different Al_2O_3 preforms shows similar behaviour as does the mildly reactive Cu-Si/C system if particles in the preform are highly angular, regardless of the presence or absence of Na impurities. Isobaric saturation rates measured between 1000°C and 1100°C give a similar activation volume as the Cu-Si/C system, on the order of $\approx 200\text{nm}^3$, and an activation energy $\approx 300 \frac{\text{kJ}}{\text{mol}}$, suggesting that the kinetics are likely limited by solid phase diffusion. It is also shown that sodium impurities in alumina serve to facilitate its infiltration by aluminium, likely because sodium alters the oxide skin that initially covers the melt.

Acknowledgements

Finally, in the infiltration of Cu-1at.pct.Cr or Cu-10at.pct.Ti into C_{Gr} , one finds that interfacial reaction does not aid pressure infiltration. In the former, it is because initial reaction between melt and preform depletes the alloy in reactive Cr, leading to similar infiltration as with pure Cu. In the latter, initial carbide formation is so extensive that it blocks ingress of the metal into the preform. For alloying elements forming a better wetted interface to aid pressure infiltration, reaction must thus be sufficiently slow compared to the rate of metal flow.

Keywords: Metal matrix composites, pressure infiltration, chemical reaction, activation energy, thermally activated process, reaction kinetics, high temperature.

Riassunto

Questa tesi è uno studio dell'interazione del flusso indotto meccanicamente di metalli fusi, dentro un solido poroso e gli effetti cinetici alla linea tripla (L-S-V). L'approccio è sperimentale e focalizza i sistemi di metallo-ceramica, i cui parametri di bagnabilità e cinetiche locali (θ , σ_{LV} e la natura dei fenomeni all'interfaccia vicino alla linea tripla) sono stati ottenuti nella letteratura, con la tecnica della goccia posata, ad alte temperature. Investighiamo le infiltrazioni dell'Al in preforme di Al_2O_3 tra $1000^\circ C$ e $1100^\circ C$ e del Cu-x (x=Si, Ti o Cr) in CGr porosa tra $1050^\circ C$ e $1200^\circ C$. Le tre leghe sono conosciute per la formazione di carburi stabili, i quali si fanno bagnare meglio dal liquido rispetto alla grafite.

Se le misure sono prese a differenti valori di sovrappressione sul metallo, in presenza di processi termicamente attivati alla linea tripla, il tempo interviene nella capillarità impedendo al fronte di stabilizzarsi. Osserviamo che il metallo continua a invadere lentamente la preforma "strisciando" gradualmente nei pori sotto l'azione dei fenomeni locali attorno alla linea tripla. Cerchiamo di caratterizzare queste infiltrazioni dinamiche, misurando i tassi di infiltrazione isobarica costante misurandone la variazione a $P_t h$ e $P_t h + 0.05 MPa$. Queste velocità di saturazione sono calcolate usando una regressione lineare su 100s dei valori registrati per ogni gradino di pressione. I dati sono interpretati facendo un'analogia con la plasticità ad alta temperatura, che ci porta ad assumere che la pressione applicata contribuisce ad una riduzione proporzionale dell'energia d'attivazione del processo, che governa il tasso d'infiltrazione della preforma. Questa costante di proporzionalità definisce un volume d'attivazione alla base del processo attivato termicamente.

Cu-46%at.Si è moderatamente reattivo con C e forma uno strato di SiC all'interfaccia L-S. I tassi di saturazione isobarica durante l'infiltrazione e la loro dipendenza sulla variazione della pressione applicata sono stati prodotti tra $1050^\circ C$ e $1200^\circ C$. Troviamo che un volume d'attivazione dell'ordine di $\approx 200 nm^3$, rende i dati compatibili con la legge di Arrhenius, ottenendo così un'energia di attivazione di $\approx 400 \frac{kJ}{mol}$, valore realistico per un processo limitato dal tasso di crescita di SiC lungo l'interfaccia L-S.

L'infiltrazione di Al in tre differenti preforme di Al_2O_3 mostrano un comportamento simile col sistema Cu-Si/C, se le particelle nella preforma sono altamente angolari, indipendentemente dalla presenza di impurità di Na. I tassi di saturazione isobarica misurati tra $1000^\circ C$ e $1100^\circ C$ danno un volume d'attivazione simile al sistema Cu-Si/C, dell'ordine di $\approx 200 nm^3$ e un'energia d'attivazione di $\approx 300 \frac{kJ}{mol}$, che suggerisce che le cinetiche sono probabilmente limitate dalla diffusione allo stato solido.

In fine, nell'infiltrazione di Cu-1%at.Cr e Cu-10%at.Ti in CGr, troviamo che la reazione non

Acknowledgements

aiuta l'infiltrazione sotto-pressione. Nel primo sistema, è dovuto al fatto che la reazione iniziale tra il liquido e la preforma consuma tutto il Cromo reattivo, producendo infiltrazioni simili al Cu puro. Nel secondo, la formazione iniziale di carburo è talmente importante che blocca l'ingresso dei pori al metallo. Questi esperimenti mostrano che l'aggiunta di leganti reattivi forma una fase all'interfaccia bagnata meglio al fine di aiutare l'infiltrazione sotto pressione, a condizione che la reazione sia abbastanza lenta comparata al tasso del flusso di metallo.

Parole chiave: Compositi a matrice metallica, infiltrazione sotto pressione, reazione chimica, energia d'attivazione, processo d'attivazione termica, cinetiche di reazione, alta temperatura.

Résumé

Ce travail de thèse étudie l'interaction d'un flux de métal liquide induit mécaniquement dans un solide poreux et les effets cinétiques à la ligne triple (L-S-V). L'approche est expérimentale et se focalise sur des systèmes métal-céramique pour lesquels la littérature donne des valeurs de paramètres de mouillage et de cinétique locale (θ , σ_{LV} , nature et vitesse des phénomènes interfaciaux locaux proche de la ligne triple) à haute température, obtenues par la méthode de la goutte posée. Plus précisément, nous investiguons les infiltrations de préformes d'alumine avec de l'aluminium à 1000°C, 1050°C et 1100°C et de graphite poreux avec du Cu-x (x = Si, Cr ou Ti) entre 1050°C et 1200°C, ces trois éléments d'alliage étant connus pour former des carbures stables qui sont mieux mouillés que le graphite par le métal liquide.

Si les mesures sont prises à différentes valeurs de surpression, en présence de processus activés thermiquement à la ligne triple, le temps intervient dans la capillarité et le front d'infiltration ne se stabilise pas. Nous observons que le métal liquide continue à envahir lentement le milieu poreux, en "fluant" dans les pores sous l'action des phénomènes qui se passent à la ligne triple. Nous cherchons à caractériser ces dynamiques en mesurant des vitesses stables d'infiltration isobares, en évaluant ces vitesses à pression seuil (threshold pressure en anglais) P_{th} et $P_{th}+0.05\text{MPa}$. Ces variations de vitesse de saturation sont calculées au moyen d'une régression linéaire évaluée sur 100s des valeurs enregistrées pour chaque pas de pression. Les données sont analysées en faisant un parallèle avec la plasticité à haute température, ce qui nous amène à supposer que la pression appliquée contribue proportionnellement à la réduction d'énergie d'activation du phénomène qui contrôle le remplissage de la préforme. La constante de proportionnalité est définie comme le volume d'activation sous-jacent aux processus activés thermiquement.

La réaction entre le graphite et le Cu-46%at.Si pendant l'infiltration est très légère et produit une couche de SiC à l'interface L-S. La mesure des vitesses de saturation isobares et de leur dépendance à la pression appliquée a été effectuée entre 1050°C et 1200°C. Un volume d'activation de l'ordre de $\approx 200\text{ nm}^3$ rend les données compatibles avec une loi d'Arrhenius, caractérisée par une énergie d'activation d'environ $400\frac{\text{kJ}}{\text{mol}}$, valeur réaliste pour un processus limité par le taux de croissance du SiC à l'interface L-S.

L'infiltration de préformes d'alumine par de l'aluminium a un comportement similaire à celui du système légèrement réactif Cu-Si dans du graphite, pour autant que les particules composant les préformes d' Al_2O_3 soient hautement angulaires, et ce, indépendamment de la présence d'impuretés de sodium. Les vitesses de saturation isobares ont été mesurées à 1000°C, 1050°C et 1100°C, donnant un volume d'activation similaire à celui du système

Acknowledgements

Cu-Si/C, soit de l'ordre de $\approx 200 \text{ nm}^3$, tandis que l'énergie d'activation est d'environ $300 \frac{\text{kJ}}{\text{mol}}$, ce qui suggère que les cinétiques sont probablement limitées par la diffusion en phase solide. Enfin, en infiltrant du graphite avec du Cu-1%at.Cr et du Cu-10%at.Ti, il a été observé qu'une réaction à l'interface n'aide pas l'infiltration sous pression. Dans le premier système, cela est dû à la réaction entre le métal fondu et le bord extérieur de la préforme qui épuise l'alliage de son élément réactif, à savoir le chrome, ce qui amène à une infiltration similaire à celle du cuivre pur dans le graphite. Dans le deuxième système, la formation de carbure initiale est tellement importante qu'elle bloque l'accès du métal aux pores. Ces expériences montrent que l'ajout d'éléments d'alliage, formant une couche de carbure qui est mieux mouillée par le métal, n'est pas la seule condition qui aide l'infiltration sous pression ; la réaction doit aussi être suffisamment lente comparée au flux de métal.

Mots clés : Composites à matrice métallique, infiltration sous pression, réaction chimique, énergie d'activation, processus activé thermiquement, cinétiques de réaction, haute température.

Contents

Acknowledgements	v
Abstract (English/Italiano/Français)	ix
List of figures	xvii
1 Introduction	1
2 Literature review	5
2.1 Metal matrix composites	5
2.1.1 Processing of metal matrix composites	6
2.2 Wetting of solids by molten metals around their melting temperature	7
2.2.1 Liquid surface tension	7
2.2.2 Contact angle measurements	8
2.2.3 Work of adhesion	11
2.2.4 Work of immersion	12
2.2.5 Wetting of Al and Cu on Al ₂ O ₃ and Graphite	12
2.2.6 β -Al ₂ O ₃ and β'' -Al ₂ O ₃	19
2.3 Kinetics of reactions at high temperature	20
2.3.1 Interfacial reactivity and dissolutive wetting	20
2.3.2 Reactive wetting due to bulk diffusion	21
2.3.3 Wetting of Cu alloyed with selected reactive elements (Si, Ti, Cr) on graphite	22
2.4 Basics of infiltration	27
2.4.1 Pressure infiltration of metal-ceramic non-reactive systems at low temperature	27
2.4.2 Capillary phenomena in infiltration	30
2.5 Wetting in pressure-infiltration	32
2.5.1 Spontaneous infiltration and critical wetting angle	33
2.5.2 Experimental methods	37
2.5.3 Experimental measurement of wettability in infiltration	37
2.6 The theory behind drainage curves	39
2.6.1 Percolation theory	40
2.6.2 Brooks and Corey model	43
2.7 Infiltration of liquid metal into ceramic preforms: data	44
	xv

Contents

2.7.1	Parameters modifying wetting in infiltration	45
2.7.2	Chemical reaction during infiltration	49
2.8	Definition of the aim of the study	53
3	Reactive pressure infiltration of Cu-46at.pct. Si into carbon	55
3.1	Disclaimer	55
3.2	Abstract	55
3.3	Introduction	56
3.4	Experimental Procedures	57
3.4.1	Materials	57
3.4.2	Infiltration velocity measurements	57
3.5	Results	60
3.5.1	Infiltration kinetics	60
3.5.2	Composite microstructure	62
3.6	Discussion	65
3.7	Conclusion	73
3.8	Acknowledgement	73
4	Kinetic processes in the high temperature pressure-infiltration of Al into Al₂O₃	75
4.1	Disclaimer	75
4.2	Abstract	75
4.3	Introduction	76
4.4	Experimental	77
4.4.1	Materials	77
4.4.2	Gas-pressure infiltration	79
4.4.3	Composite characterization	81
4.5	Results	81
4.5.1	Isobaric infiltration kinetics	81
4.5.2	Phase characterization	85
4.5.3	Composite microstructure	87
4.6	Discussion	89
4.6.1	Infiltration kinetics in the Al-Al ₂ O ₃ system	89
4.6.2	Effect of sodium impurities in alumina preforms on pressure infiltration with aluminium	92
4.7	Conclusions	97
4.8	Acknowledgement	98
5	Reactive infiltration of Cu-X (X= Cr, Ti) alloy into porous graphite	99
5.1	Disclaimer	99
5.2	Abstract	99
5.3	Introduction	99
5.4	Experimental	100
5.4.1	Materials	100

5.4.2	Infiltration apparatus	101
5.4.3	Metallographic preparation	101
5.5	Results	102
5.5.1	Infiltration experiments	102
5.5.2	Microstructure analysis	103
5.6	Discussion	105
5.6.1	Cu-1at.pct.Cr	105
5.6.2	Cu-10at.pct.Ti	106
5.7	Conclusion	107
5.8	Acknowledgement	107
6	Conclusion	109
7	Perspectives	113
	Bibliography	149
	Curriculum Vitae	151

List of Figures

2.1	2D schematic representation of the sessile drop experiment. The liquid metal droplet posed on a flat, solid surface. The contact angle θ and the forces acting on the system are highlighted, a) $\theta > 90^\circ$ where the liquid does not wet the substrate and b) $\theta < 90^\circ$ where the liquid wets the substrate (in the sense that the wetting angle is below 90 degrees).	9
2.2	Schematic representation of different method of measuring the contact angle a) classical technique, b) sessile drop with in situ alloy formation, c) dispensed drop, d) transferred drop, e) double substrate, and f) tilted plate [1–3]	11
2.3	Contact angles as a function of temperature for Al- α -Al ₂ O ₃ measured with the sessile drop experiment. Surces: Nicholas [4], Laurent <i>et al.</i> [5], John and Hausner [6], Brennan and Pask [7], Wang and Wu [8], Naidich <i>et al.</i> [9], Ksiazek <i>et al.</i> [10], Shen <i>et al.</i> [11, 12], Carnahan <i>et al.</i> [13], Klintner <i>et al.</i> [14], and Saiz <i>et al.</i> [15, 16]	15
2.4	Reported contact angles in the system Cu-Ti over carbon as a function of Ti concentration; data from: Yang <i>et al.</i> [17], Mortimer and Nicholas [18], Naidich and Kolesnichenko [19, 20], Shinozaki <i>et al.</i> [21], Scott and Nicholas [22], Li [23], Sobczak <i>et al.</i> [24], Standing and Nicholas [25], Naidich and Kolesnichenko [26], Mao <i>et al.</i> [27], and Naidich and Kolesnichenko [20].	24
2.5	Contact angles of the system Cu on TiC _x as a function of C index x with the sources: Nicholas [28], Xiao and Derby [29], Goretzki and Scheuermann [30], Mortimer and Nicholas [18], and Ramqvist [31].	26
2.6	Contact angles of the system Cu-Cr versus Cr concentration on different allotropes of carbon, with the sources: Mortimer and Nicholas [32], Tao <i>et al.</i> [33], Devincent and Michal [34], Voitovitch <i>et al.</i> [35], Landry <i>et al.</i> [36], Hodaj <i>et al.</i> [37], Nogi <i>et al.</i> [38], Yang <i>et al.</i> [17], Voitovitch <i>et al.</i> [39], Mortimer and Nicholas [18], Sobczak <i>et al.</i> [24], Naidich and Kolesnichenko [19], Scott <i>et al.</i> [22], and Naidich and Kolesnichenko [20].	27
2.7	Representative sketch of slug-flow infiltration showing the pressure as a function of position along the preform in the direction of infiltrating melt flow. From [40].	29
2.8	Schematic representation of an infiltration front during unidirectional pressure-infiltration at the scale of single pores. The contact angle and the surface tensions are highlighted for this configuration.	33

List of Figures

3.1	Mercury infiltration porosimetry curves measured on three separate graphite preforms of the type used in this work. a) full drainage curve, b) zoom on the first part of the drainage curve.	58
3.2	Infiltration of Cu-46at.pct. Si into C, a) and b) at 1200°C and c) and d) at 1150°C a) and c) raw data: h and P versus t over an entire infiltration experiment, showing up to $t = 190\text{min.}$ for 1200°C and $t = 160\text{min.}$ for 1150°C the regime of alternating pressures between $P = P_{th}$ and $P = P_{th} + 0.05\text{MPa}$ and beyond $t = 190\text{min.}$ or $t = 160\text{min.}$ the regime of stepwise increasing pressure conducted to reach $S=1$, b) and c) zoom over a pressure cycle to highlight the change of velocity and the measurement of $\frac{dS}{dt}$. The dotted arrow show the velocity at the previous pressure. Figures e) and f): corresponding curves for the infiltration of pure Cu into the same C preforms, showing that in the absence of Si in the alloy one observes stabilization of the saturation at fixed pressure after isobaric holds similar to those used in the CuSi reactive infiltration experiments.	61
3.3	Experimental infiltration velocities $\frac{dS}{dt}$ measured over time just above P_{th} at four different temperatures: 1050°C (red), 1100°C (turquoise), 1150°C (green) and 1200°C (blue).	62
3.4	Microstructure of the composite after infiltration at 1050°C and 12MPa, a) low magnification, b) high magnification.	62
3.5	Microstructure of the composite after infiltration at 1100°C and 12MPa, a) low magnification, b) high magnification.	63
3.6	Microstructure of the composite after infiltration at 1150°C and 12MPa, a) low magnification, b) high magnification.	63
3.7	Microstructure of the composite after infiltration at 1200°C and 12MPa, a) low magnification, b) high magnification.	63
3.8	EDX mapping of the composite infiltrated at 1200°C and 12MPa, a) SE image, b) C map, c) Cu map and d) Si map.	64
3.9	XRD spectra for of the composite infiltrated at 1050°C (black curve) and 1150°C (red curve) with the relative phase.	65
3.10	a) Ratio between measured rates of saturation increase across two successive stepped downward pressure changes across all experiments of this work, b) histogram of the distribution of the activation volume values deduced from Eq. 3.2 for each step across all experiments.	66
3.11	Schematic representation of the activation surface S_a for a small advancement of the infiltration front dx due to the creation of a small layer of reaction product. a) General view, b) zoom on the triple line.	69
3.12	Pressure-compensated velocities calculated from experimental values using Eq. 3.1 with $V_a=187\text{nm}^3$ at 1050°C (red), 1100°C (turquoise), 1150°C (green) and 1200°C (blue).	70
3.13	a) Arrhenius plot at different saturations for the four temperatures analysed assuming $V_a = 187\text{nm}^3$, b) activation energy calculated from the slope of the Arrhenius plot.	71

4.1	SE-SEM images of the three powders used, a) and b) AA10, c) and d) β'' -AA10 and e) and f) F1000.	78
4.2	Schematic representation of a cross section through the Al-F1000 sample produced at 1150°C for 4h under a steady applied pressure of 4MPa. Light blue is Al; the rectangular area represents the Al- Al ₂ O ₃ composite (in the inset is an optical image of its microstructure). Along the top surface a rectangle and the inset micrograph represent the region where the oxide layer covering the Al melt was investigated (see discussion).	80
4.3	Raw data for infiltration at 1000°C (a) and b)) and 1050°C (c) and d)) of the Al-F1000 system; a) and c): full infiltration displacement, b) and d): zoom showing the changes in velocity after a small pressure drop.	82
4.4	Raw saturation velocities at three different temperatures for Al-F1000 composite infiltration; 1000°C (squares), 1050°C (circles) and 1100°C (triangles).	82
4.5	Infiltration data for the Al-AA10 system at 1000°C. a) and c): full infiltration curve, b) and d): zoom at the end of the pressure step showing stabilization of the infiltration front.	83
4.6	Separately measured drainage curves for the system Al-AA10 showing the lack of reproducibility of the tests: infiltration at a): 700°C, b): 1000°C.	84
4.7	Raw infiltration data for the system Al- β'' -AA10 infiltrated at 1000° C a) full curve, b) zoom between two pressure steps showing that the front stabilizes when the pressure is held for a sufficiently long time.	85
4.8	a) Drainage curves for the Al- β'' -AA10 system at 1000° C, b) comparison between the relative drainage curve of Al- β'' -AA10 at 1000° C and Cu-AA10 at 1150° C and c) Brooks and Corey relation for the two systems.	85
4.9	XRD spectra of the as-received F1000 powder (bottom) and (from bottom to top) of the Al-F1000 composite infiltrated at 1000, 1050, 1100 and 1150°C.	86
4.10	XRD spectra of the Al- β'' -AA10 composite infiltrated at 1000°C (black, top curve) compared to β'' -AA10 (red) and AA10 (green, bottom curve) powders.	86
4.11	Microstructure of the Al-F1000 composite infiltrated at a) 700°C, b) 1000°C, c) 1050°C and d) 1100°C.	87
4.12	Microstructure of the Al-AA10 composite infiltrated at a): 700°C, b and c): 1000°C; in c) the surface is deep-etched in order to remove the matrix and highlight the shape of particles, and d): Al-AA10 composite infiltrated at 1100°C.	88
4.13	Microstructure of the Al- β'' -AA10 composite infiltrated at 1000°C a) low magnification, b) high magnification showing no modification of the particles after high temperature infiltration.	88
4.14	Schematic showing a 2D liquid front reaching a discontinuity presented by a pair of particles having sharp α angles: a) pressure is below the threshold for passage of the meniscus past the pinning point; b) coarsening causes a decrease in the critical threshold pressure, releasing the meniscus.	90

List of Figures

4.15 a) Ratio between measured rates of saturation increase across two successive stepped downward pressure changes across all experiments of this study, b) histogram of the distribution of the corresponding activation volume values across all experiments.	92
4.16 Saturation velocities corrected for the influence of pressure and temperature using Eq. 1 in [41] and the average computed activation volume across all experiments of this study $V_a=235 \text{ nm}^3$	93
4.17 Arrhenius plots for pressure-compensated infiltration rate data over the three infiltration temperatures around three values of saturation, namely $S = 0.6, 0.65$ or $0.7 S \pm 0.03$	93
4.18 Activation energy computed at three different saturations across a range of $\pm 0.03S$.	94
4.19 XRD spectra for the composite infiltrated at 700°C (black, bottom) compared to the composite infiltrated at 1150°C (red, top). The arrows mark the main sodium phase peaks, which are not present in the latter composite.	94
4.20 Drainage curves for the Al-F1000 system measured at 700°C after pre-heating the system at 900°C for three different holding time values: 10 min, 20 min and 30 min respectively.	95
4.21 Cross section of the liquid front along the top surface of the ingot used to infiltrate the F1000 preform at 1150°C for 4h at 4MPa. The locations of the EDX point analyses are labelled: at A and B one finds the sodium aluminate phase and at C the oxide layer is of pure alumina.	97
5.1 Raw infiltration data of the system Cu-1at.pct.Cr into graphite at 1150°C , a) curve of the whole experiment, b) zoom showing no advancing of the infiltration front at fixed pressure of 2.5MPa.	102
5.2 Drainage curves for the Cu-1at.pct.Cr- C_{Gr} (rounds) compared to the Cu- C_{Gr} (square) both infiltrated at 1150°C	102
5.3 Raw data for the infiltration of Cu-10at.pct.Ti into graphite, a) 1050°C 1.5MPa, b) 1050°C 3MPa, c) 1100°C under vacuum, d) 1200°C 0.7MPa.	103
5.4 Microstructure of fully infiltrated Cu-1at.pct.Cr-C composite produced at 1150°C under 12MPa, a) centre of the composite, b) exterior border of the composite with indicated phases.	104
5.5 SEM image and EDX maps of Cu-1at.pct.Cr-C after full infiltration at 1150°C and a final pressure of 12MPa, a) SE image, maps of b) Cu, c) Cr and d) C_{Gr}	104
5.6 Microstructure of the exterior border of the partially infiltrated Cu-10at.pct.Ti-C composite produced at 1100°C under vacuum, a) low magnification, b) higher magnification with indicated phases.	104
5.7 Microstructure of the exterior border of the partially infiltrated Cu-10at.pct.Ti-C composite produced at 1200°C under 0.7MPa, a) low magnification, b) higher magnification with indicated phases.	105
5.8 SEM image and EDX mapping of a partially infiltrated pore within a Cu-10at.pct.Ti-C composite at 1100°C under vacuum, a) SE image, b) C_{Gr} , c) Cu and d) Ti.	105

7.1 Schematic representation of an experiment with simplified pores. On top, the advancing infiltration, on the bottom, the displacement of the liquid as a function of time. 114

1 Introduction

The infiltration of an empty porous solid by a liquid has been the subject of numerous studies over the last century; the subject is indeed important in a number of venues, starting with Nature but also in engineering and in daily life. Watering potted plants or irrigating fields and orchards, the flow of water or petrol underground, making espresso coffee and many processes in the food or chemical industries involve infiltration. Infiltration is also important in materials processing, since it is one of the main methods by which composite materials are made.

To produce a composite by infiltration, one starts by preparing a porous body of one of the phases that compose the material. This is done by packing fibres or particles, which are generally designated as the composite's reinforcing phase; the resulting porous body is called a preform. Then, a liquid is made to penetrate all open pores of the preform and this liquid infiltrant is solidified to become the other phase of the composite, generally known as the matrix of the composite.

If a metallic infiltrant is used, one produces a metal matrix composite (MMC). Such materials generally combine a continuous metal or alloy with a reinforcement phase that is, most often, made of ceramic or graphite. Molten metals are fluids of low viscosity; this makes the process potentially rapid, which is of clear benefit given the high temperatures involved. On the other hand, molten metals have high surface tensions and seldom wet the reinforcing phase one seeks to combine them with. As a result, it is often necessary to apply an external force in order to force the metal into open pores of the preform body. Metal infiltration is therefore often conducted by applying a pressure on the liquid metal, by means of a pressurized gas, or mechanically with a piston.

With pressure infiltration it is possible to obtain in a comparatively short time fully infiltrated, pore-free composites. Understanding the mechanisms that lie behind the infiltration process, in particular capillary forces, which are particularly important when infiltrating molten metals given their high surface tension and can be probed with precision given their low viscosity, is essential if one wishes to understand and improve the processing of composite materials by

Chapter 1. Introduction

infiltration.

This thesis explores a particular aspect of pressure infiltration, namely the interaction between wetting on one hand, and kinetic phenomena that may take place around the triple line of solid/liquid/vapour contact on the other. Specifically, three different situations are explored:

- a mildly reactive system, in which there is some chemical reactivity between the metal and the reinforcement, which leads to the formation of an interfacial compound that is better wetted by the metal as compared to the preform. This drives the metal continuously into the preform, even if the pressure is kept constant, something that is not observed in non-reactive systems where, under fixed pressure, the metal stabilizes once capillary forces have equilibrated;
- a non-reactive system that behaves “normally” at low temperature, reaching static capillary equilibrium under fixed pressure, but which at more elevated temperature shows the same behaviour as a mildly reactive, wetting-inducing system. Under fixed pressure, one observes with this system the same continued penetration of the metal into the preform as that observed in the former mildly reactive system;
- and finally we investigate two highly reactive systems that again alter the solid-liquid interface by forming a new phase that is better wetted by the infiltrant than the original preform material. Here, the high rate of reaction leads to two behaviours completely different from what is found with the mildly reactive system.

This thesis is divided into five chapters. It starts with a review of the literature covering aspects of the infiltration process that are pertinent to this work. The chapter starts with a very brief introduction on metal matrix composite processing, and then covers capillarity as pertinent to infiltration, starting with the classical sessile drop experiment and then moving to findings specific to infiltration, covering briefly the underlying physical and chemical phenomena and finishing with coverage of reactive infiltration.

The following chapters present results of research performed during this thesis, and are written as articles destined to be published independently

Chapter 3 presents the first subject of the thesis, namely an exploration of high temperature infiltration with the mildly reactive system Cu-46at.pct.Si into porous graphite preforms. This system is one for which extensive sessile drop data have been produced, which include a quantitative explanation and model for the kinetic wetting data recorded. Those studies show that, in this system, chemical interaction between the matrix and the carbon forms a SiC interface which allows a better wetting between the liquid and the solid. The reaction kinetics are slow, such that a sessile drop reaches its final equilibrium position (with the contact angle between the solid and the liquid equal to that between the Cu-Si alloy and SiC) after a few thousands of seconds. Since the reaction between Si and C is a thermally activated

process, the infiltrations are performed at four different temperatures, namely 1050°C, 1100°C, 1150°C, and 1200°C. It will be shown that, in the presence of a reaction, the infiltration front does not stabilize under fixed pressure. Rather, the metal gradually “creeps” into the preform, most likely because of the gradual formation of SiC at the triple line within the pores. Interpretation of the data, which at first sight may seem to contradict expectations for a thermally activated process, is conducted by making a parallel between pressure infiltration and high-temperature dislocational plasticity, two processes that are highly similar since they both involve the gradual forward motion of a triple line under the combined action of stress and a local thermally activated process.

Chapter 4 focuses on high temperature infiltration in the Al-Al₂O₃ system. This is a non-reactive system but it has been shown in the literature, using the sessile drop method, that at temperatures equal to, or higher than, one thousand degrees Celsius, the liquid Al interacts with the solid Al₂O₃ by a process of solution/reprecipitation. Two parameters are studied, namely the influence of (i) the shape of the ceramic particles and (ii) a sodium-containing phase present in the ceramic powder, on both the rate of “creeping” metal ingress into the preform under fixed pressure at elevated temperature, an observation that parallels that made with the (reactive) system studied in Chapter 3, and on measurements of the drainage curve at lower temperatures. The first subject is investigated by comparing the infiltration curves and the resulting microstructure of the fully infiltrated composite for three different alumina powders, namely (i) a Bayer powder designated as F1000, which is an angular alumina with an average particle size of 5 μm containing some sodium impurities, (ii) high-purity AA10 alumina, which is a polygonal powder with an average particle size of 10 μm, and (iii) β''-AA10, produced from AA10 to have the same physical structure as AA10 but a composition close to that of F1000. In order to investigate the reactivity of the system, the infiltration is performed at three different temperatures, namely 1000°C, 1050°C and 1100°C.

Finally, Chapter 5 presents results for two, more reactive systems, namely Cu-10at.pct.Ti and Cu-1at.pct.Cr infiltrated into porous graphite. Sessile drop experiment data in the literature show that both systems react in a much shorter time with the graphite than does the Cu-Si/C system (sessile drops stabilize after a few hundreds of seconds), again forming a carbide at the interface that transforms the solid surface into a more wettable interface. Both concentrations are the lowest for which one can have a non-wetting wetting transformation in the sessile drop configuration. As seen, with more reactive systems, reaction does not aid pressure infiltration.

The thesis ends with a general conclusion listing its main findings and giving a few perspectives for further work in development of the present contribution.

2 Literature review

2.1 Metal matrix composites

Composites are a class of materials created by combining two distinct materials that do not mix, where each phase possesses its own properties, giving a newly formed material that features unique properties of its own. Metal matrix composites (MMC) are a class of composites that is generally composed of a metal matrix and a ceramic or metallic reinforcement. The metal matrix (usually copper, aluminium, magnesium, titanium and their alloys) represents a continuous phase that links the reinforcement and will transfer the load to it, so that the reinforcement will carry a significant fraction of the applied load. The reinforcements can have different shapes (powder, fibres, continuous body,...) and volume fraction values (from a few percent up to almost ninety percent). Some of the most common reinforcements are made of carbon, shaped in fibres, nanotubes, powders or densely packed bodies; these are interesting due to their electric, thermal and mechanical properties. Other frequent reinforcements are ionocovalently bonded compound (oxides, nitrides, carbides or borides), which can feature relatively low density values and isotropic mechanical properties.

Combining these two different materials it is possible to produce a new material that blends the properties of the matrix (high ductility, possibility of high plastic deformations, interesting thermal and electrical properties) with those of the carbon or ceramic reinforcement (wear resistance or dry lubrication, stiffness, hardness, and, at times, toughness). A frequent goal with these composites is to obtain a material that is at the same time tough and stiff, with a reasonably high ductility. As with all composites, it is possible to obtain the required properties by tailoring and controlling the reinforcement, and by producing the material to high microstructural quality via appropriate processing methods, so as to make those composite materials interesting for aerospace, automotive, jewellery or electronic industries [42–46].

2.1.1 Processing of metal matrix composites

The processing of metal matrix composites can differ from what is practised used for the more common polymer composite, due to the high temperature needed to soften or melt the matrix.

Producing MMC can be achieved by two main pathways: through solid phase processing or liquid phase processing.

For solid-phase processing, three techniques are commonly used:

- **Powder metallurgy:** This well-known process produces MMCs by blending and densifying mixtures of metal and ceramic powder. This technique allows a wide range of shape, volume, matrix, reinforcement and volume fraction of reinforcement. The two powders are blended together usually adding a binding agent, pressed (with a piston or isostatically) into a mould and then sintered. This process is similar to the processing of powder metallurgy or ceramic materials [47–52].
- **Diffusion bonding:** A series of metal sheets and fibres are stacked in the desired texture, alternating layers of the metal and the fibres. The “pre-composite” is then heated under pressure in order to weld the metal sheets together around the fibres, which are thus incorporated in its structure [48, 50–54].
- **In-situ processing:** The synthesis of MMCs by *In-situ* processing involves a reaction forming the final ceramic reinforcement phase directly within the metallic matrix. The products of the reaction are usually fine thermodynamically stable single crystal ceramic particles, often carbides, nitrides or borides. The particle size can be tailored by controlling the processing parameters, such as temperature or time. The formed MMC generally has a good interfacial bond between the metal matrix and the ceramic, since the reinforcement is made directly inside the matrix [50, 55, 56].

With liquid-state processing too, three techniques are usually used:

- **Infiltration:** In infiltration processing, the liquid metal is made to flow into open pores of the solid ceramic reinforcement (usually in the form of a green body, called “preform”). Since metal-ceramic systems are often non-wetting, an external force is usually needed in order to push the metal and force it to fill the pores. The most common metal matrix composite infiltration processes are therefore pressure infiltration processes. These include gas pressure infiltration, in which a pressure is applied to the molten metal by means of a gas, and squeeze casting, where the molten matrix is pushed with the help of a piston into a mould in which the reinforcement has been placed. The pressure is generally held applying the force until the metal has fully penetrated pores between the reinforcement and has solidified. Pressure infiltration allows to obtain shaped or semi-shaped products, with little to no porosity and a good surface quality [57].

2.2. Wetting of solids by molten metals around their melting temperature

- **Spray deposition:** In spray deposition the metal is melted first and then atomized. The ceramic particles are added to the atomized liquid metal and incorporated into it as it accumulates onto a pre-heated substrate [48].
- **In-situ processing:** reinforcements can also be produced by means of internal reaction within a molten metallic matrix. As with solid state in-situ processes, these composites generally contain particulate reinforcements that are strongly bonded to the metal [58–67].

2.2 Wetting of solids by molten metals around their melting temperature

2.2.1 Liquid surface tension

In molten metal processes, an important parameter is the degree of wetting of the molten matrix onto the reinforcement one seeks to combine it with. An important parameter in this regard, influencing in general terms the wetting of a solid by a liquid, is the liquid surface tension σ_{LV} . This is an intrinsic parameter of the liquid, which is dependent on its chemical composition and the atmosphere that the liquid is contained in. Its value reflects the degree of atomic bonding mismatch along the free liquid surface; the excess energy that this represents, coupled with the fact that liquids tend to be isotropic, explains the fact that free metal surfaces tend to adopt minimal-surface area geometries, such that a molten drop assumes a spherical shape if the drop is small enough to neglect gravity [68].

The Young-Laplace equation links the surface tension with the capillary pressure difference ΔP across the meniscus between two fluids (be they liquid/gas or liquid/liquid):

$$\Delta P = \sigma_{LV} \left(\frac{1}{R_1} + \frac{1}{R_2} \right) \quad (2.1)$$

with R_1 and R_2 the radii of curvature at each point along the meniscus. If a straight, circular cylindrical capillary tube of radius r contains a liquid and a gas, then the liquid meniscus separating the liquid from the gas is a spherical cap, the curvature radii of which are $R_1 = R_2 = r / \cos \theta$ where θ is “wetting angle”, namely the angle formed between the solid wall and the liquid. One can then rewrite Eq. 2.1 as [1]:

$$\Delta P = \frac{2\sigma_{LV}}{R} = \frac{2\sigma_{LV} \cos \theta}{r} \quad (2.2)$$

If the pressure difference between liquid and gas can be measured (for example by measur-

ing the equilibrium meniscus height in static equilibrium with a reservoir at atmospheric pressure), knowing the capillary radius and the contact angle, one can then use this equation to deduce the liquid metal surface tension. As is the case in contact angle measurements, however, this method is highly dependent on the experimental conditions such as the chemical purity of the metal, the control of the surrounding atmosphere or the solid surface state (roughness, impurities, ...). Other methods exist for the measurement of liquid metal surface tension, such as measuring the pressure for bubble formation within the metal melt, or recording the shape, in gravity, of larger metal droplets resting on a flat substrate, or studying the dynamics of oscillation in the shape of well-defined liquid geometries such as a molten levitating drop.

A review on available metal surface tension data has been written by Keene, giving the surface tension of pure metals as a function of temperature. The review also details the different methods of measurement as well as the main apparatus that are used to obtain this property namely: capillary rise, pendant drop, maximum bubble pressure, levitating drop, maximum pull and drop weight [68].

Even if many variations of the sessile drop experiment have been developed (see section 2.2.2) in order to reduce the possible interferences mentioned previously, this technique is still the most used. It is indeed possible to measure the surface tension σ_{LV} having a large drop, the shape of which will differ from a perfect sphere due to the action of gravity; from the resulting deformation it is possible to calculate σ_{LV} .

2.2.2 Contact angle measurements

The sessile drop experiment is also the most common way to measure the contact angle between a liquid metal and a solid substrate. This experiment consists in measuring optically the angle formed by the liquid metal in its equilibrium position (i.e. when the system does not move anymore and the angle becomes independent of time) assuming that there is no solid substrate deformation (except perhaps very near the liquid/solid/gas triple line), and hence writing force equilibration only for horizontal forces [1, 69, 70].

This experiment allows to access, by visual means, the contact angle θ . This can then be used, knowing the isotropic surface tension of the liquid metal, to measure the difference between the surface tension of the free surface and that of the liquid/solid interface, by neglecting any effects of anisotropy or vertical force equilibration and using the Young-Dupré equation [71]:

$$\cos\theta = \frac{\sigma_{SV} - \sigma_{LS}}{\sigma_{LV}} \quad (2.3)$$

where σ_{SV} is the surface tension of the solid-vapour interface, σ_{LV} is the surface tension of the liquid-vapour interface and σ_{LS} is the surface tension of the liquid-solid interface. The angle

2.2. Wetting of solids by molten metals around their melting temperature

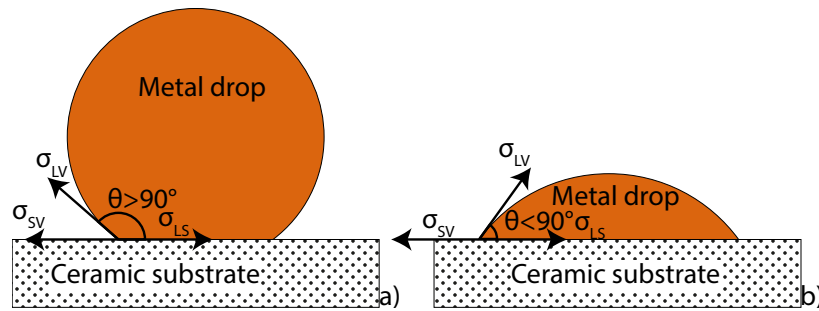


Figure 2.1: 2D schematic representation of the sessile drop experiment. The liquid metal droplet posed on a flat, solid surface. The contact angle θ and the forces acting on the system are highlighted, a) $\theta > 90^\circ$ where the liquid does not wet the substrate and b) $\theta < 90^\circ$ where the liquid wets the substrate (in the sense that the wetting angle is below 90 degrees).

θ is a characteristic of the system and measures the aptitude of the liquid to spread over a flat, smooth surface at a specific time and temperature. The liquid in the system is considered non-wetting if the angle is above 90° , and is considered wetting if the angle is smaller than 90° . Observing Eq. 2.3 it is possible to see that if σ_{LV} is reduced and/or σ_{SV} is increased, then the contact angle θ is decreased which means that the wetting is improved.

The wetting of ceramics by metals has wide relevance in multiple technological fields including brazing, lubrication, and metal matrix composite fabrication. This has motivated multiple studies into the understanding and characterization of the metal-ceramic systems by means of sessile drop experiments (some examples are in [5, 10, 15, 17, 18, 22–25, 34, 36–39, 70, 72–97, 97–114, 114–128]).

In the simplest form of the test, a small metal ingot (a few mg in order to neglect the action of gravity on the droplet) is placed on a highly polished solid substrate in a controlled atmosphere. The system is then heated to the desired temperature to have a liquid metal droplet resting on the ceramic plate. Depending on the system, a certain amount of time is required in order to reach capillary equilibrium: for non-reactive systems, static capillary equilibrium is quickly reached, but for reactive systems this can take up to a few hours before the drop reaches its equilibrium position – if it ever does.

The contact angle is then measured analysing the images of the profile of the equilibrated droplet along a horizontal axis [1]. The surface tension of the liquid-solid interface (σ_{LV}) can, as mentioned, also be measured with the sessile drop technique. Knowing the specific gravity of the liquid metal and having a drop big enough to allow gravity-induced vertical pressure gradients deform the droplet, it is possible to measure σ_{LV} as well in the same experiment [1].

In reactive systems, the contact angle will generally vary with time, due to a reaction-induced modification of the L-S interface nature. Often, the newly formed surface is better wetted by the liquid metal, meaning that the contact angle is seen to decrease with time.

Theoretically this experiment seems very easy to perform; however, in practice, it is extremely sensitive to the working conditions, especially at high temperature. Some of the parameters that may influence the measurements are: atmosphere control, substrate roughness, the purity of all phases present, the structure of the ceramic substrate, the surface quality of the droplet, the temperature and its control, and the image quality to cite the main parameters at hand. All those parameters influence greatly the results, with the consequence that data obtained by different groups on the same system can feature large discrepancies between obtained results for contact angle θ [119, 129, 130]. The dynamics of the triple line (of Solid-Liquid-Vapor intersection) movement and stabilization can also be highly dependent on external factors including oxygen absorption, interfacial or surface reactions and the potential formation of new phases. All those phenomena affect the equilibrium conditions and may lead to out-of-equilibrium, transient wetting conditions.

If the experiments are carried out at high temperature, another important factor has to be taken into account, namely local diffusion and solution-precipitation of the solid phase in contact with the liquid. Those two factors may influence the validity of the Young equation (Eq. 2.3) since the vertical force (component of θ_{LV}) might become relevant and have to be compensated in addition to horizontal forces. Triple line ridges can then be formed, as these help to compensate the otherwise present vertical force disequilibrium [15, 16, 102, 121, 122, 131, 132]. Since usually metal-ceramic systems are analysed at high temperature, some diffusion and/or precipitation/dissolution of the solid atoms into the liquid metal is possible. This will then form a small ridge at the triple line due to atom migration, and this ridge will then evolve until full 3D force equilibrium is reached. Initially, if the ridge size is much smaller than the droplet radius, the system will still display the contact angle expected from the Young-Dupré equation. If on the other hand the temperature of the system becomes comparable to the melting point of the ceramic substrate (according to Saiz *et al.* when the temperature reaches or exceeds around $0.25T_{m,s}$, where $T_{m,s}$ is the melting temperature of the solid substrate) or when the holding time is sufficiently long, the ridge grows and its size cannot be neglected any more since it becomes comparable to the radius of the droplet. At this point the contact angle formed by the system due to the ridge along the substrate surface will not correspond to the theoretical value obtained with the Young equation [15, 16, 102, 121, 122, 131, 132].

In order to reduce those issues and obtain valid and reliable wetting data, many variations of the basic sessile drop experiment have been proposed [1–3]. In order to reduce the presence and influence of the oxide layer that often covers the surface of molten metals, it is possible to melt the metal separately in a crucible and then push a drop of the metal through a small orifice on the bottom of the crucible by applying pressure on the liquid reservoir (dispensed drop technique, Fig. 2.1c)). For reactive systems, it is possible to melt the metal on an inert ceramic plate and then transfer the drop onto the desired (always pre-heated) substrate (transferred drop technique, Fig. 2.2d)).

If the substrate presents a high degree of roughness or if its composition is not homogeneous, the contact angle may differ between an advancing contact angle θ_a and a receding contact

2.2. Wetting of solids by molten metals around their melting temperature

angle θ_r . It is then possible to investigate the hysteresis using either the double substrate or the tilted plate techniques as shown in Figs. 2.2e-f).

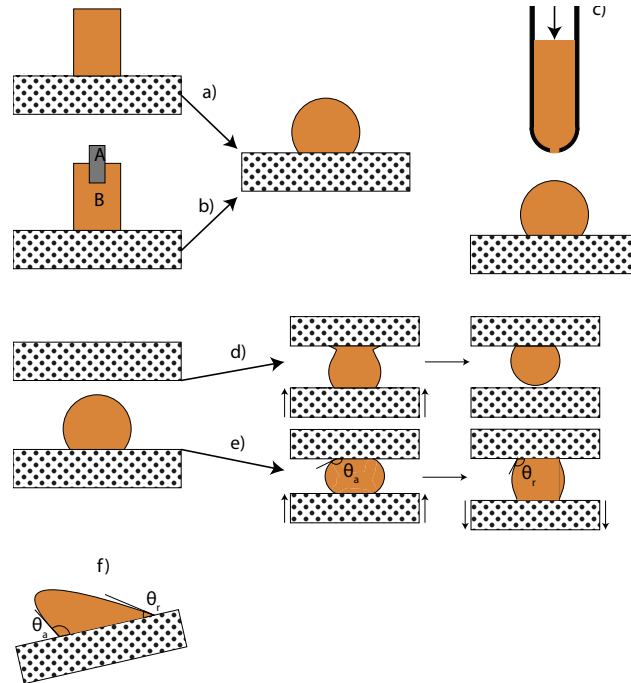


Figure 2.2: Schematic representation of different methods of measuring the contact angle: a) classical technique, b) sessile drop with in situ alloy formation, c) dispensed drop, d) transferred drop, e) double substrate, and f) tilted plate [1–3]

2.2.3 Work of adhesion

The parameters found in the sessile drop experiment give access to what is known as the work of adhesion. The work of adhesion represents the work per unit area needed to replace a solid-liquid interface at equilibrium with a solid-vapour interface of the same surface plus a liquid-vapour interface. It can be derived from the Young-Dupré equation Eq. 2.3 if one rewrites it as:

$$W_a = \sigma_{SV} + \sigma_{LV} - \sigma_{SL} = \sigma_{LV}(1 + \cos\theta) \quad (2.4)$$

This equation is commonly used in practice as a measure of the strength (energetic or mechanical) of the interface between two different bonded materials [114].

For perfect wetting, i.e. $\theta = 0^\circ$, the Young-Dupré equation only gives an upper bound ($2\sigma_{LV}$)

value of the work of adhesion :

$$W_a \leq 2\sigma_{LV} \quad (2.5)$$

Even if the data of σ_{LV} and θ are available in literature, Eustathopoulos *et al.* notes that in order to have a meaningful value of W_a it is necessary to have both σ_{LV} and θ obtained from the same experimental method and conditions with, if possible, the same substrate [114].

2.2.4 Work of immersion

If a solid is immersed within a liquid or a liquid is placed in a capillary tube of constant section, immersion wetting happens, in which the dry solid-vapour interface is replaced by a solid-liquid interface while the liquid-vapour interface area stays constant. The free energy change will then be:

$$W_i = \sigma_{SL} - \sigma_{SV} \quad (2.6)$$

Using Eq. 2.3 it is possible to link the work of immersion with the contact angle via:

$$W_i = \sigma_{SL} - \sigma_{SV} = -\sigma_{LV} \cos \theta \quad (2.7)$$

When $\sigma_{SL} > \sigma_{SV}$ the work becomes positive meaning that capillary forces oppose the immersion and $\theta > 90^\circ$; to combine the two phases an additional force has to be applied. On the other hand if $\sigma_{SL} < \sigma_{SV}$, spontaneous infiltration may be expected.

2.2.5 Wetting of Al and Cu on Al_2O_3 and Graphite

Cu- Al_2O_3

The copper-alumina system has been widely investigated due to its importance in many different field such as electronic packaging, brazing or thick film metallization. The metal has a high melting point (1083°C), thus this system can be used in applications with a wide range of service temperatures. The high metal thermal and electrical conductivity allows this system to be used in heat exchangers or in electrical applications. The disadvantage of this system is that it is strongly non-wetting. The contact angle between copper and $\alpha\text{-Al}_2\text{O}_3$ has been measured with the sessile drop experiment and reported values vary between 114° and 170°

2.2. Wetting of solids by molten metals around their melting temperature

with a high metal surface tension between 1280-1370 $\frac{mJ}{m^2}$ at 1100-1200°C under vacuum or inert atmosphere [86, 93, 133–138]. Contrary to the Al-Al₂O₃ system, wetting in the Cu-Al₂O₃ system is not reported to depend on the crystallographic orientation of the substrate [137].

It has been shown that oxygen plays a role in the wetting of alumina by copper, with a higher oxygen partial pressure leading to a decrease of the contact angle, enhancing the wetting of the substrate, due to the formation of mixed metal aluminates along the interface (CuAlO₂) which decreases the liquid/solid interfacial energy σ_{LV} [139–142].

The oxide layer formed at the copper/alumina interface has been widely studied. It has been shown that it is not only dependent on the amount of oxygen dissolved in the liquid but also on the experimental conditions such as temperature and holding time. Trumble *et al.* showed by thermodynamic analysis that a small amount of oxygen in the solid copper (on the order of 1/5 of the maximum solubility limit of oxygen in the solid, increasing from 1 at. ppm at 700°C up to 60at.ppm at 1000°C) is sufficient to form the aluminates at the interface [142–144]. While the scientific community agrees that there is formation of CuAlO₂ at the interface in the presence of oxygen, the underlying mechanisms are, however, still subject to controversy. Lee and Tuan stated that the oxide layer Cu₂O reacts with Al₂O₃ to form CuAlO₂ [145]. On the other hand, Rogers *et al.* noted that in high-vacuum, solid state diffusion-bonding is possible forming CuAlO₂ in absence of the precursor Cu₂O [146]. Gautier *et al.* noted that if the alumina surface is modified in order to reduce its surface oxygen concentration (by heating at 1400°C before depositing the copper), the copper will more likely form CuAlO₂ from the oxidized copper during deposition [147]. Bonded pre-oxidized Cu to Al₂O₃ has been investigated by Beraud *et al.* and it has been shown that after 2h at 1000°C under pressure, a 0.2-0.4 μm CuAlO₂ interphase layer is formed if bonding is performed in the solid state. If on the other hand liquid copper is deposited on the alumina substrate, then the interphase layer will appear after only a few minutes with a thickness of 0.1 μm [141].

All these studies show that oxygen greatly influences and promotes wetting in the Cu-Al₂O₃ system, and that it influences the alumina/copper interphase composition. The literature shows that the newly formed aluminates increase the interfacial strength (compared to the pure Cu-Al₂O₃ interface). It has been noted by Reimanis *et al.*, Beraud *et al.*, Lee and Tuan, and Kim and Kim that if a needle-type interlayer of CuAlO₂ is present at the interface, then the strength of the bond is improved [141, 145, 148, 149]. On the other hand, the same groups noted that Cu₂O promotes crack growth. It has been suggested that removing the oxide layer by reduction will improve the interface strength. Kim and Kim confirmed this suggestion and noted that time is an essential parameter influencing the growth and shape of the interphase [149]. Since alumina growth is very slow, they noted that a longer exposure time leads to a stronger and continuous bond. This is also the reason why in the literature the aluminate layer is not always observed [150]. Seager *et al.* on the other hand, noted the opposite trend, namely a decrease of interface strength with the formation of the aluminate. They suggested that this is due to the brittleness of the CuAlO₂ interlayer [150]. They concluded that in order to use the growth of the aluminate interphase as a bond strengthening mechanism, a very

thin layer of 1-2 μm is sufficient in order to avoid crack propagation due to the interlayer brittleness, while being extensive enough to cover the entire bonding interface [150].

Cu-Graphite

Copper-graphite finds many applications as a composite material because of its excellent thermal properties, its stiffness, its ease of shaping by machining, its dry-lubrication behaviour, and for the reduction of weight the composite brings over the pure metal due to the addition of lower-density graphite to pure copper. It can also be used in brazing to graphite or diamond with copper-based brazes [151]. Due to the strongly non-wetting behaviour of copper on graphite, alloying elements are often added in order to transit to a wetting system and simplify processing. Investigations of these systems were made on all three main allotropes of carbon, namely graphite (C_{Gr}), vitreous carbon (C_V), and diamond (C_{Dia}). The pure system is known to be non-wetting and non-reactive; furthermore, C does not have any solubility in Cu and copper does not form any stable carbide [17, 18, 22, 24, 32–35, 37, 38, 151–153]. In the literature, values of the contact angle measured with the sessile drop experiment vary from 120° to 150° under vacuum or inert atmosphere [17–20, 24, 123, 134, 152–154]. Molten copper has, as stated in the previous subsection, a surface tension around $1300 \frac{\text{mJ}}{\text{m}^2}$ at 1100°C [155–164].

Al- Al_2O_3

The aluminium-alumina system is important both as a form of MMC or in brazing. Extensive research has been conducted in order to investigate the wetting behaviour of Al on both pure sapphire and polycrystalline $\alpha\text{-Al}_2\text{O}_3$ [1, 5, 8, 10–12, 14, 75, 76, 106, 111, 115, 122, 137, 165–174]. Initially, the aluminium-alumina interface may seem a simple Al-O binary interface; however, the system is much more complicated than that, due to the oxide layer formed at the surface of liquid aluminium which, in the presence of any oxygen, does not reach equilibrium [16]. This system has only one oxygen partial pressure at each temperature in which both the contact angle and the surface tension are independent from $P(\text{O}_2)$, ranging between 10^{-60} MPa at 600°C and 10^{-23} MPa at 1500°C [16]. Those pressures are much lower than those attainable experimentally, which means that some adsorption will always be present at all interfaces (liquid-solid, liquid-vapour and solid-vapour) [16]. This oxidation process is the main reason for which the results obtained in the literature are scattered (varying from 65° - 170°). Shen *et al.* suggested that three different domains could be found as a function of temperature for the wetting of Al on $\alpha\text{-Al}_2\text{O}_3$ [11]: (a) a region of oxidation ($T < 800^\circ\text{C}$), (b) a region of change in the surface structure ($800^\circ\text{C} < T < 1100^\circ\text{C}$) and (c) a reactive region ($1100^\circ\text{C} < T < 1500^\circ\text{C}$).

Figure 2.3 gives a summary of the main results from sessile drop experiments with the Al- Al_2O_3 system showing the measured contact angle values versus temperature.

(a) Oxidation region ($T_m < T < 800^\circ\text{C}$):

In the sessile drop experiment at temperatures below 800°C , the liquid droplet of Al has an

2.2. Wetting of solids by molten metals around their melting temperature

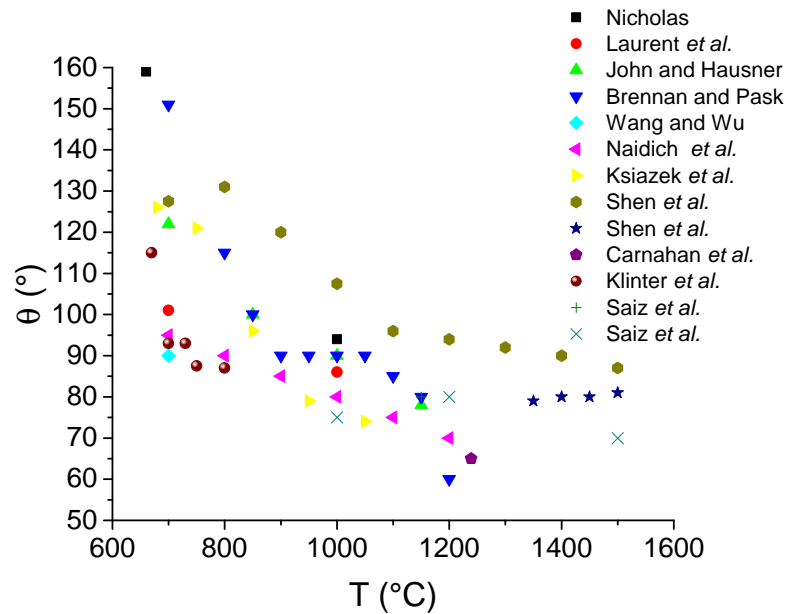


Figure 2.3: Contact angles as a function of temperature for Al- α -Al₂O₃ measured with the sessile drop experiment. Sources: Nicholas [4], Laurent *et al.* [5], John and Hausner [6], Brennan and Pask [7], Wang and Wu [8], Naidich *et al.* [9], Ksiazek *et al.* [10], Shen *et al.* [11,12], Carnahan *et al.* [13], Klinter *et al.* [14], and Saiz *et al.* [15, 16]

irregular shape and presents a matt surface [8]. This confirms the presence of a protective, mechanically strong, oxide layer on the drop surface (the thickness of the oxide depends on the temperature and the atmosphere). This film appears as soon as the metal melts, acting as a protective carapace perturbing the equilibration of capillary forces at the triple line junction (Solid-Liquid-Vapour). This gives a scatter to measured contact angle values for temperatures below 1000°C, as was noted in the review by Bao *et al.* [175]; see Fig. 2.3. In order to produce true and reproducible results of the contact angle, it could be possible to *in situ* spray Ar⁺ ion [122] in order to remove the oxygen at the surface of the droplet or one may use the dispensed drop method (Fig. 2.2c), in which the metal is melted previously in a crucible and then a droplet is dispensed through a small hole on the pre-heated substrate in order to reduce the exposure time with the atmosphere and clean the liquid of its initial oxide layer. If the oxide layer is avoided, then the droplet has a mirror-like surface and the contact angle decreases to take a value close to 90°. Even with all these precautions (namely high vacuum, a controlled atmosphere, reduced oxygen partial pressure and so on), it remains technically near-impossible to avoid the formation of this layer at low temperatures, with the consequence that perturbed and scattered results are often obtained [168].

(b) Change of the surface structure (800° C < T < 1100° C):

When the temperature is increased, the contact angle scatter becomes smaller (Fig. 2.3). This is due to a reduction in the thickness and importance of the oxide layer covering the Al droplet.

Chapter 2. Literature review

Laurent *et al.* [5] noted that even at the Al melting temperature (660°C) the oxide layer starts to be consumed by the formation of a gaseous phase following the reaction [5, 173]:



The kinetics of the process by which the equilibrium contact angle value is reached are strongly dependent on the temperature (equilibration is reached after around 1s at 1000°C and 1000s at 700°C). Basing their research on [5, 165], Levi and Kaplan [122] noted that, at high temperature, the oxide film at the surface of the liquid droplet does not play an essential role in wetting when the oxygen partial pressure is relatively low. They also noted that two main processes could be found in the interaction between the liquid Al and the solid Al₂O₃, namely (i) the growth of a new epitaxial α -Al₂O₃ on the sapphire substrate at T<1100°C or (ii) dissolution of the solid substrate when T>1100°C [122].

The fact that this system transits from non-wetting to wetting by changing time and/or temperature (between 800°C and 1100°C) is not well agreed upon in the scientific community [5, 10, 11, 115, 122, 165, 166, 170, 176]. After a simple thermodynamics calculation, Kaplan *et al.* assumed that a lowering in the Al-Al₂O₃ surface tension (σ_{LV}) causes the non-wetting/wetting transition and not a change in the two other surface tensions (σ_{SL} or σ_{SV}) [177]. The oxygen present in the working atmosphere diffuses along the S-L interface, since the dissolution of oxygen in liquid Al is negligible, creating a layer of oxygen-rich interface leading to a lowering of interfacial energy (and consequently a lowering of θ) when its value is higher than 90°. This layer also is the initiator of the epitaxial growth of new α -Al₂O₃. This diffusion process will then lead to a dynamic equilibrium contact angle between the L-S interface and the newly formed Al₂O₃ [122, 166, 170, 178]. It is to be noted that Zhang *et al.* showed, using a reactive force field, that temperatures of 850-1100°C are sufficient to drive the oxygen diffusion, leading to the wetting-non wetting transition [170]. Oh *et al.* investigated the interface of liquid Al in contact with (0001) α -Al₂O₃ with *in situ* High Resolution-Transmission Electron Microscopy (HR-TEM) by reducing an Al-O droplet deposited on the sapphire substrate via knock-on damage by electron beam radiation [166, 179, 180]. It was found that there is a self-catalytic growth of α -Al₂O₃ nanowires in a layer-by-layer way at the S-L interface [180, 181].

Chemical bonds in crystalline solid substrates tend to produce a low-range atomic ordering in the liquid lining the liquid-solid interface. This has been confirmed by simulations and also experimentally, both in diffraction studies and by HR-TEM studies [166, 180–192]. Even if the temperature plays an important role on the diffusion of oxygen and on the ordering of the L-S interface, Hashibon *et al.* noted that some ordering in the liquid is always present even at low temperature [185, 193]. Other factors influencing the degree of ordering in the liquid along the liquid-solid interface are the solid surface structure and its orientation. It is usually described as the in-plane and/or layering periodicity [180, 185, 194, 195] (a schematic of the in-layer and in-plane ordering of the liquid-solid interface can be found in Fig.1 of Ref. [194]). If the solid substrate termination is incompatible with the liquid, some perturbation will thus be formed perpendicularly to the interface, which will then decay exponentially with an

2.2. Wetting of solids by molten metals around their melting temperature

oscillation wavelength frequency proper to the liquid. The formed structure will then have more in-layer-ordering than in-plane ordering for the liquid at the interface. On the other hand, if the liquid and the crystal structure of the solid are compatible, significant ordering will happen at the interface, both in-layer and in-plane [166, 185, 195].

Lee and Kim investigated the in-plane ordering of liquid Al on α -Al₂O₃ ($\bar{1}10\bar{2}$) and noted that the segregation of oxygen at the interface coupled to the ordering lowers the interface free energy [166]. They also confirmed previous results noting that a new (0001) Al₂O₃ layer is formed at the interface [122, 180, 192, 196]. Gandman *et al.* investigated the interaction at the interface between liquid Al in multiple sapphire crystallographic planes using the procedure given in [180, 181] (aberration-corrected *in situ* HR-TEM). The authors noted the presence of both in-layer and on-plane order. They also noted that close to the melting point of Al, the ordering was slightly higher than at 750°C. They showed that the ordering is dependent on the crystallographic orientation of the solid phase surface and showed that the degree of ordering decreases as: {0006} > { $\bar{1}210$ } > { $10\bar{1}2$ } > { $\bar{1}014$ }. It was found that the lowest interface energy was on the (0001) sapphire plane in contact with liquid Al [192]. Since they measured the ordering at the L-S interface only in terms of contrast perturbation, no final conclusion could be drawn on the interface chemical composition [192, 194].

Hashibon *et al.* investigated, through atomistic simulation, the difference in ordering of a liquid drop of Al on BCC or FCC structures. They found that with a BCC lattice only in-layer ordering happens while with a FCC lattice both orderings are present [185]. Moving away from the interface, in-plane ordering gradually disappears, but faster than in-layer ordering [192, 194], before reaching the typical structure of the bulk liquid. First-principles dynamic simulations allowed to investigate theoretically the L-S interface leading to the growth of the epitaxial α -Al₂O₃ [170, 197, 198]. Kang *et al.* noted, using molecular dynamics simulations, that the liquid will form bonds with oxygen at the “abrupt” solid-liquid interface, which is characterized by a given vacancy concentration of around 10% in the liquid layer. The energy of binding of newly formed Al-O bond is greater than the Al-Al bond, leading to a decrease of chemical potential and thus reducing the interfacial energy [198].

It has been shown in the literature that anisotropy in alumina orientation is present in the wetting of Al on Al₂O₃ both by simulation and experiments performed with the sessile drop method [11, 168, 176, 199]; however, some authors do not see any anisotropy for this system [7, 76]. Such anisotropy is kept even at high temperature when the contact angle decreases [167, 168, 176]. The results of the ordering at the interface cited previously [192, 194] showed that the orientation with the maximum ordering and lowest interface energy is (0001). Experiments performed by Schmitz *et al.* by means of the sessile drop method with liquid Al on sapphire (0001), ($11\bar{2}0$) and ($\bar{1}10\bar{2}$) orientations at 1100°C, do, however, not confirm this. It was found that Al on a (1000) oriented surface of sapphire has the highest contact angle and it is the only situation that is slightly time-dependent (starting from $\approx 95^\circ$ at $t = 0$ up to $\approx 114^\circ$ at $t = 40$ s) while the two other investigated orientations are not time-dependent, and the measured contact angle reaches its equilibrium value of $\approx 85^\circ$ immediately. These results confirmed

Chapter 2. Literature review

previous data on the sessile drop experiment in different orientations performed by Shen *et al.* [11, 168] and Aguilar-Santillan [199]. The origin of this behaviour has been found in the increase of the interfacial energy σ_{SL} and the decrease of solid surface tension σ_{SV} [176].

Liu and Ning simulated two differently terminated surfaces of Al_2O_3 in contact with alumina. The first is a (1x1) stoichiometric $\alpha\text{-Al}_2\text{O}_3$ (0001) surface and the second has a $(\sqrt{31}\times\sqrt{31})R9^\circ$ reconstructed $\alpha\text{-Al}_2\text{O}_3$ surface. They showed that for the reconstructed surface the wetting was improved in both the oxidized and unoxidized conditions (oxidized has a O termination along the free surface, while the unoxidized surface has an Al termination at the surface) in the simulation of wetting at 800°C . They also noted that an Al-metal-like FCC (111) layer was found at the interface between the liquid Al and the reconstructed surface. Comparing their results with the literature, they stated that the normal surface fitted better the experiments concluding that at that temperature there is no reconstruction [200].

It was experimentally found that the (0001) surface of the $\alpha\text{-Al}_2\text{O}_3$ undergoes reconstruction at 1250°C [201–205]. The (0001) alumina surface changes from a (1x1) to a $(\sqrt{31}\times\sqrt{31})R\pm 9^\circ$ structure (R being a rotation of $\pm 9^\circ$) and the chemical termination of the surface is also modified losing the oxygen termination. It has been shown that the impoverished oxygen surface is highly stable at high temperature and that its transition to a bulk-like structure is reversible and depends on the oxygen partial pressure at the surface. If the surface is in contact with gaseous Al or Si, then the temperature at which the reconstruction happens can be lowered [201, 202]. It was also found experimentally that a layer of Al-metal-like FCC (111) forms at the interface between the liquid and the solid [203]. The “ordered” reconstructed interface has weaker bonds since it forms mainly Al-Al metallic bonds ($133\pm 6\frac{\text{kJ}}{\text{mol}}$ [167]) compared to the Al-O ionic bonds of the bulk structure ($511\pm 3\frac{\text{kJ}}{\text{mol}}$ [167]). This may explain the higher contact angle formed on the (0001) plane compared to the other orientation planes investigated, since the other orientations are unaffected by the presence of gaseous Al [11, 12, 167, 176, 199].

(c) Reactive region ($1100^\circ\text{C} < T < 1500^\circ\text{C}$):

At higher temperature it has been noticed, in sessile drop experiments, that a new phenomenon happens: the drop does not reach an equilibrium position but rather it spreads and contracts repeatedly, leaving ring-shaped traces on the substrate where the metal was in contact with the solid. This behaviour had been first noticed and investigated by Champion *et al.*, both on polycrystalline alumina and sapphire [115]. They proposed that the fast evaporation of Al leads to a decreasing drop volume, which decreases artificially the contact angle since the triple line is pinned to the substrate due to the presence of ridges. Those ridges are present because the system is able to reach, at high temperature, a 3D equilibration of surface forces at the triple line. An apparent equilibrium contact angle is then reached, which is far from that estimated theoretically by means of the Young-Dupré equation. When the triple line withdraws from the ridge, the droplet shrinks due to the surface tension σ_{LV} acting on its surface with a new triple line configuration and force equilibrium. A new ridge is then

2.2. Wetting of solids by molten metals around their melting temperature

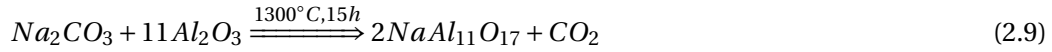
formed at the new position and the process starts again creating the spreading-contracting cycle. Immediately after the jump, when the drop is pulled by its surface tension, and before a new ridge is formed, the contact angle measured should then correspond to the theoretical contact angle predicted by the Young-Dupré equation (Eq. 2.3) [15, 16, 102, 122].

The interaction between the liquid Al and the solid Al₂O₃ at high temperature, and the ridge formation rate and mechanism, have been thoroughly investigated by Saiz *et al.*. They showed that ridge formation can be linked to the evolution of the grain boundary grooving in Al₂O₃ under a liquid Al droplet. Capillary forces are the driving forces for both the ridging and the grain boundary grooving. Using thermodynamic analysis, it was shown that the evolution of the grooving and the ridging is due to atomic transport, diffusion or solution-precipitation, and not by chemical reaction [15, 16, 102, 122, 206]. It was also shown that even if evaporation happens at high temperature, the growth of epitaxial Al₂O₃ under the liquid Al is still present [76, 122]. Ownby *et al.* observed the growth of α -Al₂O₃ at the Al-Al₂O₃ interface and proposed that this was due to the decreased solubility of oxygen in the liquid metal [76]. On the other hand, Levi and Kaplan calculated the amount of crystallite as a function of the available oxygen inside the liquid Al, and found that the crystallite number, or the thickness of newly formed α -Al₂O₃, do not match with experimental observation, being a few orders of magnitude lower than what was observed experimentally. They observed the formation of rings, which is linked to the evaporation rather than diffusion at the Al-Al₂O₃ interface. This leads to a deepening of the trough, a process that is unaffected by the oxygen activity at the L-S interface. Diffusion of dissociated products such as Al and Al-O, which are not affected by the evaporation (due to the static pressure applied by the droplet), helps the formation of new Al₂O₃ layers under the droplet [122].

2.2.6 β -Al₂O₃ and β'' -Al₂O₃

Sodium oxide and aluminium oxide can combine and form stable sodium aluminate (Na₂O-Al₂O₃ mixtures). In the literature, two main sodium aluminate phases have been investigated since they are both excellent ionic conductors [207–213]. Those two phases are named β -Al₂O₃ (Na₂O-11Al₂O₃) and β'' -Al₂O₃ (Na₂O-5Al₂O₃). Ray and Subbarao [207] noted that those two phases are very similar, both having a hexagonal symmetry, with the only difference being the *c* parameter of the lattice being 1.5 times bigger for β'' -Al₂O₃. Some authors noted that this latter phase is metastable and decomposes at high temperature due to the high vapour partial pressure of sodium [207, 212, 214, 215]. This decomposition is highly dependent on the atmosphere in which the sample is heated, with the temperature of full decomposition into α -Al₂O₃ ranging from 1300°C under vacuum or hydrogen atmosphere, and up to 1700°C for heating in air [214]. In all atmospheres, the higher the temperature, the faster the decomposition happens, leading to pure α -Al₂O₃. This decomposition will impoverish the phase in Na, which will lead to the formation of β -Al₂O₃. Before decomposing, the β phase goes through a transition stage in which needle-like shaped crystals are formed before the final transformation into α -Al₂O₃.

In the literature, the β'' - Al_2O_3 phase has been synthesised by heating to 1300°C a mixture of Al_2O_3 powder with Na_2CO_3 following the reaction [212]:



The author noted that it was not possible to have the perfect stoichiometric ratio of 1:5 $\text{Na}_2\text{O}:\text{Al}_2\text{O}_3$, the observed ratio being closer to 1:5.33 [212]. This phase has been only investigated for its electronic properties and not in metallurgy; hence, to our knowledge, no investigation was done to understand the interaction between those phases and liquid aluminium or their interaction with the oxide layer at the liquid surface.

2.3 Kinetics of reactions at high temperature

2.3.1 Interfacial reactivity and dissolutive wetting

Interfacial reactivity during infiltration is, as the name indicates, the propensity for interaction of the metal with the solid surface producing a chemical reaction product, this being often a second solid phase. This interaction can generate two different situations: i) a change in geometry at the triple line without necessarily modifying the liquid surface tension, or ii) a new L-S interface due to the reaction product which will modify the wetting parameters of the system. Surface and interface forces also modify the flatness of the substrate and the liquid drop may in some case (of solid phase dissolution) sink into the formed substrate.

For σ_{LV} -insensitive systems, there are three different stages on the path to equilibrium [1, 216]:

- The drop spreads in a non-wetting way and there is no dissolution. The contact angle is nearly equal to the Young-Dupré horizontal force equilibrium contact angle on the unreacted flat solid. This happens on the timescale of some *ms*. Relevant forces for spreading are viscosity-related and inertial.
- Dissolution of the solid starts and modifies the apparent contact angle. Dissolution is driven by diffusion due to a difference of concentration between the interface (C_i) and the surface of the drop (C_0). The interface concentration at equilibrium, C_i , in the liquid can be calculated as a function of the equilibrium concentration on a flat surface $C_{equ}(T)$ at a given temperature (given by the phase diagram) and the interface curvature κ :

$$C_i = C_{equ}(T) \left[1 + \frac{\sigma_{LV} T_m}{RT} \kappa \right] \quad (2.10)$$

where v_m is the molar volume of the liquid. This absorption induces a volume increase

v_t , which depends on the initial volume v_0 and the phase diagram of the newly formed compound (i.e. how much substrate can be dissolved by the liquid). The apparent contact angle θ_{app} is now different from the equilibrium contact angle between the flat surface and the liquid drop because the triple line is now displaced below the original surface. This change was first calculated by Warren *et al.* [216] assuming the equilibrium dihedral angle at the new position of the triple line.

- At longer times, the curvature of the liquid/solid interface will be uniform and the triple line contact angle will stabilize. This is when equilibrium is reached.

If the surface tension is modified, but the liquid-solid interface is not modified as in the previous situation, then the driving force for the change in contact angle and surface tension is the dissolution of the solid into the liquid. It has been proposed that the driving force for spreading of the liquid over the solid is then as a function of time t [1]:

$$f_d(t) = \sigma_{SV}^0 - (\sigma_{SL} + \Delta G(t)) - \sigma_{LV}^0 \cos\theta(t) \quad (2.11)$$

Where σ^0 is the surface tension before dissolution, and $\Delta G(t)$ is the change of Gibbs free energy per unit area accompanying dissolution at the interface. Since the velocity of the triple line is much higher than the rate of diffusion in the liquid bulk, equilibrium is reached when $f_d(t) = 0$ and the final contact angle is:

$$\cos\theta(t) = \cos\theta^0 - \frac{\sigma_{SL}(t) - \sigma_{SL}^0}{\sigma_{LV}^0} - \frac{\Delta G(t)}{\sigma_{LV}^0} \quad (2.12)$$

The change of contact angle was first supposed to be due to the change in Gibbs free energy [83]. Later, studies showed that the modification of θ is due to the change in surface and interfacial energies, with no direct contribution of ΔG [1].

2.3.2 Reactive wetting due to bulk diffusion

Reactive wetting happens when the liquid metal (or an alloying element in the liquid) reacts chemically with the substrate in order to form a new compound that (often) will be better wetted at the liquid-(new) solid interface. Previous studies determined that the final wetting (when thermodynamic equilibrium is reached and the reaction is stopped) is governed only by the final interface composition at the triple line and not by the kinetics of reaction or a contribution of the (volumetric) free energy change accompanying reaction to the Young-Dupré capillary force equilibrium equation [97, 99, 111, 120].

This situation allows two different kinds of interface product. The first is the case where the reaction product is the most stable system configuration in the environment of the experiment, and the product layer volume is far below that of the drop, implying also that there are sufficient reagents in the alloy for them to be fully consumed without affecting the overall experiment geometry significantly. The final contact angle will then be approximately the same as the contact angle between the product and the liquid:

$$\cos\theta_F = \cos\theta_P \simeq \frac{\sigma_{PV} - \sigma_{PL}}{\sigma_{LV}} \quad (2.13)$$

With P , V and L product, vapour and liquid respectively.

Sometimes the reaction product is metastable, which implies that the reaction product is stable only under the drop. The triple line will then not be fixed and will move slightly around the equilibrium position. The final contact angle θ_F will be given by a combination of the four interface energies:

$$\cos\theta_F \cong \frac{\sigma_{SV} - (\sigma_{SP} + \sigma_{PL})}{\sigma_{LV}} \quad (2.14)$$

Many studies show that the addition of Ti in a liquid metal drop deposited on a oxide ceramic will produce a Ti_xO_y layer that is wetted by the liquid metal [1, 74, 86, 100, 130, 217]. Other studies show that the addition of Cr to the liquid metal drop deposited on a carbon substrate, decreases the contact angle due to the formation of a layer of Cr_7C_3 and/or Cr_3C_2 with a slower reaction rate [36, 87]. Other studies show that some pure metal can react with the substrate (carbides/carbon and nitrogen/nitride) to form mainly carbides or nitrides [51] where the reaction product is better wetted by the liquid metal than the original solid substrate [75, 80, 81, 95, 113, 165]. Some examples are listed below.

2.3.3 Wetting of Cu alloyed with selected reactive elements (Si, Ti, Cr) on graphite

As mentioned previously (Section 2.2.5), some alloying elements are often added to the Cu-C system in order to improve wetting of the graphite substrate. The main elements are listed below.

Cu-Si-graphite

Silicon is a well-known carbide former. When pure liquid Si is deposited on a carbon substrate (both C_G or C_V), the liquid reacts rapidly at the interface in order to form the stable carbide SiC [75, 78, 218–221], releasing significant heat in the process. All studies of the process report

2.3. Kinetics of reactions at high temperature

the formation, at the liquid Si-solid C interface, of a SiC layer, which decreases strongly the contact angle of the system and drives spreading of the liquid over the solid. The kinetics of isothermal reaction of this system are however not rapid (order of tens of minutes in order to reach the equilibrium position in sessile drop experiment) and the temperature needed to drive it is high since $T_{m,Si}=1414^{\circ}\text{C}$. In order to decrease the temperature of the experiment, Si has been alloyed with Cu, which as seen above is inert with graphite.

Copper alloyed with silicon on a carbon substrate has been investigated by Eustathopoulos and coworkers using the sessile drop experiment [77, 78, 97, 222]. They showed that when a small droplet of Cu-Si (between 30-50at.pct.Si) is deposited both on C_{Gr} or C_V , the contact angle decreases as a function of time, increasing the drop contact surface (and curvature) radius. They noted that if the Cu alloy contains more than 15at.pct.Si, a reaction at the L-S interface happens; this reaction is the same as that observed with the pure Si-C system. The initial and final contact angles are independent of the Si concentration in Cu, starting always around 150° and ending at 40° , meaning that this system experiences a non-wetting/wetting transition. Compared to other systems (see below), the kinetics of reactions are very slow in this system. Eustathopoulos *et al.* showed that the time needed to reach the equilibrium contact angle is dependent on the Si concentration and temperature (1800s for Cu-50at.pct.Si, 8000s for Cu-30at.pct.Si at 1150°C , 3000s at 1250°C , and 6000s at 1100°C for Cu-40at.pct.Si [77, 97, 222]). The equilibrium contact angle has been shown to be approximately the same as that of pure Cu or Cu-Si alloys on a dense SiC substrate [223–225]. That the final equilibrium contact angle of the Cu-SiC and the final contact angle of Cu-Si-C systems are similar suggests that the reactive layer at the interface is a homogeneous layer of SiC, known to be better wetted by the liquid metal compared to the initial carbon substrate, a fact confirmed by microscopic characterization of the interfacial reaction layer formed between the drop and the substrate in this system.

It has been shown that the spreading kinetics of the liquid Cu-Si alloy with carbon are not limited by the diffusion rate of Si in liquid Cu but rather by the interfacial reaction kinetics [77, 101].

Cu-Ti-graphite

Another common element alloyed to copper in order to decrease the contact angle on carbon (and many other solid substrates) is titanium. Titanium is a very reactive element, which can combine quickly with carbon in order to form TiC, a carbide of high stability. Observing the phase diagram of this system, it is possible to see that this phase does not have a stoichiometric composition, being stable over a range of compositions going from 50 to 64at.pct.Ti in C at 1000°C .

When a liquid droplet of Cu alloyed with Ti is deposited on a carbon substrate, the layer of TiC that is formed at the interface is indeed not always stoichiometric and its precise composition varies with the Ti concentration of the liquid ([18, 29]). Multiple studies show that the carbide

Chapter 2. Literature review

formed at the interface is not always wetted by the liquid metal (see Fig. 2.4); there is a critical Ti concentration in Cu for which the system possesses a non-wetting/wetting transition. The critical concentration of Ti necessary for the transition has been investigated on different carbon allotropes such as diamond (C_{Dia}), graphite (C_{Gr}) and vitreous carbon (C_V).

The measured final contact angle is independent of the carbon substrate allotrope; however, it is strongly dependent on the Ti concentration in the liquid, and hence on the stoichiometry of the interfacial layer of TiC carbide formed by substrate/liquid reaction.

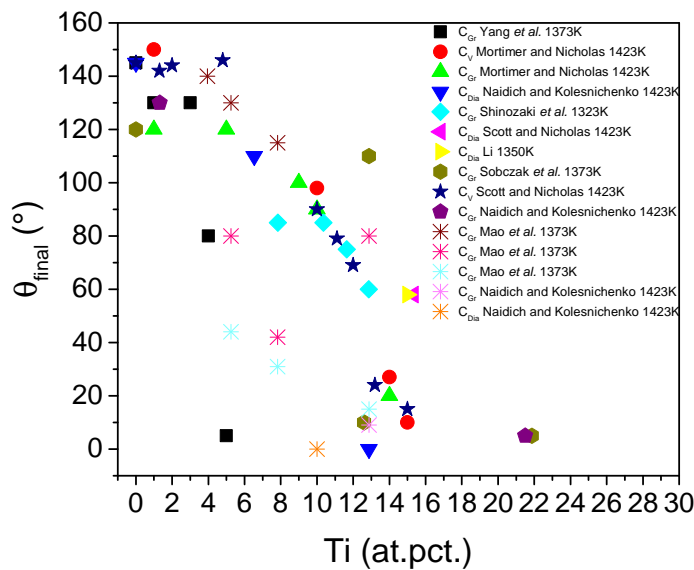


Figure 2.4: Reported contact angles in the system Cu-Ti over carbon as a function of Ti concentration; data from: Yang *et al.* [17], Mortimer and Nicholas [18], Naidich and Kolesnichenko [19,20], Shinozaki *et al.* [21], Scott and Nicholas [22], Li [23], Sobczak *et al.* [24], Standing and Nicholas [25], Naidich and Kolesnichenko [26], Mao *et al.* [27], and Naidich and Kolesnichenko [20].

Figure 2.4 shows that the transition to a wetting system happens at around 10at.pct.Ti in copper on carbon (independent of the carbon substrate allotrope or temperature).

This system is an example of diffusion-limited kinetics: here and unlike the Cu-Si/C system, the reaction kinetics are very fast. In the sessile drop experiment, the time needed for the drop to reach the final (post-reaction) equilibrium contact angle is on the order of hundreds of seconds [123].

In order to investigate the reactivity of this system, Mao *et al.* [27] produced three ingot conditions at three different concentrations (4wt.pct., 6 wt.pct. and 10 wt.pct.) for the sessile drop experiment, namely i) a pre-alloyed ingot, ii) pure Ti on top of Cu, and iii) pure Cu on top of Ti. All three systems were deposited on a graphite substrate and heated to 1100°C. The results obtained show that, as expected, the final contact angle is dependent on the Ti

concentration; however, it is also dependent on the metal ingot placement. In all cases the presence of a titanium carbide layer is observed; however, the lowest contact angle is observed in placement iii) followed by placement ii) and finally placement i). The authors proposed that this is due to the total L-S interface and the effective Ti concentration dissolved inside the liquid metal directly in contact with the graphite substrate, which is not constant for the three different placements.

The contact angle of pure Cu on a pure stoichiometric TiC substrate has been measured to be between 100° and 130° [29, 75, 134, 226, 227]; note that this is still non-wetting.

Li [75, 228], Frage *et al.* [226, 227] and Xiao and Derby [29] noted that the wetting behaviour of the Cu-TiC_x system is strongly dependent on the carbon index x . All those studies show that pure stoichiometric TiC is not wetted by molten copper; however if the carbon index x decreases, the system become wetting.

All authors agree on the fact that the lower the C index x is, the better the substrate will be wetted by the liquid copper. The underlying cause for those observations comes from the fact that the lower the x index is, the more the ceramic possesses a metallic character in its chemical bonding state, leading wetting by molten metal to be promoted. It has been proposed that this phenomenon is due to the high activity of Ti at the L-S interface which promotes wetting since its activity near the stoichiometric concentration is close to 0 [29, 75]. Another explanation could come from the fact that the more stable the carbide is, the stronger the interatomic bond will be, meaning that the interaction with the liquid will be weak leading to a high surface tension and low work of adhesion, translating into a non-wetting situation [31].

Cu-Cr-graphite

Chromium is another commonly used alloying element to bond carbon to copper and obtain a wetting system with carbon. This system, too, has been widely investigated over time since a small amount of alloying element is enough for the non-wetting/wetting transition. Published studies have focused on all three main allotropes of carbon, namely graphite (G_{Gr}), vitreous carbon (C_V) and diamond (C_{Dia}).

Figure 2.6 summarizes the main results obtained from sessile drop experiments conducted on this system, plotting the reported contact angle at equilibrium. It is possible to see that all authors agree on the fact that the contact angle decreases with increasing chromium content in copper, with the non-wetting/wetting transition happening at around 0.5at.pct.Cr in copper. It is generally found that the solid carbon substrate nature does not influence the results. There is also a general agreement that by adding Cr to Cu on graphite, one promotes wetting due to the reaction at the interface between carbon and Cr in order to form a stable carbide. On the other hand, the scientific community does not agree on the kinetics of reaction and the product formed at the interface, and its conclusions are often antithetical. This is due to the fact that two main stable chromium carbides, Cr₃C₂ and Cr₇C₃, can be formed.

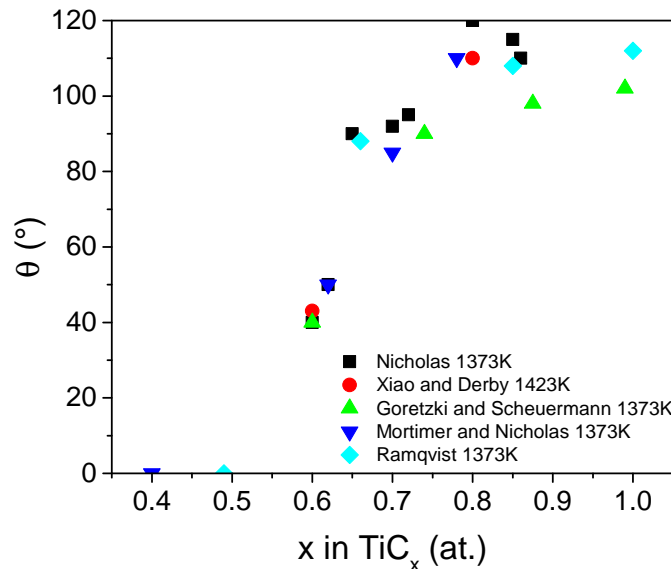


Figure 2.5: Contact angles of the system Cu on TiC_x as a function of C index x with the sources: Nicholas [28], Xiao and Derby [29], Goretzki and Scheuermann [30], Mortimer and Nicholas [18], and Ramqvist [31].

The work of Sobczak *et al.* [24] highlights the formation of both carbides, with a small preference for Cr_3C_2 at the interface at the compositions and temperatures analysed. On the other hand, Devincent and Michal [34] and Mortimer and Nicholas [32] showed that only Cr_3C_2 carbide is formed at the interface for low Cr concentrations (between 0.6-1.22at.pct.) on graphite or vitreous carbon (only Mortimer and Nicholas analysed the vitreous carbon) supporting their conclusions by XRD analysis. In opposition with this result, Voitovitch *et al.* [39] and Hodaj *et al.* [37] showed that only Cr_7C_3 carbide is formed at the interface with vitreous carbon for concentrations lower than 1.5at.pct.Cr. at 1100°C.

Yang *et al.* [17] concluded that the formation of Cr_3C_2 is preferred for low Cr concentration. If the Cr concentration increases, then Cr_7C_3 is preferentially formed; this carbide has a stronger metallic-like character which leads to better wetting. Their conclusion was supported by XRD analysis. They also noted that three stages could be observed, namely: i) the spreading is limited by the reaction rate at low Cr concentrations, ii) a switch from reaction to diffusion-limited spreading kinetics, and iii) a diffusion-limited stage.

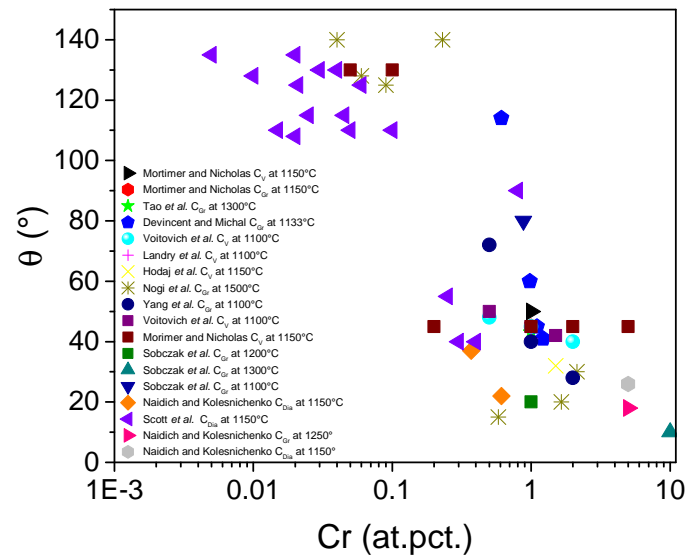


Figure 2.6: Contact angles of the system Cu-Cr versus Cr concentration on different allotropes of carbon, with the sources: Mortimer and Nicholas [32], Tao *et al.* [33], Devincent and Michal [34], Voitovitch *et al.* [35], Landry *et al.* [36], Hodaj *et al.* [37], Nogi *et al.* [38], Yang *et al.* [17], Voitovitch *et al.* [39], Mortimer and Nicholas [18], Sobczak *et al.* [24], Naidich and Kolesnichenko [19], Scott *et al.* [22], and Naidich and Kolesnichenko [20].

2.4 Basics of infiltration

2.4.1 Pressure infiltration of metal-ceramic non-reactive systems at low temperature

Infiltration consists of a fluid entering into open pores of a porous solid medium. The way that the fluid enters depends both on the kind of fluid, on solid porous medium properties, and on parameters of the infiltration process, notably the temperature and applied pressure. In order to know if the flow of the fluid entering the media is viscous-friction dominated, inertia dominated or turbulent, the Reynolds number Re , a dimensionless parameter, can be calculated to estimate the flow conditions; Re is defined as:

$$Re = \frac{r \rho_m v_0}{\mu} \quad (2.15)$$

where ρ_m is the density of the fluid, v_0 is the average velocity of the fluid, μ its viscosity and r the pore radius, the definition of which may vary from paper to paper. In general r is linked to the average distance between the two solid walls across a single pore (space between two fibres or two particles, capillary tube radius,...). If $Re \ll 1$ then viscous forces are much greater

Chapter 2. Literature review

than inertial forces and flow of the fluid is laminar, meaning that the pressure needed to drive the flow is proportional to the average fluid velocity. In metal infiltration, v_0 is on the order of $2\frac{mm}{s}$; with a viscosity of $1mPa \cdot s$ for liquid metals and a pore radius of the order of tens of μm , giving a Re which is relatively low (a few times one-hundreds).

In this condition, and for an incompressible fluid, the liquid flow follows the Navier-Stokes equations in the form [229]:

$$\nabla P = \mu \nabla^2 v \quad (2.16)$$

where P is the local pressure and v the local velocity. Integrating this equation on a representative element of volume which includes a few pores and assuming on average unidirectional fluid flow in the x direction, Eq. 2.16 becomes Darcy's law over the small volume element. For the conditions mentioned previously, this takes the form [229–231]:

$$v_0 = -\frac{k}{\mu} \frac{dP}{dx} \quad (2.17)$$

Where v_0 is the local superficial velocity of the fluid at the small volume element, defined as the volume of fluid passing through a unit area across the porous medium per unit time, k is the permeability of the porous medium (unit square metres) and dP/dx is the pressure gradient on the direction of the fluid displacement. The average fluid displacement rate \bar{v} within the porous medium is linked to the local fluid displacement v_0 through the volume fraction of reinforcement V_r as:

$$v_0 = (1 - V_r) \bar{v} \quad (2.18)$$

Assuming that the porous medium is homogeneous, that it cannot be deformed, and that the flow is unidirectional and sufficiently rapid to create a well-defined infiltration front normal to the x axis, located at $x = h$ and thus assuming that all the pores for $x < h$ are filled, then the average velocity will be $\bar{v} = dh/dt$. This simple approach supposes a planar and well defined infiltration front where a capillary pressure drop ΔP_c , defined by the difference of the liquid pressure at the infiltration front P_0 and inside the porous medium P_a (schematic in Fig. 2.7), is called the *slug flow assumption* [40, 232–234].

Taking a constant and isotropic permeability for the porous medium and a constant metal viscosity, it is possible to combine and integrate Eqs. 2.18 and 2.17 in order to find an expression linking the applied pressure on the metal P and the position of the infiltration front h as a

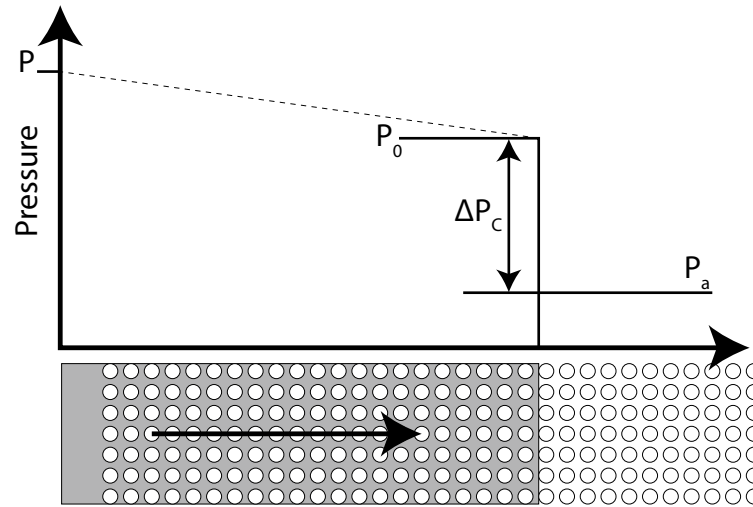


Figure 2.7: Representative sketch of slug-flow infiltration showing the pressure as a function of position along the preform in the direction of infiltrating melt flow. From [40].

function of time t as:

$$h^2 = \frac{2kt}{\mu(1 - V_r)}(P - P_0) = \frac{2kt}{\mu(1 - V_r)}(P - P_a - \Delta P_c) \quad (2.19)$$

Equation 2.19 shows that parabolic infiltration kinetics are expected if the metal is driven by a fixed pressure applied at the entrance of the preform. Such parabolic unidirectional infiltration has indeed been observed in the fixed pressure infiltration of many metal matrix composite systems.

The Washburn equation describes the flow of a liquid inside a capillary tube of constant circular section of radius r . Here, the liquid forms a meniscus at the L-V interface [235] and the system is a variant of slug-flow infiltration. In this model too, the distance is a parabola as a function of time expressed as:

$$\frac{h^2}{t} = \frac{\sigma_{LV} \cos \theta}{2\mu} r \quad (2.20)$$

This model has been used as a model of pressure infiltration in systems other than capillary tubes by several authors, for example by Dullien *et al.* [236, 237] imagining that a system composed of particulates could be seen as a network of long cylindrical capillaries with a random distribution of tube radii. Their “capillary tube bundle” model is based on the capillary rise in a series of geometrically identical tubes with a stochastic distribution of the

pore diameters.

2.4.2 Capillary phenomena in infiltration

The work needed to fully infiltrate a porous medium, if no reaction happens between the liquid and the solid, is given by the pressure difference between the initial atmosphere inside pores of the preform and the infiltrating liquid outside of the porous preform times the volume of liquid displaced in the process of infiltration. This work must at least be equal to the energy contribution that might be necessary to effect the change of surface energy from a solid-vapour interface to a solid-liquid interface ($\sigma_{LS} - \sigma_{SV}$) [92, 232, 238–240]. As mentioned previously, metals often wet poorly ceramics, which means that the work needed to infiltrate a porous ceramic with a molten metal will be positive; thus, it will be necessary to apply a pressure on the liquid metal to create the composite.

In an analysis of the processing of metal matrix composites, the fact that the pores are filled gradually by the metal is neglected, or in other words, the slug-flow is assumed: a 2D clear infiltration front separates the filled part from the empty part of the preform, as shown in Fig. 2.7. The parameters ΔP_C and P_0 can thus be calculated using the work of immersion W_i and the total amount of surface already infiltrated per unit volume, A_i , as [233]:

$$\Delta P_C = P_0 - P_a = A_i W_i = A_i (\sigma_{LS} - \sigma_{SV}) \quad (2.21)$$

It is possible to see that if $\sigma_{LS} - \sigma_{SV} < 0$, the infiltration will be spontaneous since the capillary pressure $\Delta P_C < 0$, meaning that no pressure is needed in order to fill the pores. Combining Eq. 2.3 with Eq. 2.21, it is possible to link the contact angle and the liquid-vapour surface tension to the capillary pressure as:

$$\Delta P_C = -A_i \sigma_{LV} \cos \theta \quad (2.22)$$

The parameter A_i can be calculated if we assume a porous body made of solid spherical particles (having a volume fraction V_r) with an average diameter D as:

$$A_i = \frac{6\lambda V_r}{D(1 - V_r)} \quad (2.23)$$

where λ is a geometrical factor that takes into account the deviations from a perfect sphere, including surface roughness and particle distribution. With Eqs. 2.22 and 2.23 it is possible to

write the “capillary law” in the slug-flow assumption for the infiltration of a particle bed by a molten metal as [233, 238, 241]:

$$\Delta P_C = -\frac{6\lambda V_r}{D(1-V_r)}\sigma_{LV}\cos\theta \quad (2.24)$$

Oh *et al.* noted that two parameters of this equation may be problematic, namely: the contact angle and the geometry factor. The first is because it is not always defined and the latter because it is very hard to measure experimentally [92, 238]. They suggested to express A_i using parameters that are easier to measure, such as the volume fraction of reinforcement V_r and the specific surface area per unit mass of particles A_m [m^2/kg] as:

$$A_i = A_m\rho_s\frac{V_r}{(1-V_r)} \quad (2.25)$$

where ρ_s is the density of the solid particles. The threshold pressure (lowest required pressure needed to start the infiltration) then becomes:

$$\Delta P_C = -A_m\rho_s\frac{V_r}{(1-V_r)}\sigma_{LV}\cos\theta \quad (2.26)$$

The surface area per unit preform mass can easily be measured with the Brunauer, Emmet and Teller (BET) technique, which uses Nitrogen adsorption [242, 243]. This technique however tends to give a higher surface area than the one that it is physically possible to infiltrate with metal since the gas might reach the surface of smaller pores than the ones that the metal can wet due to its high surface tension. This might lead to overestimating the threshold pressure required. Molina-Jordá *et al.* however, highlighted that it was still possible to obtain a reasonable ΔP_C value for a packed SiC bed infiltrated with liquid Al [242, 244]. Another technique that can be used to measure the surface area is laser diffraction; however, the results should be treated carefully since the measure is obtained assuming that the particles have a smooth and spherical shape [245].

Pooling results, the slug-flow assumption can be used in a first approach in order to estimate the lowest pressure required to infiltrate the preform. If the applied pressure is much higher than the capillary pressure drop required to drive the metal into the preform, then the infiltration front will tend to be well defined and, behind it, the preform will be fully infiltrated.

If the applied pressure is not far above the pressure necessary to first drive the metal into the preform, then the slug flow approach loses relevance. As particles do not have a regular

shape, size or distribution, preforms tend to have a range of pore sizes, leading to strong variations in the pressure required to fill each pore of the preform. As a result the liquid will then fill first the bigger open pores due to the low capillary force opposing it, and subsequently the smaller pores can be filled when the local metal pressure has increased [40, 53, 246–249]. This implies that the infiltration of most industrially relevant preforms such as bonded carbon, or packed ceramic particles, will require overcoming a wide range of pressures, between the first moments when the metal has first penetrated the largest open pores in the preform and final phases of the process where the smallest pores are invaded.

As a result, one cannot generally characterize capillary forces in infiltration by means of a single capillary pressure drop; rather, a range of pressures characterizes the process; furthermore, wetting in infiltration becomes then a hysteretic process [40, 233, 246].

The science of infiltration has been investigated not only in metallurgical engineering but also in many other fields, including soil science and reservoir engineering [229, 250]. In the first branch, the problem consists in pumping (or pushing) water from (or into) a porous soil and in the latter it consists in extracting oil or petroleum trapped within pores of a soil medium, such as sand. Through this work it has been shown that one can characterize capillarity in infiltration by means of drainage/imbibition curves. *Drainage* is the replacement of a wetting fluid by a non-wetting fluid within a porous medium (e.g., mercury being pushed into a porous medium); this is in opposition to *imbibition* where the opposite process is performed, i.e. a non-wetting fluid is replaced by another, better wetting fluid (such as water displacing air in a sponge). The characterization of capillary forces in those processes is usually performed by means of drainage-imbibition curves, which plot the amount of static liquid filling the porous body versus the difference between the fluid pressure and the pressure inside empty pores, at equilibrium (in the absence of fluid flow). Léger *et al.* [3, 251–253], Molina-Jordá *et al.* [254, 255], Bahraini *et al.* [249, 256], Kida *et al.* [257], Michaud *et al.* [247] and Kaufmann and Mortensen [258] extended this concept to high temperature liquid metal-ceramic systems (Section 2.7).

2.5 Wetting in pressure-infiltration

Capillary forces in high temperature infiltration tend to be particularly high (compared to what is seen in soils for example) due to the fact that liquid metals tend to have a high surface tension, in turn increasing (for a given pore size) capillary forces acting on the system, which increases the pressures needed to drive the infiltration process. This is due to the fact that interatomic bonds tends to be higher both in metal-metal and often in metal-ceramic systems compared with systems at room temperature where mainly Van der Waals and hydrogen bonds prevail [40, 232–234, 248].

The relative importance of viscous forces versus capillary forces for a fluid moving through a

porous medium is usually characterized by the capillary number C_a defined as:

$$C_a = \frac{v_0 \mu}{\sigma_{LV}} \quad (2.27)$$

where v_0 is the average superficial velocity of the fluid and μ its viscosity. For molten metals, viscosities are on the order of a few $mPa \cdot s$ and their surface tensions on the order of $1 J/m^2$. If the velocity takes a typical value of a few mm/s , one concludes that $C_a \ll 1$, meaning that capillary forces prevail over viscous forces [2]. For this reason, past phases of rapid fluid flow, in metal infiltration processing capillary forces can exert a dominant influence on the degree of infiltration and the morphology of the metal within the network of open preform pores. At the scale of individual pores, thus, the morphology of the liquid metal meniscus, and the distribution of metal along the solid pore surface, will bear a close resemblance to what is seen in a sessile drop experiment – save for the far more complicated geometry; this is sketched in Figure 2.8.

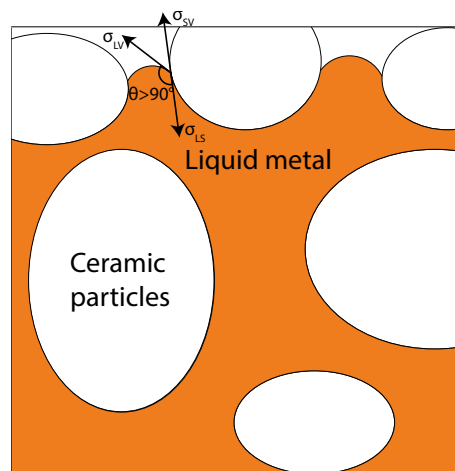


Figure 2.8: Schematic representation of an infiltration front during unidirectional pressure-infiltration at the scale of single pores. The contact angle and the surface tensions are highlighted for this configuration.

2.5.1 Spontaneous infiltration and critical wetting angle

At their melting point and under inert atmosphere, metals rarely wet ceramics, independently of the nature of the metal or the ceramic. Pressure-infiltration is therefore often used to overcome the capillary forces (P_c) acting against the penetration of the liquid, by applying on the metal a pressure $P_0 > P_c$. The Young-Laplace equation gives the pressure difference across a curved liquid meniscus at equilibrium in the presence of two fluids (usually a liquid and a

gas) as [1]:

$$\Delta P = \sigma_{LV} \left(\frac{1}{R_1} + \frac{1}{R_2} \right) \quad (2.28)$$

where R_1 and R_2 are the two principal radii of curvature of the meniscus surface, this being equal along the surface of the meniscus if there the local rate of fluid flow, and surface tension gradients, are both negligible. In the particular case of a cylindrical capillary tube of radius r , the meniscus has the shape of a spherical cap, with $R_1 = R_2 = r / \cos\theta$, such that one can rewrite the Young-Laplace equation as [1, 259]:

$$\Delta P = \frac{2\sigma_{LV}}{R} = \frac{2\sigma_{LV} \cos\theta}{r} \quad (2.29)$$

The pressure needed to infiltrate a cylindrical capillary depends only on the size of the tube, the contact angle between the solid wall of the capillary tube and the nature of the liquid since the surface tension does not change if the atmosphere is not modified. This equation is commonly used in order to estimate the pore structure of a porous body. Mercury intrusion porosimetry (MIP) uses this equation in order to back-calculate, from measurements of the drainage curve characteristic of mercury infiltrating porous bodies, their open pore sizes and their distribution. Some studies have, however, recognized that the thus-estimated pore size distribution in MIP does not always represent the real pore size [260, 261] because generally pores cannot be simplified as independent capillary tubes. For a porous body made of compacted particles, where pores are far from being perfect cylinders and rather present a tortuous path of highly varying width and shape, the pressure required to infiltrate each pore denotes rather the size of narrower pores necks, where the passage of the non-wetting metal flow is most severely hindered.

Equations 2.29, 2.24 and 2.26 clearly show that if $\theta \leq 90^\circ$, then the pressure become negative (at $\theta = 90^\circ$ the pressure is 0) meaning that if the system is wetting, the infiltration should be spontaneous. Even if some similarity exists, the infiltration process as applied to realistic preforms (such as ones produced by packing particles) differs greatly from the sessile drop experiment and also from a pure, homogeneous and smooth capillary tube. In order to observe spontaneous infiltration, it has been found that the contact angle needs to be much smaller than 90° [136, 154, 232, 234, 262, 263]. Some examples of infiltration of wetting systems which still require some pressure in order to fully infiltrate the porous preform are the study of Narciso *et al.* who investigated the Ag-Al₂O₃ system which, following sessile drop experiments, is a wetting system only when O is dissolved in Ag. They showed that for this system too, a pressure is needed in order to drive the fluid to infiltrate the preforms [264]. Travisky *et al.* investigated the Cu-O-Al₂O₃ system. This has a contact angle found by sessile drop experiments to be 44°

for Cu-2.4wt.pct.O₂: it was found that spontaneous, pressureless infiltration is not achieved when placing the preforms in contact with the molten metal. When the O₂ concentration was increased to 3.6at.pct.O₂, full pressureless infiltration was achieved; for this system, sessile drop experiments noted a contact angle of 32°. The authors concluded that the critical contact angle for spontaneous infiltration of the irregularly shaped pores should lay around 38±6° [136]. On the other hand, the studies of Ben *et al.* focused on infiltration of a mixture of ethanol and water into various particles bed that are always wetted by the liquid. It was found that the critical contact angle for spontaneous infiltration was close to 50.7° independently of the powder or the size of the particles [265].

Those observations are easily rationalized, using for example simple models of the porous medium. In a preform composed of particles, the pore size has a wide distribution, meaning that even if the liquid may penetrate inside selected pores within the preform, it will not necessarily fill completely all the open porosity due to the spread of pores size and shapes, and consequently a difference in threshold pressure needed to pass the pore necks [266]. A variety of models have been proposed by Kaptay and Bárczy [267] who proposed a new way to estimate the threshold pressure of liquid into different media assuming that not all the S-V interface is replaced by the S-L interface during infiltration, a process which is more pronounced in the case of non-wetting systems. The threshold pressure will then be a function of three semi-empirical parameters which depend on the morphology of the porous preform, leading the author to estimate a critical contact angle for spontaneous infiltration to lie between 65.5° and 90°, with a realistic approximation at 75°, a value claimed to be confirmed by the works of Yang *et al.* [234, 263]. The same authors proposed a new model for the threshold pressure of a liquid infiltrating along parallel and long fibres to find that P_0 is inversely proportional to the shortest distance between two fibres, and the contact angle for spontaneous infiltration lying between 0° and 43° as a function of the ratio between the spacing between the fibres and their diameters [268].

Models to predict a critical contact angle for spontaneous infiltration have been developed for highly idealized geometries with a meniscus having a constant curvature in a regular pore and omitting the effects of gravity. In order to have a criterion for a contact angle (or threshold pressure) which corresponds to reality, it is necessary to take into account the fact that particles are rarely perfectly spherical or cylindrical, meaning that their randomness in shape, size, packing, and roughness of the surface become important factors influencing the system. This leads to a highly complex problem of real infiltration in porous preforms [266]. Discrepancies between the experimental data and theory have been highlighted in different studies, and multiple attempts to model the critical contact angle for spontaneous infiltration have been made with different, idealized, pore shapes [265, 269–272]. For a close packed structure made of perfect spherical particles, the critical angle for spontaneous infiltration is 50.7°, a value given by the liquid entering the tetrahedral pores. Yang and Xi calculated pressure values for a perfect, ordered preform made of monosized sphere or fibres and found that even if the critical contact angle is much lower than 90° [270], the required angle for spontaneous infiltration differs greatly as a function of the infiltration direction, the particle

arrangement, and their packing density. If the particles are partially sintered, forming a ridge between them, Frage *et al.* noted that the critical angle becomes a function of the densification and the morphology of the particles [272]. Hamlett *et al.* formed a spherical bed of small spheres resting on top of an hexagonal packing of bigger spheres (modelling a soil) in order to investigate the transition between a system in which water can penetrate easily and one where it does not. They found that the critical angle depends of the radii of the big and small particles. In case of a uniform particle size (for each of the big and the small particles) a critical angle of 50.7° was found [271].

Models have also been proposed to predict the pressure required, for a given geometry, knowing relevant capillary parameters (wetting angle, surface tension), to effect infiltration. The studies of Haines described on the basis of microscopic observations the wetting and dewetting of a liquid on the contact point in a preform made of packed spheres [273]. An approximation proposed by White, called the hydraulic radius approximation, supposes a cylindrical tube having the same surface-area-to-volume rate as the pores in the porous preform and then uses Eq. 2.29 to deduce the infiltration pressure required [240]. Another approach is the Mayer and Stowe model, which reduces a close-packed system made of spheres into cylinders having the same radii of the sphere with the metal flowing between the cylinders. In all such models, the threshold pressure is a function of the contact angle and of the porosity of the preform [260].

Purcell focuses on toroid-shaped particles with the liquid located inside the hole generated. The meniscus curvature is thus somewhat simpler to calculate given the axisymmetric nature of the pore. Its curvature will only depend on its position inside the pore since the pore has a convergent-divergent shape [274]. Assembling this theory and the curvature in rods, which are nonaxisymmetric [260, 273, 275, 276], Mason and Morrow investigated the meniscus curvature in a pore made of spherical particles. They noted that the contact angle at the point of maximum curvature of the meniscus is proportional to $\cos 2\theta/3$ rather than the normal $\cos \theta$ for a cylindrical capillary tube. The experiments performed using PTFE spheres infiltrated with different partially wetting liquids confirmed their model. The authors however never addressed the effect of roughness on the surface of the particles, a parameter which can vary greatly and may significantly influence the results [261].

As mentioned before, reality is much more complicated than what models can describe assuming simple shapes for capillaries such as parallel plates, circular tubes, parallel fibres or even toroidal pores to develop analytical models which represent the shape of the liquid in contact with the solid as a function of the contact angle [266].

2.5.2 Experimental methods

2.5.3 Experimental measurement of wettability in infiltration

As mentioned previously, measuring the contact angle at high temperature can be challenging (Section 2.2.2). In pressure infiltration, another challenge comes from the fact that a simple scalar, such as the contact angle that is measured in the sessile drop experiment, is frequently insufficient to characterize capillary forces in the process of infiltrating a porous solid with a liquid. This is due to the fact that wetting in a porous network composed of a complex 3D maze of variously shaped open pores is far more complex than is the flat substrate with a drop characteristic of the sessile drop experiments. Furthermore, in the sessile drop experiment, quasi-static conditions are achieved, whereas infiltration can be a highly dynamic process, particularly if the liquid is driven by applied mechanical pressure. And finally, in infiltration, both for metals and other fluids, capillary forces become scale-dependent, given that they vary in proportion to the inverse of the size of the pore into which the fluid enters.

Two approaches have been used to characterize the forces in capillary infiltration, namely: i) highly dynamic infiltration where the capillary number C_a is high and a measurement of the pressure drop across a defined infiltration front is performed under the slug-flow assumption, and ii) quasi-static infiltration, conducted with a low C_a in order to equalize the pressure everywhere within the fluid, and thus equate the applied pressure with the (uniform) capillary force and from this plot drainage curves.

High velocity infiltration

If flow of the infiltrant is rapid, viscous friction forces will cause it to contain significant pressure gradients, such that pores will tend to get filled at a relatively well-defined infiltration front; as mentioned previously, this is a configuration called slug-flow, depicted in Fig. 2.7. If viscous forces can be estimated (from Darcy's law at sufficiently low Reynold number), then by subtracting those from the applied pressure one can deduce the pressure drop between the metal at the infiltration front and the atmosphere ahead of it (the latter being close to zero if the preform was evacuated).

The infiltration front can be observed in multiple ways. The easiest but also the slowest method is by metallography, meaning that the preform is cut longitudinally and it is analysed under a microscope in order to define the length of infiltration h . In order to obtain multiple points it is necessary to perform one infiltration for each pressure. Operationally, a pre-heated porous preform is unidirectionally infiltrated under a fixed applied pressure, which will vary from experiment to experiment and is held for one or a series of fixed time intervals, usually between 120 and 300 s. Then, by cooling the samples and measuring optically the position of the infiltration front, it is possible to deduce the infiltration kinetics and from this, using Eq. 2.19, the threshold pressure P_0 [232, 233, 238, 239, 243, 244, 277–279, 279–288]. Usually the easiest representation of those experiments is by means of a h^2 vs P plot, which should give a

linear relation between the two parameters.

Other, somewhat more complicated experiments, allow to track dynamically the infiltration front as a function of pressure, which allows, with a single experiment, to obtain the full h^2 vs P plot. Some examples of set-ups allowing such dynamic metal front tracking are the experiments of Jonas *et al.* [239], which used a system of capacitances between the liquid metal and an electrode outside the set-up calibrated in order to measure the infiltration displacement. Muscat and Drew [283] on the other hand, measured dynamically the infiltrated liquid using a microbalance which allowed to measure the weight change as a function of the applied pressure due to the metal penetrating the porous preform. Other groups developed a measurement method that tracked the metal position using measurements of electrical resistance [231,289].

Drainage-imbibition curves

The premise behind the slug-flow assumption is that the infiltration front is homogeneous and no significant porosity is left behind it; however, during infiltration of a porous medium, such is often not the case since the pressure required to infiltrate each and every pore can extend over a wide range, given the complex geometry and size distribution of pores within most porous media. As a result, in frozen partially infiltrated samples, one often notes that there is a continuous gradient in the volume fraction of voids, values of which are finite and increase as the infiltration front is approached [281, 290–292]. One has hence seen a transposition to metallurgy of approaches based on the equilibration of capillary forces and applied pressure, performed at low values of C_a that were developed in soil science and petroleum engineering [229, 250] and adapted for conditions characteristic of metals, of high temperature and high pressure. Here, capillarity is measured by drainage curves, defined as plots of the fraction of pore space that is filled with liquid, called the saturation S , versus the difference between the applied metal pressure P and the pressure inside the gas atmosphere that fills uninfiltrated pores P_a . The saturation is thus the ratio between the infiltrated liquid over the total pore volume, defined as:

$$S = \frac{V_m}{1 - V_r} \quad (2.30)$$

where V_m is the local volume fraction of liquid and V_r is the reinforcement volume fraction ($1 - V_r$ is thus the initial open pore volume fraction). When full infiltration is achieved, $V_m = 1 - V_r$ and the composite is locally pore-free if the reinforcement contains no closed pores. In metal matrix composite infiltration, $P_a = 0$ since the preform is initially under vacuum (otherwise, full saturation cannot be achieved since some compressed gas is left inside the preform after metal infiltration).

Experiments involving the infiltration of metal into porous ceramics pose specific challenges given the high temperature (as a function of the metal, but typically of the order of 1000°C) and high pressure (as a function of the particle size, but on the order of 10MPa) involved in the process. In order to measure drainage curves in such systems, various methods have been developed. One is infiltrating a series of preforms at different pressures for times long enough that fluid flow comes to a halt, and then by metallography or densitometry it is possible to determine the volume fraction of the partially infiltrated composite for each applied pressure value [247, 249, 256, 258, 293, 294]. The drawback of this method is that for each S vs P point on the drainage curve, a separate infiltration experiment is necessary, so to draw a full drainage curve, a set of 5-10 samples is necessary.

A more efficient method to measure the curve is to track dynamically the volume of metal filling the preform. A first approach is to measure the weight of the preform while the metal fills the pores; this was done for a wetting system by Muscat and Drew [295]. Another method that is suited for non-wetting systems was developed by Bahraini [2] to measure with a single sample the entire drainage curve at high temperatures and high pressures characteristic of metal-ceramic systems. The concept of the apparatus is a LVDT (Linear Variable Differential Transformer) connected via an alumina rod to a graphite plunger that floats on top of the liquid metal surface and tracks the (vertical) displacement of that liquid metal surface. The volume infiltrated will then be the measured displacement multiplied by the section of the crucible in which the preform is infiltrated. This method gave reproducible results when compared with the discontinuous methods [2] and (for mercury) results from a mercury porosimeter. This set-up, which suffered under some conditions from interference with the LVDT measurement from the induction heating system, was modified by Léger [3, 251–253, 296] who replaced the LVDT system with an optical device. This device can track the metal surface movement thanks to a series of black and white strips located on the alumina rods. This modification allows a more stable measurement, which is independent of the applied tension on the induction coil used to heat the system. This system has been proven reproducible and very accurate at high temperature and high pressure, enabling for example measurements with pure copper preforms [3, 251–253, 296].

2.6 The theory behind drainage curves

Predicting the form of drainage curves is a complex endeavour, for several reasons. The first is the complex geometry of pores in engineering preforms such as those made by packing ceramic fibres or particles. The second reason why such predictions are complex is that pore geometries are not only complex but random. Randomness in the size, shape, and hence infiltration pressure of each pore in the preform causes pressure infiltration to be a percolation process, which gives the metal flow path in initial phases of slow infiltration fractal characteristics, and gives initial portions of drainage curves certain universal characteristics. Finally in its final phases, and hence in the final, high-pressure, portion of drainage curves, one finds certain characteristics that may be a result of fractal characteristics of the inner

surface within each pore. We examine in turn below these various interpretations of drainage curves, starting with the simplest approach.

The work needed to wet a surface per unit area is called the work of immersion W_i . It represents the energy needed to replace a S-V surface with a S-L interface without creating new interfaces, and can, as we have seen, be linked to the contact angle θ and the surface tension with the Young-Dupré equation as:

$$W_i \equiv \sigma_{SL} - \sigma_{SV} = -\sigma_{LV} \cos \theta \quad (2.31)$$

where σ_i represents the surface tension of the different interfaces (all assumed to be isotropic).

If it is assumed that a drainage curve is obtained in a quasistatic infiltration where the capillary forces dominate and that all the irreversible energy losses, such as Haines jumps or viscous friction, are neglected [229, 297–299], it is then possible to link the work of immersion to the total work W spent pushing the liquid into open pores of the preform as:

$$W = (1 - V_r) \int_0^1 P dS = \Delta E_r \equiv A_s V_r \rho_s W_i \quad (2.32)$$

where A_s is the specific surface area of the preform, ρ_s is the density of the solid particles and V_r is the volume fraction of particles. The integral is obtained from the drainage curve when it is plotted as pressure versus the infiltrated pore volume per cubic metre of pore space. Léger *et al.* analysed multiple systems having different wetting parameters and found that, experimentally, this law is well followed for highly non wetting system, i.e. $W_{i,app} \simeq W_i$, while for slightly non-wetting or even wetting systems the apparent work of immersion is higher, and relatively well predicted by the correlation $W_{i,app} = 0.47(W_i + \sigma_{LV})$ [253].

If one assumes that all irreversible energy losses are negligible, or at least proportional to the reversible energy spent in the process of slow (low capillary number) infiltration, then drainage curves of the same porous preform infiltrated with various metals, of different contact angle and surface tension, collapse into a single curve if all pressures are divided by the relevant work of immersion. This is indeed often observed experimentally [2, 232, 249, 253, 254, 256, 257, 296, 300, 301].

2.6.1 Percolation theory

There is an extensive literature, largely motivated by soil science and petroleum engineering, on the physics of drainage or imbibition through porous media, comprising both experiments, theoretical analyses and numerical simulations in which infiltration is viewed as an

embodiment of percolation, potentially complicated by certain features specific to liquid infiltration [297, 302–328].

One complication that arises in infiltration is that, depending on infiltration conditions, governing forces and hence their link with characteristics of the porous medium, may vary. The forces acting on a fluid moving through a porous media act at different levels. At the pore size level the main forces are the capillary forces, and at higher scale, gravity and viscosity forces act. Lenormand *et al.* [312] and then Sukop and Or [318] investigated the influence of the ratio between the viscosity of the invading fluid to that of the invaded one (dimensionless parameter M) versus the capillary number C_a (Eq. 2.27). These authors proposed a scheme in order to separate the different parametric regions and delineate their expected infiltration patterns. They found three main patterns, namely: i) Capillary fingering, at low C_a and high M , ii) viscous fingering, at high C_a and low M , and iii) stable displacement, when both parameters are high.

Those three configurations have been intensively studied both experimentally and by simulation, with particular focus on the fractal structure of the displacing and displaced fluids. In the infiltration of evacuated preforms with a liquid metal, one is obviously within the first regime, of capillary fingering, also known as invasion percolation.

Invasion percolation

Wilkinson and Willemsen proposed a model that represents well the invasion percolation, which is a particular form of ordinary percolation [329]. In invasion percolation, the connected, invading and at some point percolating, phase can only start from the outer surface of the medium; this is unlike normal or classical transport percolation, where the invading phase builds up homogeneously throughout the medium across which it will eventually percolate.

The first analyses of invasion percolation were conducted by observation of the replacement of a fluid by another under the action of capillary forces [294, 309, 315, 319, 321, 328, 330–339]. Those studies based their results and interpretations on Eq. 2.2, which is an approximation considering the assumption that the porosity is composed by uniform cylindrical pores. Since drainage involves complex pore-scale flow paths, the networking of the pores plays an essential role [339].

In order to avoid the approximation of the long parallel tube model, new linked network models started to be proposed sixty years ago in order to better represent reality and avoid adding artificial parameters, such as tortuosity, in order to fit the models to the experiments. The new models used networks to simulate the porous medium, so as to integrate phenomena happening at different scales: the pore scale where there is wetting and fluid flow, and a larger scale, where one considers the pore size distribution. Due to the high complexity of the system, simulation of “real” systems would ask for too many resources, so simulations of fluid displacement through porous media was performed in a simplified geometry of pores and

Chapter 2. Literature review

necks of simple geometry (such as straight cylinders) connected along predetermined grids. An example is the Pore-Cor model, which approximates the 3D porous medium by giving the voids a cubic shape and connecting them by cylindrical necks of variable radius representing the connections between them [340–347].

The theory behind percolation in infiltration is tightly linked to the network model chosen. The simulated domain is often composed by square (2D) or cubic (3D) grids in which pores have characteristics linked to a random number of probability p (between 0 and 1) representing for example the pore radius. At each step of the simulation or experiment, the infiltration front is moved into new accessible pores. This method differs as mentioned from classical percolation since the pores that can be filled are only ones in contact with pores that are already filled (as opposed to any pore that has the appropriate probability characteristic). There are thus in invasion percolation two conditions for a pore to be filled at a given value of the probability number p_g : i) that its probability p is lower than p_g (or in experiments to the applied pressure), and ii) that at least one adjacent pore is already filled. Simulations of invasion percolation show that ordinary and invasion percolation have the same critical percolation threshold value $p_g = p_c$. When the displaced fluid is a collapsible vapour (such that there is no trapping of isolated blobs of the displaced fluid), then the infiltration front of the partially filled porous medium has a fractal shape at the percolation threshold and basic scaling laws of classical percolation describe the behaviour of the sample. Ordinary percolation and invasion percolation without trapping thus belong to the same universality class [312, 331, 339]. In the vicinity of p_c , the scaling laws take the form:

$$P(p) \propto (p - p_c)^\beta \quad \text{with} \quad D = d - \frac{\beta}{\nu} \quad (2.33)$$

$$\zeta(p) \propto (p - p_c)^{-\nu} \quad (2.34)$$

where $P(p)$ is the probability that a pore is connected to an already filled one, D is the fractal dimension of the infiltration front, β and ν are universal exponents and d is the Euclidian dimension. The correlation length $\zeta(p)$ is defined as the root mean square of the average distance between infiltrated pores that belong to the same infiltrated cluster. An assumption made in all models is that the probability p characteristic of each pore is related to the capillary pressure that is required to infiltrate it, and that its probability of belonging to an infiltrated cluster, p_c , is linked to the saturation S of the infiltrant (non-wetting) liquid within the infiltrated porous medium [339].

Around the percolation threshold, the critical universal exponents D , ν , and β depend only on the dimension of the system and not on its lattice structure (in 2D: $\beta=5/36$, $\nu=4/3$ and $D=91/48$ and in 3D: $\beta=0.4$, $\nu=0.875$ and $D=2.52$). On the other hand, p_c is dependent on the structure of the medium and has to be determined experimentally or by simulation.

Invasion percolation has been widely investigated, both on its simplest form and in more

complex configurations, adding for example gravity forces and viscous forces [306, 315, 338, 348–350]. Investigations of the effect of sample size in percolation theory has been carried out by Larson and Morrow and they showed that the shape of the drainage curve may be modified in its early stage when the sample size falls below a certain value. If the thickness of the sample decreases, then the accessibility of the pore space increases; hence, as the sample size decreases, at given pressure the average saturation should increase and the threshold pressure should decrease. If the flow rate remains sufficiently low, translated in a low C_a , and the length of the sample stays sufficiently low due to a critical characteristic time, then the invasion percolation domain persists [333]. If C_a and/or the infiltration rate are greater, then the displacement of the fluid is affected by the gradient in fluid pressure caused by viscous forces. Capillary fingering will then be modified, tending to a more planar infiltration front, always in a case of infiltration of a non-wetting fluid into a preform under vacuum. In the extreme, infiltration tends to the slug-flow configuration, and more classical, non-percolation continuum modeling approaches based on consideration of random elementary volumes (REV) become suitable [315, 317, 323, 351].

Near the threshold for percolation (which corresponds in a drainage curve to the lowest pressure, at which infiltration abruptly begins), the invading fluid traces at scales above the pore diameter a fractal [352]. Measurements of fractal dimension of the infiltrating fluid can be found in the works of Shaw [353] and Lenormand *et al.* [312] for non-metallic systems. The fractal dimension of a partially infiltrated metal-ceramic system was first investigated by Clément *et al.* studying the unidirectional flow of liquid metal in a bed of glass beads. These authors found a fractal pattern along the interface [294]; however, they noted that the data were strongly influenced by gravity [349]. Thompson *et al.* found similar results after infiltrating rocks with mercury [354]. More recently, Léger *et al.* investigated the fractal dimension of partially infiltrated MMC systems. The study focused on different shaped alumina and carbon preforms infiltrated with molten copper. 2D Image analysis allowed to measure a fractal dimension of the infiltrated solid, from which the 3D fractal dimension was estimated by writing that $D_{3D} = D_{2D} + 1$. Results gave values close to those predicted by theory, independently of the preform nature [252]. Due to the high values of applied pressure in their samples, gravity forces were insignificant compared to capillary forces.

2.6.2 Brooks and Corey model

At higher metal saturations, well above the threshold for percolation, it has been shown that the quasistatic infiltration of molten metal into porous ceramics of many different kinds (fibrous, particulate, other) follows the Brooks and Corey correlation [2, 3, 40, 247, 249, 252–254, 256–258, 290, 296, 355], which was originally developed in order to model soil water retention curves (SWRC), which describe the path of water through a porous soil such as sand. This

correlation takes the form:

$$S \equiv \frac{V_m}{1 - V_r} = 1 - \left(\frac{P_b}{P} \right)^\lambda \quad (2.35)$$

where S and P have their usual meaning, P_b is a parameter called the bubbling pressure, which is related to the size of the largest, continuous pore network and λ is the “pore size distribution index”, measuring the variability of sizes of the channels in the porous medium. This correlation was later shown to be compatible with the view that the pore space that is invaded at higher saturations delineates a fractal, as can be derived from the Turcotte fragmentation model [356]. All the fractal models advanced to explain the Brooks-Corey correlation assume that the soil is self-similar, meaning that it has the same geometry at all length scales (through which this power-law emerges if one writes that the pressure required for infiltration is inversely proportional to the pore size). Such models find applications in power-law linkages between solid-pore mass fractal, fractal pore-size distribution, pore-solid interface or fractal surface, pore-solid geometries and so on [357–377]. All those models represent relatively well experimental data except for both the wet and the dry ends of the infiltration process, a fact that has been imputed to the dominance of percolation-related effects [331].

2.7 Infiltration of liquid metal into ceramic preforms: data

Drainage curves for metal-ceramic alloys have been investigated for a variety of non-reactive systems in the past years, and data linked to values of the contact angle, the surface tension and the particle shape and size. Kaufmann and Mortensen investigated the infiltration of Al in fibrous Al_2O_3 producing the first drainage curves for a metal-ceramic system. Using metallography, they produced multiple samples infiltrated at different pressures, and by analysing the microstructure, they were able to measure the saturation of the partially infiltrated samples and thus plot the drainage curve [258, 378]. Several studies measured the height reached by the liquid flowing vertically upwards into a preform as a function of the applied pressure and infiltration time [379–381].

In the successive years, several papers on infiltration of metal in ceramic preform for non-reactive systems were produced by the Mortensen laboratory, using the above-mentioned apparatus able to obtain a full drainage curve in one experiment (see Section 2.5.3) by measuring the displacement of the fluid as a function of the (gradually and slowly increased) applied pressure. Multiple systems have been tested, namely Al-Si alloy infiltrated into diamond particle preforms [256], Cu into Al_2O_3 particle preforms [249], Al-Si into a mixture of SiC- Al_2O_3 particle preforms [245], or different metals into preforms of AlN particles [257]. In all of those studies, the semi-empirical model proposed by Brooks and Corey (section 2.6.2) matches data well at higher infiltration pressures. In the presence of partial reactivity, as found when carbon

2.7. Infiltration of liquid metal into ceramic preforms: data

can react with Si in the alloy to form SiC, data show an influence of the pressurization rate on the drainage curve. These studies were followed by those of Léger *et al.*, which investigated both main domains of the drainage curve, namely the (near-threshold, low-pressure) percolation dominated domain and the (higher pressure and saturation) Brooks and Corey domain, on various systems, focusing on the effect of non-reactive alloying elements and pore shape [3, 252, 253, 296]. The percolation domain for the metal-ceramic systems were shown to follow the power laws predicted by percolation theory, with drainage curves obeying the predicted power-law of exponent equal to 0.41, which showed the expected universality in that it is well followed independently of the shape, size or form of the pores within the preforms, and independently of the wetting parameters of the system. It was also found, by measuring drainage curves for multiple alloys for which wettability parameters change as a function of the alloying element concentration in the Cu-Al, Cu-Sn and Al-Sn systems, that the particle size or the wetting angle do not influence the exponent of the Brooks and Corey correlation significantly. Modifying wetting characteristics of the infiltrant, the threshold pressure is modified, switching the drainage curve (to the left if the contact angle or liquid surface tension decrease or the particle size increases, Eq. 2.29). If the shape of the particles is modified, then the Brooks and Corey exponent is modified [253].

Turning to reactive systems, Molina-Jordá *et al.* investigated the drainage curve of the reactive system Al-Si into graphite using the densitometry method [382]. The main problem of this measure of the drainage curve by densitometry, metallography or other interrupted methods is that there is no way to know for sure whether the system had reached capillary equilibrium or not (especially for spontaneous reactive systems in which flow is not controlled).

2.7.1 Parameters modifying wetting in infiltration

As mentioned previously, metals rarely wet ceramics and high pressures are needed in order to overcome the capillary forces during infiltration, increasing the production costs. Ideally a fully wetting system would be needed in order to fully infiltrate ceramics preforms without applying pressure, since (as seen above) low angles, well below 90 degrees, are needed to produce spontaneous full preform infiltration. In the last 50 years, many studies have thus focused on how to increase the wetting by modifying the parameters obtained with the sessile drop experiment such as contact angle θ and/or surface tension σ_{LV} (see Section 2.2.2). To improve the wettability of the system one seeks to decrease σ_{LV} and/or θ , as described for example in Eq. 2.26.

In order to improve the wetting, three different approaches have been pursued: i) Alloying the matrix in order to encourage reaction at the interface by the formation of a more wetting interface or to modify the L-V interface, ii) coating the reinforcement surface with a phase that is better wetted by the liquid, or iii) changing the experimental parameters such as temperature (which will improve wetting in systems such as Al with Al₂O₃ where θ decreases if T increases) and/or atmosphere (such as adding O₂ with Cu).

In the literature, the effects of those three factors have been widely investigated and the results are, sometimes, antithetical. Some reviews of the influence of the three options have been published by Narciso *et al.* and can be found in [233, 383]. The studies were made mainly on silicon carbide (SiC) infiltrated with pure or alloyed Al (usually Al-Si near the eutectic composition - 12wt.pct., Al-Mg or Al-Cu).

(i) *Alloying of the metal matrix*

Adding an alloying element to the matrix can modify σ_{LV} , σ_{LS} or the contact angle θ . All studies agree that if one of those parameters decreases, then the threshold pressure P_0 decreases too. As mentioned before, a modification of σ_{LS} due to an interfacial reaction (Section 2.3.3), produced for example by adding a highly carbide-forming element to the copper matrix, can reduce the contact angle due to the more metallic character of the newly formed product at the interface. Other studies focused on the influence of the Mg concentration in Al infiltrating a SiC particle perform [238, 281, 282, 286, 291, 379]. It was shown by Garcia-Cordovilla *et al.* that, by increasing the Mg concentration, P_0 decreases due to a decrease of σ_{LV} [384]. Maxwell *et al.* showed however an opposite tendency since the addition of 1% Mg in Al increased the threshold pressure [284]. Candan *et al.* stated that the decrease of σ_{LV} is not the only factor that promotes the wetting since the contact angle changes too (remaining non-wetting) between the liquid Al-Mg and the SiC preform [79, 238, 282].

The interaction between Al alloys and SiC has been investigated by Narciso *et al.* on both binary and ternary systems (Al-Si-Mg). It was found that Si in pure Al (up to 13wt.pct.) does not change significantly the surface tension or the contact angle, while addition of small amount of Mg (up to 4wt.pct.) generates a decrease of σ_{LV} with the contact angle remaining the same. The ternary system composed of Al-Mg-Si too shows both a decrease of the surface tension and of the contact angle [286]. Those results confirm the observations of Garcia-Cordovilla *et al.* [384]. Rodriguez *et al.* investigated ternary systems based on Al-Si-X (X=Ti, Mg) infiltrated into carbon. The results obtained with the Al-Si-Mg infiltrated into carbon particle preforms confirmed the results obtained by Narciso *et al.* on SiC, meaning that increasing the concentration of Mg in eutectic Al-Si causes the surface tension as well as the threshold pressure to decrease. For the Al-Si-Ti system, it has been shown that if the concentration of Ti increases, then the surface tension and the threshold pressure increase too [279].

Other groups investigated the effect of other alloying elements in Al, such as Al-Pb and Al-Sn (up to 1wt.pct. for both alloying elements), with both SiC and Al_2O_3 [380]. Similar results were found for both systems in which the surface tension and the threshold pressure decrease as the concentration of alloying elements increases.

Oh *et al.* investigated three Al binary alloying systems (Cu, Si and Mg) at low concentration (2 and 4.5wt.pct.) with both SiC and boron carbide (B_4C). It was shown that the threshold pressure and the work of immersion decrease more significantly for the three systems with B_4C than with SiC [238].

2.7. Infiltration of liquid metal into ceramic preforms: data

Chong *et al.* investigated the effect of alloying elements in commercial 2014 Al alloy (4.2wt.pct.Cu, 0.5wt.pct.Mg, 0.75wt.pct.Si, 0.70wt.pct.Mn and 0.43wt.pct.Fe) by comparing with a pure Al-4.2wt.pct.Cu and found that the threshold pressure decreases slightly for the 2014 Al infiltrated in SiC particles [281]. Candan *et al.* investigated a series of binary alloys in order to compare their effect on the threshold pressure infiltrated in SiC particles. They found that additions of Sr, Ca and Cu increase the threshold pressure while adding Cr, Si, Ti, Mg and Pb decreases the threshold pressure. The stronger reduction of P_0 obtained by adding Mg and Pb is due to a decrease of σ_{LV} ; however, the increase of P_0 due to the addition of Ca and Sr cannot be justified alone by the increase of σ_{LV} since, in fact, the surface tension of the liquid is reduced. The observations are explained by the increase of θ , the effect of which is more important than that of the reduction of the surface tensions [291]. These authors also investigated the effect of Mg concentration infiltrating SiC particles and confirmed that the higher the Mg concentration up to 13.9wt.pct., the lower the threshold pressure. It was also confirmed that these observations are mainly due to the effect of Mg on the melt surface tension σ_{LV} .

Some investigations were performed with silver infiltrated into SiC particle preforms to show that in the presence of oxygen, the liquid absorbs the gas, promoting an interfacial reaction that forms SiO_2 which is less wetted by the liquid, thus increasing the threshold pressure and the contact angle [277]. A similar behaviour has been observed when infiltrating Ag into Al_2O_3 particle preforms. Here too the liquid absorbs the oxygen without forming an oxide layer at the L-V interface, which is known to generally reduce wetting [264]

(ii) Reactive systems

In Section 2.3 the approach of promoting wetting by producing a more wettable layer at the interface due to a chemical reaction between the liquid and the solid substrate has been widely described with some example of specific systems that are used in this work. For completeness, other examples of reactive systems that have been infiltrated in the presence of an interfacial reaction are listed below. Usually reactive systems in infiltration have another advantage, namely a tendency towards increasing of the bond strength between the matrix and the reinforcement.

Bougiouri *et al.* investigated NiSi alloy infiltration into porous graphite. It was found that Si reacts with the reinforcement producing an interlayer of SiC at the L-S interface, which improves wetting due to the metallic character of the carbide [385–387] in a similar way to what is found with Cu-Si into graphite. Singh and Behrendt investigated too the effect of the reaction between Si and C but the liquid was an alloy of Si-Mo infiltrated into porous graphite. They found too that the reaction at the interface between Si and C promotes wetting. They noted that the addition of Mo to the system lowers the exothermicity of the reaction between Si and C; however, increasing the Mo concentration may block the path of the metal due to the formation of the intermetallic MoSi_2 only if Mo is present initially in low atomic fraction [388].

Kevorkijan explored Al infiltrating different ceramics that may produce some aluminate such as SiO_2 , Si_3N_4 , Mg_3N_2 and TiO_2 . It was found that the weaker the bond in the ceramic, the faster the reaction with the metal, decreasing P_0 [389].

(iii) Particle alteration

A system commonly used to promote wetting is to increase the particle size. In Eq. 2.2 it is possible to see that the higher the radius of the capillary tube, the lower the threshold pressure will be. If the particle size increases, the pore size will increase too, lowering P_0 [278, 281, 383]. At a more sophisticated level, the influence of the particle size distribution has been investigated by Molina-Jordá *et al.* using a bimodal mixture of SiC with both coarse and fine particles and a mixture of SiC- Al_2O_3 particles in different concentrations, which were infiltrated with molten Al. It was found that the threshold pressure is controlled by the compactness of the smaller particles [280, 285, 390, 391].

Another way to modify the reinforcement is by coating it with a layer of a better wetted material; this is not technically speaking the same system since the L-S interface is modified. An example of a coating used for infiltration of Al into SiC or C is K_2ZrF_6 which has been found to decrease σ_{LS} by reacting with Al in order to form Al_3Zr at the interface. This compound has a metallic character, leading to a surface which is better wetted by metals [379, 392–394].

Yu *et al.* coated Al_2O_3 particles with yttria (Y_2O_3) infiltrating these with Al. Results show a slight decrease of the contact angle at low temperature, and this difference increases as the temperature increases [395]. Rohatgi *et al.* on the other hand, coated fly-ash (a mixture of Al_2O_3 , SiO_2 , FeO and K_2O produced by combustion) with metallic Ni infiltrating Al. This decreased the threshold pressure by 60% thanks to the coating and intermetallic formation [396]. Finally, Chaklader and Linger coated alumina particles with pure Ni or Cu and sintered the powder in order to avoid pressurizing the system. They showed that even if a composite can be achieved, it will not be fully dense and some residual porosity is still present [397].

(iv) Temperature and atmosphere modification

One of the most important and most studied parameters (both in sessile drop and infiltration experiment) that can improve the wetting is the temperature. This parameter can influence the oxidation of the liquid surface that covers almost all metals, especially Al. Many studies showed that the wetting parameters of Al with many different ceramics decreases as the temperature increase [238, 243, 281, 284, 383, 398]. Tian *et al.* investigated both Al-SiC and Al 12wt.pct.Si-SiC from the melting temperature up to 1300K and noted that the threshold pressure has a drop at around 1173K since the contact angle drops from 125° at 1173K to 118° for pure Al and 115° for Al-Si [243]. This pressure drop was explained by the disappearance of the oxide layer that at low temperature covers the L-V interface (see Section 2.2.5). Another interesting observation was that the higher

2.7. Infiltration of liquid metal into ceramic preforms: data

the temperature, the faster the infiltration rate is; this is explained by the lowering of the viscosity of the liquid [279]. An increase in temperature can also increase the interaction between the solid and the liquid promoting wetting such as infiltration of Al in B₄C or SiC [399, 400]. Chong *et al.* showed that the porosity of the SiC-Al based alloy composite can be reduced by increasing the melt superheat [281].

Another external parameter that can be modified is the atmosphere. In the literature, the main investigated atmospheres are air, argon, argon/hydrogen and nitrogen/hydrogen. It was shown by Narciso *et al.* that wetting during infiltration of Al into preforms of different ceramic particles can be improved if an inert or reductive atmosphere is used [383]. Oh *et al.* confirmed the results noting that in air a thick oxide layer is formed at the L-V interface leading to a higher threshold pressure [238]. A different trend has been documented for Cu infiltrating Al₂O₃ particles. In the presence of oxygen, the copper dissolves partially the gas (up to 5%) and spontaneous infiltration can be achieved. The main reason of this excellent wettability is the absorption of oxygen at the L-S interface [136, 262] lowering the work of immersion, leading in turn to a lower pressure needed for full infiltration.

2.7.2 Chemical reaction during infiltration

Drainage curves have been investigated for inert systems where sessile drop experiments show that the contact angle does not change with time and the system reaches a thermodynamic equilibrium rapidly. Sessile drop experiments show also that for some systems, the contact angle changes with time, for example because the metal reacts with the oxide of the substrate or directly with the atmosphere, if it has a low but finite oxygen partial pressure [36, 111, 125, 128, 401]. Some models have also been investigated in order to understand the spreading of a sessile drop at high temperature both for ceramic-metal systems and for metal-metal systems, where intermetallic phases can be formed [112, 216, 402, 403].

From sessile drop data, two classes can be distinguished, namely reactions that are dominated by local interfacial reactivity, and those for which diffusion of the reactant to the site of reaction through the liquid is rate-limiting [1, 116].

Metal-ceramic systems are generally non-wetting [1], meaning that the work to be furnished to the system to effect infiltration is always positive. A reaction product, either oxide or carbide for metal-ceramic systems, that is created at the interface can reduce the contact angle since some carbides or oxides have a metallic behaviour. Reactions are mainly exothermic, which implies a high heat dissipation, which can induce an instability on the temperature [404]. For this reason, the exothermicity of the reaction reactions has to be known. Another point to take into account is the kinetics of reaction [39, 88, 405]. Some investigations were made for reactive systems during infiltration, in order to synthesise *in-situ* a different reinforcement as a function of alloying elements and/or substrate composition.

Hilling highlighted the infiltration product of the classic $Si_{(l)} + C_{(s)} \Rightarrow SiC_{(s)}$ system, which is one of the most studied reaction systems [406] both using pure silicon and silicon alloyed with

inert metals. The other system that has been investigated is the infiltration of liquid Al in a variety of different substrates in order to form oxides, nitrides and aluminates.

Dhandapani *et al.* investigated the reactivity of Al-Si alloys into a pre-oxidised SiC porous preform. The formation of small Al₂O₃ precipitates due to the reaction of the liquid with the oxidised layer on the particle surface was observed. It was also shown that the temperature plays an important role in determining the kinetics of reaction and infiltration: the higher the temperature, the faster the metal reacts with the oxide layer [407]. Singh and Behrendt investigated the mechanical properties of a Si-5at.pct.Nb infiltrated into packed carbon preform. It was shown that all the carbon is consumed by the reaction with the Si, forming SiC. The results were confirmed by XRD analysis where only SiC, Si, and NbSi₂ were found [408]. These authors performed the same process for a Si-3.2at.pct.Mo into porous graphite and found that, by changing the alloying elements the final composite was made of, the same SiC but with MoSi₂ instead of NbSi₂ and no Mo carbides having formed [388]. Chakrabati and Das also investigated the effect of Si alloyed with Mo infiltrating petroleum coke preform mixed with commercial SiC powder. The obtained composites showed a density of around 95% of the theoretical density and it was shown that the reaction happens at the interface with the liquid Si-Mo alloy, independently of the Mo concentration. It was also shown that in the solidified composite some MoSi₂ intermetallics were formed and that the composite shows a smooth and sharp SiC-MoSi₂ interface [409].

Hozer and Chiang investigated two different binary alloys infiltrated into porous graphite, namely Cu-Si and Al-Si at high temperature. They noticed that in order to have spontaneous infiltration, both systems need a temperature much higher than the liquidus temperature. For both systems, the entire graphite preform reacts with the liquid metal leaving a pure β -SiC reinforcement surrounded by the binary alloy [410]. Sangsuwan *et al.* investigated the influence of pore size on the infiltration of pure Si into microporous graphite preform and found that the permeability of the preform may play a role on pore closing induced by the chemical reaction [411].

Bougiouri *et al.* studied the reaction between a NiSi alloy and a porous graphite substrate in the sessile drop experiment configuration under vacuum: a metal alloy drop is placed over the porous graphite, and the rate of metal ingress into the graphite is measured. Different Si concentrations were analysed, namely 21at.pct., 47at.pct. and 67at.pct. There was a marked difference between the first and the two other concentrations since the first alloy did not form a wetting system and there was then no spontaneous infiltration through the porous substrate. On the other hand, the high Si alloys showed a wetting behaviour ($\theta = 40^\circ$) and under the droplet a wide region was infiltrated. Infiltrated regions showing SiC crystallite formation along the liquid-solid interface inside the substrate, and the authors noted that the condition for a wetting system is the formation of a SiC layer at the interface, which promotes pressureless infiltration [386, 387]. Eustathopoulos *et al.* investigated with the same experimental set-up the difference between pure liquid Si on two different substrates, namely graphite and oxidised Si₃N₄. They noted that, in the case of the Si-C couple, spreading and

2.7. Infiltration of liquid metal into ceramic preforms: data

infiltration are governed only by the local chemical process happening at the triple line, where the geometry of the pores has little influence on the infiltration, and the spreading rate is only slightly higher than the infiltration rate. They noted that, with Si alloyed to a non-reactive metal, due to the necessary diffusion of Si through the liquid, the spreading as well as the infiltration may be modified. On the other hand, the Si-oxidised Si_3N_4 couple shows a bigger difference between the spreading rate and the infiltration rate (the latter being several orders of magnitude slower) due to the presence of gaseous SiO at the infiltration front before reaction. This leads to a dependence on the pore geometry, a behaviour to be expected in all systems producing a gaseous specie at the infiltration front [412].

The first study that analysed the drainage curve of a reactive metallic system was performed by Molina-Jordá *et al.* on the system Al-SiC/ Al_2O_3 and Al 12.2at.pct.Si-SiC/ Al_2O_3 in pressure infiltration. They observed a dependence of the measured drainage curve on the pressurizing rate (and hence on the infiltration time). This was attributed to the reaction of the Al with the SiO_2 at the powder surface or to the formation of carbide by reaction of SiC with the liquid Al. They also noted that even if a reaction is present at the interface, infiltration does not become spontaneous: a pressure is always needed in order to fully infiltrate the preform [255].

Chen and Chung investigated the synthesis of Ni_3Al by infiltrating pure aluminium into a porous nickel preform. They showed that it was possible to form a homogeneous nickel aluminide reinforcement and highlighted the importance of pore volume fraction since if the preform has a high pore volume (42% porosity), the sample will contain some residual aluminium in between the grains of Ni_3Al while if the preform is dense (22% porosity) no metallic aluminium is found in the final sample, proving the complete reaction between the liquid and the solid [413]. Similar reactions were investigated by San Marchi and Mortensen, infiltrating pure Al into aligned Ni wire bundles with a volume fraction between 40 and 76% Ni. They found that the reaction between the molten Al and the solid Ni forms a large NiAl region. They noted that at the beginning the reaction rate is relatively slow, the reaction showing an incubation time, and that later, due to the reaction's exothermicity, there is a local melting of the Ni fibres which accelerates the reaction considerably [414]. Venkatesh and Dunand infiltrated liquid Al into a bed formed by Ni wires similar to the work by San Marchi and Mortensen. The composite contained no trace of the Ni fibres meaning that the reaction was fully completed. They also investigated the creep strength of the reacted composite comparing their results with literature data for a "normally" obtained NiAl-Al composite and found similar results. They added tungsten fibres prior to infiltration and showed that liquid Al reacts only with the Ni fibres leaving the W fibres unchanged. The creep strength was found similar to the normal composite showing once again the the reaction created stoichiometric NiAl having the same properties as the "normal" intermetallic [415].

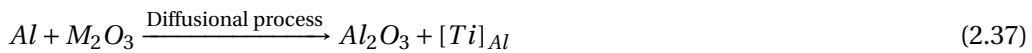
Kobashi and Choh investigated the effect of Al infiltration in different nitrides and oxides in the presence of a metallic precursor in order to form aluminates at the interface. They showed that Al in the presence of NiO cannot be infiltrated since an Al_2O_3 layer is formed at the liquid front. By adding TiB_2 to the ceramic powder, full spontaneous infiltration was achieved. The

Chapter 2. Literature review

authors justified this by the fact that the TiB_2 reduces the temperature reached due to the exothermic reaction between Al and NiO. The composite microstructure featured a mixture of Al_2O_3 and Al_3Ni proving that the reaction consumed totally the initial solid substrate. These authors then investigated the effect of boron nitride in the presence of Ti or Ta infiltrated with pure Al. They found that both Ti and Ta prefer bonding with the boron in order to form TiB_2 and TaB_2 while the Al reacts with the N to form AlN. Both systems have a similar reaction path, starting with the reaction between the two metals, which later react with the BN to form the respective borides and nitrides. For the Ti-BN system, the reaction is immediate while for the Ta-BN system, the reaction displays an incubation period to allow the Ta to react with the molten Al and later start the reaction with the ceramic [416, 417].

Another study investigating the effect of molten aluminium on different ceramic particles was performed by Kevorkijan, who investigated the kinetics of reaction between the liquid Al and the solid ceramic observing the length of the infiltrated path versus the temperature. From the data he deduced that the reaction between the liquid and the solid is a thermally activated process and is not dictated by the viscosity of the molten metal [389].

Wagner *et al.* investigated the infiltration of liquid aluminium into a mixture of titanium oxide and alumina forming $TiAl_3-Al_2O_3$ reinforced composites. By XRD analyses, they showed that the TiO_2 was completely consumed and replaced with $TiAl_3$ since only its peak with that of pure Al and Al_2O_3 were found [418]. Gheorghe and Rack investigated the process behind the reaction of molten Al infiltrating TiO_2 and forming Al_3Ti and Al_2O_3 . It was shown that the reaction fully consumes the starting oxide. Upon DSC analysis, they stated that the reaction follows the steps:



where M can be both Al and Ti. This means that the first step is the reduction of the TiO_2 into M_2O_3 and the residual Ti is dissolved into the liquid Al. Successively, the Ti atoms of M_2O_3 are slowly replaced by Al to form Al_2O_3 , a transformation which does not affect the shape of the whiskers. Finally the Ti dissolved in the liquid Al reacts to form the final Al_3Ti leaving a composite made of Al_3Ti and Al_2O_3 within an Al matrix. This is made possible because the liquid is oversaturated with Ti [419].

Another investigation on the reaction between molten aluminium and SiO_2 was performed by Yoshikawa *et al.* where they infiltrated pure Al into SiO_2 . At $1100^\circ C$ pressureless infiltration was obtained. The SiO_2 was fully consumed by the reaction and the final composite was composed of Si dissolved in Al as a matrix and $\alpha-Al_2O_3$. These results were confirmed by XRD

where only Al and α -Al₂O₃ peaks were found. This system too showed an incubation time, after which the reaction started, taking place at the interface and leading to the SiO₂ being fully consumed [420].

Swaminathan *et al.* investigated the reaction of a molten Al-Mg alloy infiltrated in Al₂O₃ in a N₂ atmosphere in order to promote the formation of AlN at high temperature (at low temperature the reaction does not happen). They showed the importance of the Mg acting as a getter in order to reduce further the oxygen partial pressure and promote the formation of AlN. They also found that the reaction is promoted at higher temperature. Having a higher amount of AlN in the composite increases the hardness of the composite for the temperature range analysed [421].

Rambo *et al.* investigated the effect of Cu-10at.pct.Ti alloy infiltrating spontaneously a 3D printed carbon preform. They noted that the obtained TiC_x has a carbon index of 0.78 after full infiltration. Since the preform was 3D printed, the porosity was high, yet the presence of residual carbon was observed. Following their EDX measurements, they found that the lowered Ti concentration in the matrix was related to the amount of TiC produced [422]. A different approach of forming a TiC reinforced composite was investigated by Wang *et al.* by mixing C and Ti and spontaneously infiltrating the mixture with magnesium alloy (AZ91D). The reaction happened during the infiltration and they showed that by reinforcing the alloy with the *in-situ* formed TiC, the tensile strength is improved, especially at high temperature [423].

Zhang *et al.* investigated the pressureless infiltration of liquid Al into NbO₂ in order to form a NbAl₃/Al₂O₃ reinforced Al composite similar to the works of Swaminathan *et al.*, Gheorghe and Rack, Kobashi and Choh, and Rambo *et al.*. The results was similar, showing full reaction between the solid and the liquid with the formation of niobium trialuminate in a Al matrix [424].

As Bougiouri *et al.* and Eustathopoulos *et al.*, Zhao *et al.* used the sessile drop experiment in order to investigate the interaction between Zr₂Cu on a polycrystalline WC substrate. The contact angle measured starts at 100° and stabilises between 41° and 28° (as a function of the temperature) at its equilibrium position, meaning that the system becomes wetting after the reaction. It was found that the liquid reacts with the carbide in order to form ZrC while W precipitates at the interface [425]. The authors successfully produced fully infiltrated samples using this technique and found that the mechanical properties such as hardness, flexural strength and fracture toughness of the composite are comparable to values in the literature obtained by a composite of ZrC and W produced by sintering [426].

2.8 Definition of the aim of the study

As seen, the infiltration of a liquid through a porous medium has been a largely investigated topic, both in soil science and petroleum engineering, and also in metallurgical engineering. In all three domains, capillarity has most precisely been quantified by means of drainage

Chapter 2. Literature review

curves, measured in quasi-static infiltration without any interaction between the liquid and the solid. The aim of the present work is to investigate to which extent the experimental approach that underlies the measurement of drainage curves can be extended to quantify infiltration in the presence of kinetic interaction phenomena occurring between the liquid infiltrant and the solid preform, be this a chemical interaction or another process; as shown by the preceding literature review, such an approach has not been developed to date.

3 Reactive pressure infiltration of Cu-46at.pct. Si into carbon

3.1 Disclaimer

This chapter has been submitted to Acta Materialia and is under consideration after revision. The preprinted version of this article is presented here below. The candidate, herewith G.S., designed and carried all experiments. The manuscript was written by G.S.. Ludger Weber (L.W.) and Andreas Mortensen (A.M.) provided supervision throughout the whole duration of this work. L.W. and A.M. revised, corrected and approved the manuscript.

Gionata Schneider, Ludger Weber, Andreas Mortensen, "Reactive pressure infiltration of Cu-46at.pct. Si into carbon", Published in Acta Materialia on the 15th of September 2019.

3.2 Abstract

We explore how reaction at the interface between a solid porous ceramic and an infiltrating molten metal influences wetting in pressure infiltration, wetting being characterized by a drainage curve that plots the metal saturation versus the applied metal pressure. Specifically, we infiltrate Cu-46at.pct. Si into graphite preforms at 1050°C, 1100°C, 1150°C or 1200°C. The Si in the copper alloy reacts with the graphite to form SiC, which is better wetted by the alloy compared to the initial graphite. We show that, unlike what is observed in non-reactive systems, at fixed applied pressure reaction prevents stabilization of the metal saturation and causes the metal to continuously flow into the preform. Interpreting the data under the assumption that the applied pressure influences the local rate of thermally activated triple line motion as does the applied stress the rate of thermally activated motion of dislocations, measured infiltration velocities can be exploited to deduce both an activation volume and an activation energy for the interfacial process that governs reaction-driven motion of the triple line in this system. The resulting activation volume is on the order of one to a few 100 nm^3 , leading to estimated activation energy values of a few times $100 \frac{\text{kJ}}{\text{mol}}$. Both are realistic for a process that is limited by the rate of SiC growth along the metal/graphite interface.

3.3 Introduction

Metal-ceramic systems are usually non-wetting, meaning that the contact angle θ formed at the Solid(S)-Liquid(L)-Vapour(V) triple line is higher than 90° [89, 120, 233, 427]. Common examples of this are Cu/Al₂O₃ and Cu/C_{Gr} under vacuum or inert gas, for which θ exceeds 130° [18, 25, 115], or Al/Al₂O₃ where θ is 100° under vacuum at the Al melting point [115].

In some metal-ceramic systems, wetting can be improved if there is, between the liquid metal or one of its alloying elements and the ceramic substrate, a chemical reaction causing the formation along the liquid/solid interface of a new phase that is better wetted by the metal than is the initial ceramic. Examples of such systems are Cu-Ti/Al₂O₃ [23, 99, 105], Cu-Ti/C_{Gr} [18, 23], Cu-Si/C_{Gr} [101, 110, 111, 117], Cu-Cr/C_{Gr} [39] or Al-C_{Gr} [111].

The presence of such a chemical reaction causes wetting characteristics of the system to become time-dependent. In sessile drop experiments the contact angles becomes a function of time. Wetting can then also be influenced, in various ways, by phenomena that govern the rate of liquid/solid reaction and/or the diffusion rate of the reactive element(s).

Unlike the sessile drop experiment, where wetting can be characterised using a few scalars, wetting as relevant to pressure infiltration is generally characterized by measuring drainage curves, which plot the fraction of liquid filling the pores of the solid “preform” to be infiltrated versus the differential applied pressure between the liquid and the atmosphere initially filling the preform (generally vacuum or a gas). Saturation measurements are conducted once liquid motion has stopped so that capillary forces alone determine the saturation level; examples of such measurements as pertinent to the pressure infiltration of ceramic preforms by liquid metals can be found in many references; examples are in [3, 249, 252, 253] for systems having engineering relevance, and also in mercury porosimetry frequently used to characterize the open pore geometry of fine-scale porous solids [428].

When interfacial chemical reaction is present, there is an interplay between reaction kinetics and the rate of ingress of the infiltrant into the porous medium: time then becomes an additional parameter of the system, which adds a new dimension to the characterization of wetting by means of drainage curve measurements. An illustration of complications that can arise in the measurement of wetting as it relates to pressure infiltration can be found in [255].

We present in what follows a study of reaction-driven infiltration using the Cu-46at.pct. Si-C system. This system is chosen because it is well-known in the sessile-drop literature and, unlike much more reactive systems where reaction drives the spontaneous penetration of melts into porous preforms [387, 412, 429], it features finite contact angles and a slow interfacial reaction whereby silicon and carbon form SiC, the latter being better wetted by the alloy than graphite [78, 97, 101, 108, 117, 118]. Sessile drop data indicate that, in this system, the spreading rate of the liquid alloy on flat carbon substrates is governed by the local reaction rate and not by that of reactant diffusion through the liquid to the triple line. More specifically, when a liquid drop of this alloy enters in contact with a solid carbon substrate, the contact angle θ

is initially between 140° [97] and 120° [101, 117, 118], and remains stable for the first 250s, until interface reaction starts. θ then decreases until it stabilizes at 45° [97, 101, 114, 118] once reaction is completed. This final contact angle is the same as that for Cu-40at.pct. Si on SiC, which implies that all the interface has changed from C to SiC during the reaction and that the influence on the S-L-V equilibrium of alloy Si depletion is negligible in the sessile-drop configuration. Dezellus *et al.* [101, 117] furthermore provide a quantitative model, which for this system explains observed wetting kinetics in the sessile drop configuration.

We present here data from drainage curve measurements for this system. We interpret those experiments using a parallel which has been made before in the seminal work of Gil Sevillano and Kubin [430, 431], between the thermally activated rate of motion of a triple line in pressure infiltration, and the rate of thermally activated dislocation motion within plastically deforming crystals. As will be seen, the parallel opens, in this system at least, a venue for the investigation of physical processes that underlie pressure infiltration in the presence of kinetic effects at the gaseous atmosphere/liquid/solid triple line.

3.4 Experimental Procedures

3.4.1 Materials

Porous graphite preforms used in this work were machined into cylinders of height 15 ± 0.03 mm and diameter 13 ± 0.03 mm from a block of EDM200 graphite purchased from Poco Graphite, Inc. (Limonest, France). The volume fraction of open pores in the graphite preform, V_p , was measured by mercury porosimetry and found to be 0.72. With mercury, of surface tension $450 \frac{mJ}{m^2}$ [68], the contact angle on graphite is strongly non-wetting and stable (124° [432]). Corresponding (reaction-free) drainage curves are given in Fig. 3.1.

The Cu-46at.pct. Si alloy was prepared in our laboratory using a high-vacuum induction furnace. The chamber atmosphere was initially purged five times with argon. The metal was then molten under an Ar pressure of 0.8 bar, starting from pure copper (> 99.9% pure) and pure silicon (> 99.99% pure). The alloy concentration was analysed with X-Ray Fluorescence (XRF) using an Orbis PC Micro EDXRF (AMETEK, Berwyn, PA, USA) analyser (50kV and 1mA) equipped with an Apollo XRF-ML50 Silicon drift detector with an energy resolution lower than 135eV in Mn $K\alpha$. The results gave an average concentration of 46 ± 2 at.pct. Si, deemed satisfactory given that wetting kinetics of graphite by copper containing Si do not differ qualitatively across the range from 40 to 50at.pct. Si [101, 117].

3.4.2 Infiltration velocity measurements

We characterize in what follows the kinetics of infiltration by measuring the rate of change with time of the metal saturation S , defined as the fraction of preform open pore space that has been filled with metal. In order to measure this rate of infiltration, we use an apparatus that can track

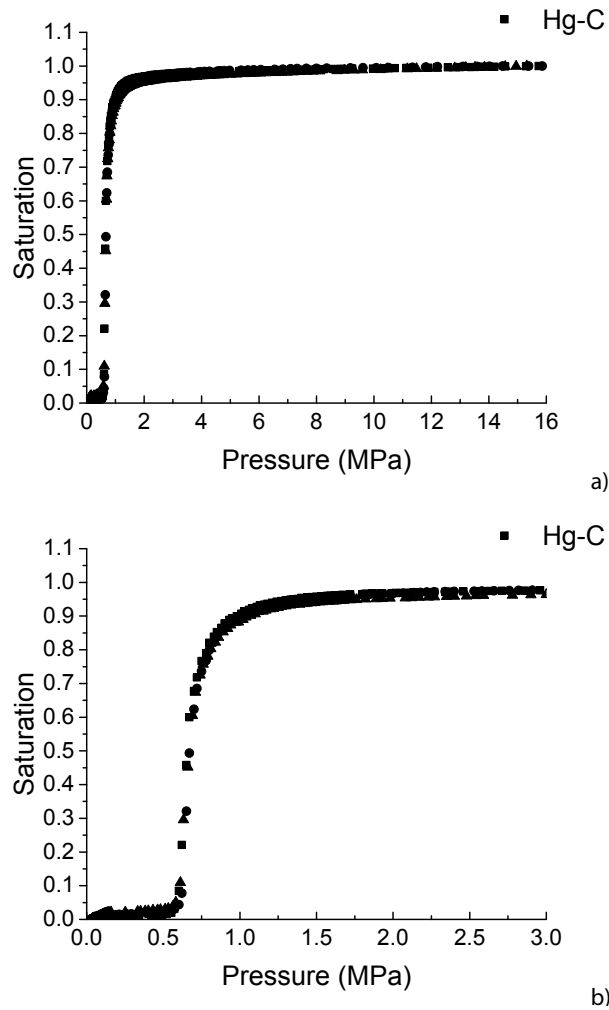


Figure 3.1: Mercury infiltration porosimetry curves measured on three separate graphite preforms of the type used in this work. a) full drainage curve, b) zoom on the first part of the drainage curve.

dynamically, to a precision of $\pm 2\mu\text{m}$, the altitude h of the liquid metal surface [253, 256, 296] (a sketch of the apparatus can be found in Fig. 2 of Ref. [296]). Tracking of the rate of metal ingress into the preform is achieved by placing, above the ingot, a plunger connected to a rod that follows the displacement of the liquid level. This displacement is measured, through a window at the top of the pressure vessel, by optical means. The rate of change of h times the cross-sectional area of the metal crucible at that location then gives the volumetric rate of metal ingress into the porous graphite preform. Given values of the total preform pore volume and the crucible cross-sectional area, the above precision in metal altitude translates into a precision in metal saturation S on the order of 0.001 (for a typical average total displacement of 2mm; the influence of error in crucible cross-sectional area is comparatively negligible).

In a system where there is no thermally activated process driving infiltration, at fixed pressure the rate of infiltration gradually slows down, causing the capillary number (which measure the ratio of viscous to capillary forces) to fall. Eventually, the system reaches capillary equilibrium and fluid flow stops. The metal level then stabilizes at a value corresponding to a fixed saturation S characteristic of initial (non-wetting) metal ingress (“drainage”) into the preform at the current value of applied pressure P . Further infiltration requires P to be increased. Increasing the pressure step by step and letting the metal saturation equilibrate at each step, one can then trace the drainage curve characteristic of the system at hand; examples for mercury are in Fig. 3.1. Such measurements, classical in areas such as soil science, reservoir engineering or mercury porosimetry, have also been reported for the high-temperature pressure infiltration of engineering metals into non-reactive solid porous “preforms”, generally with an aim to produce composite materials [2, 3, 247, 249, 251–253, 256–258, 293–296, 433].

As the present experiments will show, in the presence of kinetic phenomena that enable thermal activation to drive the metal past obstacles that limit its ingress (when the invading fluid is non-wetting, these are narrow constrictions that separate wider pore volumes), such stabilization is not observed. Rather, under fixed pressure, the triple line of contact of the metal meniscus with the solid phase continues to advance, as it does in sessile drop experiments with reactive systems. This drives more metal volume into the preform, at a rate governed by whatever process enables the triple line to move past obstacles that otherwise hinder its motion.

Measuring a single drainage curve characteristic of the system is then no longer possible since capillary equilibrium is never reached. Rather, what one may then measure is the rate of metal ingress at the applied pressure in question and its dependence on temperature and pressure. This is what we do in the present work, alternating the applied pressure between two values, namely the threshold pressure $P_1 = P_{th}$ and $P_2 = P_{th} + 0.05\text{MPa}$.

Metal ingress velocity measurements of this work were conducted over a range of saturation values that starts right after the onset of infiltration ($S \approx 0$) until $S \approx 0.85$, at which point measured velocities became too small to be measurable. At that point, in order to fully infiltrate the preform (which eases subsequent metallographic preparation of the sample), the pressure was increased rapidly to an elevated value (12MPa) at which the preform was fully infiltrated, the final saturation thus corresponding to $S=1$.

In a typical experiment, the graphite preform is placed under an ingot of Cu-46at.pct. Si inside an alumina crucible. The preform is prevented from floating while the metal is molten by wedging a small disk of graphite foil between the crucible and the preform to block mechanically motion of the preform relative to the crucible wall. With the assembly in place within the pressure infiltration apparatus, it is closed and evacuated by means of a mechanical pump. The crucible is then heated under vacuum to the desired temperature.

Once the desired infiltration temperature is reached, Ar gas is injected into the chamber, gradually under increasing pressure, until motion of the metal surface indicates that metal has

started to enter the preform. At this threshold pressure (which corresponds to the percolation threshold for infiltration of the unreacted preform by the alloy), the onset of infiltration is relatively abrupt and thus easily detected. The pressure at which this happens is the (percolation) threshold pressure P_{th} for infiltration, at the relevant temperature, of the unreacted preform by the molten Cu-46at.pct. Si alloy.

Once observable rapid infiltration has been initiated at the (threshold) pressure P_{th} , the pressure is further increased to exceed P_{th} by 0.05MPa. Then, pressurisation is halted and the pressure P is kept constant at that value. Once the rate of liquid displacement has reached a steady state value during 120s, P is decreased by 0.05MPa and again kept constant. Once again the system is let to stabilise until a steady state velocity is reached during 120 s. The pressure is then increased again to $P_{th}+0.05\text{MPa}$ and this cycle is repeated until the steady velocity becomes, at high saturation values, too small to be measurable.

“Steady” fixed-pressure infiltration velocities were more specifically measured as follows. After each change in pressure, the rate of metal ingress is seen to go through a transient. This is as observed in non-reactive systems; however, here the rate of metal flow does not fall to zero and S does not reach a stable value. Rather, it is a stable rate of saturation increase that we seek to measure. Measured infiltration rates were here only collected once $\frac{dh}{dt}$ computed over 20 data points along a sliding rule running over the curve giving h versus t at fixed pressure had stabilized to yield a fit with $R^2 \geq 0.99$ over a two-minute time span, with data collected at 5 Hz. Then, the rate of infiltration $\frac{dS}{dt}$ was computed by linear regression of the last (stabilized) set of data points, each being an average of 25 datapoints of the raw data, over a period of 100s (corresponding to 20 averaged data points), to obtain a measure of the saturation velocity at given temperature, pressure and saturation. Finally, a similar experiment was conducted using pure copper as the infiltrant (from the same source as the metal that was used to produce the alloys). The goal of this experiment was to show that, in the absence of silicon in the alloy, one does not observe the slow isobaric steady infiltration that one observes in infiltration with Cu-46at.pct. Si into carbon.

3.5 Results

3.5.1 Infiltration kinetics

Figure 3.2 gives raw plots of h and P versus t over an entire typical infiltration experiment, and also gives a view of data at higher magnification to show how $\frac{dS}{dt}$ values were measured by the above linear regression method. As seen, although infiltration rates do eventually stabilize, infiltration rates vary (in diverse ways) before a relatively steady rate can be measured over 100s, a time interval that was chosen as a compromise between gleaning measurements for relatively steady infiltration on one hand, and obtaining a sufficient number of points for comparison of the influence of pressure or saturation on the infiltration velocity on the other hand.

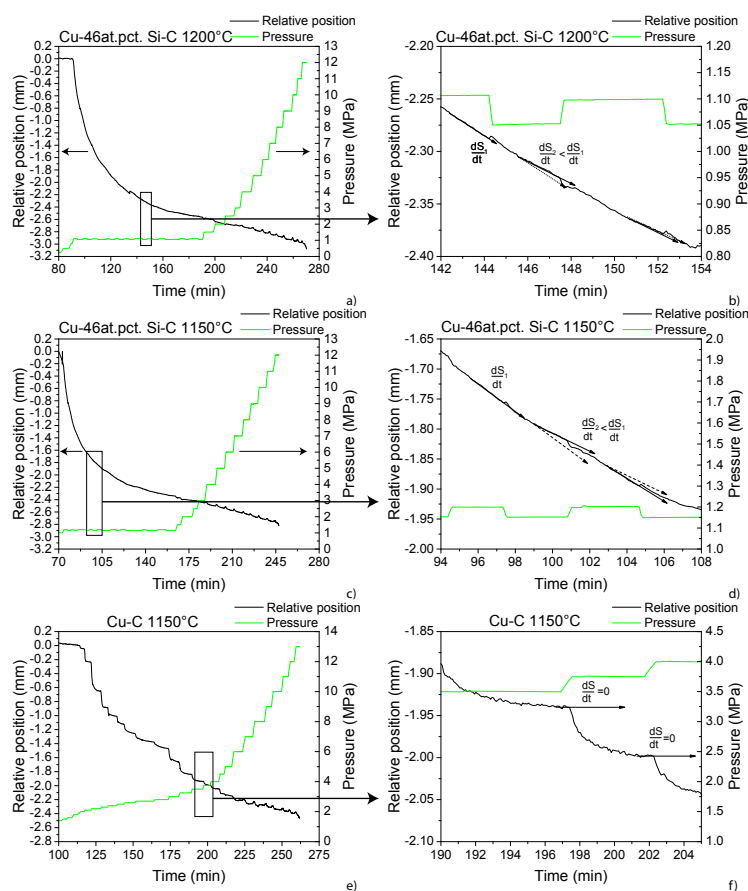


Figure 3.2: Infiltration of Cu-46at.pct. Si into C, a) and b) at 1200°C and c) and d) at 1150°C a) and c) raw data: h and P versus t over an entire infiltration experiment, showing up to $t = 190\text{min.}$ for 1200°C and $t = 160\text{min.}$ for 1150°C the regime of alternating pressures between $P = P_{th}$ and $P = P_{th} + 0.05\text{MPa}$ and beyond $t = 190\text{min.}$ or $t = 160\text{min.}$ the regime of stepwise increasing pressure conducted to reach $S=1$, b) and c) zoom over a pressure cycle to highlight the change of velocity and the measurement of $\frac{dS}{dt}$. The dotted arrow show the velocity at the previous pressure. Figures e) and f): corresponding curves for the infiltration of pure Cu into the same C preforms, showing that in the absence of Si in the alloy one observes stabilization of the saturation at fixed pressure after isobaric holds similar to those used in the CuSi reactive infiltration experiments.

Figures 3.2 (e, f) give similar data for infiltration of the same preforms in the absence of silicon. As seen, with pure copper, after a few minutes' time, $\frac{dS}{dt}$ falls to zero, showing stabilization of the infiltration front and an absence of the “creeping” isobaric infiltration that is observed with the reactive alloy. Two experiments with Cu46at.pct. Si were conducted, respectively at 1100°C and 1150°C with a low driving pressure (0.15MPa), to show that there is no spontaneous penetration of the alloy into the evacuated carbon preforms. After a four hour hold of the preforms in contact with the molten alloy, there was indeed no penetration of the alloy into the carbon preforms.

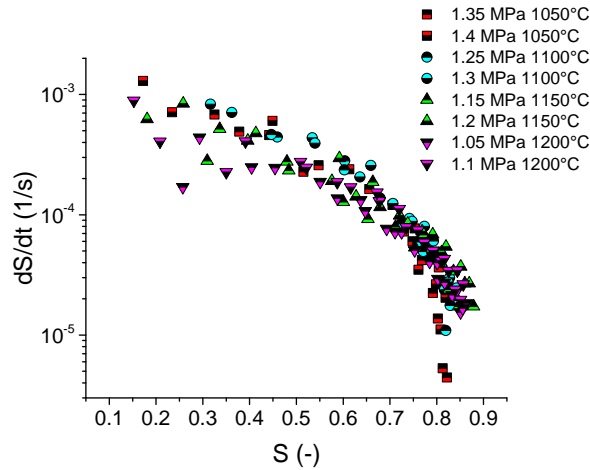


Figure 3.3: Experimental infiltration velocities $\frac{dS}{dt}$ measured over time just above P_{th} at four different temperatures: 1050°C (red), 1100°C (turquoise), 1150°C (green) and 1200°C (blue).

Figure 3.3 plots all measured values of $\frac{dS}{dt}$ for porous graphite infiltrated with Cu-46at.pct. Si under stepwise pressure change between $P_1 = P_{th}$ and $P_2 = P_{th} + 0.05\text{MPa}$ at the four different temperatures of this work, namely 1050°C, 1100°C, 1150°C and 1200°C. The experiments are repeated twice for each temperature. Error bars are not added to the graph so as to keep it readable; given the somewhat erratic transients that S showed after each pressure change, the uncertainty on measured values of $\frac{dS}{dt}$ goes beyond uncertainty in the measurement of h and is likely to be well above 10%.

3.5.2 Composite microstructure

Microstructures of fully infiltrated composites were characterized, after standard metallographic polishing, by means of secondary electron (SE) scanning electron microscopy (SEM). Phases were identified using point energy dispersive X-ray analysis (EDX).

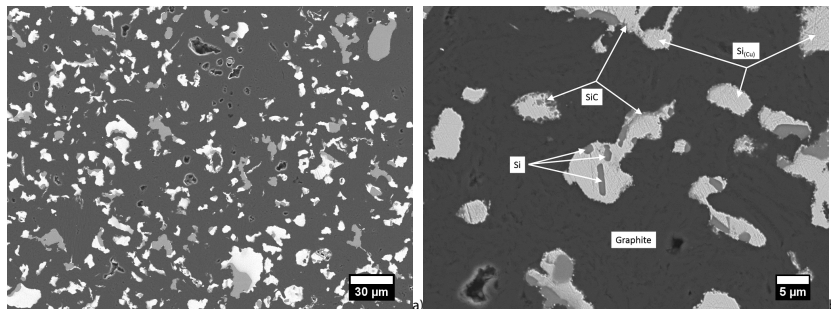


Figure 3.4: Microstructure of the composite after infiltration at 1050°C and 12MPa, a) low magnification, b) high magnification.

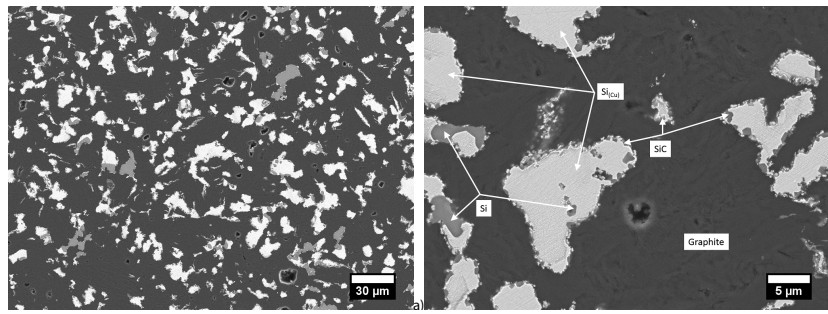


Figure 3.5: Microstructure of the composite after infiltration at 1100°C and 12MPa, a) low magnification, b) high magnification.

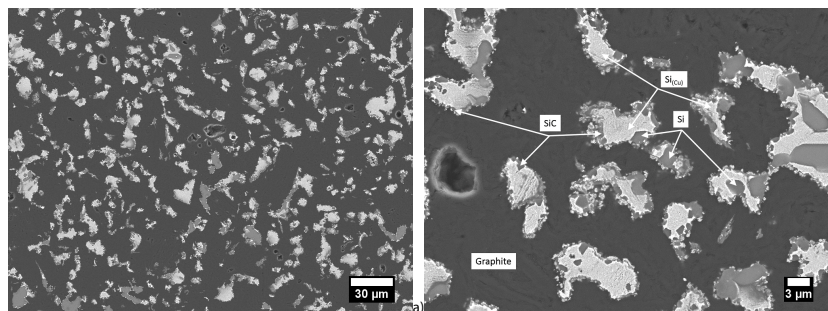


Figure 3.6: Microstructure of the composite after infiltration at 1150°C and 12MPa, a) low magnification, b) high magnification.

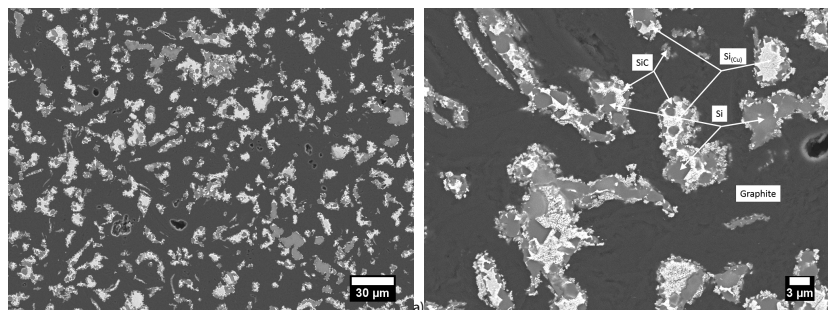


Figure 3.7: Microstructure of the composite after infiltration at 1200°C and 12MPa, a) low magnification, b) high magnification.

Figures 3.4, 3.5, 3.6 and 3.7 show the microstructure of the solidified composite after full infiltration at 1050°C, 1100°C, 1150°C, and 1200°C, respectively. All composites show the presence of a reaction product containing both Si and C, very likely to be SiC. With increasing temperature, the SiC layer at the graphite-alloy interface becomes thicker.

Fig. 3.8 shows an Energy Dispersive X-Ray (EDX) compositional map of the composite infiltrated at 1200°C and 12MPa for the three elements present in the composite. As seen, there is a lower concentration of Si on the bright part, which is the Cu-Si alloy, while at the interface with the preform the Si concentration increases.

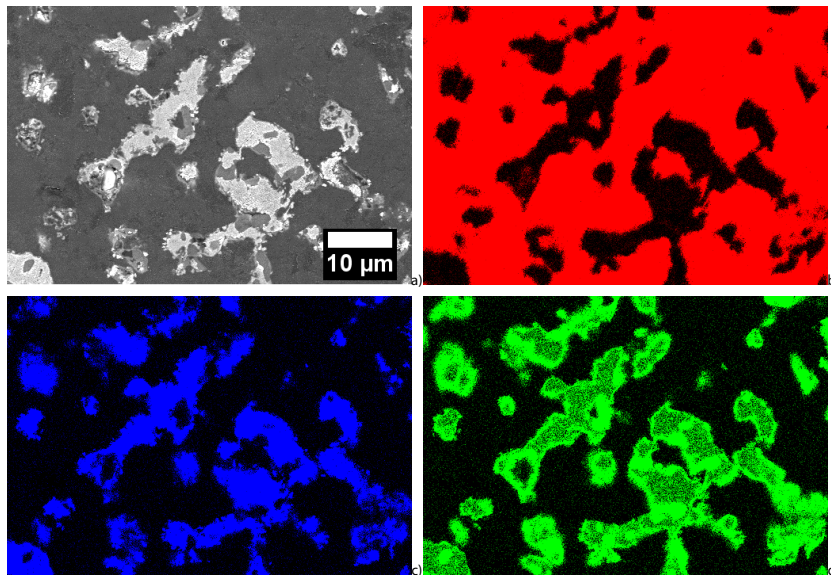


Figure 3.8: EDX mapping of the composite infiltrated at 1200°C and 12MPa, a) SE image, b) C map, c) Cu map and d) Si map.

X-Ray Diffraction (XRD) analyses were additionally conducted using a Philips X'Pert X-Ray with a diffractometer equipped with a Cu- K_{α} source on two composites infiltrated at 1050°C and 1150°C respectively. The working conditions are 45KV for the tension and 40mA for the current. Phase analysis was conducted using an Oxford Instrument mounted in the SEM. The software ETAS[®] INCA v7.0. Figure 3.9 displays collected spectra from the two composites. Data show the presence of graphite (the preform), SiC (the reaction product), Cu₃Si (an intermetallic of the matrix), Cu (the matrix with Si in solid solution), and Si (precipitates within the matrix).

Recapitulating, SEM images of the fully infiltrated composite (Figs. 3.4, 3.5, 3.6, 3.7 and 3.9) show that the graphite preform reacts with the Cu-Si matrix alloy during infiltration, forming at the interface a phase rich in both Si and C, which XRD spectra (Fig. 3.8) confirm to be SiC. Comparing the microstructures of the composites infiltrated at different temperature, one sees that if the temperature is increased, more SiC is formed at the interface. This is also confirmed by the presence of pure Si precipitates in the metal after infiltration at low temperature (between 1050°C and 1150°C) while after infiltration at 1200°C Si precipitates are not present in the composite. EDX measurements made on the metal within the infiltrated region after infiltration at 1200°C, which is the highest temperature explored and hence has the highest amount of SiC formed (and hence the highest degree of Si depletion from the alloy) of samples produced in this work, show an average Si concentration of around 25at.pct. This value is below the eutectic composition (31at.pct, [434]) and above the minimum concentration for CuSi alloys to form SiC in contact with carbon (documented to be in the range of 12 to 16at.pct. Si [110, 435]), in agreement with the dual observations of SiC formation and absence of Si in the final solidified alloy after infiltration at the elevated temperatures explored here.

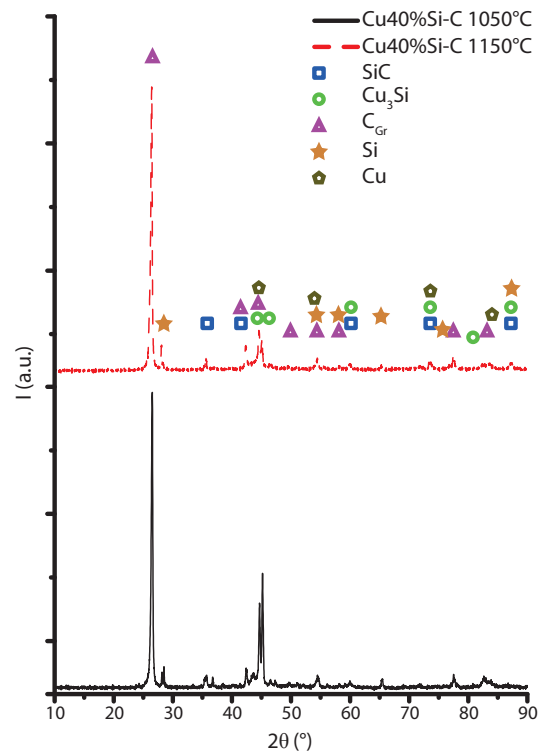


Figure 3.9: XRD spectra for of the composite infiltrated at 1050°C (black curve) and 1150°C (red curve) with the relative phase.

3.6 Discussion

To summarize, despite significant scatter in the data, we show that:

1. if one pressurizes molten Cu-46at.pct. Si to a pressure slightly (by 0.05MPa) above the threshold pressure for sudden penetration of the melt into (unreacted) microporous graphite preforms, after filling rapidly a limited portion of the preform, the metal does not reach capillary equilibration. Instead, it progresses continuously into the preform, its saturation S increasing gradually over time to approach $S = 1$.
2. Microstructural data confirm that contact between the metal alloy and the carbon preform leads to the formation of SiC along the pore surface, the amount of SiC formed increasing with increasing infiltration temperature. Silicon carbide is better wetted by the molten alloy than the initial carbon surface, so its formation explains why the metal continuously invades the preform under fixed applied pressure: interfacial reaction changes the solid preform surface to one that the metal wets well, gradually driving the (initially non-wetting) metal past narrow constrictions that initially blocked its ingress into open pores of the unreacted preform.

3. The rate $\frac{dS}{dt}$ at which the metal progresses into the preform at the threshold pressure P_{th} or at $P_{th}+0.05\text{MPa}$ depends relatively little on temperature in the range from 1050 to 1200°C, see Fig. 3.3. On the other hand $\frac{dS}{dt}$ depends measurably on (i) the level of metal saturation S that has been reached after gradual (reaction-driven) ingress of the metal into the preform and (ii) on the value of the applied pressure P that drives the metal into the preform. A decrease in applied pressure from $P_{th}+0.05\text{MPa}$ to P_{th} decreases the rate of infiltration $\frac{dS}{dt}$ by a factor that varies around a value near one-half, regardless both of temperature or S ; see Fig. 3.10(a).

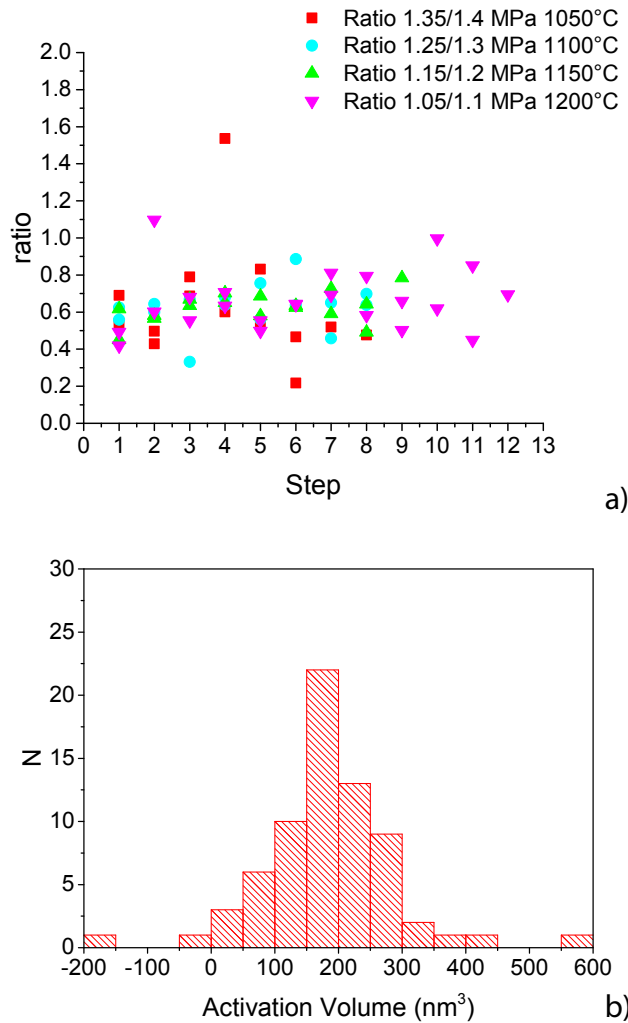


Figure 3.10: a) Ratio between measured rates of saturation increase across two successive stepped downward pressure changes across all experiments of this work, b) histogram of the distribution of the activation volume values deduced from Eq. 3.2 for each step across all experiments.

This third observation is *a priori* puzzling. Indeed, the rate of SiC growth, and hence the rate of reaction-driven penetration of the preform by the metal, should *a priori* depend strongly

on temperature. This is observed in sessile-drop experiments, where the rate of motion of the triple line driving reactive wetting of carbon by a drop of Cu-40 or 50at.pct. Si is well documented to increase strongly with temperature within the range explored here [77, 117].

Why does the observed rate of reaction-driven penetration of the preforms depend so little on temperature? We propose that the explanation lies in the role of the applied pressure in driving the metal into the preform.

The applied pressure may influence infiltration in two ways. One is that a higher pressure will increase the range of pores that can, all else constant including capillary forces at the triple line, be infiltrated by the metal. This effect might play a role in the present experiments; however, we note that the applied pressure values in the present experiments correspond to the pressure at which sudden initial ingress of the preform is observed, P_{th} , and to that value plus 0.05MPa, at each of the four temperatures explored. Given the high rate of initial metal ingress into the preform at the initiation of infiltration (see Fig. 3.2) we may assume that P_{th} values measured here correspond to, or at least approach, the (percolation-governed) threshold pressure for purely mechanically-driven pressure infiltration of the unreacted preform at the relevant temperature. Assuming that such is the case, one may then expect the (percolation-dominated) metal front geometry and the range of pores that can be rapidly infiltrated by the metal at the given (temperature-dependent) applied pressure to be roughly the same across all four temperatures explored, since experiments were conducted at roughly the same point of the process whereby the alloy is driven mechanically, by the sole action of pressure, into the unreacted preform. The geometry of infiltration flow paths being similar across the four temperatures, infiltration rates should then vary according to a simple Arrhenius law. They do not, suggesting that another explanation applies.

We propose that the influence exerted by the applied pressure on the reaction-driven pressure infiltration process is exerted more locally, at the level of the triple line of liquid/solid/vapour contact. In other words we assume that the reason why the observed rates of reaction-driven infiltration of the preform at all four temperatures are roughly the same is that the rate of reaction-driven motion of the alloy triple line itself depends also on the applied pressure. Specifically, we propose that the local rate of reaction-driven, thermally activated, forward motion of the triple line across each constriction that temporarily blocks its advance depends not only on the temperature, but also on the value of the pressure that pushes the metal forward. We base this interpretation of the present data on an analogy with the physics of thermally activated plastic deformation, this being a percolation process that has strong analogies with pressure infiltration, as was pointed out by Gil Sevillano and Kubin [430, 431] in a seminal paper that made the link between (invasion) percolation and dislocational plasticity.

In the dislocational plastic deformation of solid crystals, an applied (shear) stress pushes linear dislocations to move along crystalline planes past a series of obstacles. In pressure infiltration, a two-dimensional liquid surface is pushed by an applied pressure differential through an irregularly shaped labyrinth of voids delineated by a solid, which is contacted by the liquid

surface along the triple line of liquid/solid/vapour (L-S-V) mutual contact. In both cases, motion of the moving dislocation line or (meniscus surface) triple line is often limited by an irregular array of discrete obstacles: solute atoms, precipitates or forest dislocations for moving dislocations, narrow constrictions of the solid pore space in pressure infiltration of porous solids with non-wetting liquids. As was already noted by Gil Sevillano, Kubin *et al.* [430, 431], both phenomena fall in the same general class of invasion percolation phenomena, and show general features thereof (scaling, fractal formation, ...) [252, 253, 430, 431]. Now, it is well-known that, in the plastic deformation of crystals, thermal activation can assist dislocations in bypassing obstacles that limit their motion through the crystal [436]. As shown by the present data, the same visibly holds true in pressure infiltration, for example when (as is the case here) liquid/solid chemical interaction gradually decreases the wetting angle at narrower constriction points of the open pore space, known to be obstacles that limit ingress of a poorly wetting liquid into the porous medium.

By analogy with the theory of thermally activated plastic deformation [436, 437], we thus posit that the pressure P influences local processes that drive forward motion of the L-S-V triple line in the same way as the applied stress influences the thermally activated motion of a dislocation, i.e.:

$$\frac{dS}{dt} \propto \exp\left(\frac{-Q + V_a P}{k_B T}\right) \quad (3.1)$$

where Q is the activation energy of the thermally activated phenomenon by which obstacles limiting motion of the liquid surface through the solid preform pore space are overcome, P the pressure difference between the liquid medium and the vapour in the preform, k_B is the Boltzmann constant and T is temperature. V_a is an activation volume; this is, in addition to Q , a characteristic of the thermally activated process that drives gradual ingress of the liquid into pores within the solid under a finite applied pressure differential P .

Rearranging Eq. 3.1 one deduces that it should be possible to measure V_a if all else (including T and S) can be held constant. To do so, infiltration velocities are to be compared at two different pressures P_1 and P_2 for the same value of T and S :

$$\left. \begin{aligned} \frac{dS_1}{dt} \propto \exp\left(\frac{-Q + V_a P_1}{k_B T}\right) \\ \frac{dS_2}{dt} \propto \exp\left(\frac{-Q + V_a P_2}{k_B T}\right) \end{aligned} \right\} \begin{aligned} \ln\left(\frac{dS_1}{dt}\right) &= A + \frac{-Q}{k_B T} + \frac{V_a P_1}{k_B T} \\ \ln\left(\frac{dS_2}{dt}\right) &= A + \frac{-Q}{k_B T} + \frac{V_a P_2}{k_B T} \end{aligned}$$

$$\ln\left(\frac{dS_1}{dt}\right) - \ln\left(\frac{dS_2}{dt}\right) = \frac{V_a(P_2 - P_1)}{k_B T} \Rightarrow V_a = -\ln\left(\frac{dS_1/dt}{dS_2/dt}\right) \cdot \frac{k_B T}{\Delta P} \quad (3.2)$$

where $\Delta P = P_2 - P_1$ and $\left(\frac{dS_i}{dt}\right)$ is the measured velocity at pressure P_i .

In dislocational plasticity, the similarly defined activation volume V_a (with strain replacing the saturation S and the applied shear stress replacing the pressure P) is more rigorously viewed as an activation area times the burgers vector length $b = \|\vec{b}\|$. V_a then represents b times the total area swept in its glide plane by the dislocation as it overcomes, by means of the relevant thermally activated process while aided by the applied stress, each obstacle that hinders its movement in the direction imposed by the applied stress [436, 438].

Building on the parallel, in pressure infiltration we expect $V_a \cdot P$ to represent a reduction, contributed through work done via the applied pressure, of the energy barrier that must be overcome for the triple line of liquid/solid/vapour contact to move forward so that the infiltration front can bypass, by means of a thermally activated process, the pinning point at which its advance was blocked. Physically, given that in pressure infiltration it is a local process, occurring at the triple line, that is likely to drive forward motion of the meniscus, we expect this work to also be expressible as the liquid surface tension projected onto the direction of forward meniscus motion, times the area (width times distance of advance) swept by the triple line as it jumps forward by means of the relevant thermally activated process to free itself of the pinning point, so that it can move forward and invade the next pore(s) along its trajectory, thus increasing the saturation S , Fig. 3.11.

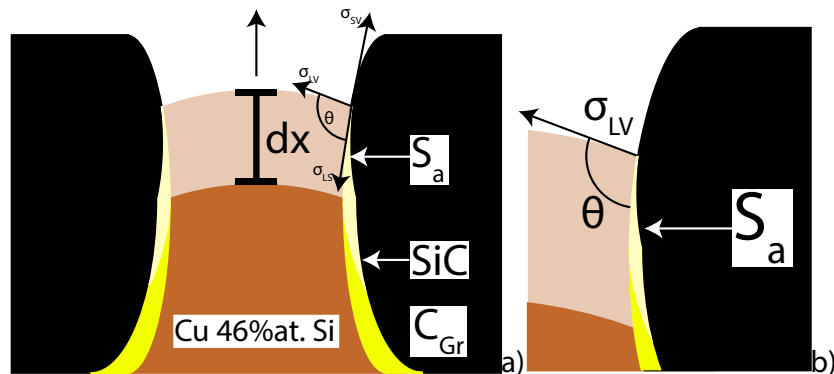


Figure 3.11: Schematic representation of the activation surface S_a for a small advancement of the infiltration front dx due to the creation of a small layer of reaction product. a) General view, b) zoom on the triple line.

Figure 3.10 (b) shows the histogram of all the activation volumes calculated using Eq. 3.2 for each pressure change step across all experiments, grouping the results using a bin size of $50nm^3$. As seen, most values congregate around $200 \pm 100nm^3$. We use in what follows the average value over all experimental points, namely $187 nm^3$ to compensate measured infiltration rates for the influence exerted by the applied pressure by multiplication of measured near-steady infiltration rate values $\frac{dS}{dt}$ with $\exp\left(\frac{-V_a P}{k_B T}\right)$. This gives Fig. 3.12. As seen, once one compensates for the effect of decreasing pressure at increasing temperature, resulting pressure-compensated infiltration rates increase significantly with increasing temperature.

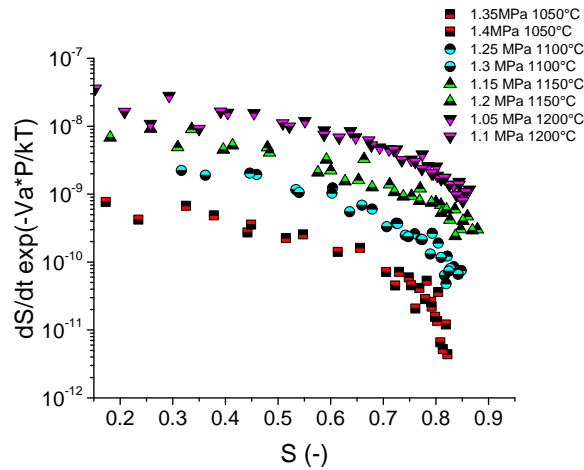


Figure 3.12: Pressure-compensated velocities calculated from experimental values using Eq. 3.1 with $V_a=187\text{ nm}^3$ at 1050°C (red), 1100°C (turquoise), 1150°C (green) and 1200°C (blue).

Having now the pressure-compensated velocities at different temperatures, we can draw an Arrhenius plot in order to find whether one can calculate a corresponding activation energy for the thermally activated process that drives forward motion of the infiltration front. The result is in Fig. 3.13. As seen, corresponding rates of infiltration, measured by the pressure-compensated rate of saturation increase at varying temperature and saturation, delineate for each value of S a relatively linear and steady relation consistent with an activation energy $Q = 440 \pm 40 \frac{\text{kJ}}{\text{mol}}$ governing the reactive infiltration process. These values are the average and standard deviation of calculated activation energy values at eight different saturations (0.5-0.85 S). In more detail one sees that the computed activation energy is quite constant at low saturation, while it increases somewhat as the saturation increases. This is likely a result of experimental uncertainty: at high saturation the velocities drop to very low values (see Fig. 3.13), such that the uncertainty on Q over those values is higher.

Comparing with the literature, $Q \approx 440 \frac{\text{kJ}}{\text{mol}}$ is well below the activation energy for bulk diffusion through SiC (above $700 \frac{\text{kJ}}{\text{mol}}$) [439, 440] and comes closer to the activation energy for grain boundary diffusion of C through SiC, which is documented to lie between 560 and $250 \frac{\text{kJ}}{\text{mol}}$ [440–446]; however, as noted below, based on the detailed study by Dezellus *et al.* [117] of the wetting of graphite by Cu-Si alloys, it is most likely that this activation energy value reflects the rupture of C-C bonds in the reaction leading to the formation of SiC, for which Dezellus *et al.* [117] found $Q=270 \frac{\text{kJ}}{\text{mol}}$.

How does this study indeed relate to previous work on the reactive wetting of carbon by Cu-Si alloys? A previous study from Dezellus *et al.* [117] characterizes, using the sessile drop technique, the rate of motion of the triple line due to the reaction at the interface of Cu-40 or 50at.pct. Si on carbon and proposes a model to explain observed triple line motion rates. Their data show that there is a relation between the rate of motion of the triple line and the instantaneous volume of the contact angle θ : in this system, the local rate of motion of the

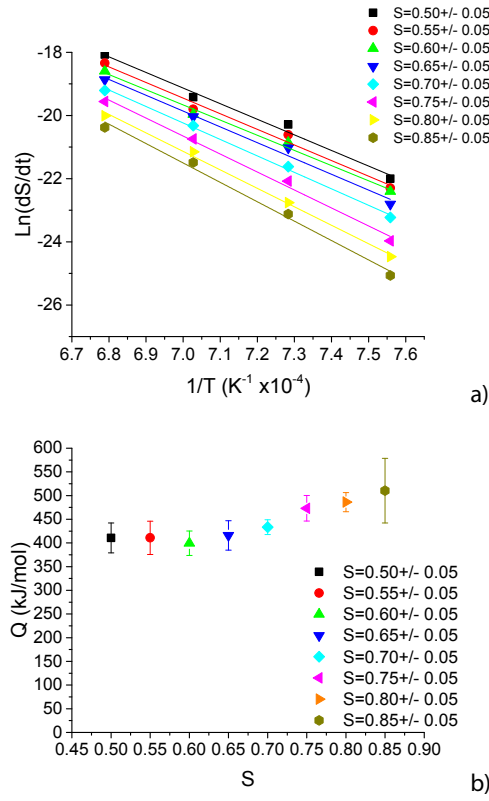


Figure 3.13: a) Arrhenius plot at different saturations for the four temperatures analysed assuming $V_a = 187 \text{ nm}^3$, b) activation energy calculated from the slope of the Arrhenius plot.

triple line is not a constant, consistent with assumptions underlying the present analysis of our data. Dezellus *et al.* [117] link the rate of triple line motion to the instantaneous contact angle θ by deriving, for a constant drop value, a relation between θ , the radius of the droplet R , the local extent of reaction at the triple line using the Cassie equation [447] and the rate of SiC formation along the surface of carbon, assumed to follow first order reaction kinetics. The end result is an equation linking the spreading rate $U = dR/dt$ and the instantaneous contact angle θ as:

$$\frac{U}{F(\theta)} = \exp\left(-\frac{Q}{k_B T}\right) K \left(\frac{3V}{\pi}\right)^{1/3} (\cos\theta_F - \cos\theta) \quad (3.3)$$

where Q is the activation energy, k_b is the Boltzmann constant, T the temperature, K is a kinetic constant, V is the drop volume and θ_F is the equilibrium contact angle of the alloy on SiC (found to be 35°). The function $F(\theta)$ is expressed as:

$$F(\theta) = -\frac{\cos\theta(2 - 3\cos\theta + \cos^3\theta) - \sin^4\theta}{\sin\theta(2 - 3\cos\theta + \cos^3\theta)^{4/3}} \quad (3.4)$$

Now in comparing data and model across our study and that of Dezellus *et al.*, one finds that

local pressures within the sessile drops of Dezellus *et al.* (which can be estimated knowing the volume, contact angle and surface tension of the alloy drop) are only on the order of 1 kPa. With $V_a \approx 200 \text{ nm}^3$, this brings $\exp\left(\frac{-V_a P}{k_B T}\right)$ very near unity. With pressure changes $\Delta P = P_2 - P_1$ in our experiments on the order of 5% of the applied pressure P , the change $\Delta\theta$ in local contact angle θ along triple lines of contact of the liquid with the solid carbon preform upon a pressure change during infiltration will also be on the order of 5% of θ (since the derivative of $\cos\theta$ is on the order of θ). Changes by a few hundredths of a radian in θ will not, according to equations (3.3) and (3.4), change the triple line rate of motion U by a factor near two. The model of Dezellus *et al.*, hence, does not explain the present data.

The two investigations in fact explore different regimes of reactive wetting: here, the applied pressure is far higher, and thus plays a role that is absent from sessile drop data. Putting together the two studies, that of Dezellus *et al.* conducted using the sessile drop technique and that of this work conducted using instrumented pressure infiltration experiments, one may surmise that the rate of advance of the triple line U could be governed by a combination of both equations leading to:

$$U = \exp\left(\frac{-Q + V_a P}{k_B T}\right) \cdot KF(\theta) \left(\frac{3V}{\pi}\right)^{1/3} (\cos\theta_F - \cos\theta) \quad (3.5)$$

Another way of combining the two studies is to assume that the activation energy for this system remains at the value measured (with higher precision than here) by Dezellus *et al.*, namely $Q=270 \frac{\text{kJ}}{\text{mol}}$ ([117]). Using this value, we can back-calculate the activation volume that best fits present data, using Eq.(3.1). This gives $V_a=135 \text{ nm}^3$ consistent, within uncertainty, with present data, Fig. 3.10(b).

With a conclusion that the thermally activated phenomenon that governs the rate of advance of the reacting (pressurized) liquid meniscus through the graphite preforms is on the order of one to a few times 100 nm^3 , we can reflect on what this measurement implies. Physically, (again by analogy with dislocational plasticity), V_a is the net volume of liquid that is pushed forward by the applied pressure during the thermally activated event by which a meniscus overcomes a pinning point. V_a values on the order of a one or a few times 100 nm^3 are small on the scale of the pore-level infiltration process, since pores in the present preforms are on the order of one to a few micrometres wide (see micrographs above; with V_a on the order of one to a few times 100 nm^3 , a meniscus of area $1 \mu\text{m}^2$ would be moving forward by a distance on the order of 10^{-27+12} metres or 10^{-5} angstrom, as the obstacle is overcome, which is not realistic). Most likely, therefore, the event by which the meniscus and triple line bypass pinning points is highly localized, and involves only a short segment of the triple line advancing forward by a short distance (likely here by the nucleation and growth of a small SiC crystal), past which the meniscus becomes unstable and spontaneously invades the next pore. Such a process bears resemblance with that by which a dislocation line glides forward by the thermally activated nucleation of (subsequently unstable) double kinks.

3.7 Conclusion

In the pressure infiltration of Cu-46at.pct. Si into graphite preforms at 1050°C, 1100°C, 1150°C or 1200°C, one observes that:

- contrary to what is found with non-reactive systems, at fixed pressure past the (percolation) threshold for forced penetration of the metal into the preform, the saturation does not reach a steady value; instead, the metal saturation steadily increases under a fixed applied pressure;
- when increasing/decreasing the applied pressure by a small amount, one observes a corresponding increase/decrease in the rate of steady infiltration under fixed pressure;
- microstructural analysis shows that the alloy reacts with the graphite preform, forming SiC as a reaction product along the interface, the SiC layer thickness increasing as the temperature increases.
- Infiltration rate data of this work can be interpreted using the same framework as is used to interpret thermally activated dislocational plasticity. This leads to the definition of an activation volume characteristic of the role played by the applied pressure on the process of reaction-driven infiltration; in the present system this activation volume equals a few times 100 nm^3 .
- This interpretation in turn leads to estimate the activation energy characteristic of the present reactive infiltration process by means of an Arrhenius plot. The thus derived value is consistent with previous work on reactive wetting in this system, suggesting that the gradual isobaric infiltration process is driven by SiC formation at a rate likely governed by the rupture of C-C bonds.
- Comparing presents results with sessile drop data of Dezellus *et al.* leads to conclude that both studies are mutually consistent but explore highly different regimes of reactive wetting.

3.8 Acknowledgement

This work was sponsored by the Swiss National Science Foundation (SNSF), Project No. 200021_149899. We gratefully acknowledge several enlightening discussions with Professor F. Stellacci, of EPFL, Professor W. C. Carter, of MIT, and Prof. J.-M. Molina-Jorda of the University of Alicante, over the course of this investigation..

4 Kinetic processes in the high temperature pressure-infiltration of Al into Al_2O_3

4.1 Disclaimer

This chapter will be submitted in a scientific journal. The preprinted version of this article is presented here below. The candidate, herewith G.S., designed and carried the infiltration experiments. G.S. and Marta Fornabaio (M.F) synthesized the β'' -AA10 powder and conducted the XRD measurements. The manuscript was written by G.S.. Ludger Weber (L.W.) and Andreas Mortensen (A.M.) provided supervision throughout the whole duration of this work. M.F, L.W. and A.M. revised, corrected and approved the manuscript.

Gionata Schneider, Marta Fornabaio, Ludger Weber, Andreas Mortensen, “Kinetic processes in the high temperature pressure-infiltration of Al into Al_2O_3 ”, to be submitted.

4.2 Abstract

We explore the influence (i) of the interaction between aluminium and alumina, and (ii) of sodium impurities present in Bayer alumina, on the pressure infiltration of alumina particle preforms with molten aluminium. At 1000°C or above, although the aluminium/alumina system is non-reactive, capillarity-driven solution-precipitation processes cause the liquid solid interface to become mobile. Data show that this can result in infiltration kinetics that resemble those observed with reaction-driven pressure infiltration, namely a continuously increasing melt saturation under fixed infiltration pressure. Resulting isobaric saturation velocities are measured at 1000°C, 1050°C and 1100°C. The role of alumina particle shape and of Na-containing inclusions is investigated. It is found that the main factors affecting the rate of high-temperature isobaric infiltration in this system are the particle shape and size. Measured steady infiltration rates give an activation volume on the order of $\approx 200\text{nm}^3$ and an activation energy in the range of 300-500 $\frac{\text{kJ}}{\text{mol}}$, suggesting that isobaric infiltration kinetics are governed by diffusion through the solid alumina. Sodium impurities of Bayer alumina are present within β'' - Al_2O_3 . They do not influence steady pressure infiltration rates but ease initial melt penetration into the preform, possibly because evaporated Na_2O alters the oxide

skin layer that lines the surface of molten aluminium.

4.3 Introduction

Pressure infiltration, one of the main processing methods used in the production of metal matrix composites (MMCs), consists in pushing a liquid metal into a porous refractory (ceramic, carbon or metal) “preform”, followed by solidification of the melt. Pressure is applied in this process to overcome capillary forces, as these usually resist penetration of the metal melt into the preform because the contact angle θ formed at the Solid-Liquid-Vapour (S-L-V) triple line is well above 0° [89, 120, 233, 427] in most molten metal/solid ceramic systems.

Often, at the high temperatures characteristic of metallurgical processes such as infiltration, metal/preform materials interact through various kinetic phenomena that can cause θ to depend on time. If the solid and liquid phases react, a new L-S interface phase may form and gradually change the degree of wetting of the solid by the liquid. In the absence of interfacial reaction, substrate dissolution and reprecipitation may cause ridging of the L-S interface, leading again the apparent contact angle measured in a sessile drop experiment to become a function of time, similar to what is observed with reactive systems [15, 16, 121, 131, 206].

Time-dependent wetting is manifest in pressure infiltration by the fact that saturation (a.k.a. “drainage”) curves, commonly used to characterize wetting of a given preform by a given infiltrant, cannot be measured because at fixed pressure the melt saturation no longer stabilizes. Instead, interfacial interaction between the liquid and the solid substrate lead to a steadily moving infiltration front even though the applied pressure driving the metal into the preform is kept constant. Such gradual isobaric pressure infiltration has recently been documented for a reactive system, namely a copper-silicon alloy infiltrating porous carbon [41]. Here, the interaction between the liquid and the solid leads to the formation of SiC which, being better wetted by the melt than is carbon, drives a steady advancement of the front at fixed pressure [41].

It was shown in Ref. [41] that a parallel can be drawn between the kinetics of elevated temperature pressure infiltration and the kinetics of high-temperature plasticity. Both processes involve the stress-driven, thermally activated, forward motion of a line (the L/S/V triple line or the dislocation line, respectively) past a series of fixed obstacles. Both processes have the same basic input parameters, namely temperature and applied stress, while the measured output parameter is, respectively, the rate of infiltration and the rate of plastic deformation.

In elevated temperature plasticity, the rate of deformation is often described as a thermally activated process, the activation energy of which is reduced by the product of an activation volume times the applied stress. It was shown in Ref. [41] that the kinetics of reactive copper-silicon alloy infiltrating porous carbon at fixed pressure can be described using this approach. Here, we apply the same methodology in the analysis and interpretation of infiltration rate measurements conducted on the non-reactive Al-Al₂O₃ system at 1000°C or higher.

This system has already been investigated by means of sessile drop experiments both at high (hundreds of degree above the aluminium melting point) and low (slightly above the Al melting point) temperatures ([5, 10, 16, 106, 115, 124, 169, 382]). The contact angle θ is known to decrease with increasing temperature, from 100° under vacuum near the Al melting point (660°C) down to roughly 70° at 1150°C .

The behaviour of this system in the context of pressure infiltration was studied by Léger *et al.* [253], who recorded saturation curves below 1000°C . At those lower temperatures, one observes a stabilization of the saturation S when the applied metal pressure P is kept constant. We show here that, at or above 1000°C , the saturation no longer stabilizes in this non-reactive system. This makes its behaviour similar to that of the reactive Cu-46at.pct. Si/graphite system. We show here that the same plasticity-inspired scheme can be used to analyse measured isobaric infiltration rates in this system.

With the aluminium/alumina system, a further complication arises at elevated temperature, in that sodium is present as an impurity in certain nominally pure alumina powders, including those that were used in the earlier study of Léger *et al.* [253]. Sodium impurities in alumina powder are quite common due to the use of NaOH in the Bayer process [448]: this can leave residual Na atoms in the alumina, which are then generally present within inclusions of the $\text{NaAl}_{11}\text{O}_{17}$ ($\text{Na}_2\text{O} \cdot 11\text{Al}_2\text{O}_3$) phase. This phase is named $\beta''\text{-Al}_2\text{O}_3$; it is a metastable [213, 449, 450] ion-conducting phase (which is used in sodium-sulphur batteries [212, 213, 449, 451]). The equilibrium phase in the $\text{Na}_2\text{O}\text{-Al}_2\text{O}_3$ system is called $\beta\text{-Al}_2\text{O}_3$ and is characterized by a lower $\text{Na}_2\text{O}:\text{Al}_2\text{O}_3$ ratio (1:7); however, $\beta''\text{-Al}_2\text{O}_3$ transforms to $\beta\text{-Al}_2\text{O}_3$ only above 1600°C and is hence often not observed in commercial alumina particles. At the high temperatures explored here, sodium atoms might intervene in the infiltration process. We therefore address here this issue as well, notably by analysing three alumina powders that differ in particle shape or composition, to separate the role played by the presence of sodium from that played by the particle geometry.

4.4 Experimental

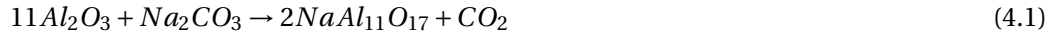
4.4.1 Materials

Ceramic samples were prepared using (i) an angular alumina $\alpha\text{-Al}_2\text{O}_3$ F1000 of average diameter $5\mu\text{m}$ purchased from Treibacher Schleifmittel (Laufenburg, Germany), or (ii) polygonal alumina $\alpha\text{-Al}_2\text{O}_3$ AA10 particles of average diameter $10\mu\text{m}$ from Sumitomo Chemical Co., Ltd. (Osaka, Japan). Powder X-Ray diffraction analyses reveal the presence in the F1000 powder of the Na-containing phase $\beta''\text{-Al}_2\text{O}_3$, together with $\alpha\text{-Al}_2\text{O}_3$. AA10 powder X-ray diffractograms show it to be pure $\alpha\text{-Al}_2\text{O}_3$.

In order to separate the effect of shape and composition of the alumina powders, a third powder was used here, namely a powder produced by reacting the pure alumina polygonal powder AA10 with sodium carbonate at 1300°C for 15h [212]. This results in the following

Chapter 4. Kinetic processes in the high temperature pressure-infiltration of Al into Al_2O_3

reaction:



thus giving the AA10 powder the same sodium-containing phase as the F-1000 Bayer alumina powder. Varying the reaction time and temperature, different molar ratios of $\text{Na}_2\text{O}:\text{Al}_2\text{O}_3$ can be produced. To reproduce as closely as possible the composition of the F1000 powder, AA10 powder was reacted to produce a ratio of 1:15 $\text{Na}_2\text{O}:\text{Al}_2\text{O}_3$. The so-produced powder has the same size and morphological features as the AA10 alumina powder, but a composition close to that of the F1000 alumina powder. It is hereafter named β'' -AA10.

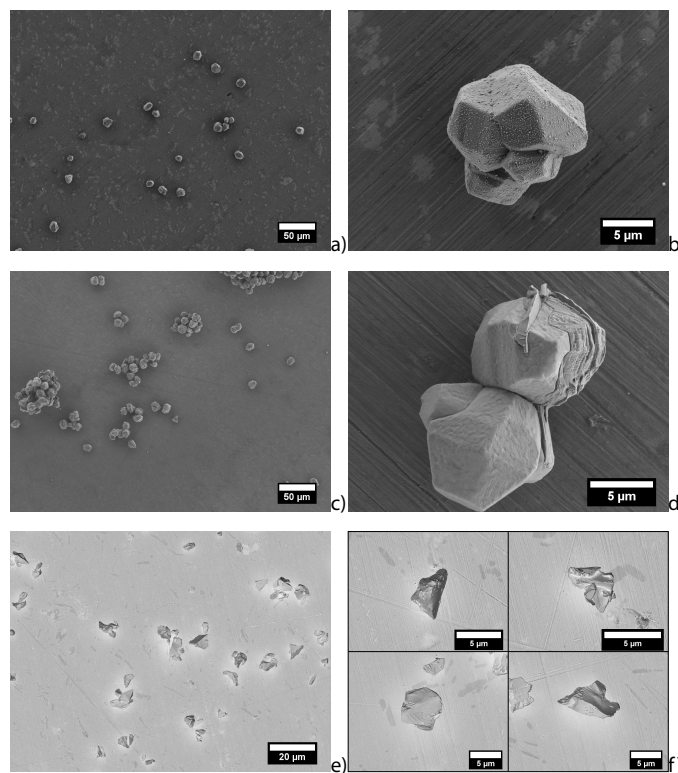


Figure 4.1: SE-SEM images of the three powders used, a) and b) AA10, c) and d) β'' -AA10 and e) and f) F1000.

To produce preforms for infiltration, alumina powders were compacted by cold isostatic pressing (CIP) at 150MPa for 1 minute. The produced CIPed preforms are cylinders approximately 14 mm in both diameter and height. The ceramic reinforcement volume fraction (V_r) in the composite was measured by characterisation of the composites after full infiltration at 700°C, by densitometry using a Sartorius MC210P microbalance of sensitivity $\pm 10\mu\text{g}$. The measured V_r for F1000 is 0.52 (same value found in [3, 252, 253, 296]). For β'' -AA10 and AA10 it is 0.58. For the metal matrix, 99.99% pure Al purchased from Hydro Aluminium GmbH

(Germany) was used as the infiltrant in all experiments reported here.

4.4.2 Gas-pressure infiltration

Infiltration experiments comprising a dynamic measurement of the saturation were conducted for F1000, AA10 and β'' -AA10 powder preforms infiltrated with molten aluminium at one of three temperatures, namely 1000°C, 1050°C or 1100°C. Each experiment was performed three times in order to test the reproducibility of the tests.

To have a reference state for the drainage curve of AA 10 powders at the same temperatures but in the presence of much slower metal/ceramic interaction, one experiment was conducted in which Copper (Cu 99.99%) was infiltrated into a preform of AA10 powder at 1150°C.

All infiltration experiments other than at 1150°C were conducted using an instrumented infiltration apparatus, by means of which one can track with comparatively high precision the volume of metal that has penetrated the preform while pressure is applied to drive infiltration. This apparatus and basic features of the experiments are described in Refs. [253, 256, 296].

To explore the role played by sodium impurities in pressure infiltration, we performed an additional Al-F1000 infiltration at 1150°C with the aim to characterize the composite microstructure after infiltration at that temperature and determine the nature of the oxide layer covering the melt after infiltration. The experiment consisted of producing a composite without tracking the fluid displacement (in order to have a clean liquid front on the top of the sample), holding the system at 1150°C for 4h under 4MPa applied pressure to effect full infiltration and to give ample time for metal/ceramic chemical interaction.

In the present work, focused on the kinetics of infiltration in the presence of preform/infiltrant interaction, instead of measuring saturation curves as was done in Refs. [253, 256, 296], we measure isobaric infiltration rates, using the same approach as in Ref. [41]. In a nutshell, after initiating infiltration once the applied pressure exceeds a threshold value P_{th} , we measure steady infiltration velocities at two different pressures that differ only slightly, changing the pressure several times during infiltration, so as to separate the influence of pressure and saturation on infiltration velocity at each temperature. As in Ref. [41], those two pressures are respectively the infiltration threshold pressure P_{th} at which the metal is observed to first penetrate the preform, and a value only slightly higher than this, namely $P_{th}+0.05\text{MPa}$.

In each infiltration experiment, once preform, metal, crucible and tracking system are assembled and placed within the apparatus and the apparatus is securely closed, the system is first evacuated and then heated to the desired temperature. The pressure is then increased until reaching the threshold pressure P_{th} , meaning until the tracking device records a displacement of the liquid front. Then, 0.05MPa is added to the applied pressure. The pressure is thereafter held at that value until the melt penetration rate becomes constant over at least 120s; more specifically, until $R^2 \geq 0.999$ over 120s in a dynamic linear regression over points of melt height versus time recorded with a frequency of 10Hz. The data used to compute the saturation

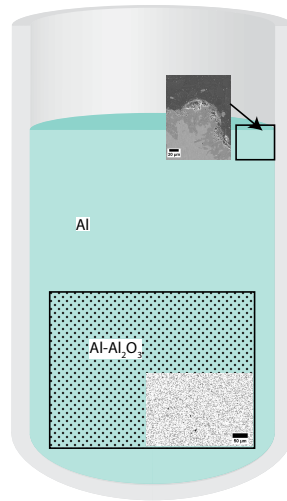


Figure 4.2: Schematic representation of a cross section through the Al-F1000 sample produced at 1150°C for 4h under a steady applied pressure of 4MPa. Light blue is Al; the rectangular area represents the Al- Al_2O_3 composite (in the inset is an optical image of its microstructure). Along the top surface a rectangle and the inset micrograph represent the region where the oxide layer covering the Al melt was investigated (see discussion).

velocity ($\frac{dS}{dt}$) are saved with a frequency of 0.2Hz. Once $\frac{dS}{dt}$ is recorded, the pressure is reduced by 0.05MPa, from $P_{th}+0.05\text{MPa}$ to P_{th} , and the rate of steady infiltration over 120s is measured following the same procedure and criterion. The pressure is then increased back to $P_{th}+0.05\text{MPa}$, and this process is repeated between the two pressures (P_{th} and $P_{th} + 0.05\text{MPa}$) until rates of infiltration are no longer measurable because steady infiltration rates decrease with increasing saturation. The pressure is then raised rapidly to 5MPa in order to fully infiltrate the composite and to record the total displacement of the fluid, as this later allows to calculate the saturation corresponding to each recorded melt surface level.

This process, of shifting the applied pressure from $P=P_{th}$ to $P=P_{th} + 0.05\text{MPa}$ and back after the front has reached a sufficiently steady velocity, was repeated several times during each infiltration experiment, the number of pressure changes being mostly a function of the time taken by the infiltration front to stabilise to a sufficiently steady and measurable saturation increase rate. The end result of those measurements is the rate of steady increase in saturation $\frac{dS}{dt}$ for each system as a function of three main parameters, namely the applied pressure, the saturation and the temperature, together with measures of the effect of pressure alone since this parameter was shifted rapidly several times at fixed temperature over a narrow range of saturation values. In effect, present experiments are the infiltration-analogue of stress-jump tests in high-temperature plasticity.

4.4.3 Composite characterization

Microstructural characterization of the composite was conducted using standard metallographic procedures, in which a cross-section of the composites is embedded in a polymeric resin and polished down to $1\mu\text{m}$ diamond paste. The morphology of Al_2O_3 particles after infiltration was revealed by soaking a polished cross section of the composite in a solution of NaOH 1[M] for 60s, followed by scanning electron microscopic characterisation of particles that remained attached to the composite surface.

The phase composition of powders (in as-received condition or within infiltrated composites) was analysed by means of a Philips X'Pert X-Ray Diffractometer (XRD) equipped with a $\text{Cu-K}\alpha$ source. Analyses were performed at 45kV and 40mA in a $5\text{-}90^\circ$ 2θ range.

Microscopy was conducted using a Zeiss[®] Merlin SEM (Carl Zeiss, Germany) scanning electron microscope. Local elemental compositions were investigated by EDX (Energy Dispersive X-Ray) analysis using an Oxford Instrument apparatus mounted in the SEM with a voltage of 10 keV and a probe current of 700 pA. The software ETAS[®] INCA v.7.0 was used to quantify EDX results.

4.5 Results

4.5.1 Isobaric infiltration kinetics

Al-F1000 system

Two representative full infiltration curves of the Al-F1000 system at 1000°C are shown in Fig. 4.3(a) and (c). The last sudden increase in pressure was conducted at elevated saturation, once the measured saturation increase rates had become too small to be measured with precision, so as to effect full infiltration of the ceramic preform.

Figures 4.3(b) and d) show close-ups over a portion of those curves. As seen, a change in the applied pressure causes a noticeable change in the saturation increase rate. This influence of the applied pressure on the infiltration rate was observed at all three temperatures of the present investigation. This differs from what was found at lower temperature in Ref. [253], where infiltration stabilized after some time, making possible at those temperatures the measurement of saturation curves, in which a single value of saturation characteristic of (static) capillary force equilibration is plotted for each value of the applied pressure.

Collating all infiltration velocity data for this system at 1000°C , 1050°C and 1100°C gives Figure 4.4. As seen, $\frac{dS}{dt}$ shows a relatively high degree of variability, yet it transpires from the data that (i) $\frac{dS}{dt}$ increases with increasing P at given saturation and temperature, (ii) decreases with increasing saturation and (iii) does not vary systematically with increasing temperature: rates are in fact lowest at the highest temperature.

Chapter 4. Kinetic processes in the high temperature pressure-infiltration of Al into Al_2O_3

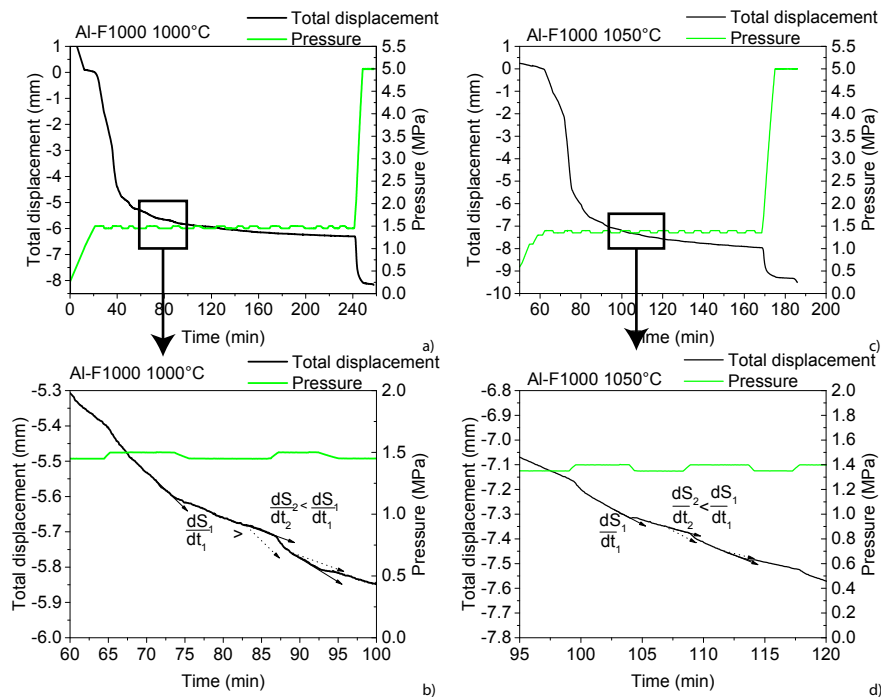


Figure 4.3: Raw data for infiltration at 1000°C (a) and b) and 1050°C (c) and d) of the Al-F1000 system; a) and c): full infiltration displacement, b) and d): zoom showing the changes in velocity after a small pressure drop.

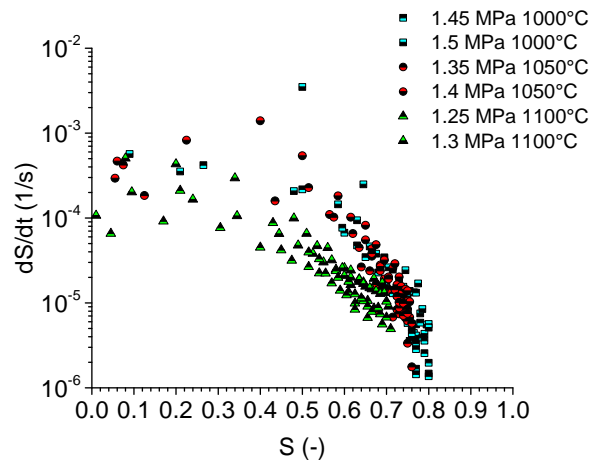


Figure 4.4: Raw saturation velocities at three different temperatures for Al-F1000 composite infiltration; 1000°C (squares), 1050°C (circles) and 1100°C (triangles).

Al-AA10 system

Illustrative infiltration curves for Al-AA10 alumina at 1000°C and 1100°C, similar to those given for the F-1000 powder, are in Fig. 4.5(a-b) and Fig. 4.5(c-d) respectively. As seen, unlike what is observed with the F1000 powder, with AA10 powders the front stabilizes after each

pressure change. The kinetic phenomenon responsible for the observation of sustained isobaric infiltration with the F1000 powder is thus either absent or much slower with the AA10 powder than it is with F1000 alumina.

Given that the front stabilizes with AA10, it is in principle possible to measure a drainage curve for this system. Such measurements were performed following the same procedure as was used for the Al-F1000 system in [253], where it was found that to obtain reproducible drainage curves with aluminium-containing melts at temperatures near the metal or alloy melting point, one had to first preheat the system to higher temperatures, of 1000°C or above, before infiltration at lower temperature. The system was thus pre-heated to 1000°C and then cooled down to 700°C before applying a sequence of increasing pressure values, recording the saturation reached after front stabilisation at each successively higher fixed infiltration pressure. Results of those measurements for the Al-AA10 system at 700°C and 1000°C are given in Fig. 4.6. As seen, the data are not reproducible: at both temperatures, a different drainage curve is obtained for each different experiment.

In summary, with the Al-AA10 system, (i) continued, steady, isobaric pressure infiltration is not observed and (ii) drainage curves are measurable, but are not reproducible. In both respects, thus, data differ from what is observed with F1000 alumina.

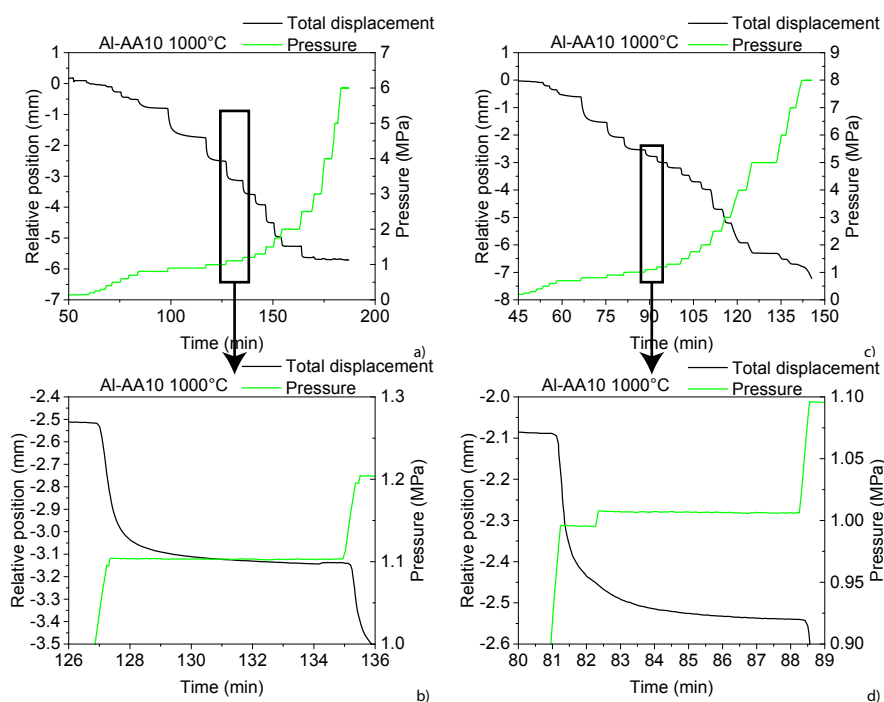


Figure 4.5: Infiltration data for the Al-AA10 system at 1000°C. a) and c): full infiltration curve, b) and d): zoom at the end of the pressure step showing stabilization of the infiltration front.

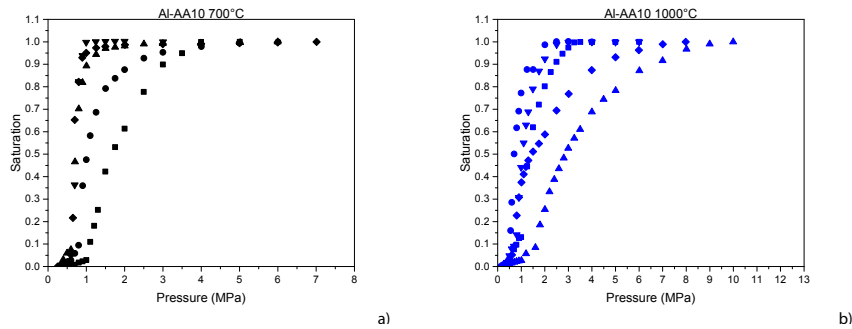


Figure 4.6: Separately measured drainage curves for the system Al-AA10 showing the lack of reproducibility of the tests: infiltration at a): 700°C, b): 1000°C.

Al- β'' -AA10 system

Repeating those experiments with the β'' -AA10 powder, produced by incorporating sodium into the AA10 powder to the same concentration as in the F1000 powder, gives data exemplified at 1000°C in Fig. 4.7. As seen, as with the AA10 powder and unlike what is observed with the F1000 powder, the infiltration front stabilizes after a sufficiently long hold at fixed pressure ($\frac{dS}{dt} \approx 0$), Fig. 4.7(b).

Repeating hence with this powder drainage curve measurements that were conducted for the Al-F1000 system at lower temperature in Ref. [253], and here for the Al-AA10 system, gives results plotted in Fig. 4.8(a). As seen, with the β'' -AA10 powder, there is sufficient reproducibility of Al infiltration at 1000°C to draw a meaningful drainage curve for this system.

For comparison purposes, we repeated these drainage curve measurements with the (non-reactive) Cu-AA10 system. To enable comparison with the Al- β'' -AA10 system, results for both systems are combined in Fig. 4.8(b) after normalisation of the pressure by division with the work of immersion (surface tension σ_{LV} times $\cos(\theta)$). As seen, within experimental uncertainty, the curves superimpose. Figure 4.8(c) shows that the Brooks and Corey relation is obeyed as has often been observed [2, 3, 40, 247, 249, 252–254, 256–258, 290, 296, 355]. The exponent λ , known to be a characteristic of the pore (and hence particle) geometry, Fig. 4.8(c), is also a constant, as expected.

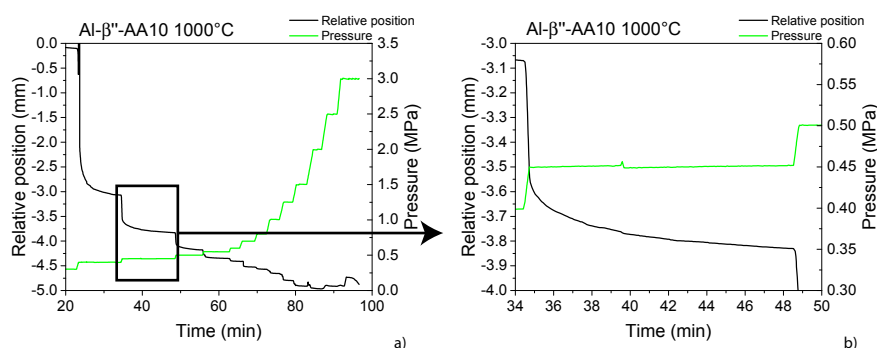


Figure 4.7: Raw infiltration data for the system Al-β''-AA10 infiltrated at 1000° C a) full curve, b) zoom between two pressure steps showing that the front stabilizes when the pressure is held for a sufficiently long time.

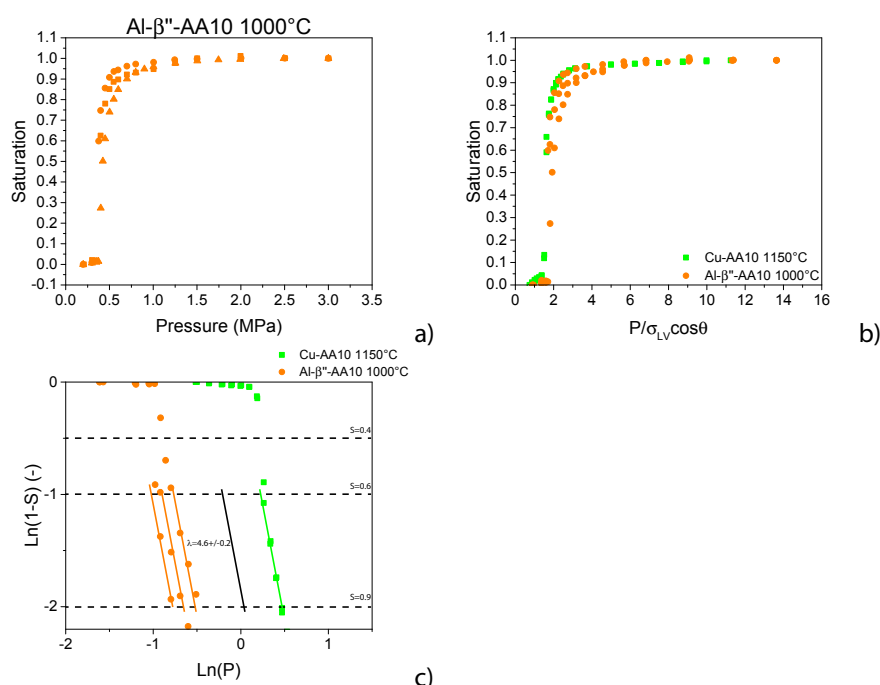


Figure 4.8: a) Drainage curves for the Al-β''-AA10 system at 1000° C, b) comparison between the relative drainage curve of Al-β''-AA10 at 1000° C and Cu-AA10 at 1150° C and c) Brooks and Corey relation for the two systems.

4.5.2 Phase characterization

Figure 4.9 shows XRD spectra collected from Al-F1000 composites after full infiltration at 1000°C, 1050°C, 1100°C and 1150°C. For comparison, the XRD pattern collected from the pristine F1000 powder is reported in the same figure. As seen, after infiltration below 1150°C, the composites show the presence of Al, α-Al₂O₃ phases and a sodium-containing phase identified as NaAl₁₁O₁₇, also known as β'' alumina (note the low sodium content in the phase).

Chapter 4. Kinetic processes in the high temperature pressure-infiltration of Al into Al_2O_3

The amount of ($\beta''\text{-Al}_2\text{O}_3$) phase relative to the amount of $\alpha\text{-Al}_2\text{O}_3$ is lower after Al infiltration compared with the raw powder. The amount of β'' alumina decreases as the infiltration temperature increases, to reach zero in the composite produced by infiltrating F1000 powder with Al at 1150°C ; here, only Al and $\alpha\text{-Al}_2\text{O}_3$ phases are detected.

Figure 4.10 compares the XRD spectra of AA10 and $\beta''\text{-AA10}$ powders: this shows the presence of $\text{NaAl}_{11}\text{O}_{17}$ in the latter, in proportions similar to what is found in F1000. The Al- $\beta''\text{-AA10}$ composite infiltrated at 1000°C shows also the presence of this phase, albeit at a lower relative concentration compared to alpha-alumina than in the initial, as-reacted and uninfiltrated, $\beta''\text{-AA10}$ powder.

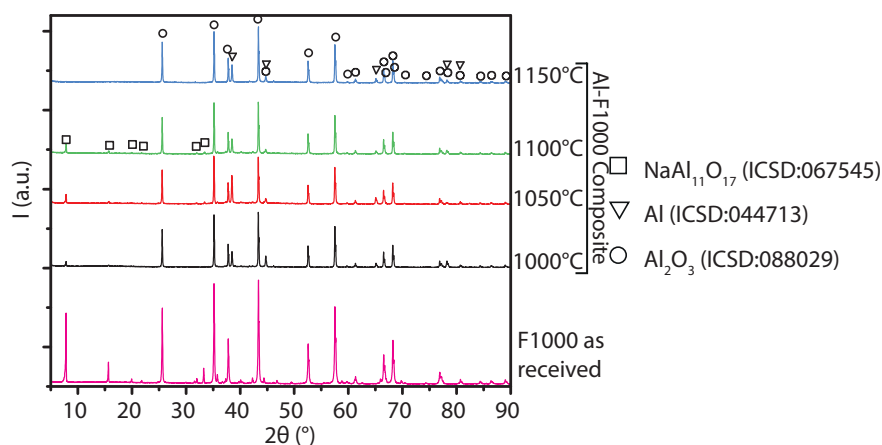


Figure 4.9: XRD spectra of the as-received F1000 powder (bottom) and (from bottom to top) of the Al-F1000 composite infiltrated at 1000, 1050, 1100 and 1150°C .

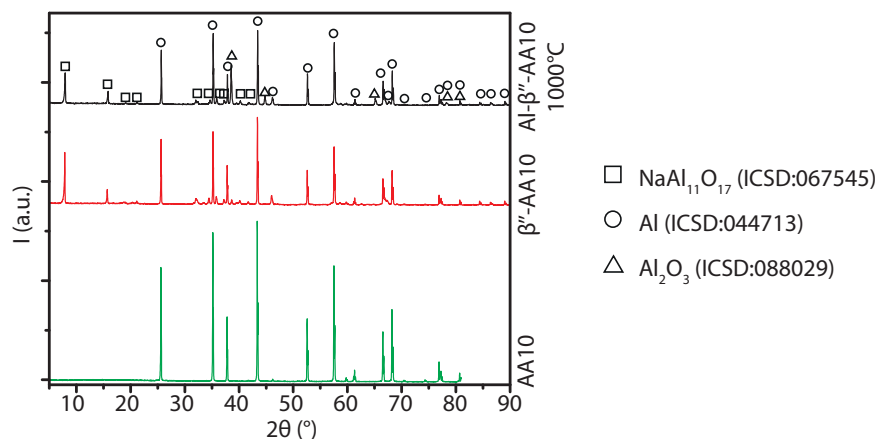


Figure 4.10: XRD spectra of the Al- $\beta''\text{-AA10}$ composite infiltrated at 1000°C (black, top curve) compared to $\beta''\text{-AA10}$ (red) and AA10 (green, bottom curve) powders.

4.5.3 Composite microstructure

Figure 4.11 shows back-scattered electron (BSE) images of the Al-F1000 composite infiltrated at 700°C (Fig. 4.11(a)) and at the three (higher) temperatures at which infiltration kinetics were measured (1000-1050-1100°C) (Figs. 4.11(b-d)). As seen, in the composite infiltrated at 700°C, F1000 particles retain their initial, highly irregular and angular, shape characteristic of comminuted powder (see Fig. 4.1(e-f)), with sharp angles separating planes along which the material fractured in its production process. Figures 4.11(b-d) show that, as the infiltration temperature increases, those sharp angles disappear. The particles have become increasingly rounded and show increasing levels of mutual coalescence.

The Al-AA10 composites (Figs. 4.12(a-d)) on the other hand do not show signs of such an evolution in their shape and size, regardless of the infiltration temperature. The etched sample (Fig. 4.12(c)) confirms that no change in powder morphology or size is visible after infiltration.

Finally, Figs. 4.13 show the microstructure of Al- β'' -AA10 composites infiltrated at 1000°C. The microstructure is similar to that in Figs. 4.12, leading to conclude that adding sodium to AA10 does not affect the observation that there is no change in particle morphology or size after high-temperature infiltration with aluminium.

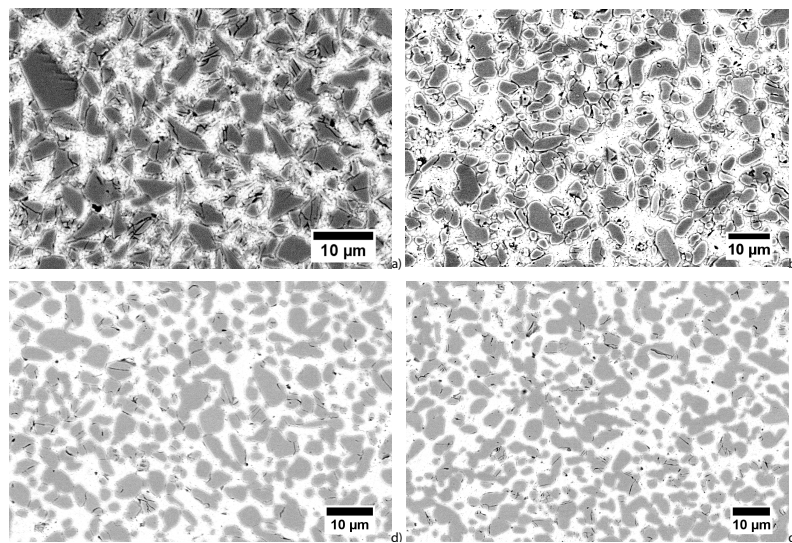


Figure 4.11: Microstructure of the Al-F1000 composite infiltrated at a) 700°C, b) 1000°C, c) 1050°C and d) 1100°C.

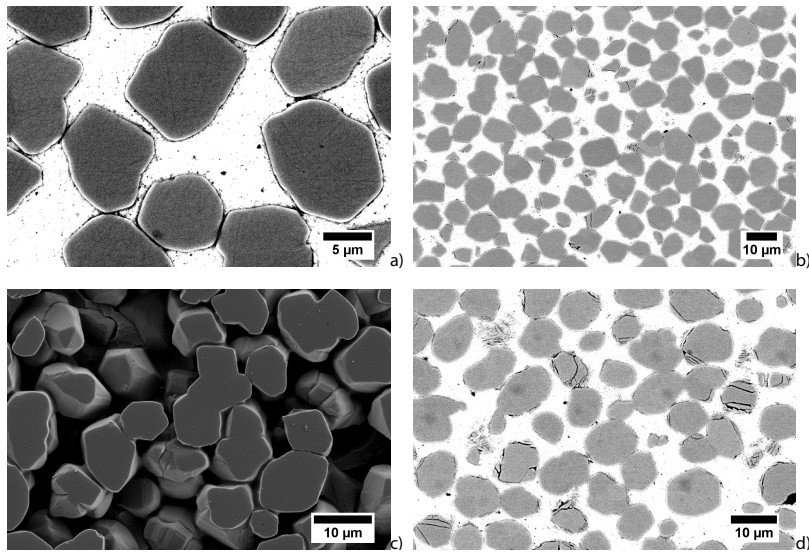


Figure 4.12: Microstructure of the Al-AA10 composite infiltrated at a): 700°C, b and c): 1000°C; in c) the surface is deep-etched in order to remove the matrix and highlight the shape of particles, and d): Al-AA10 composite infiltrated at 1100°C.

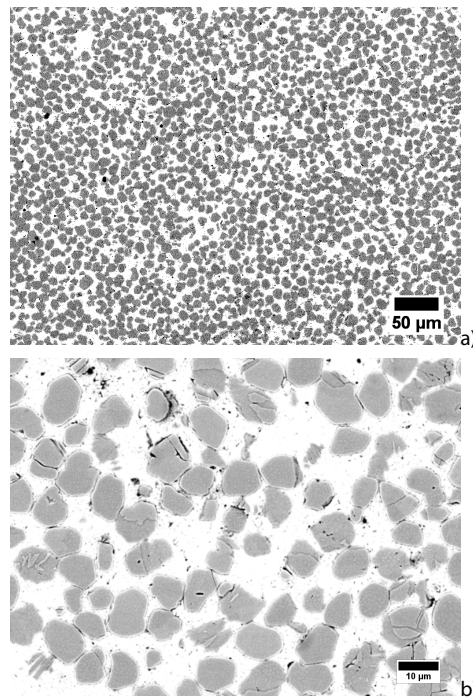


Figure 4.13: Microstructure of the Al- β'' -AA10 composite infiltrated at 1000°C a) low magnification, b) high magnification showing no modification of the particles after high temperature infiltration.

4.6 Discussion

4.6.1 Infiltration kinetics in the Al-Al₂O₃ system

Summing up, present data show that:

1. the triple line does not stabilize at, or above, 1000°C at fixed applied pressure during the pressure-infiltration of F1000 particle preforms with aluminium. An interfacial phenomenon drives the metal into the preform at fixed pressure, in the same way as does a wettability-enhancing interfacial reaction.
2. That this is observed neither with the Al-AA10 nor the Al- β'' -AA10 systems implies that the interfacial phenomenon in question is not linked with the presence of sodium impurities in the F1000 powder.
3. SEM images of Al-F1000 composites (Fig. 4.11) show that the particles have coarsened during infiltration at or above 1000°C, while after infiltration at 700°C the highly angular particle shape characteristic of comminution is retained.

These three observations lead to conclude that the reason why one observes, at 1000°C or above, continuous isobaric infiltration in this system is that the liquid/solid interface becomes sufficiently mobile to enable the liquid metal meniscus to continuously advance forward. As such, this mechanism parallels the “ridging” process that was reported for sessile drop experiment data by Saiz, Tomsia et al. [15, 16, 121, 131, 206].

How such coarsening causes the continued forward motion of the infiltration front cannot be fully ascertained from the present data; however, a simple realistic scenario can be proposed. In preforms of the highly angular F-1000 particles, sharp angles along the surface of the particles provide pinning points along the path of forward motion of the liquid metal meniscus through the open pore space within the powder preform. Now, once the liquid metal contacts such pinning points, coarsening will blunt those sharp angles, leading to an opening of the passage leading the liquid metal meniscus into the next pore. Such opening will lower the threshold pressure required for the metal surface to move past the pinning point, causing the meniscus to jump forward, despite the fact that the driving pressure is constant. A simple sketch of this process is presented in Fig. 4.14. Note also that, for a given reduction in the width of the narrowest constriction (and hence for a given decrease in the critical threshold pressure for passage of the meniscus), a greater volume of solid material must be displaced if the angle α characterizing the sharpness of the ridge along the surface of particles increases. The fact that ridges are more blunt and the particle size is larger in AA10 and β'' -AA10 particles than in F1000 alumina can thus be advanced to explain why steady isobaric infiltration is not observed with those powders, while it is seen with the sharp and highly angular F1000 powder.

Having identified a plausible physical origin of steady infiltration with the Al-F1000 system, namely coarsening of sharp ridges along the alumina particles once these are in contact with

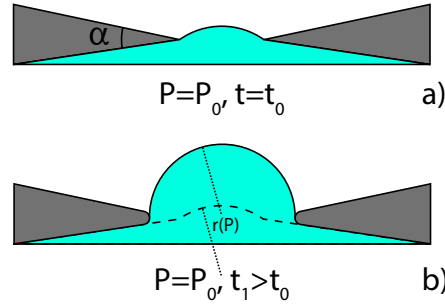


Figure 4.14: Schematic showing a 2D liquid front reaching a discontinuity presented by a pair of particles having sharp α angles: a) pressure is below the threshold for passage of the meniscus past the pinning point; b) coarsening causes a decrease in the critical threshold pressure, releasing the meniscus.

molten aluminium, we seek to quantify features of this thermally activated isobaric infiltration process, using the same approach (and assumptions) as in Ref. [41], namely we link $\frac{dS}{dt}$ with the parameters of the thermally activated process through the relation:

$$\frac{dS}{dt} \propto \exp\left(\frac{-Q + V_a P}{k_B T}\right) \quad (4.2)$$

where $\frac{dS}{dt}$ is the saturation velocity, Q is the activation energy of the thermally activated phenomenon by which obstacles limiting motion of the liquid surface through the solid preform pore space are overcome, P the applied pressure, namely the pressure difference between the liquid and the initial atmosphere (vacuum usually), k_B is the Boltzmann constant and T is temperature. V_a is the relevant activation volume; this represents, in addition to Q , a characteristic of the thermally activated process that drives gradual ingress of the liquid into pores within the solid under a finite applied pressure differential P . V_a is deduced here by measuring infiltration rates at two different pressures, by writing as in Ref [41]:

$$\left. \begin{aligned} \frac{dS_1}{dt} &\propto \exp\left(\frac{-Q + V_a P_1}{k_B T}\right) \\ \frac{dS_2}{dt} &\propto \exp\left(\frac{-Q + V_a P_2}{k_B T}\right) \end{aligned} \right\} \begin{aligned} \ln\left(\frac{dS_1}{dt}\right) &= A + \frac{-Q}{k_B T} + \frac{V_a P_1}{k_B T} \\ \ln\left(\frac{dS_2}{dt}\right) &= A + \frac{-Q}{k_B T} + \frac{V_a P_2}{k_B T} \end{aligned}$$

$$\ln\left(\frac{dS_1}{dt}\right) - \ln\left(\frac{dS_2}{dt}\right) = \frac{V_a(P_2 - P_1)}{k_B T} \Rightarrow V_a = -\ln\left(\frac{dS_1/dt}{dS_2/dt}\right) \cdot \frac{k_B T}{\Delta P} \quad (4.3)$$

where $\Delta P = P_2 - P_1$ and $\frac{dS_i}{dt}$ is the measured velocity at pressure P_i .

Using data giving the change in rate of saturation increase as one changes suddenly the infiltration pressure, we estimate the corresponding activation volume using the approach in Ref. [41]. The ratio of infiltration velocities for each successive downward change in the infiltration pressure is given in Fig. 4.15(a) for each of the three investigated temperatures (1000-1050-1100°C). As seen, there is considerable scatter in the data. This is particularly pronounced at low saturation, most likely because in early, low-saturation, phases of infiltration, measured infiltration velocities are more strongly influenced by percolation effects. These will introduce a higher level of stochasticity in infiltration data, causing more scatter in the rate of infiltration from one experiment to another, or as the saturation varies within a given infiltration experiment.

From the histogram in Fig. 4.15, one can deduce an estimated value of the activation volume for the pressure infiltration of Al into angular preforms of Al₂O₃ that is between 200 and 300 nm³ (the computed average value is 235 nm³ with a standard deviation of 80 nm³).

If we now use this value in Eq. 4.2 to correct the saturation velocities for the influence of the applied pressure, then recorded saturation increase rates in Fig. 4.4 become pressure-compensated saturation increase rates plotted in Fig. 4.16. As seen, pressure-compensated infiltration rates are (contrary to the raw data) such that the higher the temperature is, the faster the front moves, which is now as expected for a thermally activated phenomenon.

Having the pressure-compensated saturation velocities at different temperatures, one may seek to draw an Arrhenius plot to estimate the activation energy characteristic of the process driving steady pressure infiltration at high temperatures in this system. This is done in Fig. 4.17 using pressure-compensated saturation increase rates averaged over all data points in the range of saturation values within $\pm 0.03S$ of $S = 0.6, 0.65$ or 0.7 . As seen, the degree of scatter in the average slopes through data points is higher than was found for Cu-Si alloy infiltration into carbon preforms; however, using the slope given by linear regression through each of the three sets of three temperatures explored one obtains calculated activation energies in Fig. 4.18. These vary from roughly 330 to 460 $\frac{kJ}{mol}$. Those are high values, consistent with the fact that at lower temperatures gradual thermally activated isobaric infiltration is not observed. $Q \approx 400 \frac{kJ}{mol}$ is only somewhat lower than the activation energy for the diffusion of oxygen in alumina, reported to be between 450 $\frac{kJ}{mol}$ [452, 453] and 600 $\frac{kJ}{mol}$ [454–458].

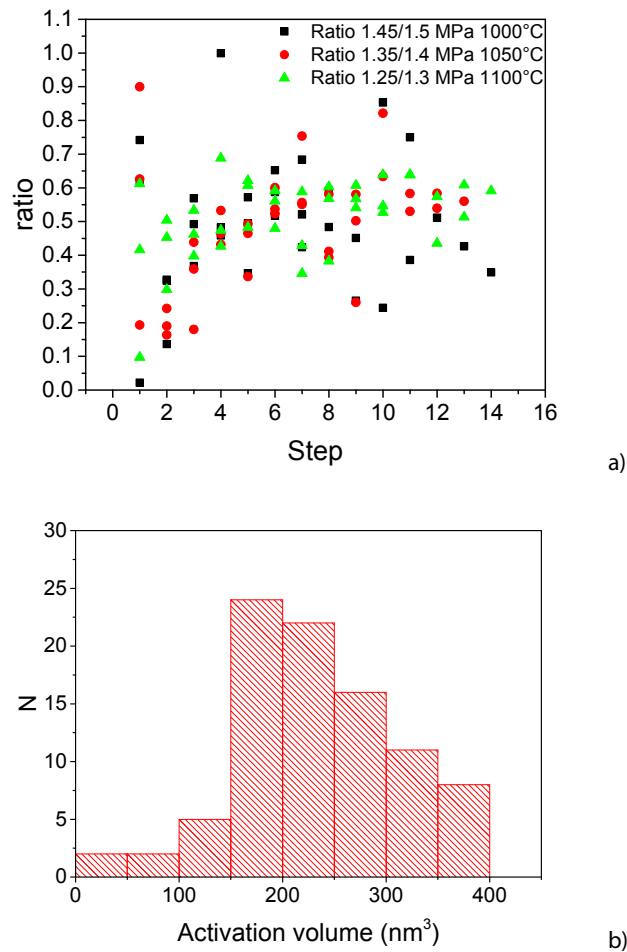


Figure 4.15: a) Ratio between measured rates of saturation increase across two successive stepped downward pressure changes across all experiments of this study, b) histogram of the distribution of the corresponding activation volume values across all experiments.

4.6.2 Effect of sodium impurities in alumina preforms on pressure infiltration with aluminium

Whereas sodium impurities in the alumina preform play no apparent role in the gradual, thermally activated, isobaric infiltration of F1000 preforms, our data show that they influence the reproducibility of drainage curve measurements in the Al- Al_2O_3 system. Specifically, comparing the behaviour of the two Al-AA10 and Al- β'' -AA10 systems, one observes that, without sodium in the alumina powder, drainage curves are (i) erratic and (ii) fall to the right of the reproducible drainage curve obtained both with the sodium-contaminated powder or (after normalisation of pressures) with molten copper, see Figs. 4.5-4.7. Without sodium, measured drainage curves become erratic and correspond to higher pressures. This suggests that “something” hinders penetration of the molten aluminium into the preform if there are

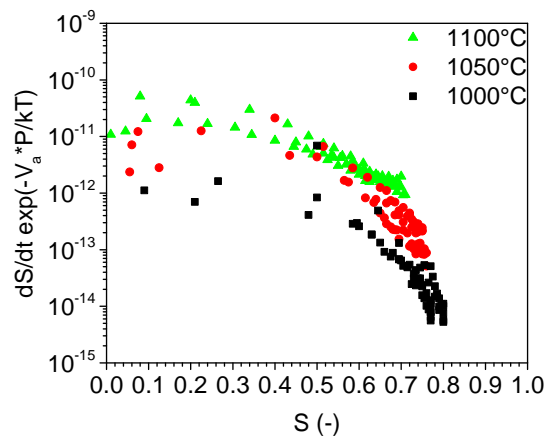


Figure 4.16: Saturation velocities corrected for the influence of pressure and temperature using Eq. 1 in [41] and the average computed activation volume across all experiments of this study $V_a=235 \text{ nm}^3$.

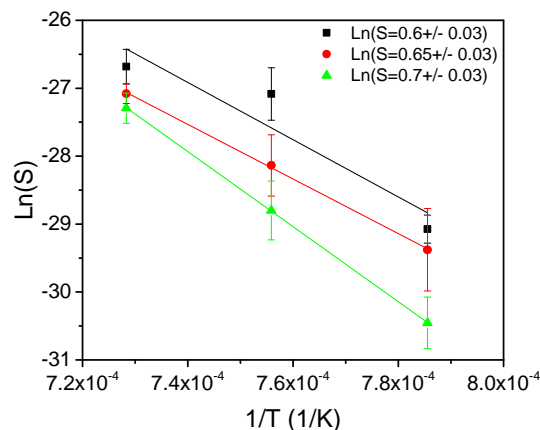


Figure 4.17: Arrhenius plots for pressure-compensated infiltration rate data over the three infiltration temperatures around three values of saturation, namely $S = 0.6, 0.65$ or $0.7 S \pm 0.03$.

no sodium atoms in the alumina powder.

The same erratic behaviour, hindering the measurement of reproducible drainage curves with aluminium-containing melts in the infiltration of Al_2O_3 preforms, was already noticed by Léger et al. in their work on the infiltration of F1000 Al_2O_3 powder preforms at lower temperature than this work ([253]). Specifically, they found that, by pre-heating the system to 1000°C before infiltration at a lower temperature (nearer 700°C), the measurement of drainage curves with aluminium-containing melt at those lower temperatures becomes reproducible. Without such a preheat, erratic results similar to those gathered here with the AA-10 powder are obtained.

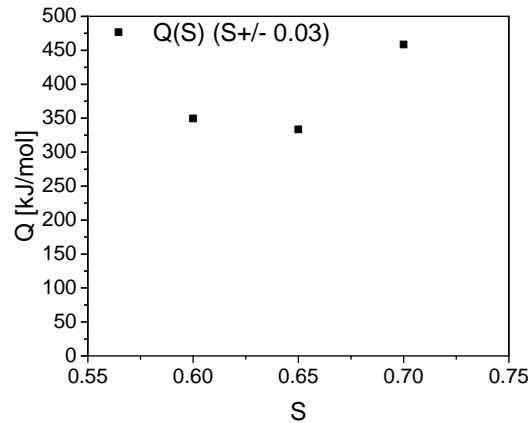


Figure 4.18: Activation energy computed at three different saturations across a range of $\pm 0.03S$.

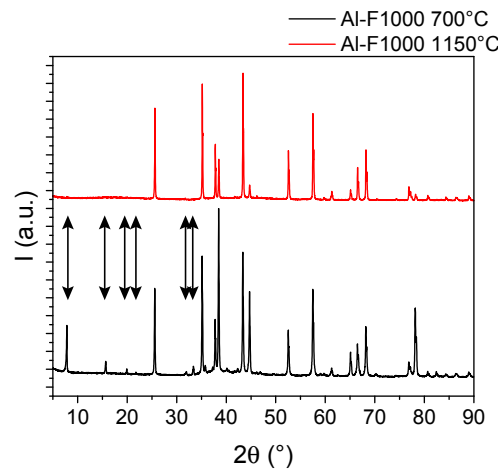


Figure 4.19: XRD spectra for the composite infiltrated at 700°C (black, bottom) compared to the composite infiltrated at 1150°C (red, top). The arrows mark the main sodium phase peaks, which are not present in the latter composite.

Pooling the present data together with those of Ref. ([253]) leads us to propose the following scenario to explain the role of sodium impurities in the infiltration of alumina preforms with aluminium-containing melts.

At elevated temperatures (significantly above 700°C), sodium within the particles reacts with the aluminium-containing melt. This is shown by the decreased proportion of sodium-containing phase in the powders after infiltration at elevated temperature, see Figs. 4.9 and 4.10. Note that this leads to no modification of the composite microstructure, other than the gradual replacement of β'' alumina with α alumina in the particles. Sodium is neither to be found in the matrix nor along the interface of the particles if the composite microstructure is examined in the electron microscope. Seemingly, sodium is absent from the composite once it has left

the ceramic powder.

It is interesting to note that, whatever interaction occurs between the melt and the powder, this interaction influences the course of infiltration *before* infiltration has started. This is evidenced by the fact that preheating the melt and (sodium-containing) alumina preforms to a temperature near 1000°C, before infiltration is conducted at a lower temperature, renders the drainage process reproducible at the lower temperature. Without such preheating, infiltration is erratic - and somehow hindered given that higher (and poorly reproducible) pressures are required to reach a given saturation.

To show that a thermally activated process occurs during the pre-heating step, we performed Al-F1000 infiltrations at 700°C after having pre-heated the system in vacuum to 900°C for respectively 10, 20 or 30 min. The corresponding drainage curves measured at 700°C are reported in Figure 4.20. One sees that after holding the system for 20 min or more at T=900°C, one starts to obtain reproducible results.

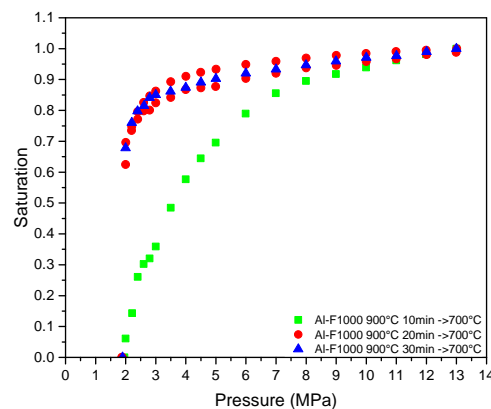


Figure 4.20: Drainage curves for the Al-F1000 system measured at 700° C after pre-heating the system at 900° C for three different holding time values: 10 min, 20 min and 30 min respectively.

The most likely cause for the observed behaviour, which is not seen with melts that do not contain aluminium, is that the oxide layer that covers the surface of aluminium-containing melts is sufficiently thick and strong to hinder penetration of the preform unless it is altered; that this is so has been suggested by many authors before us (e.g., [169, 247, 379, 459]). Léger *et al.* [253] proposed that the reason why preheating aluminium-containing melts to 1000°C before infiltration could be that the aluminium oxide film on the liquid surface transforms itself into a gaseous aluminium oxide following the reaction:



Present results show that this explanation cannot hold, since without sodium present, even when infiltration is performed at 1000°C, one does not obtain reproducible results with high-purity AA10 alumina preforms.

So why do small proportions of sodium in alumina aid infiltration with aluminium-containing melts if the melt and preform are preheated to sufficiently high temperatures for a sufficient time? Pooling data, we propose that this is because sodium is transported from the particles to the oxide that covers aluminium-containing melts, and alters it. Elrefaie and Smeltzer [212] show indeed that the $NaAl_{11}O_{17}$ phase has a partial pressure ($p(Na)=1 \cdot 10^{-7}$ at 1000°C) and if heated under vacuum it decomposes to form $Na_2O_{(l)}+Al_2O_3$. So it is plausible that at least some Na-O migrates away from the particles and reacts with the oxide layer that covers the liquid Al melt. Reported sodium aluminate densities are around $1.1 \frac{g}{cm^3}$ [460]. This phase having a lower density than Al, it may float to the surface of the liquid metal, leaving the infiltration region and thus removing or altering the oxide layer that initially covers the metal. As a result, the mechanical hindrance that the oxide creates to penetration of the melt into open pores of the ceramic powder preform is reduced or removed. The phase diagram of Al_2O_3 - NaO_2 can be found in [461].

To produce evidence of this, we performed an infiltration experiment free of melt tracking at 1150°C for 4h at 4MPa. The sample was heated under vacuum and then the chamber was pressurised to 4MPa in order to fully infiltrate the composite. In the particles of this composite, no $NaAl_{11}O_{17}$ phase remains; this is evidenced by XRD data (Figs. 4.9 and 4.19). We examined the structure and composition of the oxide layer covering the melt along the top surface using optical and SE microscopy. To this end, the top of the Al ingot was cut after infiltration and solidification along its length and its cross section was analysed by SEM-EDX. A schematic representation of this sample showing the investigated zone is given in Fig. 4.2.

Figure 4.21 shows the structure of oxide covering the metal along the top of the Al ingot: one finds alumina particles $>10 \mu m$ in size (C) together with needle- and platelet-shaped submicrometer particles (A and B) surrounded with Al metal. EDX analyses on those particles reveal the presence of Na, Al and O in the needle and platelet particles (A and B). This is consistent with the literature, which states that sodium aluminate phases often crystallise in platelet- or needle-like shapes [211]. More specifically, within error of EDX analyses, an average Na content of 1.5at.pct. was found, suggesting that this phase is $NaAl_{26}O_{40}$ ($\sim Na_2O:Al_2O_3$ 1:26).

That Na is present on the top part of the Al ingot but not inside the infiltrated composites, gives some credence to our proposal that Na impurities within alumina release sodium before infiltration, and that this sodium then interacts with the aluminium oxide film along the

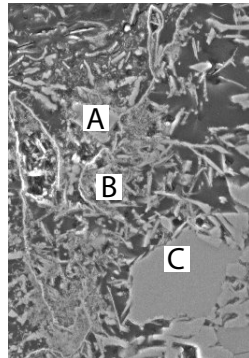


Figure 4.21: Cross section of the liquid front along the top surface of the ingot used to infiltrate the F1000 preform at 1150°C for 4h at 4MPa. The locations of the EDX point analyses are labelled: at A and B one finds the sodium aluminate phase and at C the oxide layer is of pure alumina.

L-V interface in ways that make it less resistant or to remove it, as does a flux, thus easing penetration of the melt into pores of the preform. This, in turn (i) makes drainage curve measurement reproducible and (ii) gives rise to a sodium aluminate phase that migrates to the surface of the ingot, given that it is less dense than Al.

4.7 Conclusions

We show that:

- At 1000°C and above, the pressure infiltration of aluminium into Al_2O_3 particle preforms becomes time-dependent, showing steady penetration of the melt into the porous preform under fixed metal pressure if the alumina particles are highly angular. This feature, which can also be observed in reactive infiltration, is attributed to solution-precipitation of the alumina in contact with aluminium, a process that bears strong similarity with the “ridging” mechanism that has been documented for this system in sessile drop wetting experiments. Interpreting the data using the same framework of analysis as that developed for elevated temperature dislocational plasticity leads to deduce that the thermally activated process underlying this gradual infiltration process is characterized by an activation volume on the order of $\approx 200\text{nm}^3$ and an activation energy in the range going roughly from 300 to $500 \frac{\text{kJ}}{\text{mol}}$, a range near what has been measured for bulk diffusion of oxygen through alumina.
- The presence of sodium impurities in alumina, which react with the melt at 900°C and above, eases the initiation of infiltration, rendering the measurement of drainage curves reproducible. Present data give strong evidence that this is due to a fluxing effect exerted by sodium, which migrates at those temperatures out of the preform. Sodium then likely interacts with the oxide layer that initially covers the aluminium melt, eliminating it by

flotation or reducing its mechanical strength, such that the oxide no longer opposes penetration of the melt into the powder preform.

4.8 Acknowledgement

This work was sponsored by the Swiss National Foundation (FNS), Project No. 200021_149899. The authors are grateful to Professor F. Stellacci, of EPFL, Professor W. C. Carter, of MIT, and Professor J.-M. Molina-Jorda, of the University of Alicante, for the enlightening discussions and helpful suggestions through this study.

5 Reactive infiltration of Cu-X (X= Cr, Ti) alloy into porous graphite

5.1 Disclaimer

This chapter will be submitted in a scientific journal. The preprinted version of this article is presented here below. The candidate, herewith G.S., designed and carried out all experiments. The manuscript was written by G.S.. Ludger Weber (L.W.) and Andreas Mortensen (A.M.) provided supervision throughout the whole duration of this work. L.W. and A.M. revised, corrected and approved the manuscript.

Gionata Schneider, Ludger Weber, Andreas Mortensen, "Reactive infiltration of Cu-X (X= Cr, Ti) alloy into porous graphite", to be submitted.

5.2 Abstract

We show, by adding 1at.pct.Cr or 10at.pct.Ti to copper infiltrating porous graphite that, for alloying additions forming a better wetted interfacial phase to aid pressure infiltration, reaction must be sufficiently slow to avoid reactive element depletion of the infiltrant or pore clogging along the preform periphery.

5.3 Introduction

Infiltration is a common way to produce metal matrix composites. Because most molten metals of engineering interest do not wet well the second, more refractory, composite phase with which they are to be combined in the process [89, 120, 233, 427], pressure is often applied on the liquid metal to force it to penetrate the open space between elements of the refractory phase. With sufficient pressure, even though the wetting angle as measured by the sessile drop method may be well above 0° [70, 86, 89, 97, 113, 114, 125, 128, 404], high-quality composites are produced from chemically inert systems such as Cu/Al₂O₃, Cu/C_{Gr} or Al/Al₂O₃. These are all systems where the contact angle exceeds 90° under vacuum near the metal melting

point [5, 10, 16, 18, 25, 106, 115, 115, 124, 382, 462].

Often, to aid the process, it is sought to improve wetting of the refractory phase by the liquid metal that it is to be combined with. A classical approach to this end is to add to the metal infiltrant an alloying element that reacts with the solid refractory phase in order to form, along the liquid/solid interface, a third phase that is far better wetted by the liquid. Example of such reactive systems are Cu-Ti/Al₂O₃ [23, 99, 105], Cu-Ti/C_{Gr} [18, 23], Cu-Si/C_{Gr} [101, 110, 111, 117], and Cu-Cr/C_{Gr} [39]. Such interfacial reactivity has been used to drive spontaneous (pressureless) infiltration of preforms by molten metal [45, 246]; however, it might also be useful in the context of pressure-driven infiltration. In a recent study [41] we studied the influence of silicon additions to copper on pressure infiltration of porous graphite preforms. It was found that the alloying addition drives the metal to continuously flow into the preform, instead of equilibrating at a finite saturation, under fixed applied pressure. This is explained by the formation of (better wetted) SiC along the copper/carbon interface which drives the infiltrating metal meniscus further into uninfiltrated preform pores, than would the applied pressure alone with pure copper. In the present study, we examine two other carbide-forming, copper-based infiltrants, namely Cu-1at.pct.Cr and Cu-10at.pct.Ti, flowing under pressure into the same porous graphite as in Ref. [41].

For both systems, sessile drop experiment data show that one observes the rapid formation of a uniform layer of better-wetted carbide along the liquid-solid interface. For the Cu-Cr system on graphite, 1at.pct.Cr is the minimum concentration with which one obtains a wetting system [18, 28–31]. With this alloy, it has been found that the contact angle stabilizes at around 45° after approximately 100s due to the formation of a continuous layer of Cr₃C₂ and/or Cr₇C₃ [17, 18, 24, 37–39, 101]. In the Cu-Ti system, one needs at least 10at.pct.Ti in order to transition from wetting to non-wetting [17–20, 20–27]. With Cu-10at.pct.Ti one again finds that the time to produce favourable wetting with a sessile drop is on the order of 100 seconds. The reaction product TiC has a slightly non-wetting contact angle with the liquid metal, of around 100° [18, 22, 123]; however this value may change as a function of the carbon content in the carbide formed, with stoichiometric TiC having a lower metallic character and as a result less favourable wetting compared to titanium carbide of substoichiometric carbon content [18, 28–31]. As will be seen, despite the fact that interfacial reaction forms a better wetted phase with each of these two alloys, they in fact hamper pressure infiltration, for reasons that differ between the two alloys.

5.4 Experimental

5.4.1 Materials

Porous graphite preforms are machined in cylinders of 15±0.03mm height and diameter 13±0.03mm from a block of EDM200 purchased from Poco Graphite, Inc. (Limonest, France). The volume fraction of open pores of the graphite preform, V_r , measured by mercury porosime-

try, is 0.22. The alloys are prepared starting from pure copper (> 99.9%) and pure chromium (> 99.98%, ABCR GmbH Germany) or pure titanium (>99.99%, ABCR GmbH Germany) to contain 1at.pct.Cr and 10at.pct.Ti respectively in a high-vacuum induction furnace, under an Ar pressure of 0.8 bar introduced after 5 successive purges of gas within the apparatus.

5.4.2 Infiltration apparatus

The rate of penetration of the metal into the porous preform is measured using a custom set-up designed and built in our laboratory (pictured in Fig. 2 of Ref. [296]). This set-up allows to measure dynamically the infiltrating fluid displaced volume, using dynamic measurements of the displacement of the liquid level in the crucible containing preform and alloy [253, 256, 296].

Prior to each pressure infiltration experiment the preform is blocked under an ingot the Cu alloy ingot inside an alumina crucible. After closing the chamber and pulling a primary vacuum, the system is heated up to the desired infiltration temperature, leaving sufficient time for the metal to melt completely and seal the preform from the surrounding atmosphere by forming a meniscus along the crucible periphery above the preform. On top of the ingot a graphite plunger floating on the liquid (coated with BN to prevent reaction with carbide-forming elements in the infiltrant) is connected to an alumina rod sticking out of the hot zone of the infiltration apparatus. At the top of the rod, alternating black and white strips are used to track optically the displacement of the liquid level, giving readings of the volume of liquid that has entered into the preform. The precision in readings of the rod altitude is on the order of $\pm 2\mu\text{m}$; this converts into a precision in metal saturation S (defined as the fraction open pore space filled with metal) around ± 0.001 .

When the infiltration temperature is reached, Ar gas is injected inside the chamber up to the desired pressure, which is measured continuously during the experiment. At the beginning this pressure is gradually increased until it equals the threshold infiltration pressure, this being the lowest pressure that allows the metal to enter. Then, as infiltration progresses, this pressure is kept constant and stepwise increased, tracking the kinetics of preform infiltration by the metal, until the whole preform is filled with the liquid metal.

5.4.3 Metallographic preparation

After infiltration, samples are taken out from the alumina crucible and are cut in half and hot-mounted in resin. They are ground on emery paper down to 1200 grit and are then polished using 6, 3 and $1\mu\text{m}$ diamond suspension. The SEM images are taken on a Zeiss Merlin microscope (Carl Zeiss Microscopy, Germany) in SE mode.

5.5 Results

5.5.1 Infiltration experiments

Cu-1at.pct.Cr-C

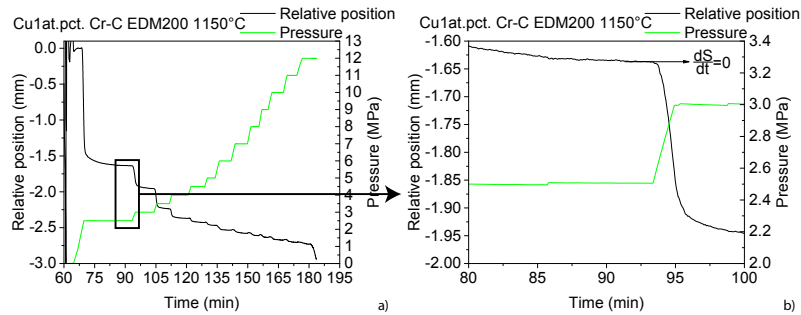


Figure 5.1: Raw infiltration data of the system Cu-1at.pct.Cr into graphite at 1150°C, a) curve of the whole experiment, b) zoom showing no advancing of the infiltration front at fixed pressure of 2.5MPa.

Figure 5.1a) shows the raw data (pressure and metal surface displacement versus time) from one of the two complete infiltration run with Cu-1at.pct.Cr. Figure 5.1b) displays a portion of the curve, showing that, after a transient, the saturation does not change over prolonged time at fixed pressure of 2.5MPa: the level of infiltration remains stable as long as the pressure is not increased. Having an infiltration curve which reaches the equilibrium at each pressure step, or in other words capillary equilibration under fixed pressure as with a non-reactive system, a drainage curve (plotting by definition the metal saturation S versus the applied pressure P) can be traced for this system, cf. Fig. 5.2.

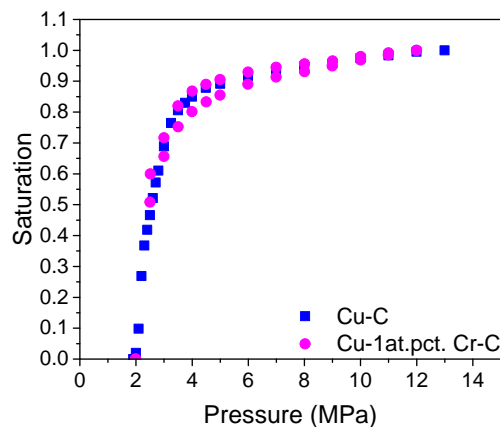


Figure 5.2: Drainage curves for the Cu-1at.pct.Cr- C_{Gr} (rounds) compared to the Cu- C_{Gr} (square) both infiltrated at 1150°C.

Figure 5.2 plots of the drainage curve for pure Cu and two drainage curves of Cu-1at.pct.Cr

into graphite preforms, all cut from the same block.

Cu-10at.pct.Ti-C

The same procedure was applied with Cu-10at.pct.Ti alloy pressure-infiltrated into the graphite preforms.

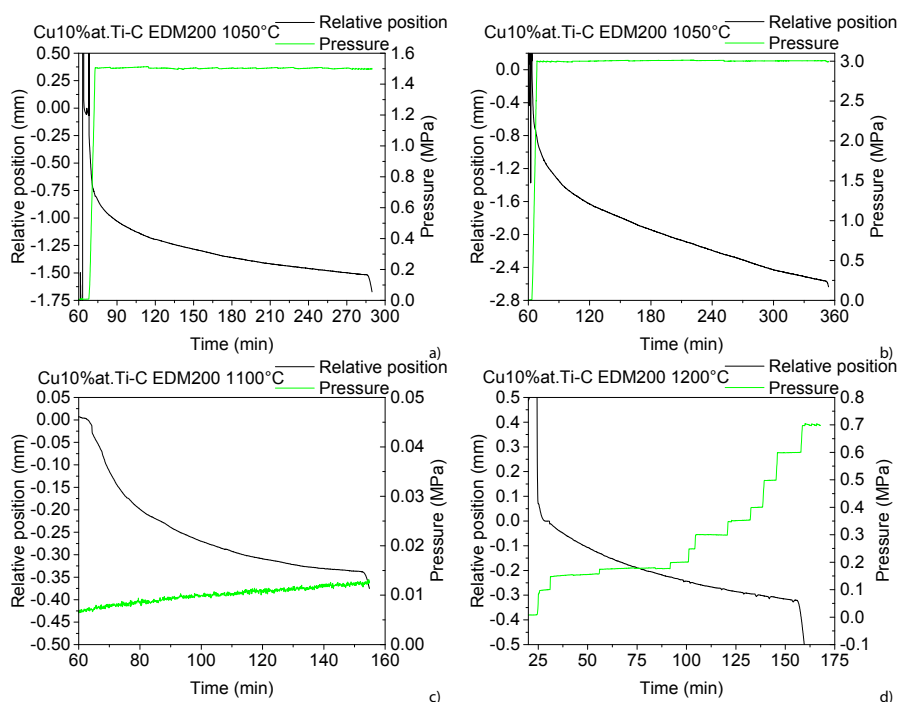


Figure 5.3: Raw data for the infiltration of Cu-10at.pct.Ti into graphite, a) 1050°C 1.5MPa, b) 1050°C 3MPa, c) 1100°C under vacuum, d) 1200°C 0.7MPa.

Figure 5.3 shows curves of pressure and metal surface displacement versus time for four different experiments conducted for the system Cu-10at.pct.Ti- C_{Gr} . Neither the pressure nor the temperature allows full infiltration of the graphite preform as confirmed by microscopical analysis (Figs. 5.6 and 5.8), while even without pressure some (limited) infiltration is obtained.

5.5.2 Microstructure analysis

In order to analyse the phases present in composites produced with both systems, scanning electron microscope (SEM) images and Energy Dispersive X-Ray (EDX) spectra were measured under 10keV in secondary electron (SE) mode.

Figure 5.4 shows the Cu-1at.pct.Cr-C composite after full infiltration at 1150°C and a final pressure of 12MPa. At the exterior border of the composite a chromium carbide layer is formed while inside the composite there is no carbide to be found along the interface. Figure 5.5

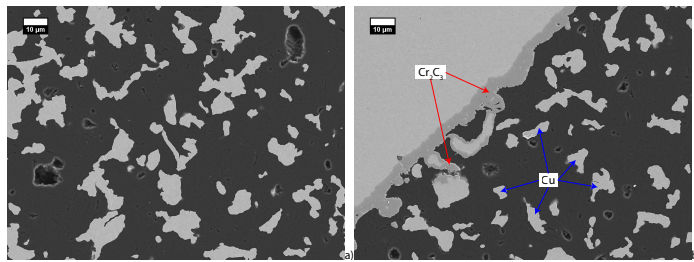


Figure 5.4: Microstructure of fully infiltrated Cu-1at.pct.Cr-C composite produced at 1150°C under 12MPa, a) centre of the composite, b) exterior border of the composite with indicated phases.

shows the result of EDX mapping, highlighting the phase present along the outer border of the composite. From these data, the composition the phase is identified as Cr_2C_3 .

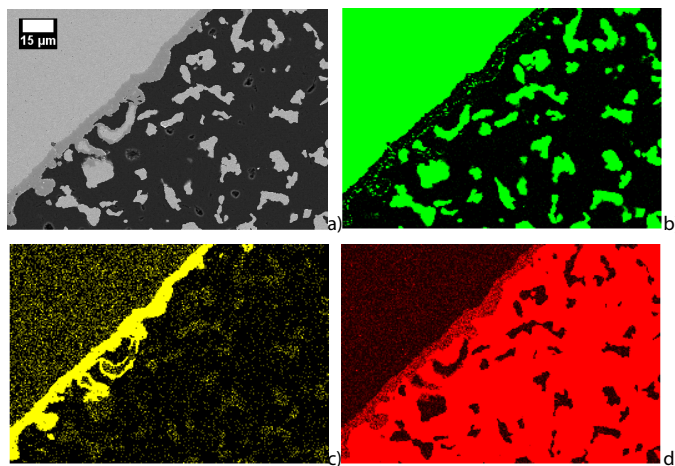


Figure 5.5: SEM image and EDX maps of Cu-1at.pct.Cr-C after full infiltration at 1150°C and a final pressure of 12MPa, a) SE image, maps of b) Cu, c) Cr and d) C_{Gr} .

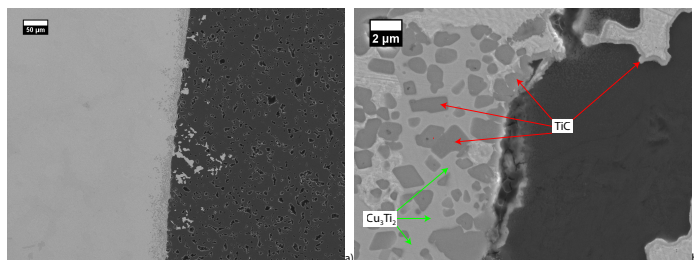


Figure 5.6: Microstructure of the exterior border of the partially infiltrated Cu-10at.pct.Ti-C composite produced at 1100°C under vacuum, a) low magnification, b) higher magnification with indicated phases.

With Cu-10at.pct.Ti-C, Figure 5.6 shows that even under vacuum, with no applied pressure, some metal enters into the preform. The formation of an intermetallic phase is also seen in the solidified alloy, which is not present inside the pores. One finds the formation of a TiC

layer on the pore walls. Figure 5.7 shows a composite infiltrated at 1200°C under 0.7MPa. A reaction product is present at the entrance of the composite as well as where the metal enters the preform. Filling of the remaining pore-space within the graphite was apparently blocked by the reaction product and the infiltration could not be completed even at high pressure (3MPa). Figure 5.8 shows at higher magnification EDX elemental maps of Cu-10at.pct.Ti-C produced at 1100°C under vacuum, imaging a single metal-filled pore along the periphery of the preform.

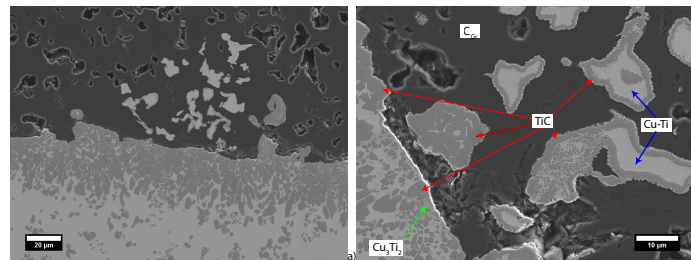


Figure 5.7: Microstructure of the exterior border of the partially infiltrated Cu-10at.pct.Ti-C composite produced at 1200°C under 0.7MPa, a) low magnification, b) higher magnification with indicated phases.

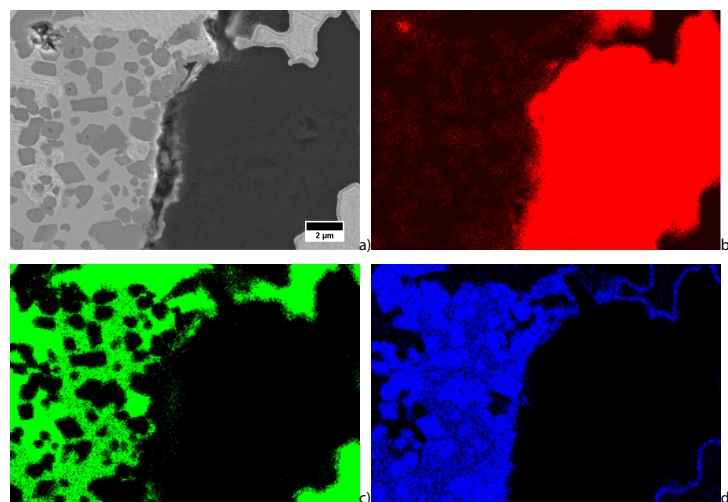


Figure 5.8: SEM image and EDX mapping of a partially infiltrated pore within a Cu-10at.pct.Ti-C composite at 1100°C under vacuum, a) SE image, b) C_{Gr} , c) Cu and d) Ti.

5.6 Discussion

5.6.1 Cu-1at.pct.Cr

The Cu-1at.pct.Cr system allowed full infiltration, indicating that the carbide layer formed at the interface did not block access of the infiltrating metal to open pores in the graphite preform. On the other hand, the alloying element was of no assistance in the pressure in-

filtration process, despite the fact that sessile drop data indicate that interfacial reaction produces a low contact angle between the metal and the solid phase [17, 24, 32, 37, 39]. Two observations, namely (i) that chromium carbide is observed along the preform periphery (Figures 5.4 and 5.5) and (ii) that the infiltrating metal behaves as does pure copper during infiltration (Figure 5.2) suggest that the lack of any beneficial effect linked with the presence of chromium in the melt originates from initial reaction of the preform with the infiltrant depleting the latter sufficiently of chromium for the interfacial reaction, and hence its effect in improving wettability of the solid by the liquid, to be suppressed. This is confirmed by EDX mapping, Figure 5.5, which shows that inner pores of the preform contain much less than 0.1at.pct.Cr (0.04at.pct.average obtained by EDX). Thermodynamic calculations indeed indicate that the limiting concentration of Cr to form a stable carbide at the interface is on the order of 0.1at.pct. [463], a threshold that is similar to that which can be deduced from sessile drop experiment data [18, 32].

5.6.2 Cu-10at.pct.Ti

With Cu-10at.pct.Ti on the other hand, it was not possible to fully infiltrate the graphite preform. Raw infiltration measurements performed at different temperature and pressure confirmed that only a small amount of metal flowed into open pores of the graphite preforms, see Figs. 5.6a-d). Observing the microstructure of the composite in Figs. 5.6 and 5.7 it is seen that a relatively dense layer of TiC is formed at the interface between the metal and the graphite preform. EDX mapping analysis confirms that the reaction product is formed by Ti and C, and that an intermetallic is formed on the outside of the preform with the composition Cu_3Ti_2 .

Comparing Fig. 5.6 and 5.7 it is seen that the higher the temperature is, the thicker is the carbide layer formed even if in both cases only a small amount of metal entered into the preform. This layer, likely formed as soon as the metal melts and contacts the preform, is apparently sufficiently thick to have blocked access to remaining open pores of the preform, preventing their full infiltration.

Summing up, we show that, although adding active elements that improve the wettability of solid preforms through the formation of a better wetted interfacial reaction product is a strategy that has frequently been used to ease infiltration with a metal to form metallic composites, in pressure infiltration, this will often not be attractive. For this approach to be beneficial, interfacial reaction kinetics must be sufficiently slow to prevent blockage of open pores within the preform and also to prevent rapid depletion of the infiltrant with the reactive element. Given the comparatively short times (seconds or minutes) required for the pressure-driven infiltration of porous preforms with molten metal, alloying to enhance preform wettability through interfacial reaction will therefore often not be an interesting approach from the perspective of eased composite processing.

5.7 Conclusion

Adding chromium or titanium to liquid copper contacting graphite is known to lead to the formation of carbides, Cr_3C_2 and TiC , respectively, which are both better wetted by the liquid metal than is the initial graphite. We show here that such interfacial reaction does not ease pressure infiltration in those two systems, for two different reasons that are likely to be found with other systems as well:

- Liquid Cu-1at.pct.Cr forms rapidly a stable carbide layer along the outer surface of the graphite preform. Subsequent pressure infiltration shows features of reactionless infiltration and the associated drainage curve is the same for pure copper into the same graphite preform. This indicates that, in this system, alloy depletion in chromium at the infiltration front prevents it from aiding infiltration over what is found with copper alone.
- Cu-10at.pct.Ti also leads to the rapid formation of carbide along the preform periphery; however, in this system the reaction layer clogs peripheral pores of the preform, preventing further infiltration.

5.8 Acknowledgement

This work was sponsored by the Swiss National Science Foundation (SFNS), Project No. 200021_149899.

6 Conclusion

Time-dependent interfacial phenomena can influence the pressure-driven liquid metal infiltration of porous ceramic or carbon solid preforms by preventing static capillary equilibrium from being reached at the triple line of metal/solid/vapour phase coexistence. This is manifest by the fact that, under fixed applied pressure, the infiltration front continuously progresses into the solid porous body to be infiltrated instead of stabilizing. Measurements of the rate of steady isobaric saturation increase are conducted, to study the interplay between applied pressure and thermally activated phenomena occurring along the triple line, for four systems at temperatures near or above 1000°C.

The main findings of this work for the infiltration of Cu-46at.pct.Si alloy into porous carbon, can be summarized as:

- Chemical interaction between the solid and the liquid, known to produce a better wetted interface (SiC) along the solid surface, prevents reaching capillary equilibrium in isobaric pressure infiltration, contrary to what is found for non-reactive systems. Pressure is however still necessary to overcome an initial capillary force and in order to first drive the metal into the porous carbon preform.
- Microstructural analysis of infiltrated composites show that SiC forms along the L-S interface and that an increase in temperature leads to a thickening of the formed carbide.
- The steady isobaric saturation rate increases with increasing applied pressure.
- Measurements of the steady isobaric rate of saturation increase conducted at, or slightly above, the threshold pressure for initial penetration of the melt into the carbon preforms produce data that can be interpreted using the analysis framework developed to interpret the kinetics of thermally activated plastic deformation. The resulting activation volume characteristic of the thermally activated process driving forward motion of the triple line is around a few 100nm³
- Performing the experiment at different temperatures enables drawing an Arrhenius plot and deducing an activation energy of the thermally activated rate of isobaric infiltration

Chapter 6. Conclusion

in this system. This gives a value near $400 \frac{kJ}{mol}$, consistent within error with data in the literature for the rate of triple line motion with this system in sessile drop experiments.

Adding Cr or Ti to Cu infiltrating the same carbon preforms leads also to the formation of carbides at the interface that are better wetted by the alloy than carbon; however, in these systems the rate of carbide formation is higher than for Cu-Si alloys. This prevents the observation of steady, isobaric infiltration observed with the more slowly reacting Cu-Si/C system. More specifically:

- The Cu-10at.pct.Ti alloy creates a thick layer of carbide at the interface along the periphery of the preform, preventing further infiltration by clogging the pore necks.
- With Cu-1at.pct.Cr, interfacial reaction along the periphery of the preform does not block flow into the porous carbon preforms; however, the reaction “cleans” the flowing alloy infiltration front of its reactive element. This leads pressure infiltration with this system to show features of non-reactive infiltration, and to a drainage curve equal to that of the (pure) Cu-C system infiltrated into the same graphite preform.

With the non-reactive system Al-Al₂O₃, it is found that:

- In the infiltration of molten Al at, or above, 1000°C into preforms of packed (comminuted) Bayer alumina particles possessing sharp angles, the infiltration front does not reach an equilibrium position, unlike what is found at lower temperature. Instead, the system shows the same characteristics in pressure infiltration as does the mildly reactive Cu-Si/C system, namely steady infiltration of the melt into the preform under fixed pressure, near the threshold pressure for initiation of preform infiltration.
- Microstructural evidence suggests that this is caused by the solution-precipitation of alumina in contact with liquid Al. This process has similarity with the “ridging” phenomenon that has been documented for this system in sessile drop experiments.
- The resulting activation volume, characteristic of the thermally activated process driving forward motion of the triple line in this system, is similar to that found with Cu-Si/C, namely a few times 100nm³
- The activation energy found for this system, by means of an Arrhenius plot for data corrected for the influence of the applied pressure, is between 300-500 $\frac{kJ}{mol}$; this is in the range of the bulk diffusion of oxygen through alumina.
- Further analyses of the Bayer alumina powder used in this, and previous, work show that it contains a sodium phase caused by the presence of sodium impurities derived from the Bayer process. The effect of this phase was analysed and it was found that it does not affect the drainage curve or steady infiltration measurements in the Al-Al₂O₃ system.

Sodium however, helps produce reproducible drainage curves with this system. We show that this is likely caused by an interaction between evaporated sodium oxide and the aluminium oxide layer that initially covers the surface of aluminium, this interaction between the two effectively fluxing the infiltration front of its oxide.

7 Perspectives

A possible future extension of this work could be to investigate other reactive systems such as Cu-V into graphite and to investigate further the effect of chemical reaction at the interface during infiltration. Another interesting development could be to perform infiltration of Cu-10at.pct.Ti into a less dense graphite preform, to see whether this would allow full infiltration and then similarly measure the activation volume and activation energy for TiC formation-driven pressure infiltration.

An interesting feature to analyse further is the activation volume. It was found to be roughly similar for the two very different analysed systems. One could investigate further the exact meaning of this parameter and determine whether it was a coincidence that the same value was found, or whether the order of magnitude 100nm^3 represents a constant value for the minimum volume needed to destabilize the capillary equilibrium and allow a steady rate of infiltration. This can be achieved by increasing the pore size through which the metal passes or by increasing the pressure difference between the two pressures used to deduce the activation volume value. To this end, other reactive systems such as Cu-Ti into Al_2O_3 , Cu-Al-Ti into Al_2O_3 , or Al-Si into graphite could be investigated. With the last system, the data would be interesting, as they may help to determine whether the activation energy remains the same as for the Si+C→SiC system, since this would confirm that it is linked to the rupture of C-C bonds.

In order to better understand the influence of reactivity, an experiment could be designed and performed using a sample with simple and well known pores in succession (See Fig. 7.1), in which a constant pressure would be kept at the threshold pressure for the biggest pore, and the system would be let to react at each pore neck, measuring the rate of infiltration thus produced.

This experiment may allow to understand the importance of the reaction velocity and how it helps the melt pass over pore necks thus, allowing the progression of infiltration even if the applied pressure is not sufficient for the infiltration front to advance without interfacial interaction between the solid and the liquid.

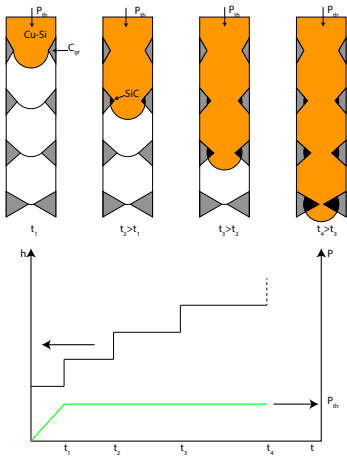


Figure 7.1: Schematic representation of an experiment with simplified pores. On top, the advancing infiltration, on the bottom, the displacement of the liquid as a function of time.

Bibliography

- [1] N. Eustathopoulos, M. G. Nicholas, and B. Drevet, *Wettability at high temperatures*. Pergamon Press, Inc, 1999.
- [2] M. Bahraini, *Characterization of capillarity forces during liquid metal infiltration*. PhD thesis, EPFL, 2007.
- [3] A. Léger, L. Weber, and A. Mortensen, "Infiltration of tin bronze into alumina particle beds: influence of alloy chemistry on drainage curves," *Journal of Materials Science*, vol. 49, pp. 7669–7678, 2014.
- [4] M. G. Nicholas, "The strength of metal/alumina interfaces," *Journal of Materials Science*, vol. 3, pp. 571–576, 1968.
- [5] V. Laurent, D. Chatain, C. Chatillon, and N. Eustathopoulos, "Wettability of monocrystalline alumina by aluminium between its melting point and 1273K," *Acta Metallurgica*, vol. 36, no. 7, pp. 1797–1803, 1988.
- [6] H. John and H. Hausner, "Wetting of aluminum oxide by liquid aluminum," *International Journal of High Technology Ceramics*, vol. 2, pp. 73–78, 1986.
- [7] J. J. Brennan and J. A. Pask, "Effect of nature of surfaces on wetting of sapphire by liquid aluminum," *Journal of the American Ceramic Society*, vol. 51, no. 10, pp. 569–573, 1968.
- [8] D.-J. Wang and S.-T. Wu, "The influence of oxidation on the wettability of aluminium on sapphire," *Acta Metallurgica et Materialia*, vol. 42, no. 12, pp. 4029–4034, 1994.
- [9] J. V. Naidich, J. N. Chubashov, N. F. Ishchuk, and V. P. Krasovskii, "Wetting of some nonmetallic materials by aluminium," *Poroshkovaya Metallurgiya*, vol. 6, no. 246, pp. 67–69, 1983.
- [10] M. Ksiazek, N. Sobczak, B. Mikulowski, W. Radziwill, and I. Surowiak, "Wetting and bonding strength in Al/Al₂O₃ system," *Materials Science and Engineering: A*, vol. 324, pp. 162–167, 2002.
- [11] P. Shen, H. Fujii, T. Matsumoto, and K. Nogi, "Wetting of (0001) α -Al₂O₃ single crystals by molten Al," *Scripta Materialia*, vol. 48, pp. 779–784, 2003.

Bibliography

- [12] P. Shen, H. Fujii, T. Matsumoto, and K. Nogi, "Reactive wetting of molten Al on different oriented α -Al₂O₃ single crystals at high temperatures," *Scripta Materialia*, vol. 49, pp. 563–569, 2003.
- [13] D. Carnahan, T. L. Johnston, and C. H. Li, "Some observations on the wetting of Al₂O₃ by aluminium," *Journal of The American Ceramic Society*, vol. 41, no. 9, pp. 343–347, 1958.
- [14] A. J. Klintner, G. Mendoza-Suarez, and R. A. L. Drew, "Wetting of pure aluminum and selected alloys on polycrystalline alumina and sapphire," *Materials Science and Engineering: A*, vol. 495, pp. 147–152, 2008.
- [15] E. Saiz, A. P. Tomsia, and R. M. Cannon, "Ridging effects on wetting and spreading of liquids on solids," *Acta Materialia*, vol. 46, no. 7, pp. 2349–2361, 1998.
- [16] E. Saiz, A. P. Tomsia, and K. Suganuma, "Wetting and strength issues at Al/ α -alumina interfaces," *Journal of the European Ceramic Society*, vol. 23, pp. 2787–2796, 2003.
- [17] L. Yang, P. Shen, Q. Lin, F. Qiu, and Q. Jiang, "Effect of Cr on the wetting in Cu/graphite system," *Applied Surface Science*, vol. 257, pp. 6276–6281, 2011.
- [18] D. A. Mortimer and M. G. Nicholas, "The wetting of carbon and carbides by copper alloys," *Journal of Materials Science*, vol. 8, pp. 640–648, 1973.
- [19] J. V. Naidich and G. A. Kolesnichenko, "Investigation of the wetting of diamond and graphite by molten metals and alloys, III. The wetting of diamond crystals," *Poroshkovaya Metallurgiya*, vol. 3, no. 21, pp. 23–28, 1964.
- [20] J. V. Naidich and G. A. Kolesnichenko, "Investigation of the wetting of and adhesion to graphite and diamond by liquid metals," in *Surface Phenomena in Metallurgical Processes*, p. 2018, 1965.
- [21] N. Shinozaki, Y. Katayama, Y. Umezawa, and K. Wasi, "Reaction and wetting between molten Cu-Ti alloy and graphite," *J. JRICu*, vol. 47, p. 187, 2008.
- [22] P. M. Scott, M. G. Nicholas, and B. Dewar, "The wetting and bonding of diamonds by Copper-base binary alloys," *Journal of Materials Science*, vol. 10, pp. 1833–1840, 1975.
- [23] J.-G. Li, "Kinetics of wetting and spreading of Cu-Ti alloys on alumina and glassy carbon substrates," *Journal of Materials Science Letters*, vol. 11, pp. 1551–1554, 1992.
- [24] N. Sobczak, J. Sobczak, P. K. Rohatgi, M. Ksiazek, W. Radziwill, and J. Morgiel, "Interaction between Ti or Cr containing copper alloys and porous graphite substrate," in *High Temperature Capillarity* (N. Eustathopoulos, N. Sobczak, ed.), (Cracow), pp. 145–152, 1997.
- [25] R. Standing and M. G. Nicholas, "The wetting of alumina and vitreous carbon by copper-titanium alloys," *Journal of Materials Science*, vol. 13, pp. 1509–1514, 1978.

- [26] J. V. Naidich and G. A. Kolesnichenko, "Study of the wetting of diamond and graphite by liquid metals, II. Angles of contact and adhesion between tin-titanium and copper-tin-titanium alloys and the graphite surface," *Poroshkovaya Metallurgiya*, vol. 1, no. 13, pp. 49–53, 1963.
- [27] W. Mao, T. Yamaki, N. Miyoshi, N. Shinozaki, and T. Ogawa, "Wettability of Cu-Ti alloys on graphite in different placement states of copper and zitanium at 1373 K (1100°C)," *Metallurgical and Materials Transactions A*, vol. 46A, pp. 2262–2272, 2015.
- [28] M. G. Nicholas, *Joining ceramics, glass and metal*. DGM Informationsgesellschaft, 1989.
- [29] P. Xiao and B. Derby, "Wetting of titanium nitride and titanium carbide by liquid metals," *Acta Materialia*, vol. 44, no. 1, pp. 307–314, 1996.
- [30] H. Goretzki and W. Scheuermann, "Einfluss der Elektronenkonfiguration auf das Benetzungsverhalten von Hartstoffmischkristallen," *High Temperatures - High Pressures*, vol. 3, pp. 649–658, 1971.
- [31] L. Ramqvist, "Wetting of metallic carbides by liquid copper, nickel, cobalt, and iron," *International Journal of Powder Metallurgy*, vol. 2, no. 4, pp. 2–21, 1965.
- [32] D. A. Mortimer and M. G. Nicholas, "The wetting of carbon by copper and copper alloys," *Journal of Materials Science*, vol. 5, pp. 149–155, 1970.
- [33] Z. Tao, Q. Guo, X. Gao, and L. Liu, "The wettability and interface thermal resistance of copper/graphite system with an addition of chromium," *Materials Chemistry and Physics*, vol. 128, pp. 228–232, 2011.
- [34] S. M. Devinent and G. M. Michal, "Reaction layer formation at the graphite/copper-chromium alloy interface," *Metallurgical Transactions A*, vol. 24A, pp. 53–60, 1993.
- [35] R. Voytovych, A. Mortensen, and N. Eustathopoulos, "Spreading kinetics of Cu-Cr alloys on carbon substrate," in *High Temperature Capillarity*, (Cracow), 1997.
- [36] K. Landry, C. Rado, R. Voytovych, and N. Eustathopoulos, "Mechanisms of reactive wetting: The question of triple line configuration," *Acta Materialia*, vol. 45, no. 7, pp. 3079–3085, 1997.
- [37] F. Hodaj, O. Dezellus, J. N. Barbier, A. Mortensen, and N. Eustathopoulos, "Diffusion-limited reactive wetting: effect of interfacial reaction behind the advancing triple line," *Journal of Materials Science*, vol. 42, pp. 8071–8082, 2007.
- [38] K. Nogi, Y. Osugi, and K. Ogino, "A new method of wettability measurement utilizing a small sample and its application to graphite or α -SiC and liquid Cu-Cr alloy systems," *ISIJ International*, vol. 30, no. 1, pp. 64–69, 1990.

Bibliography

- [39] R. Voytovych, A. Mortensen, F. Hodaj, and N. Eustathopoulos, "Diffusion-limited reactive wetting: Study of spreading kinetics of Cu-Cr alloys on carbon substrates," *Acta Materialia*, vol. 47, no. 4, pp. 1117–1128, 1999.
- [40] V. Michaud and A. Mortensen, "Infiltration processing of fibre reinforced composites: governing phenomena," *Composites Part A: Applied Science and Manufacturing*, vol. 32, pp. 981–996, 2001.
- [41] G. Schneider, L. Weber, and A. Mortensen, "Reactive pressure infiltration of Cu-46at.pct.Si into carbon," *Submitted to Acta Materialia*, 2019.
- [42] Y. Nishida, *Introduction to metal matrix composites : fabrication and recycling*. Tokyo: Tokyo : Springer, 2013.
- [43] B. Cantor, *Metal and ceramic matrix composites: an Oxford-Kobe materials text*. Bristol: Bristol : Institute of Physics Publishing, 2004.
- [44] T. W. Clyne and P. J. Withers, *An introduction to metal matrix composites*. Cambridge: Cambridge : Cambridge University Press, 1993.
- [45] N. Chawla and K. K. Chawla, *Metal matrix composites*. Boston, MA: Springer, 2006.
- [46] S. Hasanovic, A. Mortensen, L. Weber, and R. Tavangar, "Composite material comprising a precious metal, manufacturing process and use of such material," mar 2011.
- [47] D. Huda, M. A. El Baradie, and M. S. J. Hashmi, "Development of a hardness model for MMCs (Al/Al₂O₃)," *Journal of Materials Processing Technology*, vol. 44, pp. 81–90, 1994.
- [48] D. Huda, M. A. El Baradie, and M. S. J. Hashmi, "Metal-matrix composites: Manufacturing aspects. Part I," tech. rep., 1993.
- [49] D. Huda, M. A. El Baradie, and M. S. J. Hashmi, "Metal-matrix composites: Materials aspects. Part II," *Journal of Materials Processing Technology*, vol. 37, pp. 52–541, 1993.
- [50] S. N. Trinh and S. Sastry, "Processing and properties of metal matrix composites," *Mechanical Engineering and Materials Science Independent Study*, vol. 10, 2016.
- [51] B. Ralph, H. C. Yuen, and W. B. Lee, "The processing of metal matrix composites — an overview," *Journal of Materials Processing Technology*, vol. 63, no. 1-3, pp. 339–353, 1997.
- [52] R. Anish, G. Robert Singh, and M. Sivapragash, "Techniques for processing metal matrix composites; A survey," *Procedia Engineering*, vol. 38, pp. 3846–3854, 2012.
- [53] A. Evans, C. San Marchi, and A. Mortensen, *Processing of metal matrix composites*. Boston, MA: Springer, Boston, MA, 2003.
- [54] F. Delannay, C. Colin, Y. Marchal, L. Tao, F. Boland, P. Cobzaru, B. Lips, and M. Dellis, "Processing and properties of metal matrix composites reinforced with continuous fibres for the control of thermal expansion, creep resistance and fracture toughness," *Journal de Physique IV Colloque*, vol. 03, no. 3, 1993.

- [55] S. Sheibani and M. Fazel Najafabadi, "In situ fabrication of Al–TiC metal matrix composites by reactive slag process," *Metal & Design*, vol. 28, pp. 2373–2378, 2007.
- [56] A. Basumallick and S. Ghosh, "Processing of In Situ aluminium matrix composites by micro-pyretic reactive sintering," *Materials and Manufacturing Processes*, vol. 22, pp. 692–695, 2007.
- [57] M. R. Ghomashchi and A. Vikhrov, "Squeeze casting: an overview," *Journal of Material Processing Technology*, vol. 101, pp. 1–9, 2000.
- [58] Y. Chen, X. Zhang, E. Liu, C. He, C. Shi, J. Li, P. Nash, and N. Zhao, "Fabrication of in-situ grown graphene reinforced Cu matrix composites," *Scientific Reports*, vol. 6, p. 19363, may 2016.
- [59] N. Kang, P. Coddet, Q. Liu, H. Liao, and C. Coddet, "In-situ TiB/near α Ti matrix composites manufactured by selective laser melting," *Additive Manufacturing*, vol. 11, pp. 1–6, jul 2016.
- [60] Q. Gao, S. Wu, S. LÜ, X. Duan, and P. An, "Preparation of in-situ 5 vol% TiB₂ particulate reinforced Al–4.5Cu alloy matrix composites assisted by improved mechanical stirring process," *Materials & Design*, vol. 94, pp. 79–86, mar 2016.
- [61] S. Li, K. Kondoh, H. Imai, B. Chen, L. Jia, J. Umeda, and Y. Fu, "Strengthening behavior of in situ-synthesized (TiC–TiB)/Ti composites by powder metallurgy and hot extrusion," *Materials & Design*, vol. 95, pp. 127–132, apr 2016.
- [62] P. S. Bains, S. S. Sidhu, and H. S. Payal, "Fabrication and machining of metal matrix composites: a review," *Materials and Manufacturing Processes*, vol. 31, pp. 553–573, apr 2016.
- [63] S. Suarez, L. Reinert, M. Zeiger, P. Miska, S. Grandthyll, F. Müller, V. Presser, and F. Mücklich, "In-situ nanodiamond to carbon onion transformation in metal matrix composites," *Carbon*, vol. 129, pp. 631–636, apr 2018.
- [64] J. Jiang, X. He, J. Du, X. Pang, H. Yang, and Z. Wei, "In-situ fabrication of graphene-nickel matrix composites," *Materials Letters*, vol. 220, pp. 178–181, jun 2018.
- [65] V. A. Popov, M. Burghammer, M. Rosenthal, and A. Kotov, "In situ synthesis of TiC nano-reinforcements in aluminum matrix composites during mechanical alloying," *Composites Part B: Engineering*, vol. 145, pp. 57–61, jul 2018.
- [66] Y. Lei, J. Jiang, T. Bi, J. Du, and X. Pang, "Tribological behavior of in situ fabricated graphene–nickel matrix composites," *RSC Advances*, vol. 8, pp. 22113–22121, jun 2018.
- [67] L. Huang, M. Qian, Z. Liu, V. T. Nguyen, L. Yang, L. Wang, and J. Zou, "In situ preparation of TiB nanowires for high-performance Ti metal matrix nanocomposites," *Journal of Alloys and Compounds*, vol. 735, pp. 2640–2645, feb 2018.

Bibliography

- [68] B. J. Keene, "Review of data for the surface tension of pure metals," *International Materials Reviews*, vol. 38, no. 4, pp. 157–192, 1993.
- [69] P.-G. DeGennes, F. Brochard-Wyart, and D. Quéré, *Capillarity and wetting phenomena: drops, bubbles, pearls, waves*. 2004.
- [70] N. Eustathopoulos, "Wetting by liquid metals—application in materials processing: The contribution of the Grenoble group," *Metals*, vol. 5, no. 1, pp. 350–370, 2015.
- [71] T. Young, "An essay on the cohesion of fluids," *Philosophical Transactions of the Royal Society of London*, vol. 95, no. 0, pp. 65–87, 1805.
- [72] G. W. Liu, M. L. Muolo, F. Valenza, and A. Passerone, "Survey on wetting of SiC by molten metals," *Ceramics International*, vol. 36, no. 4, pp. 1177–1188, 2010.
- [73] K. Nogi, M. Tsujimoto, K. Ogino, and N. Iwamoto, "Wettability of MgO single crystal by liquid pure Pb, Sn and Bi," *Acta Metallurgica et Materialia*, vol. 40, no. 5, pp. 1045–1050, 1992.
- [74] P. Kritsalis, B. Drevet, N. Valignat, and N. Eustathopoulos, "Wetting transitions in reactive metal/oxide systems," *Scripta Metallurgica et Materialia*, vol. 30, no. 9, pp. 1127–1132, 1994.
- [75] J.-G. Li, "Wetting of ceramic materials by liquid silicon, aluminium and metallic melts containing titanium and other reactive elements: A review," *Ceramics International*, vol. 20, pp. 391–412, 1994.
- [76] P. D. Ownby, K. W. K. Li, and D. A. Welrauch, "High-temperature wetting of sapphire by aluminum," *Journal of the American Ceramic Society*, vol. 74, pp. 1275–1281, 1991.
- [77] O. Dezellus, F. Hodaj, and N. Eustathopoulos, "Progress in modelling of chemical-reaction limited wetting," *Journal of the European Ceramic Society*, vol. 23, no. 15, pp. 2797–2803, 2003.
- [78] O. Dezellus, S. Jacques, F. Hodaj, and N. Eustathopoulos, "Wetting and infiltration of carbon by liquid silicon," *Journal of Materials Science*, vol. 40, pp. 2307–2311, 2005.
- [79] E. Candan, H. V. Atkinson, and H. Jones, "Role of surface tension in relation to contact angle in determining threshold pressure for melt infiltration of ceramic powder compacts," *Scripta Materialia*, vol. 38, no. 6, pp. 999–1002, 1998.
- [80] M. Kobashi and T. Choh, "The wettability and the reaction for SiC particle/Al alloy system," *Journal of Materials Science*, vol. 28, no. 3, pp. 684–690, 1993.
- [81] H. Fujii, H. Nakae, and K. Okada, "Interfacial reaction wetting in the boron nitride/-molten aluminum system," *Acta Metallurgica et Materialia*, vol. 41, no. 10, pp. 2963–2971, 1993.

- [82] J. F. White, L. Ma, K. Forwald, and D. Sichen, "Reactions between silicon and graphite substrates at high temperature: In Situ observations," *Metallurgical and Materials Transactions B*, vol. 45B, pp. 150–160, 2014.
- [83] I. A. Aksay, C. E. Hoge, and J. A. Pask, *Wetting under chemical equilibrium and nonequilibrium conditions*, vol. 78. 1974.
- [84] P. Protsenko, A. Terlain, V. Traskine, and N. Eustathopoulos, "The role of intermetallics in wetting in metallic systems," *Scripta Materialia*, vol. 45, no. 12, pp. 1439–1445, 2001.
- [85] D. Muscat, R. L. Harris, and R. A. L. Drew, "The effect of pore size on the infiltration kinetics of aluminum in titanium carbide preforms," *Acta Metallurgica et Materialia*, vol. 42, no. 12, pp. 4155–4163, 1994.
- [86] N. Eustathopoulos and B. Drevet, "Relationship between reactivity and wettability in metal/oxide systems," *Composite Interfaces*, vol. 2, no. 1, pp. 29–42, 1994.
- [87] F. Delannay, L. Froyen, and A. Deruyttere, "The wetting of solids by molten metals and its relation to the preparation of metal-matrix composites," *Journal of Materials Science*, vol. 22, no. 1, pp. 1–16, 1987.
- [88] N. Eustathopoulos, "Dynamics of wetting in reactive metal/ ceramic systems," *Acta Materialia*, vol. 46, no. 7, pp. 2319–2327, 1998.
- [89] N. Eustathopoulos and R. Voytovich, "The role of reactivity in wetting by liquid metals: a review," *Journal of Materials Science*, vol. 51, pp. 425–437, 2016.
- [90] R. Sangiorgi, M. L. Muolo, D. Chatain, and N. Eustathopoulos, "Wettability and work of adhesion of nonreactive liquid metals on silica," *Journal of the American Ceramic Society*, vol. 71, pp. 742–748, sep 1988.
- [91] J.-G. Li, D. Chatain, L. Coudurier, and N. Eustathopoulos, "Wettability of sapphire by Sn-Al alloys," *Journal of Materials Science Letters*, vol. 7, pp. 961–963, 1988.
- [92] S.-Y. Oh, J. A. Cornie, and K. C. Russell, "Wetting of ceramic particulates with liquid aluminium alloys: Part I. Experimental techniques," *Metallurgical Transactions A*, vol. 20A, no. March, pp. 527–532, 1989.
- [93] V. Ghetta, J. Fouletier, and D. Chatain, "Oxygen adsorption isotherms at the surfaces of liquid Cu and Au-Cu alloys and their interfaces with Al₂O₃ detected by wetting experiments," *Acta Materialia*, vol. 44, no. 5, pp. 1927–1936, 1996.
- [94] R. N. Murarka, W. K. Lu, and A. E. Hamielec, "Effect of dissolved oxygen on the surface tension of liquid iron," *Canadian Metallurgical Quarterly*, vol. 14, no. 2, pp. 111–115, 1975.
- [95] K. Nogi and K. Ogino, "Wettability of SiC by liquid pure metals," *Transaction of the Japan Institute of Metals*, vol. 29, no. 9, pp. 742–747, 1988.

Bibliography

- [96] R. Sangiorgi, M. L. Muolo, and A. Passerone, "Surface tension and adsorption in liquid silver-oxygen alloys," *Acta Metallurgica*, vol. 30, no. 8, pp. 1597–1604, 1982.
- [97] K. Landry, C. Rado, and N. Eustathopoulos, "Influence of interfacial reaction rates on the wetting driving force in metal / ceramic systems," *Metallurgical and Materials Transactions A*, vol. 27, pp. 3181–3186, 1996.
- [98] C. Toy and W. Scott, "Wetting and spreading of molten aluminium against AlN surfaces," *Journal of Materials Science*, vol. 2, pp. 3243–3248, 1997.
- [99] P. Kritsalis, L. Coudurier, and N. Eustathopoulos, "Contribution to the study of reactive wetting in the CuTi/Al₂O₃ system," *Journal of Materials Science*, vol. 26, pp. 3400–3408, 1991.
- [100] L. Espié, B. Drevet, and N. Eustathopoulos, "Experimental study of the influence of interfacial energies and reactivity on wetting in metal / oxide systems," *Metallurgical and Materials Transactions A*, vol. 25, no. March, pp. 1994–1994, 1994.
- [101] O. Dezellus and N. Eustathopoulos, "Fundamental issues of reactive wetting by liquid metals," *Journal of Materials Science*, vol. 45, no. 16, pp. 4256–4264, 2010.
- [102] E. Saiz, R. M. Cannon, and A. P. Tomsia, "Reactive spreading: adsorption, ridging and compound formation," *Acta Materialia*, vol. 48, pp. 4449–4462, 2000.
- [103] W. D. Kaplan, D. Chatain, P. Wynblatt, and W. C. Carter, "A review of wetting versus adsorption, complexions, and related phenomena: The rosetta stone of wetting," *Journal of Materials Science*, vol. 48, pp. 5681–5717, 2013.
- [104] J.-G. Li, "Wetting and interfacial bonding of metals with ionocovalent oxides," *Journal of the American Ceramic Society*, vol. 75, pp. 3118–3126, 1992.
- [105] B. Drevet, K. Landry, and N. Eustathopoulos, "Influence of substrate orientation on wetting kinetics in reactive metal/ceramic system," *Scripta Materialia*, vol. 35, no. 11, pp. 1265–1270, 1996.
- [106] S. Bao, K. Tang, A. Kvithyld, T. A. Engh, and M. Tangstad, "Wetting of pure aluminium on graphite, SiC and Al₂O₃ in aluminium filtration," *Transactions of Nonferrous Metals Society of China*, vol. 22, pp. 1930–1938, 2012.
- [107] H. Do-Suck, H. Jones, and H. V. Atkinson, "The wettability of silicon carbide by liquid aluminium," *Journal of Materials Science*, vol. 28, pp. 2654–2658, 1993.
- [108] D. Zhang, D.-Y. Zhu, T. Zhang, and Q.-F. Wang, "Kinetics of reactive wetting of graphite by liquid Al and Cu-Si alloys," *Transactions of Nonferrous Metals Society of China*, vol. 25, pp. 2473–2480, 2015.

- [109] N. Sobczak, R. Nowak, W. Radziwill, J. Budzioch, and A. Glenz, "Experimental complex for investigations of high temperature capillarity phenomena," *Materials Science and Engineering: A*, vol. 495, no. 1-2, pp. 43–49, 2008.
- [110] C. Rado, B. Drevet, and N. Eustathopoulos, "The role of compound formation in reactive wetting: the Cu/SiC system," *Acta Materialia*, vol. 48, pp. 4483–4491, 2000.
- [111] K. Landry and N. Eustathopoulos, "Dynamics of wetting in reactive metal/ceramic systems," *Acta Materialia*, vol. 44, no. 10, pp. 3923–3932, 1996.
- [112] F. G. Yost and E. J. O'Toole, "Metastable and equilibrium wetting states in the Bi-Sn system," *Acta Materialia*, vol. 46, no. 14, pp. 5143–5151, 1998.
- [113] K. Landry, S. Kalogeropoulou, and N. Eustathopoulos, "Wettability of carbon by aluminium and aluminium alloys," *Materials Science and Engineering: A*, vol. 254, no. 1-2, pp. 99–111, 1998.
- [114] N. Eustathopoulos, N. Sobczak, A. Passerone, and K. Nogi, "Measurement of contact angle and work of adhesion at high temperature," *Journal of Materials Science*, vol. 40, pp. 2271–2280, 2005.
- [115] J. A. Champion, B. J. Keene, and J. M. Sillwood, "Wetting of aluminium oxide by molten aluminium and other metals," *Journal of Materials Science*, vol. 4, pp. 39–49, 1969.
- [116] R. Voytovych, F. Robaut, and N. Eustathopoulos, "The relation between wetting and interfacial chemistry in the CuAgTi/alumina system," *Acta Materialia*, vol. 54, no. 8, pp. 2205–2214, 2006.
- [117] O. Dezellus, F. Hodaj, and N. Eustathopoulos, "Chemical reaction-limited spreading: The triple line velocity versus contact angle relation," *Acta Materialia*, vol. 50, no. 19, pp. 4741–4753, 2002.
- [118] K. Nogi, Y. Hirata, T. Matsumoto, and H. Fujii, "Reactive wetting in liquid Cu alloy – carbon and silicon carbide systems," *Journal of Physics: Conference Series*, vol. 165, 2009.
- [119] N. Sobczak, M. Singh, and R. Asthana, "High-temperature wettability measurements in metal/ceramic systems - Some methodological issues," *Current Opinion in Solid State and Materials Science*, vol. 9, no. 4-5, pp. 241–253, 2005.
- [120] N. Eustathopoulos, D. Chatain, and L. Coudurier, "Wetting and interfacial chemistry in liquid metal-ceramic systems," *Materials Science and Engineering: A*, vol. 135, no. C, pp. 83–88, 1991.
- [121] G. Levi and W. D. Kaplan, "Aluminium-alumina interface morphology and thermodynamics from dewetting experiments," *Acta Materialia*, vol. 51, pp. 2793–2802, 2003.
- [122] G. Levi and W. D. Kaplan, "Oxygen induced interfacial phenomena during wetting of alumina by liquid aluminium," *Acta Materialia*, vol. 50, pp. 75–88, 2002.

Bibliography

- [123] L. Yang, P. Shen, Q. Lin, F. Qiu, and Q. Jiang, "Wetting of porous graphite by Cu-Ti alloys at 1373K," *Materials Chemistry and Physics*, vol. 124, pp. 499–503, 2010.
- [124] A. Sangghaleh and M. Halali, "Effect of magnesium addition on the wetting of alumina by aluminium," *Applied Surface Science*, vol. 255, pp. 8202–8206, 2009.
- [125] N. Eustathopoulos and B. Drevet, "Determination of the nature of metal–oxide interfacial interactions from sessile drop data," *Materials Science and Engineering: A*, vol. 249, no. 1-2, pp. 176–183, 1998.
- [126] B. S. Ellefson and N. W. Taylor, "Surface properties of fused salts and glasses. I. Sessile-drop method of determining surface tension and density of viscous liquids at high temperatures," *Journal of the American Ceramic Society*, vol. 21, no. 6, pp. 193–205, 1938.
- [127] R. Sangiorgi, G. Caracciolo, and A. Passerone, "Factors limiting the accuracy of measurements of surface tension by the sessile drop method," *Journal of Materials Science*, vol. 17, no. 10, pp. 2895–2901, 1982.
- [128] A. Mortensen, B. Drevet, and N. Eustathopoulos, "Kinetics of diffusion-limited spreading of sessile drops in reactive wetting," *Scripta Materialia*, vol. 36, no. 6, pp. 645–651, 1997.
- [129] V. Merlin and N. Eustathopoulos, "Wetting and adhesion of Ni-Al alloys on α -Al₂O₃ single crystals," *Journal of Materials Science*, vol. 30, pp. 3619–3624, 1995.
- [130] G. Kumar and K. N. Prabhu, "Review of non-reactive and reactive wetting of liquids on surfaces," *Advances in Colloid and Interface Science*, vol. 133, no. 2, pp. 61–89, 2007.
- [131] E. Saiz and A. P. Tomsia, "Atomic dynamics and Marangoni films during liquid-metal spreading," *Nature materials*, vol. 3, no. December, pp. 903–909, 2004.
- [132] E. Saiz and A. P. Tomsia, "Kinetics of high-temperature spreading," *Current Opinion in Solid State and Materials Science*, vol. 9, no. April, pp. 167–173, 2005.
- [133] M. Diemer, A. Neubrand, K. P. Trumble, and J. Rödel, "Influence of oxygen partial pressure and oxygen content on the wettability in the copper-oxygen-alumina system," *Journal of the American Ceramic Society*, vol. 82, pp. 2825–2832, dec 1999.
- [134] J. V. Naidich, "The wettability of solids by liquid metals," in *Progress in Surface and Membrane Science*, vol. 14, pp. 353–484, Elsevier, jan 1981.
- [135] I. Egry, E. Ricci, R. Novakovic, and S. Ozawa, "Surface tension of liquid metals and alloys — Recent developments," *Advances in Colloid and Interface Science*, vol. 159, pp. 198–212, 2010.
- [136] N. Travitzky and A. Shlayan, "Microstructure and mechanical properties of Al₂O₃ /Cu-O composites fabricated by pressureless infiltration technique," *Materials Science and Engineering: A*, vol. 244, pp. 154–160, 1998.

- [137] J. Schmitz, J. Brillo, and I. Egry, "Surface tension of liquid Cu and anisotropy of its wetting of sapphire," *Journal of Materials Science*, vol. 45, pp. 2144–2149, 2010.
- [138] S. K. Rhee, "Critical surface energies of Al₂O₃ and graphite," *Journal of the American Ceramic Society*, vol. 55, no. 6, pp. 300–303, 1972.
- [139] A. C. D. Chaklader, A. M. Armstrong, and S. K. Misra, "Interfacial reactions between metals and ceramics: IV, wetting of sapphire by liquid copper-oxygen alloys," *Journal of the American Ceramic Society*, vol. 51, pp. 630–633, 1968.
- [140] T. E. O'Brien and A. C. D. Chaklader, "Effect of oxygen on the reaction between copper and sapphire," *Journal of the American Ceramic Society*, vol. 57, no. 8, pp. 329–332, 1974.
- [141] C. Beraud, M. Courbiere, C. Esnouf, D. Juve, and D. Treheux, "Study of copper-alumina bonding," *Journal of Materials Science*, vol. 24, pp. 4545–4554, 1989.
- [142] K. P. Trumble, "Prediction of a critical temperature for aluminate formation in alumina/copper – oxygen eutectic bonding," *Journal of the American Ceramic Society*, vol. 82, pp. 2919–2920, 1999.
- [143] K. P. Trumble, "Thermodynamic analysis of aluminate formation at Fe/Al₂O₃ and Cu/Al₂O₃ interfaces," *Acta Metallurgica et Materialia*, vol. 40, pp. 105–110, 1992.
- [144] S. Yi, K. P. Trumble, and D. R. Gaskell, "Thermodynamic analysis of aluminate stability in the eutectic bonding of copper with alumina," *Acta Materialia*, vol. 47, no. 11, pp. 3221–3226, 1999.
- [145] S.-K. Lee and W.-H. Tuan, "Formation of CuAlO₂ at the Cu/Al₂O₃ interface and its influence on interface strength and thermal conductivity," *International Journal of Applied Ceramic Technology*, vol. 10, pp. 780–789, 2013.
- [146] K. A. Rogers, K. P. Trumble, B. J. Dalgleish, and I. E. Reimains, "Role of oxygen in microstructure development at solid-state diffusion-bonded Cu/ α -Al₂O₃ interfaces," *Journal of the American Ceramic Society*, vol. 77, no. 8, pp. 2036–2042, 1994.
- [147] M. Gautier, J.-P. Duraud, and L. Pham Van, "Influence of the Al₂O₃ (0001) surface reconstruction on the Cu/Al₂O₃ interface," *Surface Science Letters*, vol. 249, pp. L327–L332, 1991.
- [148] I. E. Reimains, K. P. Trumble, K. A. Rogers, and B. J. Dalgleish, "Influence of Cu₂O and CuAlO₂ interphases on crack propagation at Cu/ α -Al₂O₃ interfaces," *Journal of the American Ceramic Society*, vol. 80, no. 2, pp. 424–432, 1997.
- [149] S. T. Kim and C. H. Kim, "Interfacial reaction product and its effect on the strength of copper to alumina eutectic bonding," *Journal of Materials Science*, vol. 27, pp. 2061–2066, 1992.

Bibliography

- [150] C. W. Seager, K. Kokini, K. P. Trumble, and M. J. M. Krane, "The influence of CuAlO₂ on the strength of eutectically bonded Cu/Al₂O₃ interfaces," *Scripta Materialia*, vol. 46, pp. 395–400, 2002.
- [151] J. V. Naidich and G. A. Kolesnichenko, "Investigation of the wetting of diamond and graphite by molten metals and alloys," *Poroshkovaya Metallurgiya*, vol. 2, pp. 76–79, 1968.
- [152] O. Dezellus, F. Hodaj, S. Janaqi, and N. Eustathopoulos, "Influence of evaporation-condensation in reactive spreading," *Acta Materialia*, vol. 50, pp. 4727–4740, 2002.
- [153] O. Dezellus and N. Eustathopoulos, "The role of Van Der Waals interactions on wetting and adhesion in metal/carbon system," *Scripta Materialia*, vol. 40, no. 11, pp. 1283–1288, 1999.
- [154] A. R. Kennedy, J. D. Wood, and B. M. Weager, "The wetting and spontaneous infiltration of ceramics by molten copper," *Journal of Materials Science*, vol. 35, pp. 2909–2912, 2000.
- [155] S. K. Rhee, "Wetting of AlN and TiC by liquid Ag and liquid Cu," *Journal of the American Ceramic Society*, vol. 53, pp. 639–641, dec 1970.
- [156] E. Ricci, D. Giuranno, I. Grosso, T. Lanata, S. Amore, R. Novakovic, and E. Arato, "Surface tension of molten Cu-Sn alloys under different oxygen containing atmospheres," *Journal of Chemical and Engineering Data*, vol. 54, pp. 1660–1665, jun 2009.
- [157] K. Nogi, K. Oishi, and K. Ogino, "Wettability of solid oxides by liquid pure metals," *Materials Transactions, JIM*, vol. 30, no. 2, pp. 137–145, 1989.
- [158] G. Metsger, "Über die Temperaturabhängigkeit der Oberflächenspannung von Kupfer und die Oberflächenspannung von schmelzflüssigen Silber-Blei-, Silber-Wismut- und Kupfer-Blei-Legierungen," *Zeitschrift für Physikalische Chemie*, vol. 40, no. 211, pp. 1–25, 1959.
- [159] R. Novakovic, E. Ricci, D. Giuranno, and A. Passerone, "Surface and transport properties of Ag-Cu liquid alloys," *Surface Science*, vol. 576, pp. 175–187, feb 2005.
- [160] I. Egry, S. Sauerland, and G. Jacobs, "Surface tension of levitated liquid noble metals," *High Temperatures - High Pressures*, vol. 26, pp. 217–223, 1994.
- [161] F. Pawlek, W. Thielsch, and W. Wuth, "Der Einfluss von Temperatur und Legierungszusätzen auf die Oberflächenspannung von Silber, Kupfer und Kupferlegierungen," *Metall*, vol. 15, no. 11, pp. 1076–1078, 1961.
- [162] J. V. Naidich and V. N. Eremenko, "Method "Big Drops" to determine the surface tension and density molten metals at high temperatures," *Fiz. Met. Metalloved*, vol. 11, no. 6, pp. 883–888, 1961.

- [163] N. A. Bykov and V. G. Shevchenko, "Density and surface tension of Copper, Aluminium, Gallium, Indium and Tin," *Physical and Chemical Research of Liquid Metals and Alloys*, no. 29, pp. 42–46, 1974.
- [164] V. F. Ukhov, N. A. Vatolin, and V. P. Chenstov, "The dependence of the surface tension of alloys based on palladium and silver on the temperature," *Works of the Institute of Metallurgy*, no. 25, pp. 30–36, 1970.
- [165] X. B. Zhou and J. T. M. De Hosson, "Reactive wetting of liquid metals on ceramic substrates," *Acta Materialia*, vol. 44, no. 2, pp. 421–426, 1996.
- [166] S. B. Lee and Y.-M. Kim, "Direct observation of in-plane ordering in the liquid at a liquid Al/ α -Al₂O₃ (1102) interface," *Acta Materialia*, vol. 59, pp. 1383–1388, 2011.
- [167] P. Shen, H. Fujii, T. Matsumoto, and K. Nogi, "The influence of surface structure on wetting of α -Al₂O₃ by aluminum in a reduced atmosphere," *Acta Materialia*, vol. 51, pp. 4897–4906, 2003.
- [168] P. Shen, H. Fujii, T. Matsumoto, and K. Nogi, "Critical factors affecting the wettability of α -alumina by molten aluminum," *Journal of The American Ceramic Society*, vol. 87, pp. 2151–2159, 2004.
- [169] S. Bao, K. Tang, A. Kvithyld, M. Tangstad, and T. A. Engh, "Wettability of aluminum on alumina," *Metallurgical and Materials Transactions A*, vol. 42B, pp. 1358–1366, 2011.
- [170] Q. Zhang, T. Cagin, A. Van Duin, W. A. Goddard, Y. Qi, and L. G. Hector, "Adhesion and nonwetting-wetting transition in the Al/ α -Al₂O₃ interface," *Physical Review B*, vol. 69, pp. 045423–1–045423–11, 2004.
- [171] S. W. Ip, M. Kucharski, and J. M. Toguri, "Wetting behaviour of aluminium and aluminium alloys on Al₂O₃ and CaO," *Journal of Materials Science Letters*, vol. 12, pp. 1699–1702, 1993.
- [172] A. Sangghaleh and M. Halali, "An investigation on the wetting of polycrystalline alumina by aluminium," *Journal of Materials Processing Technology*, vol. 197, pp. 156–160, 2008.
- [173] H. John and H. Hausner, "Influence of oxygen partial pressure on the wetting behaviour in the system Al/Al₂O₃," *Journal of Materials Science Letters*, vol. 5, pp. 549–551, 1986.
- [174] H.-N. Ho and S.-T. Wu, "The influence of temperature and residual gas in the wettability of aluminium melt on sapphire," *Japanese Journal of Applied Physics*, vol. 37, pp. 274–278, 1998.
- [175] S. Bao, A. Kvithyld, S. Gaal, T. A. Engh, and M. Tangstad, "Wetting of pure aluminium on filter materials Graphite, AlF₃ and Al₂O₃," *Light metals*, pp. 767–771, 2009.
- [176] J. Schmitz, I. Egry, and J. Brillo, "Anisotropy in wetting of oriented sapphire surfaces by liquid Al-Cu alloys," *Journal of Materials Science*, vol. 49, pp. 2286–2297, 2014.

Bibliography

- [177] A. Bellosi and NATO and Advanced Research Workshop on Interfacial Science in Ceramic Joining, *Interfacial science in ceramic joining*. Dordrecht [etc.: Kluwer Academic, nato scien ed., 1998.
- [178] X. B. Zhou and J. T. M. De Hosson, "Wetting kinetics of liquid aluminium on an Al₂O₃ surface," *Journal of Materials Science*, vol. 30, pp. 3571–3575, jan 1995.
- [179] G. P. Pells, "Radiation damage effects in alumina," *Journal of the American Ceramic Society*, vol. 77, pp. 368–377, feb 1994.
- [180] S. H. Oh, Y. Kauffmann, C. Scheu, W. D. Kaplan, and M. Rühle, "Ordered liquid aluminum at the interface with sapphire," *Science (New York, N.Y.)*, vol. 310, pp. 661–3, oct 2005.
- [181] S. H. Oh, M. F. Chisholm, Y. Kauffmann, W. D. Kaplan, W. Luo, M. Rühle, and C. Scheu, "Oscillatory mass transport in vapor-liquid-solid growth of sapphire nanowires," *Science (New York, N.Y.)*, vol. 330, pp. 489–93, oct 2010.
- [182] T. P. Swiler and R. E. Loehman, "Molecular dynamics simulations of reactive wetting in metal–ceramic systems," *Acta Materialia*, vol. 48, pp. 4419–4424, dec 2000.
- [183] F. Spaepen, "A structural model for the solid-liquid interface in monatomic systems," *Acta Metallurgica*, vol. 23, pp. 729–743, jun 1975.
- [184] F. F. Abraham and Y. Singh, "The structure of a hard-sphere fluid in contact with a soft repulsive wall," *The Journal of Chemical Physics*, vol. 67, p. 2384, aug 1977.
- [185] A. Hashibon, J. Adler, M. W. Finnis, and W. D. Kaplan, "Atomistic study of structural correlations at a liquid–solid interface," *Computational Materials Science*, vol. 24, pp. 443–452, jul 2002.
- [186] R. L. Davidchack and B. B. Laird, "Direct calculation of the hard-sphere crystal / melt interfacial free energy," *Physical Review Letters*, vol. 85, pp. 4751–4754, nov 2000.
- [187] H. Reichert, O. Klein, H. Dosch, M. Denk, V. Honkimäki, T. Lippmann, and G. Reiter, "Observation of five-fold local symmetry in liquid lead," *Nature*, vol. 408, pp. 839–841, dec 2000.
- [188] C.-J. Yu, A. Richter, A. Datta, M. K. Durbin, and P. Dutta, "Observation of molecular layering in thin liquid films using X-Ray reflectivity," *Physical Review Letters*, vol. 82, pp. 2326–2329, mar 1999.
- [189] A. K. Doerr, M. Tolan, J.-P. Schlomka, and W. Press, "Evidence for density anomalies of liquids at the solid/liquid interface," *Europhysics Letters (EPL)*, vol. 52, pp. 330–336, nov 2000.
- [190] O. M. Magnussen, B. M. Ocko, M. J. Regan, K. Penanen, P. S. Pershan, and M. Deutsch, "X-Ray reflectivity measurements of surface layering in liquid mercury," *Physical Review Letters*, vol. 74, pp. 4444–4447, may 1995.

- [191] J. M. Howe and H. Saka, "In Situ transmission electron microscopy studies of the solid-liquid interface," *MRS Bulletin*, vol. 29, pp. 951–957, dec 2004.
- [192] M. Gandman, Y. Kauffmann, C. T. Koch, and W. D. Kaplan, "Direct quantification of ordering at a solid-liquid interface using aberration corrected transmission electron microscopy," *Physical Review Letters*, vol. 110, p. 086106, feb 2013.
- [193] A. Hashibon, J. Adler, M. W. Finnis, and W. D. Kaplan, "Ordering at solid-liquid interfaces between dissimilar materials," *Interface Science*, vol. 9, no. 3/4, pp. 175–181, 2001.
- [194] Y. Kauffmann, S. H. Oh, C. T. Koch, A. Hashibon, C. Scheu, M. Rühle, and W. D. Kaplan, "Quantitative analysis of layering and in-plane structural ordering at an alumina-aluminum solid-liquid interface," *Acta Materialia*, vol. 59, pp. 4378–4386, 2011.
- [195] W. D. Kaplan and Y. Kauffmann, "Structural order in liquids induced by interfaces with crystals," *Annual Review of Materials Research*, vol. 36, pp. 1–48, aug 2006.
- [196] G. Levi and W. D. Kaplan, "Iron as an oxygen tracer at the aluminum-alumina interface," *Journal of the American Ceramic Society*, vol. 85, pp. 1601–1606, jun 2002.
- [197] W. Zhang and J. R. Smith, "Nonstoichiometric interfaces and Al₂O₃ adhesion with Al and Ag," *Physical Review Letters*, vol. 85, pp. 3225–3228, oct 2000.
- [198] J. Kang, J. Zhu, C. Curtis, D. Blake, G. Glatzmaier, Y.-H. Kim, and S.-H. Wei, "Atomically abrupt liquid-oxide interface stabilized by self-regulated interfacial defects: the case of Al/Al₂O₃ interfaces," *Physical Review Letters*, vol. 108, p. 226105, may 2012.
- [199] J. Aguilar-Santillan, "The influence of surface anisotropy crystalline structure on wetting of sapphire by molten aluminum," *Metallurgical and Materials Transactions A*, vol. 44, pp. 2299–2306, may 2013.
- [200] Y. Liu and X.-S. Ning, "Influence of α -Al₂O₃ (0001) surface reconstruction on wettability of Al/Al₂O₃ interface: A first-principle study," *Computational Materials Science*, vol. 85, pp. 193–199, apr 2014.
- [201] T. M. French and G. A. Somorjai, "Surface structure of the (0001) face of α -alumina composition and surface structure of the (0001) face of α -alumina by low-energy electron diffraction," *The Journal of Physical Chemistry*, vol. 74, no. 12, pp. 2489–2495, 1970.
- [202] M. Vermeersch, R. Sporken, P. Lambin, and R. Caudano, "The Al-Al₂O₃ interface formation as studied by electron spectroscopies," *Surface Science*, vol. 235, pp. 5–14, sep 1990.
- [203] M. Gautier, G. Fenaud, L. Pham Van, B. Villette, M. Pollak, N. Thromat, F. Jollet, and J.-P. Duraud, " α -Al₂O₃ (0001) surfaces: Atomic and electronic structure," *Journal of the American Ceramic Society*, vol. 77, pp. 323–334, feb 1994.

Bibliography

- [204] G. Renaud, B. Villette, I. Vilfan, and A. Bourret, "Atomic structure of the α -Al₂O₃(0001)(V31×V31)R +/- 9° reconstruction," *Physical Review Letters*, vol. 73, pp. 1825–1828, sep 1994.
- [205] E. Gillet and B. Ealet, "Characterization of sapphire surfaces by electron energy-loss spectroscopy," *Surface Science*, vol. 273, pp. 427–436, jul 1992.
- [206] E. Saiz, R. M. Cannon, and A. P. Tomsia, "Energetic and atomic transport at liquid metal/Al₂O₃ interfaces," *Acta Materialia*, vol. 41, no. 15, pp. 4209–4220, 1999.
- [207] A. K. Ray and E. C. Subbarao, "Synthesis of sodium β and β' alumina," *Materials Research Bulletin*, vol. 10, pp. 583–590, 1975.
- [208] S. Yamaguchi, K. Terabe, Y. Iguchi, and A. Imai, "Formation and crystallization of beta-alumina from precursor prepared by sol-gel method using metal alkoxides," *Solid State Ionics*, vol. 25, pp. 171–176, 1987.
- [209] K. Terabe, S. Yamaguchi, Y. Iguchi, and A. Imai, "Characterization of sodium β -alumina prepared by sol-gel method," *Solid State Ionics*, vol. 40/41, pp. 111–114, 1990.
- [210] S. Sartori, A. Martucci, A. Muffato, and M. Guglielmi, "Sol-gel synthesis of Na⁺ beta-Al₂O₃ powders," *Journal of the European Ceramic Society*, vol. 24, pp. 911–914, 2004.
- [211] C. Zhu, J. Xue, and G. Ji, "Effect of Na₂O content on properties of beta alumina solid electrolytes," *Materials Science in Semiconductor Processing*, vol. 31, pp. 487–492, 2015.
- [212] E. A. Elrefaie and W. W. Smeltzer, "Thermodynamic properties of the ionic conduction phases of Na-Al-O system between 800 and 1200 K," *Solid State Ionics*, vol. 12, pp. 517–524, 1984.
- [213] R. Stevens and J. G. P. Binner, "Review structure, properties and production of β -alumina," *Journal of Materials Science*, vol. 19, pp. 698–715, 1984.
- [214] J. Gallup, "The transformation of aluminium oxide from the beta to the alpha form," *Journal of the American Ceramic Society*, vol. 18, pp. 144–148, dec 1935.
- [215] E. A. Elrefaie and W. W. Smeltzer, "The stability of β -Al₂O₃ (Na₂O:11Al₂O₃) in oxygen atmospheres," *Journal of The Electrochemical Society*, vol. 128, p. 1443, jul 1981.
- [216] J. A. Warren, W. J. Boettinger, and A. R. Roosen, "Modeling reactive wetting," *Acta Materialia*, vol. 46, no. 9, pp. 3247–3264, 1998.
- [217] V. S. Zhuravlev and M. A. Turchanin, "Reasons for the formation of various titanium oxide phases upon wetting aluminum oxide with titanium-containing metallic solutions," *Poroshkovaya Metallurgiya*, vol. 36, no. 3-4, pp. 141–146, 1997.
- [218] J.-G. Li and H. Hausner, "Reactive wetting in the liquid-silicon/solid-carbon system," 1996.

- [219] T. J. Whalen and A. T. Anderson, "Wetting of SiC, Si₃N₄, and Carbon by Si and binary Si alloys," *Journal of The American Ceramic Society*, vol. 58, no. 9-10, pp. 396–399, 1975.
- [220] J. V. Naidich, V. M. Perevertailo, and G. M. Nevodnik, "Kinetics of spreading of molten metals on solid surfaces," *Poroshkovaya Metallurgiya*, vol. 7, no. 115, pp. 51–55, 1972.
- [221] D. A. Cadenhead and J. F. Danielli, *Progress in surface and membrane science. Volume 14*. New York: Academic press INC., academic press ed., 1981.
- [222] O. Dezellus, F. Hodaj, and N. Eustathopoulos, "Role of diffusion and chemical reactions in reactive spreading kinetics: the case of Cu-Si/C," in *High Temperature Capillarity* (N. Eustathopoulos and N. Sobczak, eds.), (Cracow), pp. 18–22, 1997.
- [223] M. Shimbo, M. Naka, and I. Okamoto, "Wettability of silicon carbide by aluminium, copper and silver," *Journal of Materials Science Letters*, vol. 8, pp. 663–666, 1989.
- [224] S. Takahashi and O. Kuboi, "Study on contact angles of Au, Ag, Cu, Sn, Al and Al alloys to SiC," *Journal of Materials Science*, vol. 31, pp. 1797–1802, 1996.
- [225] C. Rado and N. Eustathopoulos, "The role of surface chemistry on spreading kinetics of molten silicides on silicon carbide," *Interface Science*, vol. 12, pp. 85–92, 2004.
- [226] N. Frage, N. Froumin, and M. P. Dariel, "Wetting of TiC by non-reactive liquid metals," *Acta Materialia*, vol. 50, pp. 237–245, 2002.
- [227] N. Frage, N. Froumin, M. Aizenshtein, L. Kutsenko, D. Fuks, and M. P. Dariel, "Reactive wetting in titanium carbide/non-reactive metal systems," *Current Opinion in Solid State and Materials Science*, vol. 9, pp. 189–195, 2005.
- [228] J.-G. Li, "Influence of oxygen partial pressure on the wetting behaviour of titanium carbide by molten copper and other metals," *Materials Letters*, vol. 17, pp. 74–78, 1993.
- [229] J. Bear, *Dynamics of fluid in porous media*. New York: Dover Publications, INC., american edition, 1972.
- [230] A. Mortensen, L. J. Masur, J. A. Cornie, and M. C. Flemings, "Infiltration of fibrous preforms by a pure metal: Part I. Theory," *Metallurgical Transactions A*, vol. 20A, pp. 2535–2547, 1989.
- [231] L. J. Masur, A. Mortensen, J. A. Cornie, and M. C. Flemings, "Infiltration of fibrous preforms by a pure metal: Part II. Experiment," *Metallurgical Transactions A*, vol. 20A, pp. 2549–2557, 1989.
- [232] A. Mortensen and T. Wong, "Infiltration of fibrous preforms by a pure metal: Part III. Capillary phenomena," *Metallurgical Transactions A*, vol. 21A, pp. 2257–2263, 1990.
- [233] C. García-Cordovilla, E. Louis, and J. Narciso, "Pressure infiltration of packed ceramic particulates by liquid metals," *Acta Materialia*, vol. 47, no. 18, pp. 4461–4479, 1999.

Bibliography

- [234] Y.-W. Yang, G. Zografi, and E. E. Miller, "Capillary flow phenomena and wettability in porous media: I. Static characteristics," *Journal of Colloid and Interface Science*, vol. 122, no. 1, pp. 24–34, 1988.
- [235] E. W. Washburn, "The dynamics of capillary flow," *The Physical Review*, vol. XVII, no. 3, pp. 273–283, 1921.
- [236] F. A. L. Dullien, "New network permeability model of porous media," *AIChE Journal*, vol. 21, no. 2, pp. 299–307, 1975.
- [237] F. A. L. Dullien, M. S. El-Sayed, and V. K. Batra, "Rate of capillary rise in porous media with nonuniform pores," *Journal of Colloid and Interface Science*, vol. 60, no. 3, pp. 497–506, 1977.
- [238] S.-Y. Oh, J. A. Cornie, and K. C. Russell, "Wetting of ceramic particulates with liquid aluminum alloys: Part II. Study of Wettability," *Metallurgical Transactions A*, vol. 20, pp. 533–541, 1989.
- [239] T. R. Jonas, J. A. Cornie, and K. C. Russell, "Infiltration and wetting of alumina particulate preforms by aluminum and aluminum-magnesium alloys," *Metallurgical and Materials Transactions A*, vol. 26, pp. 1491–1497, 1995.
- [240] L. R. White, "Capillary rise in powders," *Journal of Colloid and Interface Science*, vol. 90, no. 2, pp. 536–538, 1982.
- [241] P. C. Carman, "Capillary rise and capillary movement of moisture in fine sands," *Soil Science*, vol. 52, no. 1, pp. 1–14, 1941.
- [242] J.-M. Molina-Jordá, R. Arpón, R. A. Saravanan, C. García-Cordovilla, E. Louis, and J. Narciso, "Threshold pressure for infiltration and particle specific surface area of particle compacts with bimodal size distributions," *Scripta Materialia*, vol. 51, pp. 623–627, 2004.
- [243] J. Tian, E. Piñero, J. Narciso, and E. Louis, "Effects of temperature on pressure infiltration of liquid Al and Al-12wt.%Si alloy into packed SiC particles," *Scripta Materialia*, vol. 53, pp. 1483–1488, 2005.
- [244] J.-M. Molina-Jordá, J. Narciso, and E. Louis, "On the triple line in infiltration of liquid metals into porous preforms," *Scripta Materialia*, vol. 62, pp. 961–965, 2010.
- [245] J.-M. Molina-Jordá, R. Prieto, M. Duarte, J. Narciso, and E. Louis, "On the estimation of threshold pressures in infiltration of liquid metals into particle preforms," *Scripta Materialia*, vol. 59, pp. 243–246, 2008.
- [246] A. Mortensen and I. Jin, "Solidification processing of metal matrix composites," *International Materials Reviews*, vol. 37, no. 3, pp. 101–128, 1992.

- [247] V. Michaud, L. Compton, and A. Mortensen, "Capillarity in isothermal infiltration of alumina fiber preforms with aluminum," *Metallurgical and Materials Transactions A*, vol. 25, no. 10, pp. 2145–2152, 1994.
- [248] A. Mortensen, "Melt infiltration of metal matrix composites," in *Comprehensive Composite Materials* (T. W. Clyne, ed.), ch. 3.20, pp. 521–555, Amsterdam: Elsevier Science, elsevier ed., 2000.
- [249] M. Bahraini, L. Weber, J. Narciso, and A. Mortensen, "Wetting in infiltration of alumina particle preforms with molten copper," *Journal of Materials Science*, vol. 40, no. 9-10, pp. 2487–2491, 2005.
- [250] F. A. L. Dullien, *Porous media fluid transport and pore structure*. Elsevier Science, academic p ed., 1979.
- [251] A. Léger, *Capillarity in pressure-infiltration of ceramic preforms by molten metals*. PhD thesis, EPFL, 2014.
- [252] A. Léger, J.-M. Molina-Jordá, L. Weber, and A. Mortensen, "Percolation and universal scaling in composite infiltration processing," *Materials Research Letters*, vol. 3, no. 1, pp. 7–15, 2015.
- [253] A. Léger, L. Weber, and A. Mortensen, "Influence of the wetting angle on capillary forces in pressure infiltration," *Acta Materialia*, vol. 91, pp. 57–69, 2015.
- [254] J.-M. Molina-Jordá, A. Rodríguez-Guerrero, M. Bahraini, L. Weber, J. Narciso, F. Rodríguez-Reinoso, E. Louis, and A. Mortensen, "Infiltration of graphite preforms with Al–Si eutectic alloy and mercury," *Scripta Materialia*, vol. 56, pp. 991–994, jun 2007.
- [255] J.-M. Molina-Jordá, M. Bahraini, L. Weber, and A. Mortensen, "Direct measurement of drainage curves in infiltration of SiC particle preforms: influence of interfacial reactivity," *Journal of Materials Science*, vol. 43, no. 15, pp. 5061–5067, 2008.
- [256] M. Bahraini, J.-M. Molina-Jordá, M. Kida, L. Weber, J. Narciso, and A. Mortensen, "Measuring and tailoring capillary forces during liquid metal infiltration," *Current Opinion in Solid State and Materials Science*, vol. 9, no. 4-5, pp. 196–201, 2005.
- [257] M. Kida, M. Bahraini, J.-M. Molina-Jordá, L. Weber, and A. Mortensen, "High-temperature wettability of aluminum nitride during liquid metal infiltration," *Materials Science and Engineering: A*, vol. 495, no. 1-2, pp. 197–202, 2008.
- [258] H. Kaufmann and A. Mortensen, "Wetting of SAFFIL alumina fiber preforms by aluminum at 973 K," *Metallurgical Transactions A*, vol. 23, no. 7, pp. 2071–2073, 1992.
- [259] E. Kissa, *Dispersion, characterization, testing, and measurements*, vol. 84. New York: Marcel Dekker INC., taylor & f ed., 1999.

Bibliography

- [260] R. P. Mayer and R. A. Stowe, "Mercury porosimetry—breakthrough pressure for penetration between packed spheres," *Journal of Colloid Science*, vol. 20, pp. 893–911, oct 1965.
- [261] G. Mason and N. R. Morrow, "Effect of contact angle on capillary displacement curvatures in pore throats formed by spheres," *Journal of Colloid and Interface Science*, vol. 168, pp. 130–141, nov 1994.
- [262] E. J. Gonzalez and K. P. Trumble, "Spontaneous infiltration of alumina by copper-oxygen alloys," *Journal of American Ceramic Society*, vol. 79, no. 1, pp. 114–120, 1996.
- [263] Y.-W. Yang, G. Zografi, and E. E. Miller, "Capillary flow phenomena and wettability in porous media: II. Dynamic flow studies," *Journal of Colloid and Interface Science*, vol. 122, pp. 35–46, mar 1988.
- [264] J. Narciso, C. García-Cordovilla, and E. Louis, "Pressure infiltration of packed Al₂O₃ particulates by pure silver," *Scripta Materialia*, vol. 36, no. 4, pp. 363–368, 1997.
- [265] S. Ban, E. Wolfram, and S. Rohrsetzer, "The condition of starting of liquid imbibition in powders," *Colloids and Surfaces*, vol. 22, pp. 301–309, 1987.
- [266] J. L. Hilden and K. P. Trumble, "Spontaneous infiltration of non-cylindrical porosity: Lagers pores," *Materials Science Forum*, vol. 308-311, pp. 157–162, 1999.
- [267] G. Kaptay and T. Bárczy, "On the asymmetrical dependence of the threshold pressure of infiltration on the wettability of the porous solid by the infiltrating liquid," *Journal of Materials Science*, vol. 40, pp. 2531–2535, may 2005.
- [268] G. Kaptay, "The threshold pressure of infiltration into fibrous preforms normal to the fibers' axes," *Composites Science and Technology*, vol. 68, pp. 228–237, jan 2008.
- [269] K. P. Trumble, "Spontaneous infiltration of non-cylindrical porosity: Close-packed spheres," *Acta Materialia*, vol. 46, pp. 2363–2367, apr 1998.
- [270] X. F. Yang and X. M. Xi, "Critical wetting angle for spontaneous liquid infiltration into orderly packed fibres or spheres," *Journal of Materials Science*, vol. 30, no. 20, pp. 5099–5102, 1995.
- [271] C. A. E. Hamlett, N. J. Shirtcliffe, G. McHale, S. Ahn, R. Bryant, S. H. Doerr, and M. I. Newton., "Effect of particle size on droplet infiltration into hydrophobic porous media as a model of water repellent soil," *Environmental Science & Technology*, vol. 45, pp. 9666–9670, nov 2011.
- [272] N. Frage, N. Froumin, L. Rubinovich, and M. P. Dariel, "Infiltrated TiC/Cu composites," in *15th International Plansee Seminar* (G. Kneringer, P. Rodhammer, and H. Wildner, eds.), vol. 1, (Reutte), pp. 202–216, 2001.

- [273] W. B. Haines, "Studies in the physical properties of soils: IV. A further contribution to the theory of capillary phenomena in soil," *The Journal of Agricultural Science*, vol. 17, p. 264, apr 1927.
- [274] W. R. Purcell, "Interpretation of capillary pressure data," *Journal of Petroleum Technology*, vol. 1, pp. 11–12, 1950.
- [275] H. M. Princen, "Capillary phenomena in assemblies of parallel cylinders: I. Capillary rise between two cylinders," *Journal of Colloid and Interface Science*, vol. 30, pp. 69–75, may 1969.
- [276] H. M. Princen, "Capillary phenomena in assemblies of parallel cylinders: II. Capillary rise in systems with more than two cylinders," *Journal of Colloid and Interface Science*, vol. 30, pp. 359–371, jul 1969.
- [277] J. Narciso, C. García-Cordovilla, and E. Louis, "Pressure infiltration in a reactive system: Packed SiC particulates infiltrated by pure silver with dissolved oxygen," *Acta Materialia*, vol. 45, no. 12, pp. 5111–5118, 1997.
- [278] A. Rodríguez-Guerrero, S. A. Sánchez, J. Narciso, E. Louis, and F. Rodríguez-Reinoso, "Pressure infiltration of Al-12 wt.% Si-X (X = Cu, Ti, Mg) alloys into graphite particle preforms," *Acta Materialia*, vol. 54, pp. 1821–1831, 2006.
- [279] A. Rodríguez-Guerrero, S. A. Sánchez, J. Narciso, E. Louis, and F. Rodríguez-Reinoso, "Pressure infiltration of Al-Si alloys into compacts made of carbon particles," *Journal of Materials Science*, vol. 40, pp. 2519–2523, 2005.
- [280] J.-M. Molina-Jordá, R. A. Saravanan, R. Arpón, C. García-Cordovilla, E. Louis, and J. Narciso, "Pressure infiltration of liquid aluminium into packed SiC particulate with a bimodal size distribution," *Acta Materialia*, vol. 50, pp. 247–257, 2002.
- [281] S. Y. Chong, H. V. Atkinson, and H. Jones, "Effect of ceramic particle size, melt superheat, impurities and alloy conditions on threshold pressure for infiltration of SiC powder compacts by aluminium-based melts," *Materials Science and Engineering*, vol. A173, pp. 233–237, 1993.
- [282] E. Candan, H. V. Atkinson, and H. Jones, "Effect of magnesium alloying additions on infiltration threshold pressure and structure of SiC powder compacts infiltrated by aluminium-based melts," *Journal of Materials Science*, vol. 2, pp. 289–294, 1997.
- [283] D. Muscat and R. A. L. Drew, "Modeling the infiltration kinetics of molten aluminum into porous titanium carbide," *Metallurgical and Materials Transactions A*, vol. 25, no. November, pp. 2357–2370, 1994.
- [284] P. B. Maxwell, G. P. Martins, D. L. Olson, and G. R. Edwards, "The infiltration of aluminum into silicon carbide compacts," *Metallurgical Transactions B*, vol. 21B, pp. 475–485, 1990.

Bibliography

- [285] J.-M. Molina-Jordá, E. Piñero, J. Narciso, C. García-Cordovilla, and E. Louis, "Liquid metal infiltration into ceramic particle preforms with bimodal size distributions," *Current Opinion in Solid State and Materials Science*, vol. 9, pp. 202–210, 2005.
- [286] J. Narciso, A. Alonso, J. Pamies, C. García-Cordovilla, and E. Louis, "Wettability of binary and ternary alloys of the system Al-Si-Mg with SiC particulates," *Scripta Metallurgica et Materialia*, vol. 31, no. 1, pp. 1495–1500, 1994.
- [287] T. R. Fletcher, J. A. Cornie, and K. C. Russell, "Cast reinforced metal composites," in *ASM International* (S. G. Fishman and A. K. Dhingra, eds.), (Chicago), p. 393, ASM International, 1988.
- [288] R. Asthana and P. K. Rohatgi, "Melt infiltration of silicon carbide compacts," *Zeitschrift für Metallkunde*, vol. 83, no. 12, pp. 887–892, 1992.
- [289] S. K. Senotrusov and V. A. Perezhogina, "Method of determining the kinetics of infiltration of capillary-porous solids by melts," *Poroshkovaya Metallurgiya*, vol. 25, no. 6, pp. 467–470, 1986.
- [290] T. Dopler, A. Modaressi, and V. Michaud, "Simulation of metal-matrix composite isothermal infiltration processing," *Metallurgical and Materials Transactions B*, vol. 31B, pp. 225–234, 2000.
- [291] E. Candan, H. V. Atkinson, and H. Jones, "Effect of alloying additions on threshold pressure for infiltration and porosity of aluminium-based melt infiltrated silicon carbide powder compacts," *Key Engineering Materials*, vol. 127-131, no. 463-470, 1997.
- [292] S. Long, Z. Zhang, and H. M. Flower, "Characterization of liquid metal infiltration of a chopped fibre preform aided by external pressure- I. Visualization of the flow behaviour of aluminium melt in a fibre preform," *Acta Metallurgica et Materialia*, vol. 43, no. 9, pp. 3489–3498, 1995.
- [293] E. Clément, C. Baudet, and J. P. Hulin, "Multiple scale structure of non wetting fluid invasion fronts in 3D model porous media," *Journal de Physique Lettres*, vol. 46, no. 24, pp. 1163–1171, 1985.
- [294] E. Clément, C. Baudet, E. Guyon, and J. P. Hulin, "Invasion front structure in a 3-D model porous medium under a hydrostatic pressure gradient," *Journal of Physics D: Applied Physics*, vol. 20, no. 5, pp. 608–615, 1987.
- [295] D. Muscat and R. A. L. Drew, "A method of measuring metal infiltration rates in porous preforms at high temperature," *Journal of Materials Science Letters*, vol. 12, pp. 1567–1569, 1993.
- [296] A. Léger, N. Rojo-Calderon, R. Charvet, W. Dufour, C. Bacciarini, L. Weber, and A. Mortensen, "Capillarity in pressure infiltration: Improvements in characterization of high-temperature systems," *Journal of Materials Science*, vol. 47, no. 24, pp. 8419–8430, 2012.

- [297] N. R. Morrow, "Physics and thermodynamics of capillary, a thermodynamic theory and a detailed mechanism of immiscible displacement in porous media are developed in terms of a quantized model," *Industrial and Engineering Chemistry*, vol. 62, pp. 32–56, 1970.
- [298] F. A. L. Dullien, *Porous media : Fluid transport and pore structure*. San Diego: Harcourt Brace Jovanovich Publishers, academic p ed., 1991.
- [299] A. Mortensen, "Interfacial phenomena in the solidification processing of metal matrix composites," *Materials Science and Engineering: A*, vol. 135, pp. 1–11, mar 1991.
- [300] M. Bahraini, J.-M. Molina-Jordá, L. Weber, and A. Mortensen, "Direct measurement of drainage curves in infiltration of SiC particle preforms," *Materials Science and Engineering: A*, vol. 495, pp. 203–207, nov 2008.
- [301] Q. Liu, F. Ye, Y. Gao, S. Liu, H. Yang, and Z. Zhou, "Fabrication of a new SiC/2024Al co-continuous composite with lamellar microstructure and high mechanical properties," *Journal of Alloys and Compounds*, vol. 585, pp. 146–153, feb 2014.
- [302] R. Lenormand, "Flow through porous media: Limits of fractal patterns," in *Fractals in the natural sciences : a discussion* (M. Fleischmann, D. J. Tildesley, and R. C. Ball, eds.), pp. 159–168, Royal Society (Great Britain), 1988.
- [303] R. Lenormand and C. Zarcone, "Capillary fingering: Percolation and fractal dimension," *Transport in Porous Media*, vol. 4, pp. 599–612, dec 1989.
- [304] R. Lenormand, "Liquids in porous media," *Journal of Physics: Condensed Matter*, vol. 2, pp. SA79–SA88, dec 1990.
- [305] K. J. Måløy, F. Boger, J. Feder, T. Jøssang, and P. Meakin, "Dynamics of viscous-fingering fractals in porous media," *Physical Review A*, vol. 36, pp. 318–324, jul 1987.
- [306] G. Løvoll, Y. Méheust, K. J. Måløy, E. Aker, and J. Schmittbuhl, "Competition of gravity, capillary and viscous forces during drainage in a two-dimensional porous medium, a pore scale study," *Energy*, vol. 30, no. 6, pp. 861–872, 2005.
- [307] G. M. Homsy, "Viscous fingering in porous media," *Ann. Rev. Fluid Mech*, vol. 19, pp. 271–311, 1987.
- [308] J.-D. Chen and D. Wilkinson, "Pore-scale viscous fingering in porous media," *Physical Review Letters*, vol. 55, pp. 1892–1895, oct 1985.
- [309] J. H. Kang, K.-J. Lee, J. H. Nam, C.-J. Kim, H. S. Park, S. Lee, and I. Kwang, "Visualization of invasion-percolation drainage process in porous media using density-matched immiscible fluids and refractive-index-matched solid structures," *Journal of Power Sources*, vol. 195, pp. 2608–2612, may 2010.

Bibliography

- [310] R. Lenormand and C. Zarcone, "Invasion percolation in an etched network: measurement of a fractal dimension," *Physical Review Letters*, vol. 54, pp. 2226–2229, may 1985.
- [311] R. Lenormand, "Pattern growth and fluid displacements through porous media," *Physica A: Statistical Mechanics and its Applications*, vol. 140, no. 1-2, pp. 114–123, 1986.
- [312] R. Lenormand, E. Touboul, and C. Zarcone, "Numerical models and experiments on immiscible displacements in porous media," *Journal of Fluid Mechanics*, vol. 189, p. 165, apr 1988.
- [313] K. J. Måløy, J. Feder, and T. Jossang, "Viscous fingering fractals in porous media," *Physical Review Letters*, vol. 55, no. 24, pp. 2688–2691, 1985.
- [314] M. Blunt, M. J. King, and H. Scher, "Simulation and theory of two-phase flow in porous media," *Physical Review A*, vol. 46, pp. 7680–7699, dec 1992.
- [315] B. Xu, Y. C. Yortsos, and D. Salin, "Invasion percolation with viscous forces," *Physical Review E*, vol. 57, pp. 739–751, jan 1998.
- [316] L. Furuberg, K. J. Måløy, and J. Feder, "Intermittent behavior in slow drainage," *Physical Review E*, vol. 53, pp. 966–977, jan 1996.
- [317] Y. C. Yortsos, B. Xu, and D. Salin, "Phase diagram of fully developed drainage in porous media," *Physical Review Letters*, vol. 79, pp. 4581–4584, dec 1997.
- [318] M. C. Sukop and D. Or, "Invasion percolation of single component, multiphase fluids with lattice Boltzmann models," *Physica B: Condensed Matter*, vol. 338, pp. 298–303, oct 2003.
- [319] A. D. Araujo, M. C. Romeu, A. A. Moreira, R. F. S. Andrade, and J. S. Andrade, "Multiple-well invasion percolation," *Physical Review E*, vol. 77, p. 041410, apr 2008.
- [320] M. Ferer, W. N. Sams, R. A. Geisbrecht, and D. H. Smith, "Scaling of fractal flow," *Physica A: Statistical Mechanics and its Applications*, vol. 177, pp. 273–280, sep 1991.
- [321] M. Ferer, G. S. Bromhal, and D. H. Smith, "Pore-level modeling of immiscible drainage: validation in the invasion percolation and DLA limits," *Physica A: Statistical Mechanics and its Applications*, vol. 319, pp. 11–35, mar 2003.
- [322] M. Ferer, G. S. Bromhal, and D. H. Smith, "Fractal dimension and avalanches of invasion percolation: the effect of aspect ratio," *Physica A: Statistical Mechanics and its Applications*, vol. 334, pp. 22–38, mar 2004.
- [323] M. Ferer, G. S. Bromhal, and D. H. Smith, "Two-phase flow in porous media: Crossover from capillary fingering to compact invasion for drainage," *Physical Review E*, vol. 71, p. 026303, feb 2005.

- [324] M. Ferer, G. S. Bromhal, and D. H. Smith, "Crossover from capillary fingering to compact invasion for two-phase drainage with stable viscosity ratios," *Advances in Water Resources*, vol. 30, pp. 284–299, feb 2007.
- [325] M. Ferer, G. S. Bromhal, and D. H. Smith, "Miscible viscous fingering in three dimensions: Fractal-to-compact crossover and interfacial roughness," *Physical Review E*, vol. 80, p. 011602, jul 2009.
- [326] M. Ferer, S. L. Anna, P. Tortora, J. R. Kadambi, M. Oliver, G. S. Bromhal, and D. H. Smith, "Two-phase flow in porous media: Predicting its dependence on capillary number and viscosity ratio," *Transport in Porous Media*, vol. 86, pp. 243–259, jan 2011.
- [327] D. Wilkinson, "Percolation effects in immiscible displacement," *Physical Review A*, vol. 34, no. 2, 1986.
- [328] M. Sahimi, *Flow and transport in porous media and fractured rock : from classical methods to modern approaches*. Wiley-VCH, 1995.
- [329] D. Wilkinson and J. F. Willemsen, "Invasion percolation: a new form of percolation theory," *Journal of Physics A: Mathematical and General*, vol. 16, pp. 3365–3376, oct 1983.
- [330] T. J. Perham, D. Chrzan, and L. C. De Jonghe, "Invasion percolation model of co-interpenetrating ceramic-metal composites," *Modelling and Simulation in Materials Science and Engineerign*, vol. 10, pp. 103–119, 2002.
- [331] A. G. Hunt, R. P. Ewing, and B. Ghanbarian, *Percolation theory for flow in porous media*. springer i ed., 2009.
- [332] R. Lenormand and C. Zarcone, "Invasion percolation in an etched network: measurement of a fractal dimension," *Physical Review Letters*, vol. 54, no. 20, 1985.
- [333] R. G. Larson and N. R. Morrow, "Effects of sample size on capillary pressures in porous media," *Powder Technology*, vol. 30, pp. 123–138, nov 1981.
- [334] B. Koiller, H. Ji, and M. O. Robbins, "Fluid wetting properties and the invasion of square networks," *Physical Review B*, vol. 45, pp. 7762–7767, apr 1992.
- [335] M. Sahimi, "Flow phenomena in rocks: from continuum models to fractals, percolation, cellular automata, and simulated annealing," *Reviews of Modern Physics*, vol. 65, pp. 1393–1534, oct 1993.
- [336] A.-L. Barabási, "Invasion percolation and global optimization," *Physical Review Letters*, vol. 76, pp. 3750–3753, may 1996.
- [337] A. G. Hunt, "Continuum percolation theory for pressure–saturation characteristics of fractal soils: extension to non-equilibrium," *Advances in Water Resources*, vol. 27, pp. 245–257, mar 2004.

Bibliography

- [338] M. Sara and M. Mohsen, "Invasion percolation in presence of gravity," *Iranian Journal of Chemistry and Chemical Engineering*, vol. 29, no. 1, pp. 71–82, 2010.
- [339] M. Sahimi, *Applications of percolation theory*. Taylor & Francis Group, apr 1994.
- [340] T. Mathews, G. P. Matthews, and S. Huggett, "Estimating particle size distributions from a network model of porous media," *Powder Technology*, vol. 104, pp. 169–179, sep 1999.
- [341] M. Spearing and G. P. Matthews, "Modelling characteristic properties of sandstones," *Transport in Porous Media*, vol. 6, pp. 71–90, feb 1991.
- [342] P. A. C. Gane, J. P. Kettle, G. P. Matthews, and C. J. Ridgway, "Void space structure of compressible polymer spheres and consolidated calcium carbonate paper-coating formulations," *Industrial & Engineering Chemistry Research*, vol. 35, no. 5, pp. 1753–1764, 1996.
- [343] A. Johnson, I. M. Roy, G. P. Matthews, and D. Patel, "An improved simulation of void structure, water retention and hydraulic conductivity in soil with the Pore-Cor three-dimensional network," *European Journal of Soil Science*, vol. 54, pp. 477–490, sep 2003.
- [344] J. Schoelkopf, C. J. Ridgway, P. A. C. Gane, G. P. Matthews, and D. C. Spielmann, "Measurement and network modeling of liquid permeation into compacted mineral blocks," *Journal of Colloid and Interface Science*, vol. 227, pp. 119–131, jul 2000.
- [345] G. P. Matthews, C. L. Levy, G. M. Laudone, K. L. Jones, C. J. Ridgway, I. L. Hallin, S. A. Gazze, L. Francis, W. R. Whalley, J. Schoelkopf, and P. A. C. Gane, "Improved interpretation of mercury intrusion and soil water retention percolation characteristics by inverse modelling and void cluster analysis," *Transport in Porous Media*, vol. 124, pp. 631–653, sep 2018.
- [346] J. Gostick, M. Aghighi, J. Hinebaugh, T. Tranter, M. A. Hoeh, H. Day, B. Spellacy, M. H. Sharqawy, A. Bazylak, A. Burns, W. Lehnert, and A. Putz, "OpenPNM: a pore network modeling package," *Computing in Science & Engineering*, vol. 18, pp. 60–74, jul 2016.
- [347] Z. Liu, Y. Wang, F. J. Muzzio, G. Callegari, and G. Drazer, "Capillary drop penetration method to characterize the liquid wetting of powders," *Langmuir*, vol. 33, pp. 56–65, jan 2017.
- [348] D. Wilkinson, "Percolation model of immiscible displacement in the presence of buoyancy forces," *Physical Review A*, vol. 30, pp. 520–531, jul 1984.
- [349] J. F. Gouyet, M. Rosso, E. Clément, C. Baudet, and J. P. Hulin, "Invasion of a porous medium under gravity: A quantitative analysis," *Physica A: Statistical Mechanics and its Applications*, vol. 157, pp. 497–498, may 1989.
- [350] H. Ouerfelli, M. Najjari, Z. Baouab, and S. B. Nasrallah, "Experimental study of the influence of gravity and injected-gas flow rate on drainage in two-dimensional porous media," *Journal of Porous Media*, vol. 11, no. 8, pp. 781–789, 2008.

- [351] V. Sarrot and M. Prat, "Hyperslow drainage in a porous medium: Influence of retention curve," *Advances in Water Resources*, vol. 33, pp. 987–996, sep 2010.
- [352] B. B. Mandelbrot, *The fractal geometry of nature*. San Francisco :: W.H. Freeman, 1982.
- [353] T. M. Shaw, "Drying as an immiscible displacement process with fluid counterflow," *Physical Review Letters*, vol. 59, pp. 1671–1674, oct 1987.
- [354] A. H. Thompson, A. J. Katz, and C. E. Krohn, "The microgeometry and transport properties of sedimentary rock," *Advances in Physics*, vol. 36, pp. 625–694, jan 1987.
- [355] V. Michaud and A. Mortensen, "On measuring wettability in infiltration processing," *Scripta Materialia*, vol. 56, no. 10, pp. 859–862, 2007.
- [356] D. L. Turcotte, "Fractals and fragmentation," *Journal of Geophysical Research*, vol. 91, no. 5, pp. 1921–1926, 1986.
- [357] G. Tao, Y. Chen, L. Kong, H. Xiao, Q. Chen, and Y. Xia, "A simple fractal-based model for soil-water characteristic curves incorporating effects of initial void ratios," *Energies*, vol. 11, p. 1419, jun 2018.
- [358] J. Peng, H. Han, Q. Xia, and B. Li, "Evaluation of the pore structure of tight sandstone reservoirs based on multifractal analysis: a case study from the Kepingtage Formation in the Shuntuoguole uplift, Tarim Basin, NW China," *Journal of Geophysics and Engineering*, vol. 15, pp. 1122–1136, aug 2018.
- [359] A. M. Tarquis, I. G. Torre, J. J. Martín-Sotoca, J. C. Losada, J. B. Grau, N. R. A. Bird, and A. Saa-Requejo, "Scaling characteristics of soil structure," *Springer Nature*, 2018.
- [360] N. R. A. Bird and E. Perrier, "The pore-solid fractal model of soil density scaling," *European Journal of Soil Science*, vol. 54, pp. 467–476, sep 2003.
- [361] T. A. Cousins, B. Ghanbarian, and H. Daigle, "Three-dimensional lattice boltzmann simulations of single-phase permeability in random fractal porous media with rough pore–solid interface," *Transport in Porous Media*, vol. 122, pp. 527–546, apr 2018.
- [362] J. Zhou and Y. Tang, "Experimental inference on dual-porosity aggravation of soft clay after freeze-thaw by fractal and probability analysis," *Cold Regions Science and Technology*, vol. 153, pp. 181–196, sep 2018.
- [363] E. Perrier, M. Rieu, G. Sposito, and G. De Marsily, "Models of the water retention curve for soils with a fractal pore size distribution," *Water Resources Research*, vol. 32, pp. 3025–3031, oct 1996.
- [364] S. W. Tyler and S. W. Wheatcraft, "Fractal processes in soil water retention," *Water Resources Research*, vol. 26, pp. 1047–1054, may 1990.

Bibliography

- [365] H. Millán, M. González-Posada, M. Aguilar, J. Domínguez, and L. Céspedes, “On the fractal scaling of soil data. Particle-size distributions,” *Geoderma*, vol. 117, pp. 117–128, nov 2003.
- [366] M. Rieu and G. Sposito, “Fractal fragmentation, soil porosity, and soil water properties: I. Theory,” *Soil Science Society of America Journal*, vol. 55, no. 5, p. 1231, 1991.
- [367] M. Rieu and G. Sposito, “Fractal fragmentation, soil porosity, and soil water properties: II. Applications,” *Soil Science Society of America Journal*, vol. 55, no. 5, p. 1239, 1991.
- [368] E. Perfect, “Estimating soil mass fractal dimensions from water retention curves,” *Geoderma*, vol. 88, pp. 221–231, mar 1999.
- [369] E. Perfect, “Fractal models for the fragmentation of rocks and soils: a review,” *Engineering Geology*, vol. 48, pp. 185–198, dec 1997.
- [370] E. Perfect, M. Diaz-Zorita, and J. H. Grove, “A prefractal model for predicting soil fragment mass-size distributions,” *Soil and Tillage Research*, vol. 64, pp. 79–90, feb 2002.
- [371] N. R. A. Bird, F. Bartoli, and A. R. Dexter, “Water retention models for fractal soil structures,” *European Journal of Soil Science*, vol. 47, pp. 1–6, mar 1996.
- [372] A. K. Guber, Y. A. Pachepsky, and E. V. Levkovsky, “Fractal mass–size scaling of wetting soil aggregates,” *Ecological Modelling*, vol. 182, pp. 317–322, mar 2005.
- [373] N. R. A. Bird, E. Perrier, and M. Rieu, “The water retention function for a model of soil structure with pore and solid fractal distributions,” *European Journal of Soil Science*, vol. 51, pp. 55–63, mar 2000.
- [374] D. Gimenez, R. R. Allmaras, D. R. Huggins, and E. A. Nater, “Mass, surface, and fragmentation fractal dimensions of soil fragments produced by tillage,” *Geoderma*, vol. 86, pp. 261–278, nov 1998.
- [375] P.-G. DeGennes, “Partial filling of a fractal structure by a wetting fluid,” in *Physics of Disordered Materials*, pp. 227–241, Boston, MA: Springer US, 1985.
- [376] T. Kutlu, S. Ersahin, and B. Yetgin, “Relations between solid fractal dimension and some physical properties of soils formed over alluvial and colluvial deposits,” *Journal of food, agriculture & environment*, vol. 6, no. 3-4, pp. 445–449, 2003.
- [377] E. Perrier and N. R. A. Bird, “Modelling soil fragmentation: the pore solid fractal approach,” *Soil and Tillage Research*, vol. 64, pp. 91–99, feb 2002.
- [378] A. Mortensen and J. A. Cornie, “On the infiltration of metal matrix composites,” *Metalurgical Transactions A*, vol. 22, pp. 1160–1163, 1991.

- [379] A. Alonso, A. Pamies, J. Narciso, C. García-Cordovilla, and E. Louis, "Evaluation of the wettability of liquid aluminum with ceramic particulates (SiC, TiC, Al₂O₃) by means of pressure infiltration," *Metallurgical Transactions A*, vol. 24, no. June, pp. 1423–1432, 1993.
- [380] A. Alonso, C. García-Cordovilla, E. Louis, J. Narciso, and A. Pamies, "Evaluation of the wettability of Al-Pb and Al-Sn alloys with SiC and Al₂O₃ particulates by means of pressure infiltration," *Journal of Materials Science*, vol. 29, pp. 4729–4735, 1994.
- [381] M. A. Taha and N. A. El-Mahallawy, "Metal–matrix composites fabricated by pressure-assisted infiltration of loose ceramic powder," *Journal of Materials Processing Technology*, vol. 73, pp. 139–146, jan 1998.
- [382] J.-M. Molina-Jordá, R. Voytovych, E. Louis, and N. Eustathopoulos, "The surface tension of liquid aluminium in high vacuum: The role of surface condition," *International Journal of Adhesion & Adhesives*, vol. 27, pp. 394–401, 2007.
- [383] J. Narciso, A. Alonso, A. Pamies, C. García-Cordovilla, and E. Louis, "Factors affecting pressure infiltration of packed SiC particulates by liquid aluminum," *Metallurgical and Materials Transactions A*, vol. 26, pp. 983–990, 1995.
- [384] C. García-Cordovilla, E. Louis, and A. Pamies, "The surface tension of liquid pure aluminium and aluminium-magnesium alloy," *Journal of Materials Science*, vol. 21, p. 2792, 1986.
- [385] V. Bougiouri, R. Voytovych, O. Dezellus, and N. Eustathopoulos, "Wetting and reactivity in Ni-Si/C system: experiments versus model predictions," *Journal of Materials Science*, vol. 42, pp. 2016–2023, 2007.
- [386] V. Bougiouri, R. Voytovych, N. Rojo-Calderon, J. Narciso, and N. Eustathopoulos, "The role of the chemical reaction in the infiltration of porous carbon by NiSi alloys," *Scripta Materialia*, vol. 54, pp. 1875–1878, 2006.
- [387] R. Voytovych, V. Bougiouri, N. Rojo-Calderon, J. Narciso, and N. Eustathopoulos, "Reactive infiltration of porous graphite by NiSi alloys," *Acta Materialia*, vol. 56, pp. 2237–2246, 2008.
- [388] M. Singh and D. R. Behrendt, "Reactive melt infiltration of silicon-molybdenum alloys into microporous carbon preforms," *Materials Science and Engineering*, vol. A194, pp. 193–200, 1995.
- [389] V. M. Kevorkijan, "The reactive infiltration of porous ceramic media by a molten aluminum alloy," *Composites Science and Technology*, vol. 59, pp. 683–686, apr 1999.
- [390] E. Piñero, J.-M. Molina-Jordá, J. Narciso, and E. Louis, "Liquid metal infiltration into ceramic particle compacts chemically and morphologically heterogeneous," *Materials Science and Engineering: A*, vol. 495, pp. 288–291, 2008.

Bibliography

- [391] E. Piñero, J.-M. Molina-Jordá, J. Narciso, C. García-Cordovilla, and E. Louis, "The intrinsic permeability of packed SiC particles with monomodal and bimodal size distributions," *Journal of Composite Materials*, vol. 42, no. 26, pp. 2795–2804, 2008.
- [392] J. P. Rocher, J. M. Quenisset, and R. Maslain, "A New casting process for carbon (or SiC-based) fibre-aluminium matrix low-cost composite materials," *Journal of Materials Science Letters*, vol. 4, pp. 1527–1529, 1985.
- [393] J. P. Rocher, J. M. Quenisset, and R. Naslain, "Wetting improvement of carbon or silicon carbide by aluminium alloys based on a K2ZrF6 surface treatment: application to composite material casting," *Journal of Materials Science*, vol. 24, pp. 2697–2703, 1989.
- [394] S. Schamm, R. Fedou, J. P. Rocher, J. M. Quenisset, and R. Naslain, "The K2ZrF6 wetting process: Effects of surface chemistry on the ability of a SiC fibre preform to be impregnated by aluminium," *Metallurgical Transactions A*, vol. 22A, no. September, pp. 2133–2139, 1991.
- [395] Z. Yu, G. Wu, D. Sun, and L. Jiang, "Coating of Y2O3 additive on Al2O3 powder and its effect on the wetting behaviour in the system Al2O3p/Al," *Materials Letters*, vol. 57, pp. 3111–3116, 2003.
- [396] P. K. Rohatgi, Q. Guo, H. Iksan, E. J. Borchelt, and R. Asthana, "Pressure infiltration technique for synthesis of aluminum-fly ash particulate composite," *Materials Science and Engineering: A*, vol. A244, pp. 22–30, 1998.
- [397] A. C. D. Chaklader and K. R. Linger, "Ceramic/metal composites using metal-coated alumina powder," *Composites*, vol. October, pp. 239–243, 1976.
- [398] S. A. Sánchez, J. Narciso, E. Louis, F. Rodríguez-Reinoso, E. Saiz, and A. P. Tomsia, "Wetting and capillarity in the Sn/graphite system," *Materials Science and Engineering: A*, vol. 495, pp. 187–191, 2008.
- [399] W.-F. Du and T. Watanabe, "High-toughness B4C-AlB12 composites prepared by Al infiltration," *Journal of the European Ceramic Society*, vol. 17, pp. 879–884, 1997.
- [400] K. Janghorban, "Processing of Ceramic Matrix SiC-Al Composites," *Journal of Materials Processing Technology*, vol. 38, pp. 361–368, 1993.
- [401] N. Eustathopoulos, "Progress in understanding and modeling reactive wetting of metals on ceramics," *Current Opinion in Solid State and Materials Science*, vol. 9, no. 4-5, pp. 152–160, 2005.
- [402] R. R. Rye, F. G. Yost, and E. J. O'Toole, "Capillary flow in irregular surface grooves," *Langmuir*, vol. 14, no. 14, pp. 3937–3943, 1998.
- [403] F. G. Yost, P. A. Sackinger, and E. J. O'Toole, "Energetics and kinetics of dissolutive wetting processes," *Acta Materialia*, vol. 46, no. 7, pp. 2329–2336, 1998.

- [404] A. Mortensen, F. Hodaj, and N. Eustathopoulos, "On thermal effects in reactive wetting," *Scripta Materialia*, vol. 38, no. 9, pp. 1411–1417, 1998.
- [405] F. Hodaj, J. N. Barbier, A. Mortensen, O. Dezellus, and N. Eustathopoulos, "Modelling kinetics of diffusion controlled reactive wetting: the role of reaction behind the triple line," *Solid State Phenomena*, vol. 72, pp. 91–98, 2000.
- [406] W. B. Hillig, "Making ceramic composites," *American Ceramic Society Bulletin*, vol. 73:4, pp. 56–62, 1993.
- [407] S. P. Dhandapani, V. Jayaram, and M. K. Surappa, "Growth and microstructure of Al₂O₃-SiC-Si(Al) composites prepared by reactive infiltration of silicon carbide preforms," *Acta Metallurgica et Materialia*, vol. 42, pp. 649–656, mar 1994.
- [408] M. Singh and D. R. Behrendt, "Reactive melt infiltration of silicon-niobium alloys in microporous carbons," *Journal of Materials Research*, vol. 9, pp. 1701–1708, jul 1994.
- [409] O. Chakrabarti and P. K. Das, "Reactive infiltration of Si-Mo alloyed melt into carbonaceous preforms of silicon carbide," *Journal of the American Ceramic Society*, vol. 83, pp. 1548–1550, jun 2000.
- [410] L. Hozer and Y.-M. Chiang, "Reactive-infiltration processing of SiC-metal and SiC-intermetallic composites," *Journal of Materials Research*, vol. 11, pp. 2346–2357, sep 1996.
- [411] P. Sangsuwan, S. N. Tewari, J. E. Gatica, M. Singh, and R. Dickerson, "Reactive infiltration of silicon melt through microporous amorphous carbon preforms," *Metallurgical and Materials Transactions B*, vol. 30, pp. 933–944, oct 1999.
- [412] N. Eustathopoulos, R. Israel, B. Drevet, and D. Camel, "Reactive infiltration by Si: infiltration versus wetting," *Scripta Materialia*, vol. 62, pp. 966–971, jun 2010.
- [413] Y. Chen and D. L. Chung, "Nickel aluminide (Ni₃Al) fabricated by reactive infiltration," *Journal of Materials Science*, vol. 31, no. 8, pp. 2117–2122, 1996.
- [414] C. San Marchi and A. Mortensen, "Reactive infiltration processing of aluminum-nickel intermetallic compounds," *Metallurgical and Materials Transactions A*, vol. 29A, pp. 2819–2828, 1998.
- [415] T. A. Venkatesh and D. C. Dunand, "Reactive infiltration processing and secondary compressive creep of NiAl and NiAl-W composites," *Metallurgical and Materials Transactions A*, vol. 31, pp. 781–792, mar 2000.
- [416] M. Kobashi and T. Choh, "Synthesis of Al₂O₃ matrix composites by reactive infiltration," *Journal of Materials Science*, vol. 32, no. 23, pp. 6279–6282, 1997.
- [417] M. Kobashi and T. Choh, "Synthesis of boride and nitride ceramics in molten aluminium by reactive infiltration," *Journal of Materials Science*, vol. 32, no. 23, pp. 6283–6289, 1997.

Bibliography

- [418] F. Wagner, D. E. Garcia, A. Krupp, and N. Claussen, "Interpenetrating Al₂O₃-TiAl₃ alloys produced by reactive infiltration," *Journal of the European Ceramic Society*, vol. 19, pp. 2449–2453, oct 1999.
- [419] I. Gheorghe and H. J. Rack, "Reactive infiltration of 25 vol.pct. TiO₂/Al composites," *Metallurgical and Materials Transactions A*, vol. 33, pp. 2155–2162, jul 2002.
- [420] N. Yoshikawa, S. Funahashi, S. Taniguchi, and A. Kikuchi, "Fabrication and mechanical properties of Al/Al₂O₃ composite bodies by reactive infiltration of molten Al into SiO₂ preform," *Journal of Materials Research*, vol. 15, pp. 2314–2321, nov 2000.
- [421] S. Swaminathan, B. Srinivasa Rao, and V. Jayaram, "The production of AlN-rich matrix composites by the reactive infiltration of Al alloys in nitrogen," *Acta Materialia*, vol. 50, pp. 3095–3106, jul 2002.
- [422] C. R. Rambo, N. Travitzky, K. Zimmermann, and P. Greil, "Synthesis of TiC/Ti-Cu composites by pressureless reactive infiltration of TiCu alloy into carbon preforms fabricated by 3D-printing," *Materials Letters*, vol. 59, pp. 1028–1031, apr 2005.
- [423] J.-J. Wang, J.-H. Guo, and L.-Q. Chen, "TiC/AZ91D composites fabricated by in situ reactive infiltration process and its tensile deformation," *Transactions of Nonferrous Metals Society of China*, vol. 16, pp. 892–896, aug 2006.
- [424] W. Zhang, N. Travitzky, and P. Greil, "Formation of NbAl₃/Al₂O₃ composites by pressureless reactive infiltration," *Journal of the American Ceramic Society*, vol. 91, pp. 3117–3120, sep 2008.
- [425] Y.-W. Zhao, Y.-J. Wang, Y. Zhou, and P. Shen, "Reactive wetting and infiltration of polycrystalline WC by molten Zr₂Cu alloy," *Scripta Materialia*, vol. 64, pp. 229–232, feb 2011.
- [426] Y.-W. Zhao, Y.-J. Wang, L. Chen, Y. Zhou, G.-M. Song, and J.-P. Li, "Microstructure and mechanical properties of ZrCW matrix composite prepared by reactive infiltration at 1300°C," *International Journal of Refractory Metals and Hard Materials*, vol. 37, pp. 40–44, mar 2013.
- [427] N. Eustathopoulos and B. Drevet, "Interfacial bonding, wettability and reactivity in metal/oxide systems," *Journal de Physique III*, vol. 4, pp. 1865–1881, oct 1994.
- [428] H. Giesche, "Mercury porosimetry," in *Handbook of Porous Solids*, pp. 309–351, Weinheim, Germany: Wiley-VCH Verlag GmbH, 2002.
- [429] D. Camel, B. Drevet, and N. Eustathopoulos, "Capillarity in the processing of photovoltaic silicon," *Journal of Materials Science*, vol. 51, pp. 1722–1737, feb 2016.
- [430] J. Gil Sevillano, E. Bouchaud, and L. P. Kubin, "The fractal nature of gliding dislocation lines," *Scripta Metallurgica et Materialia*, vol. 25, pp. 355–360, feb 1991.

- [431] J. Gil Sevillano, I. Ocaña Arizcorreta, and L. P. Kubin, "Intrinsic size effects in plasticity by dislocation glide," *Materials Science and Engineering: A*, vol. 309-310, pp. 393–405, jul 2001.
- [432] T. E. Hutchinson, "Direct measurement of microscopic contact angle," *Thin Solid Films*, vol. 8, pp. R25–R29, oct 1971.
- [433] M. Kida, *High-temperature wettability and thermal conductivity of aluminium nitride reinforced metal matrix composites*. PhD thesis, EPFL, 2008.
- [434] H. Okamoto, "Cu-Si (Copper-Silicon)," *Journal of Phase Equilibria and Diffusion*, vol. 33, pp. 415–416, oct 2012.
- [435] C. Rado, *Contribution à l'étude du mouillage et de l'adhésion thermodynamique des métaux et alliages liquides sur le Carbure de Silicium*. PhD thesis, Institut National Polytechnique de Grenoble, 1997.
- [436] D. Caillard and J.-L. Martin, *Thermally activated mechanisms in crystal plasticity*, vol. 8. Pergamon, 2003.
- [437] L. P. Kubin, *Dislocations, mesoscale simulations and plastic flow*. Oxford: OUP Oxford, 1 ed., 2013.
- [438] U. F. Kocks, A. S. Argon, and M. F. Ashby, *Thermodynamics and kinetics of slip*. Pergamon Press, 1975.
- [439] D. P. Birnie, "A model for dilicon self-diffusion in silicon carbide: anti-site defect motion," *Journal of the American Ceramic Society*, vol. 69, no. 2, pp. C–33–C–35, 1986.
- [440] M. H. Hon and R. F. Davis, "Self-diffusion of ^{14}C in polycrystalline $\beta\text{-SiC}$," *Journal of Materials Science*, vol. 14, pp. 2411–2421, 1979.
- [441] C. Greskovich and J. H. Rosolowski, "Sintering of covalent solids," *Journal of the American Ceramic Society*, vol. 59, no. 7-8, pp. 336–343, 1976.
- [442] F. K. Van Dijen and R. Metselaar, "The chemistry of the carbothermal synthesis of $\beta\text{-SiC}$: reaction mechanism, reaction rate and grain growth," *Journal of the European Ceramic Society*, vol. 7, pp. 177–184, 1991.
- [443] K. Ono and Y. Kurachi, "Kinetic studies on $\beta\text{-SiC}$ formation from homogeneous precursors," *Journal of Materials Science*, vol. 26, pp. 388–392, 1991.
- [444] T. L. Francis and R. L. Coble, "Creep of polycrystalline silicon carbide," *Journal of the American Ceramic Society*, vol. 51, no. 2, pp. 115–116, 1968.
- [445] V. I. Gorovenko, V. A. Knyazik, and A. S. Shteinberg, "High-temperature interaction between silicon and carbon," *Ceramics International*, vol. 19, pp. 129–132, 1993.

Bibliography

- [446] C. Pantea, G. A. Voronin, T. Waldek Zerda, J. Zhang, L. Wang, Y. Wang, T. Uchida, and Y. Zhao, "Kinetics of SiC formation during high P-T reaction between diamond and silicon," *Diamond & Related Materials*, vol. 14, pp. 1611–1615, 2005.
- [447] A. B. D. Cassie, "Contact angle," *Discussions of the Faraday Society*, vol. 3, pp. 5–11, 1948.
- [448] A. R. Hind, S. K. Bhargava, and S. C. Grocott, "The surface chemistry of Bayer process solids: a review," *Colloids and Surfaces A: Physicochemical and Engineering Aspects*, vol. 146, pp. 359–374, 1999.
- [449] G. Yamaguchi and K. Suzuki, "On the structures of alkali polyaluminates," *Bulletin of the Chemical Society of Japan*, vol. 41, pp. 93–99, 1968.
- [450] R. C. De Vries and W. L. Roth, "Critical evaluation of the literature data on beta alumina and related phases: I, phase equilibria and characterization of beta alumina phases," *Journal of the American Ceramic Society*, vol. 52, no. 7, pp. 364–369, 1969.
- [451] T. Takahashi and K. Kuwabara, " β -Al₂O₃ synthesis from m-Al₂O₃," *Journal of Applied Electrochemistry*, vol. 10, pp. 291–297, 1980.
- [452] A. E. Paladino and W. D. Kingery, "Aluminum ion diffusion in aluminum oxide," *The Journal of Chemical Physics*, vol. 37, pp. 957–962, sep 1962.
- [453] J. H. Harding, K. J. W. Atkinson, and R. W. Grimes, "Experiment and theory of diffusion in alumina," *Journal of the American Ceramic Society*, vol. 86, pp. 554–59, apr 2003.
- [454] Y. Oishi and W. D. Kingery, "Self-diffusion of oxygen in single crystal alumina," *Journal of Chemical Physics*, vol. 33, p. 1679, 1960.
- [455] Y. Oishi, K. Ando, and Y. Kubota, "Self-Diffusion of oxygen in single crystal and polycrystalline aluminum oxide," *The Journal of Chemical Physics*, vol. 73, pp. 1410–1412, 1980.
- [456] K. P. R. Reddy and A. R. Cooper, "Oxygen diffusion in sapphire," *Journal of the American Ceramic Society*, vol. 65, pp. 634–638, dec 1982.
- [457] D. Prot, M. Le Gall, B. Lesage, A. M. Huntz, and C. Monty, "Self-diffusion in α -Al₂O₃. IV. Oxygen grain-boundary self-diffusion in undoped and yttria-doped alumina polycrystals," *Philosophical Magazine A*, vol. 73, pp. 935–949, apr 1996.
- [458] D. J. Reed and B. J. Wuensch, "Ion-probe measurement of oxygen self-diffusion in single-crystal Al₂O₃," *Journal of the American Ceramic Society*, vol. 63, no. 1-2, pp. 88–92, 1980.
- [459] A. Demir and N. Altinkok, "Effect of gas pressure infiltration on microstructure and bending strength of porous Al₂O₃/SiC-reinforced aluminium matrix composites," *Composites Science and Technology*, vol. 64, pp. 2067–2074, oct 2004.

- [460] J. G. Reynolds and R. Carter, "Density model for sodium hydroxide-sodium aluminate solutions," *Hydrometallurgy*, vol. 89, pp. 233–241, 2007.
- [461] E. Yazhenskikh, K. Hack, and M. Müller, "Critical thermodynamic evaluation of oxide systems relevant to fuel ashes and slags Part 2: Alkali oxide–alumina systems," *Calphad*, vol. 30, pp. 397–404, dec 2006.
- [462] K. C. Russell, S.-Y. Oh, and A. Figueredo, "Theoretical and experimental studies of ceramic : Metal wetting," *MRS bulletin*, pp. 46–52, 1991.
- [463] L. Weber and R. Tavangar, "On the influence of active element content on the thermal conductivity and thermal expansion of Cu–X (X = Cr, B) diamond composites," *Scripta Materialia*, vol. 57, pp. 988–991, dec 2007.

GIONATA SCHNEIDER

Ph.D en Science et Génie des Matériaux, EPFL



Curieux et dynamique, je suis à la recherche de nouveaux défis professionnels qui me permettront d'élargir mes connaissances et de développer mes compétences, tout en faisant bénéficier mon employeur de mes connaissances en recherche acquise à l'EPFL.

Contact

Route de Divonne 9

1291 Commugny

gionata.schneider@gmail.com

+41 (0)79 716 00 06

www.linkedin.com/in/gionata-schneider

Informations personnelles

Suisse, Marié, né le 28 août 1987

Compétences techniques

Coulée et mise en œuvre de métaux et alliages	Excellent
Tests mécaniques	Excellent
Métallurgie	Excellent
Métallographie	Excellent
Caractérisation de poudres	Très bon
Microscopie électronique (SEM)	Très bon
Infiltration et production de composites à matrice métallique	Excellent
Mathematica	Bon
C++	Bon
LaTeX	Très bon
OriginLab	Très bon

Langues

Italien	Langue maternelle
Français	Excellent (C1)
Anglais	Excellent (C1)
Allemand	Basique (A2)
Indonésien	Basique (A2)

Formation

2014- 2019, EPFL Lausanne

Thèse de doctorat en Science et Génie des Matériaux,

Laboratoire de Métallurgie Mécanique (LMM)

Supervision: Prof. A. Mortensen et Dr. L. Weber

2012- 2014, EPFL Lausanne,

Master en Science et Génie des Matériaux,

2008-2012, EPFL Lausanne,

Bachelor en Science et Génie des Matériaux

Centres d'intérêts:

Fitness, promenades entre amis, cuisine du monde, voyages, mécanique, cinéma.

Expérience

Etudiant doctorant, EPFL Lausanne

Mouillage dynamique dans l'infiltration sous pression de préformes céramique par des métaux liquides

Le but de cette thèse était d'investiguer l'effet de l'interaction entre le solide et le liquide pendant l'infiltration sous pression. Les données collectées ont été mises en relation avec la thermodynamique de la réaction.

2014- 2019 (juillet 2019)

Ce projet m'a permis d'affiner:

- Mon **sens pratique** afin de résoudre les différents problèmes techniques rencontrés lors de la réalisation des expériences.
- Mon **ingéniosité**, en augmentant la résolution d'analyse de l'appareil de mesure d'un facteur 2 et en amenant la température maximale d'utilisation à 1500°C.
- Mon **sens de l'organisation** et ma capacité à **travailler sur plusieurs tâches**, en traitant mon projet sur plusieurs fronts à la fois.
- Mes **capacités de communication**, afin de présenter mon travail dans plusieurs conférences et de publier mes résultats dans des journaux scientifiques.
- Ma **rigueur scientifique** afin de mettre en évidence et de résoudre des problèmes liés à la caractérisation de systèmes particulièrement complexes.
- Mes **capacités à travailler en équipe** en développant une collaboration entre plusieurs groupes d'universités différentes dans plusieurs pays.
- Mon **sens de la pédagogie** en donnant plusieurs cours et travaux pratiques aux étudiants.
- Mes **capacités managériales** afin de suivre un projet d'étudiant Master.

Thèse de Master, Novelis SA, Sierre

Cinétique de précipitation des alliages d'aluminium 6xxx

Août 2013- Février 2014

Ce projet m'a permis d'affiner:

- Mon **sens de l'organisation**, en travaillant simultanément sur les propriétés mécaniques de trois alliages différents.
- Mon **sens pratique** en développant une technique permettant d'observer l'évolution des précipités dans les alliages aluminium qui n'avait jamais été utilisée dans l'entreprise.

